Volume 70A
Number 6
Nov.–Dec. 1966

Physics and Chemistry

U.S. DEPARTMENT OF COMMERCE

SECTION A

JOURNAL OF RESEARCH

NATIONAL BUREAU OF STANDARDS

Journal of Research

of the

National Bureau of Standards

A. Physics and Chemistry

Nov.–Dec. • 1966

VOLUME • 70A

NUMBER • 6

Editor: C. W. Beckett

Associate Editors: D. D. Wagman
J. M. Richardson

Publication dates:
Feb. 1, Apr. 1, June 1, Aug. 1, Oct. 1, Dec. 1, 1966

JOURNAL OF RESEARCH

The National Bureau of Standards Journal of Research reports research and development in the fields of activity shown at right. Also included from time to time are survey articles on topics closely related to the Bureau's scientific and technical program.

The Journal is published in three separate sections as follows:

A. Physics and Chemistry

Contains papers of interest primarily to scientists working in these fields. Issued six times a year. Annual subscription: domestic, $5.00; foreign, $6.00. Single copy, $1.00.

B. Mathematics and Mathematical Physics

Presents studies and compilations designed mainly for the mathematician and the theoretical physicist. Issued quarterly. Annual subscription: domestic, $2.25; foreign, $2.75. Single copy, 75c.

C. Engineering and Instrumentation

Reports research and development results of interest chiefly to the engineer and the applied scientist. Issued quarterly. Annual subscription: domestic, $2.75; foreign, $3.50. Single copy, 75c.

The National Bureau of Standards is a principal focal point in the Federal Government for assuring maximum application of the physical and engineering sciences to the advancement of technology in industry and commerce. Its responsibilities include development and maintenance of the national standards of measurement, and the provision of means for making measurements consistent with those standards; determination of physical constants and properties of materials; development of methods for testing materials, mechanisms, and structures, and making such tests as may be necessary, particularly for government agencies; cooperation in the establishment of standard practices for incorporation in codes and specifications; advisory service to government agencies on scientific and technical problems; invention and development of devices to serve special needs of the Government; assistance to industry, business and consumers in the development and acceptance of commercial standards and simplified trade practice recommendations; administration of programs in cooperation with United States business groups and standards organizations for the development of international standards of practice; and maintenance of a clearinghouse for the collection and dissemination of scientific, technical and engineering information. The scope of the Bureau's activities is suggested in the following listing of its three Institutes and their organizational units.

Institute for Basic Standards. Applied Mathematics. Electricity. Metrology. Mechanics. Heat. Atomic Physics. Physical Chemistry. Laboratory Astrophysics.* Radiation Physics. Radio Standards Laboratory.* Radio Standards Physics & Radio Standards Engineering. Office of Standard Reference Data.

Institute for Materials Research. Analytical Chemistry. Polymers. Metallurgy. Inorganic Materials. Reactor Radiations. Cryogenics.* Materials Evaluation Laboratory. Office of Standard Reference Materials.

Institute for Applied Technology. Building Research. Information Technology. Performance Test Development. Electronic Instrumentation. Textile and Apparel Technology Center. Technical Analysis. Office of Weights and Measures. Office of Engineering Standards. Office of Invention and Innovation. Office of Technical Resources. Clearinghouse for Federal Scientific and Technical Information.**

*Located at Boulder, Colo. 80302.
**Located at 5285 Port Royal Road, Springfield, Va. 22151.

U.S. DEPARTMENT OF COMMERCE
John T. Connor, Secretary

NATIONAL BUREAU OF STANDARDS
A. V. Astin, Director

Order all publications from the Superintendent of Documents
U.S. Government Printing Office, Washington, D.C. 20402

Use of funds for printing this publication approved by the Director of the Bureau of the Budget (June 22, 1966).

JOURNAL OF RESEARCH of the National Bureau of Standards—A. Physics and Chemistry
Vol. 70A, No. 6, November–December 1966

Absolute Isotopic Abundance Ratios and Atomic Weight of Magnesium

Edward J. Catanzaro, Thomas J. Murphy, Ernest L. Garner, and William R. Shields

Institute for Materials Research, National Bureau of Standards, Washington, D.C., 20234

(August 16, 1966)

Absolute values have been obtained for the isotopic abundance ratios of magnesium, using surface emission mass spectrometry. Samples of known isotopic composition, prepared from nearly pure separated magnesium isotopes, were used to calibrate the mass spectrometers. The resulting absolute values are $^{25}Mg/^{24}Mg = 0.12663 \pm 0.00013$ and $^{26}Mg/^{24}Mg = 0.13932 \pm 0.00026$, yielding an atomic weight ($^{12}C = 12$) of 24.30497 ± 0.00044. The indicated uncertainties are overall limits of error based on 95 percent confidence limits for the mean and allowances for effects of known sources of possible systematic error.

Key Words: Absolute ratios, atomic weight, isotopic abundances, magnesium.

1. Introduction

The NBS is conducting a long-term program of physical atomic weight determinations using solid-source mass spectrometry. Previous determinations include silver [1],[1] chlorine [2], copper [3], bromine [4], and chromium [5]. The present work extends the study to magnesium.

A number of mass spectrometric determinations of magnesium isotope abundances have been reported in the literature, including: Dempster [6], Blewett and Jones [7], White and Cameron [8], Hibbs and Redmond [9], White et al. [10], Daughtry et al. [11], Shima [12], and Catanzaro and Murphy [13]. Of these studies, only the pioneer work of Dempster ($^{24}Mg = 77.4\%$, $^{25}Mg = 11.5\%$, $^{26}Mg = 11.1\%$) and the later works of White and Cameron ($^{24}Mg = 78.60\%$, $^{25}Mg = 10.11\%$, $^{26}Mg = 11.29\%$) and Hibbs and Redmond ($^{24}Mg = 78.98\%$, $^{25}Mg = 10.03\%$, $^{26}Mg = 11.00\%$) were conducted with the aim, or hope, of measuring absolute values. The results obtained by White and Cameron [8] were accepted as best estimates by the ICAW (1961 Report) while those of Hibbs and Redmond [9], which are virtually identical with the absolute values obtained in the present study, were apparently ignored. In any case, none of the above-noted studies included calibration of the instruments with separated magnesium isotope mixtures, so none of the results could be considered absolute.

In the present study the mass spectrometers used were calibrated for bias by the use of samples of known isotopic composition, prepared from nearly pure separated magnesium isotope samples. The measured biases were then used to obtain the absolute magnesium isotope ratios of a reference sample of magnesium metal. The atomic weight was then calculated using masses from Mattauch et al. (14).

The collector and recorder systems used in this laboratory have been designed so that any biases they may contribute are constant. The only "random" bias associated with the isotopic ratio measurements is due to the mass-dependent fractionation of the isotopes during ionization, and this bias is independent of the isotopic composition of the samples. Thus, for each instrumental system used in this study, a single experimentally determined mass-dependent correction factor is valid over the entire range of isotopic compositions measured [5].

The calibration samples were prepared by mixing aliquots of "Mg 24" and "Mg 26" separated isotope solutions. The use of the two extreme-mass isotopes gives the maximum sensitivity for determining the bias in the source region of a mass spectrometer. Four of the six calibration samples were prepared so as to give $^{24}Mg/^{26}Mg$ ratios which bracketed the natural $^{24}Mg/^{25}Mg$ and $^{24}Mg/^{26}Mg$ ratios. Amplifier attenuator positions used for these samples were identical to those used in the reference sample analyses, so that amplifier attenuator corrections were unnecessary. The other two calibration samples had unnatural $^{24}Mg/^{26}Mg$ ratios of approximately 1 and 2 and comparison of the correction factors given by these two samples with those given by the four "more-natural" samples served as a test of the single-correction-factor assumption.

[1] Figures in brackets indicate the literature references at the end of this paper.

2. Experimental Procedure

2.1. Mass Spectrometry

Isotopic measurements of the calibration and reference samples were made with two different single-focusing solid-source mass spectrometers. One instrument, MS–2, has a 6-in radius of curvature 60° analyzer tube and 48° sector magnet; the other, MS–4, has a 12-in radius of curvature 68° analyzer tube and 60° sector magnet. The electronic components and source and collector design are basically the same in both instruments. A third instrument, MS–3, which is identical with MS–4 except that it has a Z lens in the source assembly, was used to measure the isotopic compositions of the separated isotope solutions. Triple-filament rhenium-ribbon (1×30 mils) sources were used and Mg^+ currents were measured by means of a vibrating-reed electrometer with an expanded-scale recorder. Ratios were measured by varying the magnetic field at constant ion-accelerating potential (8kV on MS–2, 5 kV on MS–4).

The magnesium was deposited on the sample filaments in the form of aqueous solutions containing 5 mg Mg/ml, 5 mg U/ml, and 10 percent HNO_3. The uranyl nitrate was added to all solutions to act as a binding agent, because pure MgO did not adhere well to rhenium filaments. One drop of solution (~ 100 μgMg) was deposited on each sample filament and dried with a heat lamp and an electrical current which was slowly increased until an orange uranium oxide was formed.

To minimize the variability in isotopic fractionation (the $^{24}Mg/^{26}Mg$ ratio usually decreased by approximately 0.5% during an analyses), all analyses were performed in an identical manner. The temperature of the ionizing filament (~ 2100 °C) was held constant for all analyses by monitoring the strength of the Re^+ signal. A strict pattern of filament heating was followed and all data were taken on stable or slowly growing ion signals ($5–7 \times 10^{-12}$ A on MS–2 and $3–4 \times 10^{-12}$ A on MS–4) between 25 and 48 min after the filaments were turned on. The peak-top data were taken by step-wise changes in the magnet current and each peak-top was monitored for 30 sec. All analyses which did not have the normal signal-growth pattern were discarded.[2]

Ionizing filaments were prebaked (1/2 hr at 5 A) in a vacuum and under a potential field (300 V) to reduce the Na^+ signal from the rhenium-ribbon. Although there was no problem in resolving the ^{23}Na and ^{24}Mg peaks, preliminary tests showed that the scattering of secondary electrons produced by large Na^+ beams could affect the baselines under the ^{25}Mg and ^{26}Mg peaks. The prebaking of the ionizing filaments, combined with the efficient secondary electron suppression grids in the collector, eliminated this problem. Aside from an alcohol wash, the sample filaments were not pretreated in any manner; prebaked sample filaments increased the liklihood of sample flake-off. The magnesium background signal of the entire filament setup was negligible, being $< 3 \times 10^{-15}$ A.

In preliminary studies, a small amount ($< 1\%$) of source memory was sometimes detected, when samples of significantly different isotopic composition were analyzed back-to-back. Experiments showed that the memory was due to particulate matter which had flaked off the sample filaments, during one or more aborted analyses, and had adhered to the first or second source plates. To insure against this memory effect, the shield and first two plates of the source were replaced with a clean set whenever a sample change was made.

2.2. Purification of the Separated Isotopes

Electromagnetically separated ^{24}Mg and ^{26}Mg isotopes, in the form of magnesium oxide, were obtained from the Isotopes Division, Oak Ridge National Laboratory of the Union Carbide Nuclear Company. The ^{24}MgO and ^{26}MgO were designated Series KM, Sample 1256(A) and Series RS, Sample 129(A), respectively. The certificate of analysis accompanying each sample included a semiquantitative spectrographic analysis which indicated that calcium was present in both samples at about the 0.2 percent level and that several other elements could be present at concentrations up to 0.05 percent. To reduce these impurities to a level low enough so that they could not cause a significant error in the determination of the magnesium ion in solutions of these isotopes, the separated isotope samples were further purified by a method, based on work by Bricker and Parker [16] and Brunisholz [17], which had been previously found by this laboratory to be effective in removing these impurities and preparing pure MgO.

Each separated isotope sample was treated as follows: The magnesium oxide (about 1.7 g) was dissolved in 15 ml of (1 + 1) redistilled hydrochloric acid and the solution was filtered and diluted to about 300 ml. To this solution was added a solution containing 13 g (a 1 g excess) of (ethylenedinitrilo) tetraacetic acid (EDTA) in sufficient dilute (1 + 4) NH_4OH to just dissolve the acid. [The EDTA was purified by dissolving it in sufficient dilute (1 + 4) NH_4OH to effect solution and recrystallizing the EDTA by adjusting the *p*H of the solution to 1.0 with dilute (1 + 4) redistilled hydrochloric acid. The recrystallization was repeated twice. The ammonium hydroxide was prepared by passing ammonia gas into water.]

The solution containing the Mg isotope and EDTA was adjusted to *p*H 4.0 with dilute NH_4OH and allowed to stand at room temperature for two days. The magnesium salt of EDTA ($MgC_{10}H_{14}O_8N_2H_2O$) began to form after approximately 1 hr and precipitation was substantially complete ($> 98\%$) at the end of two days. The precipitated Mg-EDTA salt was recovered by filtering the solution through porous glass and was thoroughly washed with water. The

[2] A detailed description of the analytical procedure is given in reference [15].

salt was dissolved in dilute NH_4OH and reprecipitated as before. The Mg-EDTA from this second precipitation was transferred to a Vycor dish and dried. The temperature was slowly increased until the salt decomposed, and the residue was converted to MgO by ignition for 8 hr at 800 °C.

Samples of the purified ^{24}MgO and ^{26}MgO were analyzed by quantitative emission spectrography. The results of these analyses are shown in table 1. The concentration of each of the detected elements was low enough so that their total could not cause a significant error in the magnesium concentration determinations. To conserve the samples, the alkali metals were not determined. However, tests showed that when natural MgO, to which had been added 0.1 percent each of sodium, potassium, rubidium, and cesium, was purified by this method, none of the alkali metals was detected in the purified product, indicating that the concentration of each had been reduced to less than 0.0001 percent.

TABLE 1. *Results of spectrochemical analysis of purified isotope samples*

Quantitative (with standards) determinations of concentrations

Element	^{24}MgO	^{26}MgO	Estimated limits of detection
	ppm	*ppm*	*ppm*
Ag	10	2	0.2
B	–	–	0.2
Cd	–	–	1.
Cr	–	–	2.
Cu	1	< 1	0.1
Fe	< 1	< 1	0.5
In	1	–	1.
Pb	–	–	2.
Mn	–	–	0.5
Ni	–	–	1.
Sn	–	–	1.
Si	< 1	< 1	0.5
Ti	1	–	1.
V	–	–	5
Zn	–	–	

Semiquantitative (without standards) estimates of concentration ranges

	%	%
Al	–	0.0001 – 0.001
Ca	0.0001 – 0.001	< 0.0001
Pt	< 0.0001	< 0.0001
Rh	–	–

Notes: dash (–), not detected; <, less than.

2.3. Preparation and Magnesium Concentration of the Separated Isotope Solutions

The purified ^{24}MgO and ^{26}MgO samples were dissolved in dilute HNO_3 and the solutions were evaporated to near dryness to eliminate most of the excess nitric acid. The residues were taken up in water and diluted to approximately 40 ml. The solutions were then filtered and transferred to 100 ml volumetric flasks whose necks had been cut off so that only about 1 cm remained. The solutions were then diluted to about 65 ml and thoroughly mixed by swirling the flasks for several minutes. Each flask was then sealed with a rubber serum septum and left overnight in the case of a semimicrobalance, to insure that thermal equilibrium was achieved. The flasks and contents were then weighed on the balance to ± 0.02 mg. Samples were withdrawn from each flask by inserting a platinum needle, attached with a Kel-F hub to a glass hypodermic syringe, through the rubber septum and withdrawing the desired amount of solution. A second needle which just punctured the septum served as a vent. The syringe and needle were washed with distilled water and the washings were combined with the bulk of the sample in a 100 ml beaker. The weight of the sample was determined from the weights of the flask before and after the withdrawal of solution.

Four samples of from 7 to 8 g each were withdrawn from each solution by this method. The quantity of magnesium in each of these samples was from 4.0 to 4.5 millimoles (mM). Each sample was concentrated to a small volume by evaporation and transferred to a 15 ml platinum crucible. The beaker was washed several times with water and the washings were caught in the platinum crucible. As necessary, the contents of the crucible was concentrated by evaporation, to make space for the washings. Two ml of (1 + 1) redistilled sulfuric acid was added and the solution was evaporated to constant volume on a steam bath. The crucible and contents were transferred to a hot plate and the temperature was slowly increased until fumes of sulfuric acid were noted. The crucibles were then cooled, the contents taken up in water, and the evaporation to fumes of sulfuric acid was repeated. This process was repeated a third time, to insure removal of nitrate and chloride. [Tests with solutions of natural magnesium nitrate showed that after this sulfuric acid treatment the nitrate content was reduced to less than 0.001%, based on a colormetric determination using brucine sulfate(18). When solutions of natural magnesium chloride were treated in the same manner, the chloride content was reduced to less than 0.0005%, based on a turbidimetric silver analysis(18).]

At this point, the salt contained in the crucible was magnesium bisulfate, $Mg(HSO_4)_2$, which loses H_2SO_4 at about 400 °C, to form $MgSO_4$. After the fumes of sulfuric acid had been driven off the $MgSO_4$ was ignited at 600 °C overnight in an electric furnace.

The crucible was covered with a small piece of platinum foil and the furnace was cooled to 500 °C. The crucible was transferred to a special individual desiccator which was kept in an oven at 150 °C to lessen the thermal shock of transfer. [The individual desiccator was constructed by sealing a small glass drying bulb to a 70 ml glass weighing bottle. The drying bulb was packed with P_2O_5 and closed with a rubber stopper, when cool.] The desiccator containing the covered crucible was transferred from the oven, cooled, stoppered, and allowed to stand 4 hr to insure that thermal equilibrium was attained. The covered crucible was then weighed against time on a microbalance because of the hygroscopic nature of magnesium sulfate. The weight was recorded each minute for 5 min. The weight at "zero time" was determined from a weight-time plot. The weight of magnesium

sulfate was equal to the "zero time" weight minus the weight of the crucible and cover. All weights were corrected to vacuum.

This procedure of ignition, cooling, and weighing was repeated until a constant weight was obtained for the magnesium sulfate; that is, until the weighings agreed to within 50 μg. For simplicity of calculation, the average of the two weighings was converted to millimoles (mM) of magnesium using the 1964 atomic weights [19] for sulfur and oxygen and a calculated atomic weight for the isotopic magnesium based on the ORNL analyses. The results of these determinations are shown in table 2.

This method for the determination of the concentration of the magnesium isotope solutions was adopted after it became apparent that none of the conventional methods for magnesium analysis were capable of yielding precise enough results. It is a valid method as long as the purity of the magnesium sulfate is known. As stated previously, the total of the cationic impurities, as determined by emission spectrography, would cause a negligible error, and the only two likely anionic impurities, nitrate and chloride, would have been reduced to negligible amounts by the repeated sulfuric acid evaporations.

TABLE 2. *Concentration of magnesium isotope solutions*

Soln	Sample No.	Wt soln	Mg	Conc. soln Mg/g soln
		g	*mM*	*mM*
"Mg 24"	1	7.53528	4.203714	0.557871
	2	7.47788	4.171849	.557892
	3	7.37865	4.116165	.557848
	4	7.20773	4.020761	.557840
			Avg.	0.557863 [a]
"Mg 26"	1	7.43629	3.895881	0.523901
	2	7.42701	3.890721	.523861
	3	7.70054	4.034620	.523940
	4	7.59321	3.978122	.523905
			Avg.	0.523902 [a]

[a] The standard error of the average is calculated to be 0.000067 and the uncertainty of the value of concentration at the 95 percent confidence level is 0.000141 mM Mg/g soln.

This method for determining the concentration of magnesium nitrate solutions was tested on solutions containing known amounts of magnesium. Four such solutions were prepared from high purity (99.99+%) magnesium metal crystals in the approximate concentration of the isotopic solutions. Four samples containing from 3.8 to 5.5 mM of magnesium were withdrawn from each solution and the magnesium ion concentrations were determined as described above. Comparison of the known and measured concentrations of the four solutions showed that: (a) the concentration of magnesium ion as determined by this method agreed to within 0.01 percent of the known magnesium concentration, (b) systematic errors were negligible, and (c) the analyses of the four solutions were of equal precision.

From these analyses and from the analyses of the separated isotope solutions the standard deviation of an individual measurement of the concentration of a magnesium solution was computed to be 0.000133 mM Mg/g soln, with 18 deg of freedom. The standard error of the average of four determinations is therefore

$$\frac{0.000133}{\sqrt{4}} \text{ or } 0.000067 \text{ mM Mg/g soln,}$$

and the uncertainty of the concentration is 2.110×0.000067 or 0.000141 mM Mg/g soln (95% confidence limits). This corresponds to an uncertainty of 0.025 percent for solutions containing 0.55 mM Mg/g soln.

2.4. Isotopic Analyses of the Separated Isotope Solutions

The separated isotope solutions were analyzed five times each on a 12-in. mass spectrometer equipped with a Z-lens (MS-3). The source was dismantled and thoroughly cleaned before the analyses of each solution; clean sources gave negative memory tests.

Because of the large ratios involved, accurate analysis of the separated isotope solutions required larger ion currents than were used in the analyses of the calibration and reference samples. These larger signals ($3-4 \times 10^{-11}$ A) were obtained by a combination of the Z-lens source (a gain of $\times 4$) and the use of slightly higher sample filament temperatures. The bias for this analytical set up was zero, as determined by analyses of calibration sample No. I (see below) under the identical analytical conditions.

TABLE 3. *Isotopic composition of separated magnesium isotopes used in calibration samples*

Isotope	Isotopic composition (atom percent)		
"Mg 24"	^{24}Mg	99.95642	±0.00184 [a]
	^{25}Mg	0.02707	
	^{26}Mg	.01651	
"Mg 26"	^{24}Mg	0.39751	
	^{25}Mg	.44772	
	^{26}Mg	99.15477	±0.00413

[a] The uncertainties are based on the 95 percent confidence limits on the ratio determinations.

The isotopic compositions of the separated isotopes are given in table 3. The isotopic compositions reported by ORNL are "Mg 24," 99.96 ±0.02 atom percent ^{24}Mg, 0.03 ±0.01 atom percent ^{25}Mg, and <0.02 ±0.01 atom percent ^{26}Mg; "Mg 26," 0.42 ±0.02 atom percent ^{24}Mg, 0.42 ±0.02 atom percent ^{25}Mg, and 99.16 ±0.05 atom percent ^{26}Mg. The ORNL limits quoted express the precision of the measurements. From known sources of systematic error, the absolute error is estimated by ORNL to be less than 1 percent.

2.5. Preparation of the Calibration Samples

Six calibration samples were prepared by mixing weighed portions of the "Mg 24" and "Mg 26" solutions to produce ratios ranging from ^{24}Mg/^{26}Mg=1 to

$^{24}Mg/^{26}Mg=8.2$ (table 4). The portions were withdrawn from the flasks and weighed in the manner previously described. To eliminate any possibility of change in concentration of the isotope solutions with time, the portions for the calibration samples were withdrawn from the flasks on the same day that the samples for determining the magnesium concentration were withdrawn.

TABLE 4. *Composition of magnesium calibration samples*

Sample No.	Isotope Mg	Wt soln	Conc. soln Mg/g soln	Magnesium
		g	*mM*	*mM*
I	24	1.01244	0.557863	0.564803
	26	1.08547	.523902	.568680
II	24	2.01208	.557863	1.122465
	26	1.14635	.523902	0.600575
III	24	5.17735	.557863	2.888252
	26	0.83234	.523902	0.436065
IV	24	4.92722	.557863	2.748714
	26	0.64225	.523902	0.336476
V	24	5.01471	.557863	2.797521
	26	0.77441	.523902	0.405715
VI	24	5.13324	.557863	2.863645
	26	0.74109	.523902	0.388259

Each calibration sample was thoroughly mixed by stirring, and concentrated to a small volume by evaporation on a steam bath. Since pure MgO did not adhere well to the rhenium filaments, uranyl nitrate was added to act as a binding agent. The uranyl nitrate was prepared from standard reference material 950a, U_3O_8, uranium chemical standard, which has a magnesium content of only one part per million. Sufficient nitric acid was added so that the final solution contained 5 mg Mg/ml + 5 mg U/ml and was 10 percent HNO_3.

2.6. Isotopic Analyses of the Calibration and Reference Samples

Three complete sets of analyses of the calibration and reference samples were made, two on MS–2 and one on MS–4. Each set consisted of eight analyses of the reference, in four sets of two, and two analyses (made in succession) each of the six calibration samples; with duplicate reference analyses being made before and after successive duplicate analyses of two calibration samples. The $^{24}Mg/^{25}Mg$ and $^{24}Mg/^{26}Mg$ ratios were measured in the analyses of the reference sample but only the $^{24}Mg/^{26}Mg$ ratio was measured in the analyses of the calibration samples.

The entire source was dismantled and cleaned between the two complete sets of analyses on MS–2. The shields and first two plates of all sources were replaced with clean sets whenever a sample change was made. With this precaution, no memory effects were noted.

3. Results and Discussion

Table 5 summarizes the results for the six calibration samples. The mean correction factors given in this table and used in subsequent calculations are averages of the results of only the four calibration samples with approximately normal $^{24}Mg/^{26}Mg$ ratios (III, IV, V, and VI). The two "abnormal" calibration samples (I and II) were prepared and analyzed to show that the bias (per mass unit) of each instrument is single valued over the entire range of isotopic composition. The agreement between results is well within analytical error. Had the results for calibration samples I and II been included in the averaging for the final correction factors, an estimate of possible amplifier attenuator errors would have had to have been included in the final error statements, since the attenuator positions used in the analyses of these two samples were different from those used in the analyses of the reference sample.

The differences between the correction factors for MS–2, MS–4, and MS–3 (zero bias) is due primarily to the different techniques used on each instrument. The $^{24}Mg/^{26}Mg$ and $^{24}Mg/^{25}Mg$ ratios decrease steadily during an analysis; the higher the sample filament temperature, the higher the rate of change of these ratios. The technique used in MS–4 included the lowest sample filament temperature and smallest ion signals. This technique gave the smallest change in ratio with time, resulting in the best precision, but highest observed bias.

TABLE 5. *Determination of mass spectrometric bias*

Calibration sample No.	Isotopic ratio, $^{24}Mg/^{26}Mg$				Correction factor (2 mass units)	
	Calc.	MS–2(a)	MS–2(b)	MS–4	MS–2 (Avg. a+b)	MS–4
I	1.005055	1.01045	1.01270	1.02055	0.993556	0.984817
II	1.88752	1.89905	1.90170	1.91525	.993231	.985521
III	6.67364	6.72875	6.71645	6.77655	.992718	.984814
IV	8.22798	8.27785	8.30795	8.33550	.992174	.987101
V	6.94706	7.01270	7.01215	7.04800	.990679	.985678
VI	7.43012	7.50615	7.47955	7.53350	.991631	.986277
Mean of samples III, IV, V, and VI					0.991801	0.985968

Table 6 gives the observed and corrected magnesium isotope ratios for each mass spectrometer, and the average values, with uncertainty components. The correction factors for $^{25}Mg/^{24}Mg$ were calculated by assuming the biases to be one-half of those measured for the $^{26}Mg/^{24}Mg$ ratios. The statistical error per analysis was somewhat greater for MS–2 than for MS–4. However, since two sets of analyses were obtained on MS–2, the final standard errors for each mass spectrometer were almost identical and they were given equal weight in the averaging.

With the nuclidic masses given by Mattauch et al. (14), the results yield an atomic weight of 24.30497 $\pm$0.00044 on the unified scale ($^{12}C=12$). These cal-

TABLE 6. *Observed and corrected isotope ratios for the reference sample*

Mass spectrometer	Observed ratios		Correction factors		Corrected ratios	
	$^{25}Mg/^{24}Mg$	$^{26}Mg/^{24}Mg$	$^{25}Mg/^{24}Mg$	$^{26}Mg/^{24}Mg$	$^{25}Mg/^{24}Mg$	$^{26}Mg/^{24}Mg$
MS-2	0.1261426	0.1382371	0.995901	0.991801	0.1266618	0.1393799
MS-4	.1257059	.1373016	.992984	.985968	.1265941	.1392556
Mean [a]					0.1266280	0.1393178
Overall limit of error [b]					± 0.0001255	± 0.0002621
Uncertainty Components:						
95 percent confidence limits on ratio determination					± 0.0000812	± 0.0001652
Bounds due to possible systematic error in chemical analyses					± 0.0000398	± 0.0000870
Bounds due to possible systematic error in isotopic composition of separated isotopes					± 0.0000045	± 0.0000099

[a] The standard errors for the final results of both mass spectrometers were approximately the same so the results are averaged with equal weight.
[b] The overall limit of error is the sum of the 95 percent confidence limits for the ratio determinations and the terms covering effects of known sources of possible systematic error.

TABLE 7. *Summary calculations of the atomic weight of magnesium*

	Value	Overall limit of error [a]	Uncertainty components		
			Mass spectrometric analytical error	Possible systematic error in chemical analyses	Possible systematic error in composition of separated isotopes
Atomic weight	24.30497	± 0.00044	± 0.00026 [d]	± 0.00016	± 0.00002
Nuclidic masses [14] ($^{12}C = 12$)					
^{24}Mg	23.9850417	± .0000019			
^{25}Mg	24.9858390	± .0000020			
^{26}Mg	25.9825930	± .0000020			
Atom percent					
^{24}Mg	78.992	± .025	± .0154 [d]	± .0082	± .0009
^{25}Mg	10.003	± .009	± .0071 [d]	± .0021	± .0002
^{26}Mg	11.005	± .019	± .0123 [d]	± .0058	± .0007
Isotopic ratios [b]					
25/24	0.12663	± .00013	± .000081 [c]	± .000040	± .000005
26/24	.13932	± .00026	± .000165 [c]	± .000087	± .000010

[a] The overall limit of error is the sum of the limits based on the 95 percent confidence limits for the ratio determinations and the terms covering effects of known sources of possible systematic error.
[b] From table 6.
[c] 95 percent confidence limits.
[d] Limits based on 95 percent confidence limits on isotopic ratios.

culations are summarized in table 7. The value given here is significantly different from that presently accepted by the ICAW(24.312).

Catanzaro and Murphy [13] report no variations in the isotopic composition of 60 samples of natural magnesium from various localities and origins, so the atomic weight of magnesium should be constant.

We are indebted to Mrs. Martha Darr for the spectrochemical analysis of the magnesium isotope samples and to Hsien H. Ku for the statistical analysis of the experimental data.

4. References

[1] W. R. Shields, E. L. Garner, and V. H. Dibeler, J. Res. NBS **66A** (Phys. and Chem.), No. 1, 1 (1962).
[2] W. R. Shields, T. J. Murphy, E. L. Garner, and V. H. Dibeler, J. Am. Chem. Soc. **84,** 1519 (1962).
[3] W. R. Shields, T. J. Murphy, and E. L. Garner, J. Res. NBS **68A** (Phys. and Chem.), No. 6, 589 (1964).
[4] E. J. Catanzaro, T. J. Murphy, E. L. Garner, and W. R. Shields, J. Res. NBS **68A** (Phys. and Chem.), No. 6, 593 (1964).
[5] W. R. Shields, T. J. Murphy, E. J. Catanzaro, and E. L. Garner, J. Res. NBS **70A** (Phys. and Chem.), No. 2, 193 (1966).
[6] A. J. Dempster, Phys. Rev. **18,** 421 (1921).
[7] J. P. Blewett and E. J. Jones, Phys. Rev. **50,** 464 (1936).
[8] J. R. White and A. E. Cameron, Phys. Rev. **74,** 991 (1948).
[9] R. F. Hibbs and J. W. Redmond, Y-290, AECU-24 Dep. (1948).
[10] J. R. White, T. L. Collins, and F. M. Rourke, Phys. Rev. **101,** 1786 (1956).
[11] A. C. Daughtry, D. Perry, and M. Williams, Geochim. Cosmochim. Acta **26,** 857 (1962).
[12] M. Shima, Bull. Chem. Soc. Japan **37,** 284 (1964).
[13] E. J. Catanzaro and T. J. Murphy, J. Geophys. Res. **71,** 1271 (1966).
[14] J. H. E. Mattauch, W. Thiele, and A. H. Wapstra, Nuclear Physics **67,** 1 (1965).
[15] W. R. Shields, editor, NBS Tech. Note 277, 1966.
[16] C. E. Bricker and G. H. Parker, Anal. Chem. **29,** 1470 (1957).
[17] G. Brunisholz, Chima. (Switz.) **11,** 363 (1959).
[18] Committee on Analytical Reagents, Reagent Chemicals—American Chemical Society Specifications 1960, p. 289 (Amer. Chem. Society, Wash., D.C., 1961).
[19] A. E. Cameron and E. Wichers, J. Am. Chem. Soc. **84,** 4175 (1962).

(Paper 70A6-416)

JOURNAL OF RESEARCH of the National Bureau of Standards—A. Physics and Chemistry
Vol. 70A, No. 6, November–December 1966

Mass Spectrometric Study of Photoionization V. Water and Ammonia

Vernon H. Dibeler, James A. Walker, and Henry M. Rosenstock

Institute for Basic Standards, National Bureau of Standards, Washington, D.C. 20234

(August 11, 1966)

Photoionization efficiency curves are obtained for the molecule and fragment ions of H_2O and NH_3 in the wavelength region extending from onset of ionization to 600 Å. Threshold values of 12.593 eV and 10.162 eV are observed for the H_2O^+ and NH_3^+ ions, respectively. Vibrationally excited states of the molecule ions and autoionization of Rydberg levels are observed. A determination of the bond angle of the H_2O^+ ion from the Franck-Condon factors of the bending overtones results in a value of 112 degrees. Threshold values of the fragment ions permit calculations of heats of formation of the OH^+ and NH_2^+ ions and result in the ionization energies,

$$I(OH) = 12.94 \text{ eV and } I(NH_2) = 11.22 \text{ eV}.$$

Key Words: Autoionization, electronic, excited states, H_2O^+, NH_3^+, NH_2^+, OH^+ ions, heats of formation, ionization thresholds, mass spectrometer, photoionization, radicals, Rydberg levels, vacuum monochromators.

1. Introduction

Photon absorption in the wavelength region 600 to 1100 Å, and photoionization cross sections for H_2O have recently been remeasured [1–3][1] using photoelectric techniques. In general, the results are in good agreement with previous photographic [4–6] and photoelectric [7–8] studies, although only one [2] has suggested the possibility of autoionization in the wavelength region 850 to 950 Å.

The threshold for photoionization of H_2O, 12.59 $\pm$0.01 eV [9,10] seems to be well established although possibly not within the stated limits as recently published studies by Watanabe [2] would seem to indicate. However, it is in good agreement with recent electron impact measurements (12.60 $\pm$ 0.01 eV) [11] and with the value (12.61 eV) obtained from retarding potential measurements of photoejected electrons [12]. The latter two studies also report thresholds for two higher electronic states of the H_2O^+ ion. Only the electron impact study [11] employed mass analysis to identify the ionic species. Furthermore, no recent measurements of thresholds for dissociative ionization of water have been reported although these have long been known to exist in this energy region [13].

The photon absorption and photoionization of NH_3 have also been remeasured recently by photoelectric [1,3,14] and by photographic [15–17] means. These are generally in agreement with earlier measurements by both techniques [18–20]. However, some inconsistencies are observed among the photoelectric measurements [1] particularly in regions in which dissociative ionization is known to occur [13].

The threshold for photoionization of NH_3 is reported to be 10.15 eV [9] probably with an uncertainty of $\pm$0.01 eV. This is in fair agreement with the value of 10.18 eV obtained by extrapolation of Rydberg levels [15]. Recent electron impact measurements have been consistently higher than this value, usually by an amount which is nearly an order of magnitude greater than the claimed uncertainties. For examples, compare the electron impact values: 10.40 $\pm$ 0.02 eV [11], 10.52 $\pm$ 0.04 [22], and 10.34 $\pm$ 0.07 eV [23]. However, measurements of the kinetic energy of photoejected electrons [12] result in the threshold value of 10.16 eV, in excellent agreement with other photoionization data.

In the present study, mass analysis is combined with nearly monoenergetic photon beams to examine the ionization efficiency curves for the molecule and fragment ions of water and ammonia and to remeasure the threshold energies of the specific ionization and dissociative ionization processes.

2. Experimental Procedure

The windowless vacuum ultraviolet monochromator and mass spectrometer, described in detail in the first paper of this series [24], were used in the present work with only minor modifications. Both Hinteregger-type and microwave discharge lamps were used as photon sources. To obtain suitable overlapping of the spectral regions, the argon continuum was used in the wavelength region from threshold to about 1060 Å. The hydrogen many-line spectrum was used from about 1060 to 950 Å and the Hopfield continuum of helium employed from 950 to 600 Å.

[1] Figures in brackets indicate the literature references at the end of this paper.

Data were obtained principally by the use of 100-micron optical slits and a 600 grooves/mm, MgF_2-coated aluminum grating blazed at 1500 Å. In the 1-meter monochromator, this provided an optical resolving power of about 2 Å. Some threshold measurements were made using a 1200 grooves/mm, gold-coated grating blazed at 800 Å, providing a resolution of about 1 Å. The photon intensity for a 2 Å band width at the maximum of the argon continuum (about 1080 Å) was estimated from photoelectric yield curves for a tungsten detector [25] to be of the order of 2×10^8 photons/sec.

At each selected wavelength above the first onset a sufficient number of ion counts were obtained to result in a probable error of less than one percent. No correction was made to the observed relative abundances of ions for differences in detector response resulting from ions of different mass or structure. The estimated uncertainty in the measured photon intensity was about 3 percent at most wavelengths.

The ammonia was obtained from the Matheson Corporation and was used without further purification. The purity, stated by the supplier, is better than 98 mole percent NH_3 and no impurities were detected in the mass spectrum obtained at 21.23 eV.

The water sample was obtained from the laboratory supply of distilled water. When introducing H_2O, the sample inlet line in the vicinity of the pinhole leak was warmed to about 30 °C to prevent condensation or freezing at the leak.

3. Results and Discussion

H_2O: The respective relative abundances of the H_2O^+, OH^+, and O^+ ions of water observed at 584Å (21.23 eV) were found to be identical with the values reported by Samson and Cook [26]; namely, 1.0, 0.4, and 0.05. The low abundance of the O^+ ion prevents the measurement of the ionization efficiency curve for that ion in the present study. Also, an unsuccessful search was made for the negative ions, OH^- and O^-.

Figure 1 shows a typical set of photoionization efficiency curves for the H_2O^+ and the OH^+ ions. The wavelength in angstroms is plotted as the abscissa and ion current per photon transmitted is plotted in arbitrary units as the ordinate. The ordinate scale for the OH^+ ion is four times that of the H_2O^+ ion. The energies in electron-volts equivalent to several wavelengths are also given. If the ionization efficiency curves for the two ions are summed with proper consideration for the relative sensitivities as indicated above, a total ionization curve is obtained which is quite similar to that reported by Metzger and Cook [1].

The first long-wavelength onset of the H_2O^+ ion curve is ascribed to the (000)–(000) transition to the ground ($^2B_1$) state of the ion. The point of steepest ascent is 984.5 ± 1 Å (12.59_3 eV). This is in excellent agreement not only with previous photoionization values [9, 10], but also with electron impact data [11]. This agreement between adiabatic and vertical ionization energies in the case of H_2O would appear to support Mulliken's prediction [27] regarding the comparison of threshold measurements for electrons in nonbonding orbitals as obtained by spectroscopic and by electron impact methods.

Above the threshold there are two pronounced steps at 970 Å (12.78 eV) and 955 Å (12.98 eV), two small steps at about half these intervals and, at wavelengths shorter than 955 Å, considerable structure attributable to autoionization.

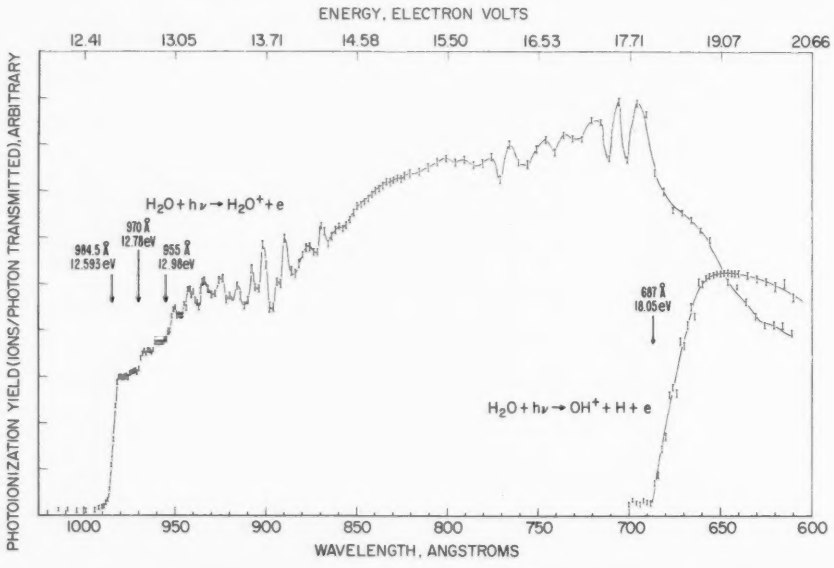

FIGURE 1. *Photoionization efficiency curves for the H_2O^+ and OH^+ ions of water.*

The $\Delta\nu$ between onset and 970 Å is about 1500 cm^{-1}, suggesting a bending overtone. The corresponding value for the 955 Å-step (ca 3100 cm^{-1}) could correspond to either the second bending overtone or the first stretching overtone of the ion.

Krauss [28] has calculated the geometries of the H_2O molecules and ion using SCF-Gaussian basis methods. His results indicate that the equilibrium bond angle in the ion is 119 deg or some 15 deg greater than in the neutral molecule. Johns [6] has carried out a rotational analysis of the first member of the $^1B_1$ Rydberg series in the 1220 to 1240 Å region leading to a bond angle of 106.9 deg for H_2O and 107.6 deg for D_2O with an increase in bond length of 0.06 Å. More recently, Bell [29] has measured the intensities of the vibrational structure of the $^1B_1$ and $^1A_1$ transitions for D_2O, determining the geometry by means of the Franck-Condon method of Coon and co-workers [30]. Bell obtained bond angles of 109.7 deg and 113.0 deg for the $^1B_1$ and $^1A_1$ states, respectively, with a probable error of ± 1.8 deg. The increases in bond length were 0.065 and 0.067 Å, respectively.

Using the method of Sharp and Rosenstock [31], and the force constants for the $^1A_1$ state given by Bell [29], we have calculated the intensities of the bending and symmetric stretching overtones relative to the (000–000) transition for various bond lengths and angles of the ion. These are plotted in figure 2. From the photoionization curve (figure 1) the 010/000 intensity ratio is 0.18 ±0.03. This leads to a value for the angle quite close to Bell's estimate. Accepting the increase in bond length determined by Johns and by Bell we obtain a value of about 112 deg for the H_2O^+ ion, see figure 2c.

The intensity of the second prominent step identified with the (100)–(000) transition cannot be determined accurately because of the autoionization structure. We have no explanation for the steps of $\Delta\nu = 800$ cm^{-1}, although progressions of this interval have been observed in absorption spectra [32] but not assigned.

Beginning at about 950 Å, the H_2O^+ ion curve shows more or less regularly spaced peaks which merge to a continuum at about 860 Å. These peaks are attributed to autoionizing Rydberg levels converging to the 14.2 eV [11, 12] threshold of the $^2A_1$ state of H_2O^+. This observation confirms an earlier suggestion [2] that diffuse bands observed in this region of absorption spectra might result from autoionization.

Initial members of another group of autoionizing Rydberg levels appear at about 780 Å, apparently merging to a continuum at about 690 Å (18.0 eV). If so, this would be in excellent agreement with the reported threshold of 18.02 eV [12] for the second excited state ($^2B_2$) of the H_2O^+ ion. The value 16.34 eV for the second ionization potential obtained by RPD electron impact methods [11] is located near the onset of this autoionizing series. The break in the electron impact ionization efficiency curve may well be due to excitation of these levels.

Except for the sharp onset, the OH^+ ionization efficiency curve is apparently featureless. The threshold occurs at 687 Å (18.05 eV). It is interesting to note that this is very near the wavelength (690 Å) at which the ionization efficiency for the molecule ion shows a marked decrease. It is probably also just above the threshold for the $^2B_2$ state of the H_2O^+ ion. It is suggested, therefore that the OH^+ ion arises from that state of the molecule ion. No metastable transition was observed in a very detailed study of the electron impact mass spectrum.

The observed value for the onset of dissociative ionization is considerably below the previously accepted electron impact value of 18.8 eV [13] and the photoionization value of 18.3 ±0.2 eV [26]. Assuming no excess kinetic energy of the fragments at threshold, the heat of reaction of the process $H_2O + h\nu \rightarrow OH^+ + H + e$ is 18.05 eV or 416.2 kcal [33] with an estimated uncertainty of 0.5 kcal. From this value and the heats of formation [34] of water and of the hydrogen atom, we calculate the $\Delta Hf°(OH^+) = 307.5$ kcal-mol^{-1}

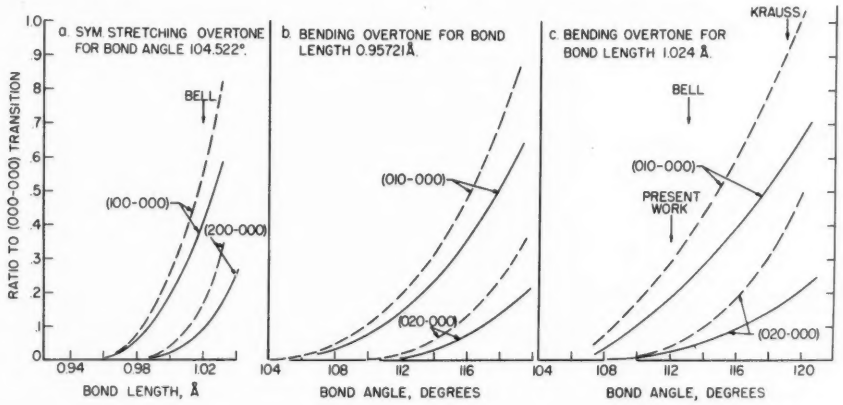

FIGURE 2. *Calculated intensities of the bending and symmetric stretching overtones relative to the (000–000) transition for various bond lengths and angles of the* H_2O^+ *ion* (——— H_2O^+, – – – D_2O^+).

at 0 °K. As the $\Delta Hf°_0(OH) = 9.25$ kcal [34] is well established, this results in I(OH) = 298.3 kcal (12.94 eV) with an estimated uncertainty of about 0.5 kcal. This is lower than the direct determination of I(OH) = 13.18 ±0.1 eV (304 ±2 kcal) reported by Foner and Hudson [35] but would be in agreement if the experimental error of the electron impact results were somewhat greater than quoted. The present results would appear to rule out the still higher value of I(OH) = 13.49 ±0.08 eV reported by Lindeman and Guffy [36].

NH_3: The relative abundances of the NH_3^+, NH_2^+, and NH^+ ions observed with the 584 Å line of He were 1.0, 1.5, and 0.01, respectively. The N^+ ion was not observed at this energy and there was no indication of the negative ions NH_2^- or NH^- at any of a number of wavelengths longer than 584 Å. The low abundance of the NH^+ ion does not permit accurate threshold measurements in the present experiments.

Figure 3 shows typical photoionization efficiency curves for the NH_3^+ and NH_2^+ ions of ammonia plotted as in fig. 1. The scale for the NH_2^+ ion is reduced to one-half that of the NH_3^+ ion. Below the onset of fragmentation, the curve looks very similar to the total ionization curve recently obtained by Watanabe and Sood [14]. If the two curves are properly added, a total ionization curve is obtained that is also in good agreement with that reported by Metzger and Cook [1]. There is no clear evidence for autoionization within the energy region covered.

The initial portion of the curve for NH_3^+ is quite unlike that for H_2O^+. The first unequivocal step at 1220 ±1 Å (10.162 ±0.008 eV) is ascribed to the 0–0 transition of the ion. This value is in good agreement with 10.154 eV from recent photoionization data [9, 12] and with 10.166 eV from recent Rydberg band analysis [14]. It is considerably lower than recent electron impact results [11, 21, 22] although the latter are not entirely consistent among themselves. There is some spectroscopic [37] evidence for a difference of about 0.5 eV between the adiabatic and vertical ionization thresholds.

On a large scale, the NH_3^+ ion curve shows some indication of hot bands as suggested by Watanabe and Mottl [38]. However, the transition probability is only of the order of 0.1 of the 0–0 transition. The 0–0 transition is followed by about nine steps at wavelength intervals of about 13 Å (900 cm^{-1}). The first four of these give indications of splitting into two steps each with nearly equal intervals of 6 or 7 Å (450 cm^{-1}). Walsh and Warsop [39] have shown that the NH_3^+ ion is very nearly planar and have estimated that the ν_2, out-of plane, vibrational frequency of the ground state of the ion is 920 ±10 cm^{-1}. The intervals for the larger steps shown in figure 3 are in good agreement with that value. The increase in intensity of the progression and the general relation of the transition probabilities are in essential agreement with the conclusions reported by Walsh and Warsop.

From about 1100 to 925 Å, the ionization efficiency for NH_3^+ is essentially constant. Above 925 Å, the curve rises to a maximum at about 785 Å and then drops rapidly to the end of the wavelength region. The threshold of an electronically excited state of the NH_3^+ ion has been reported to be about 15.0 eV [11, 12]. There is no indication of a threshold in this region of figure 3 although it may be completely masked by unresolved autoionizing levels.

The NH_2^+ ion shows a sharp onset at 788 ±2 Å (15.73 ±0.02 eV) at almost exactly the wavelength at which the intensity of the molecule ionization de-

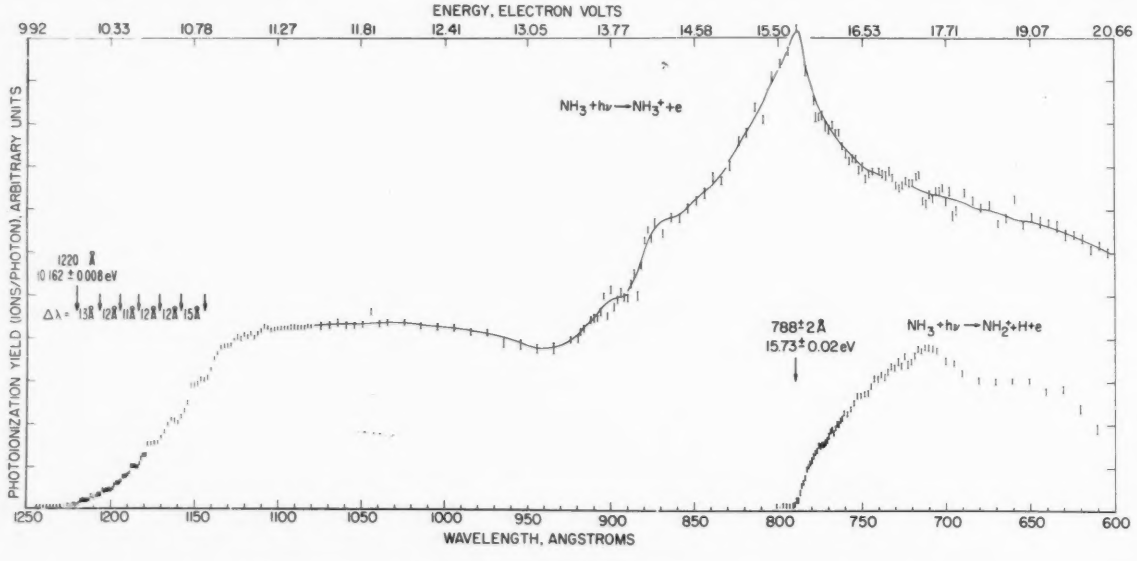

FIGURE 3. *Photoionization efficiency curves for the NH_3^+ and NH_2^+ ions of ammonia.*

creases sharply. The threshold of fragmentation is also above the reported onset of the first excited state of NH_3^+; i.e. 15.02 eV [12] and probably arises from that state. The value is again about 0.3 eV below the electron impact threshold as reported by Foner and Hudson [40] but is possibly in agreement with an earlier value (15.8 eV) [41] within the limits of combined estimated errors. Thus, from the heat of reaction of the process, $NH_3 + h\nu \rightarrow NH_2^+ + H + e$ of 15.73 eV or 362.6 kcal-mol^{-1} we calculate the $\Delta Hf°(NH_2^+) = 301.6$ kcal-mol^{-1} at 0 °K. Also, using D $(NH_2 - H) = 104 \pm 2$ kcal-mol^{-1} given by Altshuller [42] we calculate the ionization energy, $I(NH_2) = 258.6$ kcal-mol^{-1} (11.22 eV) or about 0.2 eV below that obtained by direct electron impact measurement.

We wish to acknowledge the assistance of Itiro Omura in obtaining some of the photoionization data.

4. References

[1] P. H. Metzger and G. R. Cook, J. Chem. Phys. **41,** 642 (1964).
[2] K. Watanabe and A. S. Jursa, J. Chem. Phys. **41,** 1650 (1964).
[3] G. R. Cook and B. K. Ching, Rept. No. TDR-469 (9260-01)4 Laboratory Operations, Aerospace Corp., Los Angeles, Calif. 30 Jan. 1965.
[4] W. C. Price, J. Chem. Phys. **4,** 147 (1936).
[5] P. G. Wilkinson and H. L. Johnston, J. Chem. Phys. **18,** 190 (1950).
[6] J. W. C. Johns, Can. J. Phys. **41,** 209 (1963).
[7] N. Wainfan, W. C. Walker, and G. L. Weissler, Phys. Rev. **99,** 542 (1955).
[8] K. Watanabe and M. Zelikoff, J. Opt. Soc. Am. **43,** 753 (1953).
[9] K. Watanabe, T. Nakayama, and J. Mottl, J. Quant. Spectry. Radiative Transfer **2,** 369 (1962).
[10] A. J. C. Nicholson, J. Chem. Phys. **43,** 1171 (1965).
[11] D. C. Frost and C. A. McDowell, Can. J. Chem. **36,** 39 (1958).
[12] M. I. Al-Joboury and D. W. Turner, J. Chem. Soc. (London) 1964, 4434.
[13] F. H. Field and J. L. Franklin, Electron Impact Phenomena and Properties of Gaseous Ions (Academic Press, Inc., New York, 1957).
[14] K. Watanabe and S. P. Sood, Science of Light **14,** 36 (1965).
[15] A. D. Walsh and P. A. Warsop, Trans. Faraday Soc. **57,** 345 (1961).
[16] A. E. Douglas and J. M. Hallas, Can. J. Phys. **39,** 479 (1961).
[17] A. E. Douglas, Discussions Faraday Soc. **35,** 158 (1963).
[18] A. B. F. Duncan, Phys. Rev. **50,** 700 (1936); J. Chem. Phys. **27,** 423 (1957).
[19] H. Sun and G. L. Weissler, J. Chem. Phys. **23,** 1160 (1955).
[20] W. C. Walker and G. L. Weissler, J. Chem. Phys. **23,** 1540 (1955).
[21] K. Watanabe and J. R. Mottl, J. Chem. Phys. **26,** 1773 (1957).
[22] J. D. Morrison and A. J. C. Nicholson, J. Chem. Phys. **20,** 1021 (1952).
[23] J. Collin, Can. J. Chem. **37,** 1053 (1959).
[24] V. H. Dibeler and R. M. Reese, J. Res. NBS **68A,** (Phys. and Chem.) No. 4, 409 (1964).
[25] H. E. Hinteregger and K. Watanabe, J. Opt. Soc. Am. **43,** 604 (1953).
[26] J. A. R. Samson, Private Communication. Also, see J. A. R. Samson and G. R. Cook, Bull. Am. Phys. Soc. **4,** 454 (1959).
[27] R. S. Mulliken, J. Chem. Phys. **3,** 506 (1935).
[28] M. Krauss, J. Res. NBS **68A,** (Phys. and Chem.) No. 6, 635 (1965).
[29] S. Bell, J. Mol. Spectry. **16,** 205 (1965).
[30] J. B. Coon, R. E. DeWames, and C. M. Loyd, J. Mol. Spectry. **8,** 285 (1962).
[31] T. E. Sharp and H. M. Rosenstock, J. Chem. Phys. **41,** 3453 (1964).
[32] K. Watanabe and M. Zelikoff, J. Opt. Soc. Am. **43,** 753 (1953).
[33] 1 thermochemical calorie = 4.1840 joules.
[34] D. D. Wagman, W. H. Evans, I. Halow, V. B. Parker, S. M. Bailey and R. H. Schumm, NBS Tech. Note 270-1 (Oct. 1, 1965).
[35] S. N. Foner and R. L. Hudson, J. Chem. Phys. **25,** 602 (1956).
[36] L. P. Lindeman and J. C. Guffy, J. Chem. Phys. **30,** 322 (1959).
[37] K. Watanabe, J. Chem. Phys. **22,** 1564 (1954).
[38] K. Watanabe and J. Mottl, J. Chem. Phys. **26,** 1773 (1957).
[39] A. D. Walsh and P. A. Warsop, Trans. Faraday Soc. **57,** 345 (1961).
[40] S. N. Foner and R. L. Hudson, J. Chem. Phys. **29,** 442 (1958).
[41] M. M. Marin, A. Hustrulid, and J. T. Tate, Phys. Rev. **58,** 340 (1940).
[42] A. P. Altshuller, J. Chem. Phys. **22,** 1947 (1954).

(Paper 70A6-417)

JOURNAL OF RESEARCH of the National Bureau of Standards—A. Physics and Chemistry
Vol. 70A, No. 6, November–December 1966

Interpretation of the Third Spectrum of Gold (Au III)*

Laura Iglesias**

(July 17, 1966)

A revision of the analysis of the Au III spectrum is presented. Of 9 energy levels considered doubtful on the basis of a recent theoretical treatment, 6 are found to be real and 3 have been rejected as incorrect. Three new energy levels have also been found in agreement with theoretical predictions.

Key Words: Corrections to analysis of Au III, gold, spectrum of Au III, third spectrum.

The analysis of the structure of the third spectrum of gold was published in 1960.[1] Recently, Shadmi[2] published the corresponding theoretical interpretation and some discrepancies between both papers justify the present comments.

In our 1960 paper we reported 17 even levels of the Au^{++} ion and 43 odd ones. In order to make them easily identifiable we labeled the even levels with *LS* symbols, pointing out that this coupling scheme did not apply, but was used only as a simple means of identification. Many of the odd levels were identified only by numbers, indicating that the *LS* designation was still more doubtful.

In his theoretical paper, Shadmi interprets the levels by the use of the *jj*-coupling scheme. When theory predicts a dominant *LS* character of the even levels, it is in good agreement with the experimental results, as is also the case as regards the value of the levels. Among the odd levels the situation is quite different. The largest component in *LS* coupling deduced theoretically does not always agree with the experimental designation, which is not surprising; but the theoretical results seem to indicate, also, that some of the experimental levels are incorrect. This result is worth discussing in detail.

Table 1 contains some of the data in table 6 of Shadmi's paper, and the symbols in column 4 have the following meanings:

A dash indicates experimental levels which have such large deviations from the theoretical ones that they are subject to rejection by Shadmi. A question mark indicates doubtful levels.

In this table the results of a new revision of the experimental data are also included, and the following comments are appropriate to each particular level. The levels designated 5°, 18°, and 33°, are rejected as incorrect, since the assumed combinations that were supporting them can now be considered as only numerical coincidences.

The levels 8° and 36° could be considered doubtful because they are based on only one combination. Nevertheless, only two lines are theoretically predicted as combinations of these two levels having $J=11/2$ with the known even ones. We may point out also, that the combinations $a^4F_{9/2}-8°_{11/2}$ and $a^2G_{9/2}-36°_{11/2}$ are expected to be strong. The lines chosen to identify these levels are the only two intense unclassified lines in the appropriate regions. An unsuccessful search has been made to see whether any of the already classified lines would give levels in better agreement with the theoretical predictions. We conclude, therefore, that these levels can be considered correct from the experimental point of view.

* An invited Paper. ** Present address: Instituto de Optica, Madrid, Spain.
[1] L. Iglesias, J. Res. NBS **64 A** (Phys. and Chem.) No. 6, 481 (1960).
[2] Y. Shadmi, J. Res. NBS **69 A** (Phys. and Chem.) No. 6, 511 (1965).

TABLE 1. *Doubtful levels of* Au III ($5d^8$ 6p *configuration*)

Exper. desig.	*J*	Level	(Shadmi)	Present situation	Theoretical value	O−C
5°	1/2	98559.1	−	Incorrect	− − −	
8°	11/2	102993.7	?	Probably good	102069	925
18°	1/2	113749.9	+?	Incorrect	− − −	
19°	1/2	113764.9	−	Good	113664	101
20°	7/2	115339.9	−	Good, $J=9/2$	115091	249
24°	3/2	116892.1	?	Good	115987	905
33°	9/2	123508.8?	−	Incorrect	− − −	
34°	3/2	125767.0	−	Good, $J=5/2$	125580	188
36°	11/2	127467.0?	?	Probably good	127104	363
42°	5/2	133058.9	−	Good, $J=3/2$	133181	−122

The level 24° is clearly correct. It is one of the levels giving a large number of combinations. From 12 lines theoretically possible 10 have been observed experimentally. One needs to assume too great a chance for fortuitous coincidences to be able to discard it. If this were done, several intense lines would remain without alternative explanation.

The levels 20°, 34°, and 42° are also correct, but the J-values have to be changed to agree with the theoretical predictions. It was very difficult to assign a J value of 9/2 to the level 20° since there are no even levels having $J=11/2$. By admitting that the assumed transition $a\,^2F_{5/2}-20°$ was just a coincidence, the level can be accepted as having $J=9/2$.

By assuming that the transition $a\,^2P_{1/2}-34°$ leads to a fortuitous coincidence, the level 34° combines only with levels of $J=3/2$ or 5/2. The J-value can, therefore, be changed to 5/2 as is done in table 1.

The level 42° is real. Its J-value can be changed to 3/2, since it combines only with levels having $J=5/2$ and 3/2.

The level 19° is also correct but the alternative level 18°, has to be rejected.

As a further result of the present revision three new levels, designated 46°, 47°, and 48° have been found. They correspond to theoretical predicted levels, as shown in table 2.

TABLE 2. *New levels of* Au III ($5d^8\,6p$)

Desig.	J	Dominant *LS* character	Level observed	Level calculated	O−C
46°	1/2	61% (^{3}P)^{4}P	108183.2	108293	−110
47°	7/2	48% (^{1}D)^{2}F	134891.1	135014	−123
48°	1/2	45% (^{1}D)^{2}P	137705.7	137443	263

TABLE 3. *New classified lines of* Au III

$\lambda_{vac.}$ (Å)	Int.	ν (cm^{-1})	Combination
799.928	50	125011.2	$a\,^2D_{3/2}-48°$
1207.264	10	82831.5	$a\,^2F_{5/2}-47°$
1259.81	2 H	79377.0	$a\,^2P_{1/2}-48°$
1297.486	3	77072.1	$a\,^2G_{9/2}-47°$
1310.488	5	76307.5	$a\,^2G_{7/2}-47°$
1350.715	50	74034.9	$a\,^2P_{3/2}-48°$
1415.487	80	70647.1	$b\,^2D_{5/2}-47°$
1717.820 [a]	300	58213.3	$a\,^4P_{3/2}-46°$
1850.149	80	54049.7	$b\,^2D_{3/2}-46°$
2005.764	30	49856.3	$a\,^2P_{1/2}-46°$

[a] The classification $a\,^4F_{3/2}-z\,^4D^\circ_{1/2}$ assigned to this line in our first paper is not valid.

Table 3 contains the lines classified as combinations of these new levels.

The lines $\lambda=1540.258$ Å, $\lambda=1580.277$ Å, and $\lambda=1996.853$ Å previously classified with unreal levels are now left unclassified.

Finally, we wish to emphasize that the interpretation of this spectrum gives a new and good example of fruitful cooperation of the theoretical spectroscopists in the interpretation of our experimental results.

The author thanks Mrs. Charlotte Moore-Sitterly and William C. Martin for their kind cooperation in the correction of the English manuscript and during the editorial stages of this paper.

(Paper 70A6–418)

JOURNAL OF RESEARCH of the National Bureau of Standards—A. Physics and Chemistry
Vol. 70A, No. 6, November–December 1966

A Formal Solution for Slit Corrections in Small-Angle X-Ray Scattering

Jacob Mazur and Andrew M. Wims

Institute for Materials Research, National Bureau of Standards, Washington, D.C., 20234

(May 5, 1966)

Slit shaped apertures are usually used in small-angle x-ray scattering measurements in order to obtain easily measured intensities of scattered radiation. As a result, the scattering intensity at a given angle determined by the camera, the center of the sample, and the central incident x-ray beam is not simply related to the scattering from the sample only at that angle. The experimentally determined intensities $\tilde{I}(x)$ are related to the true scattering intensities by the following integral equation:

$$\tilde{I}(x)=\int_{-\infty}^{\infty} I[(x^2+t^2)^{1/2}]W(t)dt.$$

This integral equation has been previously solved only for certain simplified functional forms for $W(t)$ and $\tilde{I}(x)$. In this paper, a formal procedure is developed for calculating $I(x)$ from the observed angular measurements, which does not necessitate making any a priori assumption about the form of $W(t)$ and $\tilde{I}(x)$.

Key words: Distribution of intensity, integral equation, scattering cross section, slit correction, small-angle x-ray scattering.

1. Introduction

Narrow slits are often used in small-angle x-ray scattering measurements to collimate the incident beam sufficiently to allow scattering measurements extremely close to the incident beam. Compared to a pinhole of diameter approximately equal to the slit width, the slit system increases the available scattering energy. However, the scattered radiation measured in a given solid angle can no longer be simply described as the scattering coming from a point source. Instead, the actual angular scattering measurements. which are summations of the scattering contributed by each scattering center along the height of the sample slit, must be resolved to give the scattering of an infinitely small area at the center of the sample slit. In this paper, a formal procedure is described for calculating the true scattering cross sections from the observed angular measurements when long but very narrow-width slits are used for collimation.

A diagram for the slit system of a small angle x-ray system is given in figure 1. This is a modification of the diagram given by Shull and Roess [1].[1] The plane of the quadrangle *txyr* is perpendicular to the camera axis which is in the vertical plane containing the collimating slit and the sample slit. The collimating slit nearest the x-ray tube has length $2l_1$, the effective length of the slit at the sample is $2l_2$, and the

[1] Figures in brackets indicate the literature references at the end of this paper.

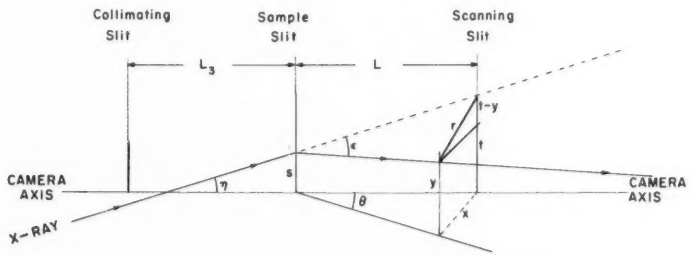

FIGURE 1. *Diagram of a slit collimation system.*

scanning slit at the detector is of length $2y_0$. The scanning slit and sample slit are shown in figure 1 to be in a plane making an angle θ with the plane containing the camera axis and the collimating slit. Let us consider a ray which makes an angle η with the camera axis and after it hits the sample is scattered by an angle ϵ with its original direction. Since the angles ϵ, θ, and η are in practice small, they can be replaced by the following ratios:

$$\epsilon = r/L, \quad \theta = x/L, \tag{1}$$

and $\eta = (t-s)/L$.
Since $r^2 = x^2 + (t-y)^2$, it follows that

$$\epsilon^2 = \theta^2 + \left[\eta + \left(\frac{s-y}{L}\right)\right]^2. \tag{2}$$

Let $\tilde{I}(\theta)$ be the intensity striking the scanning slit centered at θ, and let $I(\epsilon)d\eta$ represent the increment in intensity of scattering in an element $d\eta$. The following equation defines $\tilde{I}(\theta)$ by averaging $I(\epsilon)$ over the entire scanning area.

$$\tilde{I}(\theta) = \frac{1}{2y_0}\int_{-y_0}^{y_0} dy \int_{-l_2}^{l_2} ds \int_{(s-l_1)/L_3}^{(s+l_1)/L_3} I(\epsilon)d\eta. \tag{3}$$

Equation (3) is the one obtained by Shull and Roess [1].

The triple integral in eq (3) can be reduced to a single integral. One way to do it is by the method employed by Schmidt [2]. By changing y, s, and η into the dimensionless variables

$$y_1 = y/L_1, \; s_1 = s\left(\frac{1}{L_3}+\frac{1}{L}\right), \; \eta_1 = \eta - \frac{s}{L_3}$$

the limits of the integrations are replaced by constants which are descriptive of the geometrical parameters of the slit system. One can then integrate the resulting expression over s_1 and y_1. After substituting $t_1 = \frac{t}{L}$ for $\eta_1 + s_1$, the resulting integral equation is

$$\tilde{I}(\theta) = A\int_0^\infty I[(\theta^2 + t_1^2)^{1/2}]W(t_1)dt_1. \tag{4}$$

However, $W(t_1)$ is a complicated function of the geometrical parameters of the system. In general, $W(t_1)$ is a quadratic function of t_1, represented by different functions for different intervals of t_1. Also, $W(t_1)$ must be premultiplied by a unit step function which becomes zero when

$$t > \left| y_0 + l_2 + (l_1 + l_2)\frac{L}{L_3} \right|.$$

The advantage of starting with eq (3) is that $L_3\eta_1$ is the coordinate of the length of the slit nearest to the x-ray tube. Thus, in the more general case when the intensity along η_1 is not uniform, but is given by a general distribution function $g(\eta_1)$, eq (4) will still be obtained. However, $W(t_1)$ will be represented by double integrals of the general form

$$\int\int g(\eta_1 - s_1 - y_1)ds_1 dy_1,$$

with the ranges of integration being determined by the parameters of the system. In other words, $W(t_1)$ in eq (4) results from the projections of the variables s_1 and y_1 onto the plane of registration, corrected for a possible nonuniformity in the distribution of intensity of scattered ratiation along η_1. The only restrictions imposed are on the variables s_1, η_1, and y_1. These angles must be sufficiently small to justify their replacements by ratios of coordinates (eq (1)).

In the process of determining the formal solution of the integral eq (4), one has to calculate derivatives of $W(t)$, and for this reason, it would be more advantageous to start with a continuous expression for this function. This difficulty is eliminated if one starts with the experimentally determined $W(t)$ or by using the smoothed curve obtained from the calculated segments.

Starting with eq (3), but omitting the slit coordinate η_1, we have the following equation, with $w(t)$ representing the intensity distribution in the t direction

$$\tilde{I}(x) = \int_{-\infty}^{\infty}\int_{-\infty}^{\infty} w(t)I\{[x^2 + (t-y)^2]^{1/2}\}dtdy. \tag{5}$$

Interchanging the order of integration and making use of the fact that $W(t) = W(-t)$, we obtain

$$\tilde{I}(x) = 2\int_0^\infty W(t)I[(x^2 + t^2)^{1/2}]dt \tag{6}$$

with

$$W(t) = \int_{-\infty}^{\infty} w(t-y)dy. \tag{7}$$

$W(t)$ can be determined by measuring the intensity in the plane of registration. This is done by taking various intervals equal to $2y_0$ along the t axis. These intervals are equal to the length of the scanning slit. The finite length of the scanning slit restricts the range of the variable y in eq (7). Therefore, a unit step function $h(y)$ has to be introduced, with $h(y) = 0$ for $y > k$ and $h(y) = 1$ for $0 < y < k$. This process will modify $W(t)$ into a convolution integral of $w(t)$ and $h(t)$,

$$W(t) = \int_{-\infty}^{\infty} w(y)h(t-y)dy. \tag{8}$$

The only known solutions of the integral eq (6) were obtained for certain special forms of $W(t)$ and of $\tilde{I}(x)$. Guinier [3], Fournet [4], and DuMond [5] have solved this integral equation for slits of infinite height ($W(t) = 1$). Their method was extended by Kratky, Porod, and Kahovec [6], and by Gerold [7] to finite beams where $W(t)$ could be represented by a step function, or a Gaussian distribution, or a particular trapezoidal distribution. Shull and Roess [1] have

presented a solution for an arbitrary $W(t)$ if the scattering curve $\tilde{I}(x)$ can be resolved into a packet of Gaussian functions. The earlier attempts to solve eq (6) have been recently reviewed by Beeman, Kaesberg, Anderegg, and Webb [8], and by Kratky, Porod, and Skala [9].

In the following section a formal solution to eq (6) is presented which does not require any a priori assumptions about the particular forms of $\tilde{I}(x)$ and of $W(t)$.

2. Solution of the Integral Equation

2.1. General Considerations and Discussions

Equation (6) is rewritten as

$$\tilde{I}(x)=2\int_x^\infty \frac{yI(y)W[(y^2-x^2)^{1/2}]dy}{(y^2-x^2)^{1/2}}. \tag{9}$$

To solve this integral equation in one of the standard forms it is essential to remove its singularity, since the kernel of the equation is infinite at $y=x$. The transformation of this equation, which removes this singularity follows the method employed in connection with the celebrated Abel's integral equation. A new variable in a suitable form is introduced, and both sides of the resulting integral equation are integrated over the variable x between the value of the new variable and infinity. This, combined with the interchange in the order of integration of the right-hand side of the resulting integral equation, through the use of the Dirichlet formula, has the effect of removing the singularity. The new kernel is finite everywhere, but it is replaced by a bounded integral whose integrand involves the original distribution function $W(t)$.

The solution thus obtained is an implicit one, since the left-hand side of the integral equation involves the integrated form of the experimental function $\tilde{I}(x)$. In order to obtain an explicit form for the integral equation, two additional steps are required: (1) Solution of a subsidiary integral equation for another function, which essentially compensates for the slit weighting function W, (see following section), and (2) differentiation of the experimental intensity function $\tilde{I}(x)$ with respect to x. The details of the solution are given in the following section. Here we give the two solutions, the implicit and the explicit one in their final forms:
Implicit Solution:

$$\int_0^\infty \tilde{I}[(v^2+u^2)^{1/2}]dv=2\int_u^\infty yI(y)K[(y^2-u^2)^{1/2}]dy, \tag{10}$$

with

$$K(v)=\int_0^1 \frac{W(vx)}{(1-x^2)^{1/2}}\,dx; \qquad v^2=y^2-u^2. \tag{10a}$$

Explicit Solution:

$$I(u)=\frac{1}{\pi}\int_0^\infty \frac{\tilde{I}[(y^2+u^2)^{1/2}]}{(y^2+u^2)^{1/2}}F(y)dy. \tag{11}$$

The function F satisfies the following Volterra equation of the second kind:

$$F(y)=1-\frac{2}{\pi}y\int_0^y F(z)K[(y^2-z^2)^{1/2}]dz, \tag{12}$$

$$K(v)=\frac{1}{v}\int_0^1 \frac{xW'(vx)dx}{(1-x^2)^{1/2}}; \qquad v^2=y^2-z^2. \tag{12a}$$

The kernels of the implicit and explicit solutions, eqs (10a) and (12a), are similar in their general forms, except that the first one involves the slit correction function W, and the second one involves its derivative. The implicit solution is suitable only with the use of a digital computer. Both sides of eq (10) are solved simultaneously as a set of simultaneous linear equations through a matrix inversion method. This method can be employed also in order to obtain $F(u)$ from eq (12). However, the latter equation can be solved by expansion of $F(u)$ in a Liouville-Neumann series. These series will converge rapidly, if a good initial assumption is made about the approximate form of the function $F(u)$.

Summarizing, one can demonstrate that the solution to the problem of slit correction always leads to a single integral equation provided that all angular variables of the x-ray camera-slit system are small. The solution of this integral equation invariably leads to a solution of the Volterra equation of the second kind which has for its inhomogeneous part a constant term, and whose kernel involves an integrated expression of the derivative of the experimentally determinable slit correction function.

At the present time a computer program for the numerical solution of the eqs (10–12) is being developed.

2.2. Derivation of Equations (10–12)

In Abel's integral equation, the kernel $K(x, y)$ is of the form $\frac{1}{(x-y)^\alpha}$, with $0<\alpha<1$ and $x>y$. For $\alpha=1/2$, the singularity of the kernel is removed by multiplication of both sides of the integral equation by $\frac{dx}{(u-x)^{1/2}}$ and integrating with respect to x. This is done to make use of the fact that

$$\int_y^u \frac{dx}{[(x-y)(u-x)]^{1/2}}=\pi. \tag{13}$$

With $W[(y^2-x^2)^{1/2}]=K(x, y)$, eq (6) is written in

230-736 O-66—2

Abelian form:

$$\tilde{I}(x)=2\int_x^\infty \frac{yI(y)K(x,\,y)}{(y^2-x^2)^{1/2}}\,dy. \tag{14}$$

For this particular equation, the transformation which removes the singularity is based not on eq (13), but on an equivalent form: Use is made of the fact, that

$$\int_u^y \frac{x\,dx}{[(y^2-x^2)(x^2-u^2)]^{1/2}}=\frac{\pi}{2}, \tag{15}$$

since eq (15) can be shown to reduce to eq (13). We therefore multiply both sides of eq (14) by

$$\frac{xdx}{(x^2-u^2)^{1/2}}$$

and integrate over x from u to ∞, obtaining

$$\int_u^\infty \frac{x\tilde{I}(x)dx}{(x^2-u^2)^{1/2}}=2\int_u^\infty\int_x^\infty \frac{xyI(y)W[(y^2-x^2)^{1/2}dydx}{[(y^2-x^2)\,(x^2-u^2)]^{1/2}}$$

$$=2\int_u^\infty yI(y)K_1(u,\,y)dy, \tag{16}$$

with

$$K_1(u,\,y)=\int_u^y \frac{xW[y^2-x^2)^{1/2}]dx}{[(x^2-u^2)\,(y^2-x^2)]^{1/2}}. \tag{17}$$

In obtaining eq (16) and (17), the order of integration was exchanged using the following Dirichlet formula:

$$\int_u^\infty dx\int_x^\infty G(y,\,x)dy=\int_u^\infty dy\int_u^y G(y,\,x)dx. \tag{18}$$

The implicit solution (eq (10–10a)) is obtained from (16) and (17) in a straightforward way: we replace y^2-x^2 by t^2. The kernel (17) simplifies to

$$K_1(u,\,y)=\int_0^{(y^2-u^2)^{1/2}} \frac{W(t)dt}{(y^2-u^2-t^2)^{1/2}}, \tag{19}$$

and eq (10–10a) follow directly. To obtain the explicit solution of eq (14), we multiply the integrands of both sides of eq (16) by $F[(x^2-u^2)^{1/2}]$. $F(z)$ is an unknown function to be determined subsequently. In the right-hand side of eq (16) $K_2(u,\,y)$ replaces $K_1(u,\,v)$ and is given by eq (20):

$$K_2(u,\,y)=\int_u^y \frac{xF[(x^2-u^2)^{1/2}]W[(y^2-x^2)^{1/2}]dx}{[(y^2-x^2)(x^2-u^2)]^{1/2}}. \tag{20}$$

Both sides of the resulting eq (16) are now differentiated with respect to u:

$$\frac{d}{du}\int_u^\infty \frac{x\tilde{I}(x)F[(x^2-u^2)^{1/2}]}{(x^2-u^2)^{1/2}}\,dx$$

$$=-2uI(u)K_2(u,\,u)+2\int_u^\infty yI(y)\frac{dK_2(u,\,y)}{du}\,dy. \tag{21}$$

We need a function $F(z)$, $(z^2=x^2-u^2)$, which leads to $K_2(u,\,y)=\lambda$, independent of u and y. If $K_1(x,\,y)$ is constant, $F(z)$ then would be a constant also, equal to $2/\pi$. We would then have an Abel-related integral quation with a well-known solution for $I(x)$. With $K_2(u,\,y)=\lambda$, the solution of eq (21) is readily obtained:

$$I(u)=-\frac{1}{2u\lambda}\frac{d}{du}\int_0^\infty \tilde{I}[(z^2+u^2)^{1/2}]F(z)dz, \tag{22}$$

or

$$I(u)=-\frac{1}{2\lambda}\int_0^\infty \frac{\tilde{I}[(z^2+u^2)^{1/2}]}{(z^2+u^2)^{1/2}}F(z)dz. \tag{23}$$

Equation (23) was obtained by Kratky, Porod, and Kahovec [6], using a different method of derivation.

At first glance, the difficulty we encountered in solving the original integral eq (14), which is brought on by the singularity of its kernel, does not seem to be removed. The integral equation for the new function $F(z)$ still possesses a similar singularity. However, the integral equation for $F(z)$ (eq (20)) is considerably simpler than the original integral equation for $I(x)$ if $K_2(u,\,y)=$ constant. The same procedures which were used to remove the singularity in the kernel of eq (14) lead to a straight-forward solution for $F(z)$ by reducing it to a Volterra-type equation of the second kind. Equation (20) is rewritten as

$$\int_0^{(y^2-u^2)^{1/2}} \frac{F(z)W[(y^2-u^2-z^2)^{1/2}]}{(y^2-u^2-z^2)^{1/2}}\,dz=\lambda,$$

or

$$\int_0^s \frac{F(z)W[(s^2-z^2)^{1/2}]}{(s^2-z^2)^{1/2}}\,dz=\lambda, \tag{24}$$

with $s^2=y^2-u^2$.

Both sides of eq (24) are then multiplied by $s(u^2-s^2)^{-1/2}$ and integrated over s from o to u. The following equation is obtained:

$$\int_0^u\int_0^s \frac{sF(z)W[(s^2-z^2)^{1/2}]dzds}{[(s^2-z^2)(u^2-s^2)]^{1/2}}=\lambda\int_0^u \frac{sds}{(u^2-s^2)^{1/2}}=\lambda u. \tag{25}$$

We again interchange the order of integration in the l.h.s of eq (25), using the Dirichlet formula to obtain

$$\int_0^u F(z)dz\int_z^u \frac{sW[(s^2-z^2)^{1/2}ds}{[(s^2-z^2)(u^2-s^2)]^{1/2}}=\lambda u. \tag{26}$$

Next we subtract and add $W(z=s)=W(0)$ and integrate eq (26) to obtain

$$\frac{\pi}{2}W(0)\int_0^u F(z)dz-\int_0^u F(z)M(u,\,z)dz=\lambda u, \tag{27}$$

$$M(u,\,z)=\int_z^u \frac{s\{W(0)-W[(s^2-z^2)^{1/2}]\}}{[(s^2-z^2)(u^2-s^2)]^{1/2}}\,ds. \tag{27a}$$

After differentiating (27) with respect to u we obtain the following Volterra-type equation of the second kind

$$F(u)=\frac{2\lambda}{\pi W(0)}+\frac{2}{\pi W(0)}\int_0^u \frac{dM(u,z)}{du}F(z)dz, \qquad (28)$$

since $M(u, u)=0$.

Equation (28) can also be further simplified. If we set $W(0)=1$ and $\lambda=\pi/2$, then

$$F(u)=1+\frac{2}{\pi}\int_0^u \frac{dM(u,z)}{du}F(z)dz. \qquad (29)$$

Equation (27a) is integrated by parts,

$$M(u,z)=\frac{\pi}{2}[1-W[(u^2-z^2)^{1/2}] + \int_z^u \frac{sW'[s^2-z^2)^{1/2}]}{(s^2-z^2)^{1/2}}\cdot \sin^{-1}\left[\left(\frac{s^2-z^2}{u^2-z^2}\right)^{1/2}\right]ds.$$

Therefore,

$$\frac{dM(u,z)}{du}=-\frac{u}{(u^2-z^2)}\int_z^u \frac{sW'[(s^2-z^2)^{1/2}]}{[(u^2-s^2)]^{1/2}}ds. \qquad (30)$$

Integral eq (29) assumes the following form

$$F(u)=1-\frac{2}{\pi}\int_0^u F(z)K(u,z)dz, \qquad (31)$$

with

$$K(u,z)=\frac{u}{(u^2-z^2)}\int_0^{(u^2-z^2)^{1/2}}\frac{yW'(y)dy}{[(u^2-z^2-y^2)]^{1/2}}. \qquad (32)$$

The kernel of eq (31) is finite for all values of z, including $z=u$.

Equations (12–12a) follow directly by exchanging variables, u being replaced by y.

3. References

[1] C. G. Shull and L. C. Roess, J. Appl. Phys. **18,** 295 (1947).
[2] P. Schmidt (private communication).
[3] A. Guinier and G. Fournet, J. Phys. Radium **8,** 345 (1947a).
[4] A. Guinier and G. Fournet, Nature, London **160,** 504 (1947b).
[5] J. Du Mond, Phys. Rev. **72,** 83 (1947).
[6] O. Kratky, G. Porod, and L. Kahovec, Z. Electrochem. **58,** 49 (1951).
[7] V. Gerold, Acta Cryst. **10,** 287 (1957).
[8] Beeman, Kaesberg, Anderegg, and Webb, Handbuch Der Physik **XXXII,** 321 (1957).
[9] O. Kratky, G. Porod, Z. Skala, Acta Phys. Austriaca **13,** 76

(Paper 70A6–419)

JOURNAL OF RESEARCH of the National Bureau of Standards—A. Physics and Chemistry
Vol. 70A, No. 6, November–December 1966

High–Temperature Reactions of Hexafluorobenzene

Joseph M. Antonucci and Leo A. Wall

Institute for Materials Research, National Bureau of Standards, Washington, D.C., 20234

(July 19, 1966)

The direct replacement of aromatic fluorine in hexafluorobenzene has hitherto been possible only by the use of nucleophilic reagents. In this investigation, the replacement of nuclear fluorine by nonnucleophilic, or weakly nucleophilic, reagents was achieved by reaction at relatively high temperatures, 300 to 850 °C. For example, the reaction of hexafluorobenzene with such reagents as bromine, chlorine, and tetrafluoroethylene gave as major products bromopentafluorobenzene, chloropentafluorobenzene, and octafluorotoluene. In addition, pentafluorohalobenzenes can also be produced by passage of hexafluorobenzene over the appropriate alkali or alkaline earth-metal halides at elevated temperatures.

The mechanism of the pyrolytic reactions of hexafluorobenzene and the nonionic coreactants are considered to involve free-radical intermediates. The reaction of hexafluorobenzene with the ionic coreactants may proceed by an ionic mechanism similar to that advanced for the usual, relatively low-temperature, nucleophilic substitution reactions of aromatic systems. However, a more complicated free radical-ionic process cannot be ruled out for these reactions.

Key Words: Direct replacement, high temperature, mechanisms, nonionic or ionic coreactants, nuclear fluorine, pentafluorohalobenzenes.

1. Introduction

Aromatic hydrocarbons can undergo substitution or displacement reactions by attack of an electrophilic, nucleophilic, or free-radical species. The most common aromatic substitution reactions, however, involve the attack of an electrophilic reagent on the aromatic ring, e.g., nitration, sulfonation, halogenation, and the Friedel–Crafts reaction.

In contradistinction to this behavior, the principal mode of aromatic substitution in hexafluorobenzene is by attack of a nucleophilic reagent. In fact, with few exceptions [1–6],[1] all of the reactions of hexafluorobenzene that have been reported in the literature may be classed as bimolecular, nucleophilic, substitution reactions [3, 7–15]. The feature common to all these reactions is the displacement of one or more of the ring fluorines as the fluoride ion, by a nucleophile of sufficient strength. The general reaction is indicated by the following equation,

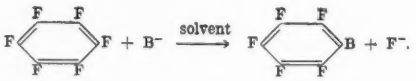

B^- represents the nucleophilic reagent, which may be (1) an anionic base, such as potassium hydroxide, sodium hydrogen sulfide, sodium amide, sodium ethoxide, etc., (2) a carbanionic base, such as various Grignard reagents and organolithium reagents, or (3) an uncharged base such as ammonia, primary and secondary amines, hydrazine, etc. In general, these nucleophilic reactions are usually conducted in solvents and at moderate temperatures, usually well below 300 °C.

Although hexafluorobenzene undergoes nucleophilic attack with comparative ease, the molecule appears to be quite inert to electrophilic attack [1, 2]. Obviously, the highly unfavorable energetics involved in the expulsion of a nuclear fluorine atom as the fluorine cation, F^+, would make such electrophilic reactions as halogenation, sulfonation, nitration, and the Friedel–Crafts reaction rather difficult, if not totally impossible.

Thus, the very nature of the electronic structure of hexafluorobenzene would appear to preclude, for this aromatic molecule, the usual electrophilic reactions that are associated with aromatic hydrocarbons.

Hexafluorobenzene, however, is susceptible to free-radical attack. The few nonnucleophilic reactions of this molecule that have been reported have indeed involved this type of attack. For example, hexafluorobenzene adds chlorine quite readily under rather mild conditions to give hexachlorohexafluorocyclohexane [1–3]. The catalytic reduction of hexafluorobenzene with hydrogen to penta- and tetra-fluorobenzene at 300 °C, using a platinum catalyst, probably proceeds by a free-radical mechanism [4]. Although the addition of chlorine to hexafluorobenzene is an example of a free-radical addition reaction, the reduction of hexafluorobenzene with hydrogen is classified as a free-radical substitution reaction.

[1] Figures in brackets indicate the literature references at the end of this paper.

One of the earliest and, perhaps, most complicated reactions of hexafluorobenzene is one reported by Desirant [1, 2]. This interesting reaction, which is the only example of a high-temperature (above 300 °C) reaction of hexafluorobenzene reported to date, involves the pyrolysis of the molecule in a platinum reactor at 850 °C. Among the many products produced in this reaction, octafluorotoluene and decafluorobiphenyl were identified. This highly complex reaction probably could also be classified, in some respects, as a free-radical substitution reaction.

There is also some less direct evidence that high-temperature reactions of hexafluorobenzene do occur. In the synthesis of hexafluorobenzene by the pyrolysis of tribromofluoromethane [1,2,9,16,17], bromopentafluorobenzene is a significant by-product. Lesser amounts of higher brominated fluorocarbons are formed as well, along with copious quantities of bromine. This rather complex reaction is illustrated below,

$$CFBr_3 \xrightarrow{630\text{–}640\ ^\circ C} C_6F_6 + Br_2$$

$$+ C_6F_5Br + C_6F_4Br_2 + \text{etc.}$$

Two similar mechanisms have been postulated for the formation of hexafluorobenzene [9,16,17], but none for the formation of the important by-product, bromopentafluorobenzene.

Since the pyrolysis of tribromofluoromethane could conceivably lead to the formation of bromofluorocarbene (>CBrF) and bromine, one possible mechanism for the formation of hexafluorobenzene is that involving the transient intermediate, > CBrF as shown below,

$$(1)\quad 2\ {>}CBrF \longrightarrow CBrF{=}CBrF$$
$$(2)\quad 3\ CBrF{=}CBrF \longrightarrow C_6Br_6F_6$$
$$(3)\quad C_6Br_6F_6 \longrightarrow C_6F_6 + 3\ Br_2$$

A second possible mechanism that has been postulated would involve the formation of difluoroacetylene ($CF \equiv CF$) and its subsequent cyclic trimerization to hexafluorobenzene [7,9].

The latter mechanism, since it does not involve any precursors that contain bromine, cannot account for the direct formation of any of the brominated derivatives of hexafluorobenzene. The former mechanism, although it does involve bromine-containing precursors, can only explain the formation of such products as bromopentafluorobenzene if debromofluorination (loss of BrF) can occur to some extent along with the energetically more favored process of debromination (loss of Br_2). It is conceivable that this situation may exist in a particular stereoisomer of hexabromohexafluorocyclohexane ($C_6Br_6F_6$) that has a conformation that permits the loss of BrF to occur. Since the yield of bromopentafluorobenzene is small compared to that of hexafluorobenzene, it would seem that, if the transient intermediate ($C_6Br_6F_6$) does exist, it exists primarily in stereoisomeric forms that favor the elimination of Br_2 rather than that of BrF, although the latter elimination could also occur if isomerization to a more favorable conformation developed during the debromination process. Two other possible transient intermediates that could also account for the formation of bromopentafluorobenzene are $C_6Br_2F_6$ and $C_6Br_4F_6$. The foregoing argument assumes, of course, that dehalogenation can only occur by means of a *cis*-elimination mechanism.

Also, it is conceivable that bromopentafluorobenzene and similar by-products might arise from secondary reactions of bromine with the newly formed hexafluorobenzene by a mechanism such as that shown,

$$C_6F_6 + Br_2 \rightarrow C_6F_5Br + BrF, \text{ etc.}$$

In the light of the early work of Desirant [1,2], which indicated that hexafluorobenzene does undergo high-temperature reactions without benefit of a coreagent, it would appear feasible that a reaction between hexafluorobenzene and such a coreagent as bromine could take place at the elevated temperatures employed in the pyrolysis of tribromofluoromethane.

2. High-Temperature Reactions of Hexafluorobenzene

2.1. Reaction With Halogens

a. Bromine

In order to test the possibility that hexafluorobenzene can undergo a free-radical substitution reaction with bromine at elevated temperatures, both these reagents were simultaneously passed through a heated reactor tube under various conditions. The reactor tube was usually made of high-silicate glass and packed with borosilicate glass helices. Other reactor tubes employed were platinum, steel, and quartz. In addition to borosilicate glass helices, other packing material included glass wool, carbon pellets, platinum gauze, and nickel turnings. A few experiments involving unpacked reactors were also tried. The results in all these cases were similar.

The examination of the pyrolyzates from several runs revealed the presence of significant amounts of bromopentafluorobenzene. In some cases, smaller amounts of polybromo derivatives of hexafluorobenzene were also noted. The conversion of hexafluorobenzene into products ranged from a few percent to about 25 percent. The yield of bromopentafluorobenzene, based on unrecovered hexafluorobenzene, was 85 to 95 percent. The yield of bromopentafluorobenzene, as expected, is dependent on such variables as (1) the temperature of the reactor, (2) the molar ratio of the reactants, (3) the contact time in the heated zone, and (4) the packing material and reactor material. The nature of the products is also dependent on the conditions of the reaction. For example, hexafluorobenzene and bromine, in the molar ratio of 1 to 3, when passed through a reactor packed with

borosilicate glass helices, gave at 650 °C an 8 percent conversion into bromopentafluorobenzene (95% yield). However, at 740 °C and with the other variables approximately the same, the conversion into products was increased to 25 percent. Although bromopentafluorobenzene was still the major product (85% yield), other more highly brominated products began to appear. The yield of these products was about 10 percent, and the main constituent appeared to be, from an examination of its retention time on the vapor-phase chromatogram, one of the isomers of dibromotetrafluorobenzene.

b. Chlorine

The successful replacement of one or more nuclear fluorines in hexafluorobenzene by bromine suggested that other high-temperature substitution reactions might be feasible with similar coreactants. The copyrolysis of chlorine or sulfuryl chloride and hexafluorobenzene at 700 °C gave good conversions into products. Again, the monosubstituted product, in this case chloropentafluorobenzene, was formed in high yield (80 to 85%). The conversion of hexafluorobenzene into products (primarily chloropentafluorobenzene) was even higher in this case than in the bromination reaction. However, as in the bromination reaction, chlorination of hexafluorobenzene at high temperatures gave also some polyhalogenated products which have not yet been characterized (except to note that, from its retention time on the vapor-phase chromatogram, the major constituent of these products appears to be an isomer of dichlorotetrafluorobenzene).

c. Iodine

The copyrolysis of iodine and hexafluorobenzene gave rather low conversions into products. The low conversion, perhaps, may have resulted from the experimental difficulties encountered in the simultaneous addition of the two reagents. However, the yield of pentafluoroiodobenzene based on unrecovered hexafluorobenzene was excellent (90%). No evidence of more highly iodinated products was found, although this may be attributable to the very low conversion into products.

2.2. Reaction With Water and Ammonia

Similarly, water and ammonia gave only trace amounts of the corresponding pentafluorophenyl derivatives, pentafluorophenol and pentafluoroaniline, on copyrolysis with hexafluorobenzene. However, it may be possible to increase these low conversions by modifications of certain of the conditions of the copyrolysis reaction.

The results of the above reactions are shown in table 1.

TABLE 1. *Inorganic coreactants*
High-temperature reactions of hexafluorobenzene/copyrolysis over glass helices.

Reactant	Temp	Products	Conversion into products	Yield of major mono derivative
	°C		%	%
Br_2	650	C_6F_5Br	8	94, 95
	740	C_6F_5Br $C_6F_4Br_2$ (?)	25–30	85–90
Cl_2	700	C_6F_5Cl $C_6F_4Cl_2$ (?) etc.	50	85
SO_2Cl_2	700	C_6F_5Cl, $C_6F_4Cl_2$, etc.	75	80
I_2	650	C_6F_5I	< 5	90
H_2O	700	C_6F_5OH C_6F_5H	< 5	90
NH_3	650	$C_6F_5NH_2$	< 5	90

2.3. Reaction With Fluorohaloalkanes

Fluorohaloalkanes can undergo an analogous high-temperature reaction with hexafluorobenzene. As before, the pentafluorohalobenzene was the major product. In these reactions, the fluorohaloalkanes serve as the source of reactive halogen species. For example, bromopentafluorobenzene was obtained in excellent yield and fair to good conversions by the copyrolysis of hexafluorobenzene and such bromofluoroalkanes as 1,2-dibromotetrafluoroethane, dibromodifluoromethane, and tribromofluoromethane. The last compound gave the best conversion into bromopentafluorobenzene. In addition to bromopentafluorobenzene, the first two bromofluoroalkanes also gave lesser, though significant, amounts of octafluorotoluene. Trace quantities of what appeared to be dibromo derivatives of hexafluorobenzene were also present in the product mixtures.

Higher conversions of hexafluorobenzene into octafluorotoluene were obtained when trifluoroiodomethane was the coreactant (table 2). In this case, the pentafluorohalobenzene (pentafluoroiodobenzene) was the minor product.

These results are summarized in table 2.

TABLE 2. *Coreactant fluorohaloalkanes*

Reactant	Temp	Products	Conv. into products	Yield of major mono derivative
	°C		%	%
$CFBr_3$	680	C_6F_5Br (major) (?) $C_6F_4Br_2$ (minor)	50	90
CF_2Br_2	680	C_6F_5Br (major) $C_6F_5CF_3$ (minor) (?) $C_6F_4Br_2$ (trace)	35	90
CF_2BrCF_2Br	670	C_6F_5Br (major) $C_6F_5CF_3$ (minor) (?) $C_6F_4Br_2$ (trace)	30	85
CF_3I	700	$C_6F_5CF_3$ (major) C_6F_5I (minor)	10	90
	760	same products. $C_6F_5CF_3$ (major)	20	85

2.4. Reaction With Fluorohaloalkenes

Early attempts to synthesize octafluorostyrene by copyrolysis of hexafluorobenzene with chlorotrifluoroethylene or bromotrifluoroethylene gave little if any of the desired olefin. However, the corresponding pentafluorohalobenzene was formed in fair conversions and excellent yields. Smaller amounts of higher-boiling products were also produced in these pyrolyses, but have not been further characterized.

The results are shown in table 3.

TABLE 3. *Coreactant fluoroolefins*

Reactant	Temp	Products	Conversion into products	Yield of major mono derivative
	°C		%	%
CF_2=CFCl	670	C_6F_5Cl, etc.	30	80–85
CF_2=CFBr	690	C_6F_5Br, etc.	20	80–85
CF_2=CF_2	850	$C_6F_5CF_3$	20	90–95
CF_3CF=CF_2	800	$C_6F_5CF_3$	15	90–95

2.5. Reaction With Perfluoroalkenes

The copyrolysis of hexafluorobenzene with perfluoroolefins, such as tetrafluoroethylene and hexafluoropropylene, resulted in excellent yields of octafluorotoluene. The conversion into products was of the order of 15 to 20 percent at temperatures of 800 to 850 °C (table 3).

2.6. Reaction With Inorganic Salts

A related study was made of the behavior of hexafluorobenzene at high temperatures with certain inorganic salts. The technique employed in these reactions usually involved the passage of hexafluorobenzene under a stream of nitrogen through a fused silica tube filled throughout the heated zone with carbon pellets which had been impregnated with the appropriate inorganic salt. The results are shown in table 4.

TABLE 4. *Pyrolysis of C_6F_6 in contact with inorganic salt sorbed by carbon pellets*

Tube packing	Temp	Products and approximate yield	Conversion
	°C		%
KOH/carbon	500	C_6F_5OH (40%), C_6F_5H (40%)	10
LiI/carbon	570	C_6F_5I (20%), C_6F_5H (40%)	30
KI/carbon	500	C_6F_5I (40%), C_6F_5H (40%)	15
KBr/carbon	600	C_6F_5Br (60%), C_6F_5H (30%)	20
KCN/carbon	570	C_6F_5CN (70%), C_6F_5H (20%)	5
$CaCl_2$ (4 mesh)[a]	700	C_6F_5Cl (90%)	10

[a] Without carbon pellets.

The substitution of chlorine, bromine, or iodine in aromatic compounds by fluorine by means of alkali fluorides, such as potassium fluoride, is a well-known process [18–22]. The reverse process, the replacement of a nuclear fluorine atom by a less electronegative halogen atom by means of its alkali or alkaline earth salt, has not yet been reported. However, as shown in table 4, it is indeed possible to replace at least one of the fluorines of hexafluorobenzene by a less electronegative halogen by reaction of this organic compound with an alkali or alkaline earth salt at elevated temperatures. For example, hexafluorobenzene and lithium iodide impregnated on carbon pellets gave, at 570 °C, a 20 percent yield of pentafluoroiodobenzene along with a 40 percent yield of pentafluorobenzene. The conversion into products was 30 percent. A fair quantity of free iodine was also produced, but only a small quantity of higher-boiling (above 162 °C) products. The other salts impregnated on carbon pellets gave similar results with hexafluorobenzene. The principal products were the expected monosubstituted derivatives and pentafluorobenzene. The origin of the pentafluorobenzene is at present unknown. Conceivably, it may arise from the decomposition of the initially formed, monosubstituted derivative in the presence of some hydrogen source. Direct hydrogenolysis of the hexafluorobenzene is also possible. The formation of pentafluorobenzene apparently requires the use of carbon pellets. The impregnated pellets were usually formed by evaporation of an aqueous solution of the salt in the presence of the carbon pellets. The impregnated pellets were dried in the reactor at about 500 °C until no more water could be detected in the trapping system. The reactor was then heated to the appropriate reaction-temperature and the traps were checked again for the presence of any moisture. Unless some water remained tightly occluded to the impregnated pellets, it would not seem to be the source of hydrogen for the hydrogenation reaction. Nonvolatile, hydrogen-containing impurities in the carbon pellets are another possible source of hydrogen.

In one experiment, the carbon pellets were omitted and only the inorganic salt, calcium chloride ($CaCl_2$), was employed as the packing material. The passage of hexafluorobenzene over anhydrous calcium chloride (4 mesh) heated to 700 °C gave a 10 percent conversion into products. The major product (90%) was the expected chloropentafluorobenzene. A small amount of higher-boiling material (polychloro derivatives of hexafluorobenzene) was also present. However, no trace of pentafluorobenzene was observed in the products of this pyrolysis. The results of these experiments are summarized in table 4.

3. Discussion

As previously indicated, earlier work seemed to suggest that the displacement of nuclear fluorine in polyfluoro aromatics could be achieved only by reaction with certain basic nucleophiles. However, recent work in these and other laboratories [4–6] has shown that homolytic substitution reactions are indeed possible with hexafluorobenzene. The results of the present study clearly demonstrate that the replacement

of nuclear fluorine can also be accomplished by the reaction of hexafluorobenzene with nonnucleophilic or weakly nucleophilic reagents at elevated temperatures.

The excellent thermal stability of hexafluorobenzene [1, 2, 23–25] lends itself quite well to high-temperature reactions where extensive decomposition and carbonization are common problems in the pyrolytic reactions of many organic compounds.

Other polyfluoro aromatic compounds can also be used in these high-temperature substitution reactions. However, some modifications of the reaction conditions may be necessary, depending on the nature of the polyfluoro aromatic compound employed. For example, a recent experiment involving the high-temperature bromination of pentafluorobenzene demonstrated that it is possible, by lowering the reaction temperature, to replace selectively the nuclear hydrogen rather than a nuclear fluorine. Thus, at 500 to 550 °C, the nuclear hydrogen only was displaced by bromine, whereas, at 650 to 700 °C, the bromination was less selective and fluorine was displaced as well.

Another important factor to be considered is the thermal stability of the polyfluoro aromatic compound. If it is thermally less stable than hexafluorobenzene, this fact must be considered in the copyrolysis reaction. In this connection, it would seem important to consider also the relative thermal stability of the expected product or products of the pyrolytic reaction. If the product breaks down at the temperature of reaction, it may be necessary to work at either lower temperatures or at shorter contact times, or both. In summary, it would appear that the several variables involved in these high-temperature reactions of polyfluoro aromatic compounds, such as the types of reactor tube, its dimensions, the packing material, the relative concentration of the reactants, the contact time, etc., should all be evaluated in order to optimize the yield of the desired product.

4. Mechanism of the High-Temperature Substitution Reactions

4.1. Free-Radical Substitution Mechanisms

The copyrolysis experiments on hexafluorobenzene with such reactants as bromine, chlorine, dibromodifluoromethane, or trifluoroiodomethane probably proceed by a free-radical mechanism. Several mechanisms for the halogenation type of reaction can be postulated.

One possible mechanism is similar to that postulated for the high-temperature vapor-phase halogenation of benzene [26–28]. This mechanism is analogous to that of most free-radical, aliphatic, substitution reactions and involves such chain-propagating steps as the following:

$$(1)\ X\cdot + C_6H_6 \longrightarrow C_6H_5\cdot + HX$$
$$(2)\ C_6H_5\cdot + X_2 \longrightarrow C_6H_5X + X\cdot$$

X = Br, Cl, etc.

Applied to the high-temperature reactions of hexafluorobenzene, this mechanism becomes:

$$(1)\ X\cdot + C_6F_6 \longrightarrow C_6F_5\cdot + XF$$
$$(2)\ C_6F_5\cdot + X_2 \longrightarrow C_6F_5X + X\cdot$$

X = H, Cl, Br, I, or CF_3.

Another possible mechanism involves the addition of the radical species, $X\cdot$, to hexafluorobenzene to give the intermediate cyclohexadienyl radical (I), which then can give the monosubstitution product by displacement of fluorine (probably as XF). This mechanism can be represented as shown below:

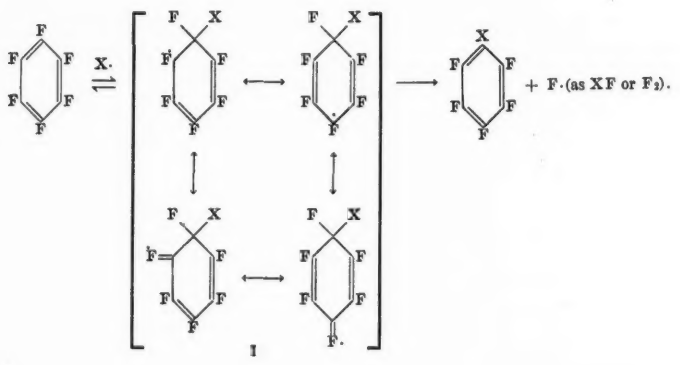

I

A third possible mechanism, somewhat similar to the preceding one, is represented by the sequence of reactions shown below:

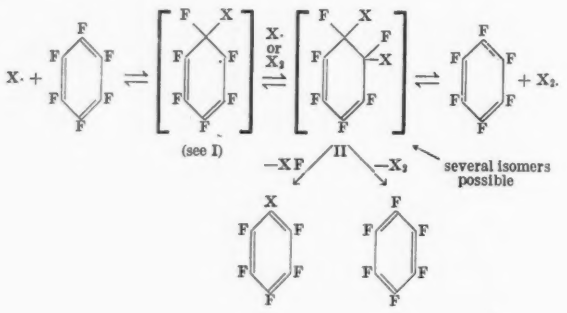

Unlike the preceding mechanism, the intermediate (II) in this case is not a cyclohexadienyl radical, but an unstable cyclohexadiene which can undergo elimination of *X*F. The intermediate cyclohexadiene can be formed either in two steps from hexafluorobenzene by successive addition of the radical species *X* or in one step by a simultaneous addition of the elements of X_2 across vinylic positions of the aromatic ring. Aromatization of the unstable cyclohexadiene intermediate can then proceed by loss of either *X*F or X_2 to give the desired monosubstituted pentafluorobenzene or the starting material, hexafluorobenzene. Presumably, the loss of *X*F can take place, as well as the energetically more favored loss of X_2, if it is assumed that a *cis*-elimination process is necessary, or at least favored, in dehalogenation. Then, the *trans* isomer of the cyclohexadiene intermediate (II) should lead to the formation of the monosubstituted pentafluorobenzene by loss of *X*F. Conversely, the *cis* isomer of the cyclohexadiene intermediate (II) should revert to hexafluorobenzene by loss of X_2. The formation of disubstituted derivatives can occur either by a similar, secondary reaction involving the primary product, or, perhaps, from hexafluorobenzene by the transient formation of the correct stereoisomer of a cyclohexene derivative. As an extension of this mechanism, it could also be argued that, in the high-temperature halogenation reactions, the transient intermediates may be certain stereoisomers of the hexafluorohexahalocyclohexane that could, by *cis* elimination, lead to the observed products.

4.2. Difluoromethylene Mechanism for the Formation of Octafluorotoluene

In the copyrolysis of hexafluorobenzene with such coreactants as dibromodifluoromethane, tetrafluoroethylene, and hexafluoropropylene, octafluorotoluene is one of the principal products. The formation of this compound can be explained by a "net insertion" mechanism [29] involving the reactive species, difluoromethylene. Several mechanistic paths are possible for this type of reaction, as shown below:

Disproportionation-Combination

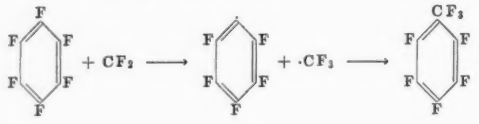

Addition-Rearrangement

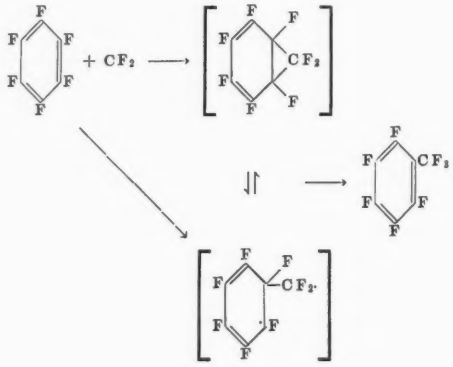

Net insertion reactions of difluoromethylene have previously been reported involving insertion into P—F, N—F, and C—F bonds [29–31]. The few reported insertion reactions of difluoromethylene into CF bonds all seem to involve a vinylic C—F bond [30], such as is demonstrated by the following reaction:

$$CF_2 + CF_2{=}CF_2 \rightarrow CF_3CF{=}CF_2.$$

Insertion reactions at other than vinylic sites have thus far not been observed for difluoromethylene and fluorocarbons. The exclusive reaction of difluoromethylene with a vinylic C—F bond seems to be borne out by the following reaction, in which only perfluoroisobutylene is formed [30],

$$CF_2 + CF_3CF{=}CF_2 \rightarrow (CF_3)_2C{=}CF_2.$$

It is not unexpected, therefore, that hexafluorobenzene would undergo an analogous reaction with difluoromethylene.

4.3. Mechanism of High-Temperature Reaction of Hexafluorobenzene With Inorganic Salts

The reaction of hexafluorobenzene with certain inorganic, ionic compounds, sorbed by carbon pellets, may follow the usual ionic mechanism for nucleophilic attack on hexafluorobenzene [15]. On the other hand, the mechanism may be more complex, and may actually involve some free-radical process as well. The

same may be said for the reaction of hexafluorobenzene with calcium chloride. Whether the elevated temperature of these reactions permit what are normally weak nucleophiles to react with hexafluorobenzene by a nucleophilic path, or whether a more complicated mechanism is, indeed, involved, remains to be determined. Continued study along these lines is planned in order to elucidate further the nature of these reactions.

5. Conclusion

Because of their high thermal stability, perfluoro aromatic compounds, such as hexafluorobenzene, can undergo many reactions at high temperatures without danger of excessive substitution or destruction of the aromatic nucleus. In this respect, they offer definite advantages over analogous aromatic hydrocarbons in the field of high-temperature chemistry. Furthermore, it appears that perfluoro aromatic compounds differ significantly from perfluoro aliphatic conpounds in their chemical behavior at high temperatures. For example, the reaction of perfluoroalkanes with such reactants as bromine and chlorine results in cleavage of the carbon–carbon bond rather than the carbon–fluorine bond of the fluorocarbon [32]. With hexaflurorbenzene, however, cleavage of the carbon–fluorine bond predominates over cleavage of the carbon–carbon bond.

Of special theoretical interest are the results obtained from the high-temperature reactions of bromine and tribromofluoromethane, respectively, with hexafluorobenzene. From these results, a plausible case can be made for the formation of bromopentafluorobenzene in the pyrolysis of tribromofluoromethane by a secondary reaction of the initially formed hexafluorobenzene with bromine radicals or some type of bromine-containing species.

In addition to their theoretical interest, these high-temperature reactions are of great potential value in that they provide a direct method for the synthesis of pentafluorohalobenzenes and other similar derivatives from hexafluorobenzene in one step, a process not previously known.

6. Experimental Procedure

6.1. Apparatus and Method

The reactor used in this study was a fused silica tube, 54 cm by 2 cm (ID), equipped with a 24/40 standard-taper joint at each end. The tube was placed in the vertical position in an electric furnace, and the lower end was connected to three traps in series cooled by a solid carbon dioxide-acetone slurry. The last trap carried a drying tube filled with anhydrous calcium sulfate. The upper end of the tube was equipped with one or two pressure-equalizing dropping funnels carrying a gas inlet-tube. The pyrolysis temperature was ascertained by an iron-constantan thermocouple fastened at one end to the outside of the reactor tube, midway in the heated zone (about 25 cm), and connected at the other end to a pyrometer. In the copyrolysis experiments, the fused silica tube was packed throughout the heated zone with borosilicate glass helices (⅛ in). In the high-temperature reactions with inorganic salts, the reactor tube was packed throughout the heated zone with activated carbon pellets (4 to 6 mesh), which had been impregnated with the appropriate inorganic salt. The ratio of inorganic salt to carbon pellets was usually 1 to 1 by weight. The impregnated pellets were dried prior to use by gradually preheating the reactor for about 24 hr until the desired reaction-temperature was attained. All the pyrolytic reactions of hexafluorobenzene were performed under a slow stream of nitrogen gas at approximately atmospheric pressure.

In the copyrolysis experiments, the following techniques were employed:

(1) For reactants miscible with hexafluorobenzene, a solution of known concentration was added at a low drop-rate (approximately 1 per 10 sec) to the reactor by means of a pressure-equalizing dropping funnel.

(2) Gaseous reactants, such as chlorine, were allowed to distil slowly into the reactor through a gas inlet-tube, the end of which was immersed in the hexafluorobenzene contained in the dropping funnel. The hexafluorobenzene was added dropwise, or by codistillation with the gaseous reactant.

(3) For reactants that were not completely miscible with hexafluorobenzene (e.g., bromine), it was necessary to employ two pressure-equalizing dropping funnels, connected in parallel and attached to the reactor by means of a Y-adapter. The drop-rate for each reactant was adjusted accordingly, so that the two reactants were always present in the reactor in low concentration.

In the experiments involving inorganic salts as the coreactant, the hexafluorobenzene was simply added at a certain drop-rate (approximately 1 drop per 15 or 20 sec) to the reactor via the dropping funnel. An alternative technique was to distil the hexafluorobenzene slowly through the reactor, either at atmospheric or reduced pressure.

The pyrolyzates from the various runs were processed by the usual techniques, such as washing to remove corrosive materials, drying, and distillation. When separation of product by distillation was difficult or impractical, preparative vapor-phase chromatography was employed.

Since the major products from these reactions were known compounds, preliminary identification was made by comparison of physical properties. When the compound was available, comparison of vapor-phase chromatographic retention-times was used to establish identity. Mass-spectroscopic analysis was used to confirm the preliminary identification. Yields were usually calculated by vapor-phase chromatographic analysis of the washed and dried pyrolyzate.

6.2. Copyrolysis of Hexafluorobenzene and Bromine

Approximately 14.4 g (0.09 mole) of bromine and 5.5 g (0.03 mole) of hexafluorobenzene were copyrolyzed at 650 °C. The pyrolyzate, after removal of

unreacted bromine, weighed 5.7 g. Examination of the pyrolyzate revealed that two components were present. About 90 percent of the mixture was hexafluorobenzene; the other component accounted for the remaining 10 percent. The second component was shown to be bromopentafluorobenzene by comparison of retention times with that of an authentic sample. Isolation of the components, by preparative vapor-phase chromatography, using an 8-ft by $^3/_4$-in column packed with 40/60 mesh acid-washed chromosorb W, which was coated with 25 percent by weight of silicone elastomer, gave 5.1 g of recovered hexafluorobenzene and 0.5 g of bromopentafluorobenzene. The identification of the second component was confirmed by mass-spectroscopic analysis (parent mass peak at 247) and by comparison of boiling points (bp 136 °C). The conversion into the bromo derivative was 8 percent and the yield was 94 percent.

The same experiment was repeated, but at 740 °C. Vapor-phase chromatographic analysis revealed that the conversion of hexafluorobenzene into bromopentafluorobenzene was increased about three-fold. Two other products (higher boiling) were also formed, in addition to the monobromobenzene, but they were present to the extent of only 5 to 10 percent. The conversion into products was about 25 to 30 percent, and the yield of bromopentafluorobenzene was 85 to 90 percent. The higher-boiling products have not yet been characterized.

6.3. Reaction of Hexafluorobenzene With Lithium Iodide

Approximately 11.0 g (0.44 mole) of hexafluorobenzene was dropped (4 drops/min) through the reactor, packed with carbon pellets which had been impregnated with lithium iodide (1 to 1 weight ratio). The reactor tube was kept at 570 °C, and the reaction was performed under a slow stream of nitrogen at atmospheric pressure. A fair quantity of free iodine formed on adding the hexafluorobenzene. The pyrolyzate, after removal of the iodine by washing with a saturated solution of sodium thiosulfate and drying, weighed 8.6 g. Vapor-phase chromatographic analysis revealed the presence of three components. The first component (90%) was hexafluorobenzene. After isolation the second component was shown by mass-spectroscopic analysis to be pentafluorobenzene. Similarly, the third component was identified as pentafluoroiodobenzene. A very small amount of a higher-boiling component was also isolated, but this has not yet been characterized. The conversion into products, based on unrecovered hexafluorobenzene, was 30 percent (7.8 g of hexafluorobenzene was recovered). The yield of the iodo derivative was about 20 percent, and that of pentafluorobenzene was about 40 percent.

7. References

[1] Y. Desirant, Bull. Acad, Roy, Belg. Classe Sci. **41,** [5], 759 (1955).
[2] Y. Desirant, Bull. Soc. Chim. Belg. **67,** 676 (1958).
[3] J. A. Godsell, M. Stacey, and J. C. Tatlow, Nature **178,** 199 (1956).
[4] R. E. Florin, W. J. Pummer, and L. A. Wall. J. Res. NBS **62,** 119 (1959) RP 2940.
[5] J. M. Antonucci and L. A. Wall, Abstracts Papers 145th Am. Chem. Soc. Meeting, **18M** (1963).
[6] P. A. Claret, J. Coulson, and G. H. Williams, Chem. Ind. (London) 228 (1965).
[7] W. J. Pummer and L. A. Wall, Science **127,** 643 (1958).
[8] E. J. Forbes, R. D. Richardson, and J. C. Tatlow, Chem. Ind. (London) 630 (1958).
[9] J. M. Birchall and R. N. Haszeldine, J. Chem. Soc. **13** (1959).
[10] E. J. Forbes, R. D. Richardson, M. Stacey, and J. C. Tatlow, ibid. 2019 (1959).
[11] G. M. Brooke, J. Burdon, M. Stacey, and J. C. Tatlow ibid. 1768 (1960).
[12] F. Robson, M. Stacey, R. Stephens, and J. C. Tatlow, ibid. 4754 (1960).
[13] A. K. Barbour, M. W. Buxton, P. L. Coe, R. Stephens, and J. C. Tatlow, ibid. 808 (1961).
[14] J. M. Birchall and R. N. Haszeldine, ibid. 3719 (1961).
[15] L. A. Wall, W. J. Pummer, J. E. Fearn, and J. M. Antonucci, J. Res. NBS **67A** (Phys. and Chem.) No. 5, 481 (1963).
[16] M. Hellman, E. Peters, W. J. Pummer, and L. A. Wall, J. Am. Chem. Soc. **79,** 5654 (1957).
[17] J. E. Fearn, R. E. Lowry, W. J. Pummer, and L. A. Wall, J. Res. NBS **65A** (Phys. and Chem.) No. 3, 167 (1959).
[18] G. C. Finger and C. W. Kruse, J. Am. Chem. Soc. **78,** 6034 (1956).
[19] G. C. Finger and L. D. Starr, ibid. **81,** 2674 (1959).
[20] N. N. Vorozhtsov, Jr., and G. G. Yakobson, Nauch. Dokl. Vyshei Shkoly Khim. i. Khim Technol. [1] 122 (1958).
[21] G. C. Finger, L. D. Starr, D. R. Dickerson, H. S. Gutowsky, and J. Hamer, J. Org. Chem. **28,** 1666 (1963).
[22] J. T. Maynard, ibid. **28,** 112 (1963).
[23] V. H. Dibeler, R. M. Reese, and F. L. Mohler, J. Chem. Phys. **26,** 304 (1957).
[24] R. E. Donadio, W. J. Pummer, and L. A. Wall, J. Am. Chem. Soc. **82,** 4846 (1960).
[25] P. L. Coe, C. R. Patrick, and J. C. Tatlow, Tetrahedron **9,** 240 (1960).
[26] O. C. Derner and M. T. Edmison, Chem. Rev. **57,** 77 (1957).
[27] G. H. Williams, Homolytic Aromatic Substitution (Pergamon Press, N.Y., 1960).
[28] E. S. Huyser and E. Bedard, J. Org. Chem. **29,** 1588 (1964).
[29] S. Andreades, Chem. Ind. (London) 782 (1962).
[30] B. Atkinson and V. A. Atkinson, J. Chem. Soc. 2086 (1957).
[31] W. Mohler, Preprints of the Second Intern. Symp. Fluorine Chem., Estes Park, Colorado, July 1962, p. 411.
[32] J. Brice, W. H. Pearlson, and J. H. Simons, J. Am. Chem. Soc. **71,** 2499 (1949).

(Paper 70A6–420)

JOURNAL OF RESEARCH of the National Bureau of Standards—A. Physics and Chemistry
Vol. 70A, No. 6, November–December 1966

The Melting Temperatures of the n–Paraffins and the Convergence Temperature for Polyethylene

Martin G. Broadhurst

Institute for Basic Standards, National Bureau of Standards, Washington, D.C. 20234

(July 19, 1966)

The extrapolation of the melting points, T_m, of the n-paraffins to large chain lengths ($n \to \infty$) is reexamined in order to resolve the differences in the proposed values of the convergence temperature $T_0 = \lim_{n \to \infty} T_m$. Experimental liquid entropies can be made consistant with a term, $R \ln n$, proposed by Flory and Vrij. This term effectively replaces the well-known expression $T_m = T_0 (n+a)/(n+b)$ with an expression $T_m = T_0 (n+a)/(n+\ln n+b)$; thus, slowing the convergence rate and increasing T_0 from 141.1 °C to 144.7 °C. Independent estimates of the parameters in the melting relationship were obtained from thermodynamic data and the least squares estimate of $T_0 = 144.7$ °C (calculated from 33 melting points with a standard deviation of $T_m = 0.3$ °C) could not be altered by more than ± 0.5 °C by any reasonable variation of the parameters. A simplified melting expression is obtained for polyethylene which includes both the chain end and fold surface energies, and it is shown that chain end effects partly account for the discrepancy between the 144.7 °C convergence temperature and experimental melting temperatures (~ 139 °C) of extended chain polyethylene crystals.

Key Words: Convergence temperature, melting temperatures, methyl surfaces, n-paraffins, polyethylene, thermodynamic properties.

1. Introduction

In 1962, I published a paper [1][1] which was intended to establish on thermodynamic grounds an analytical expression $T_m = f(n)$ for the orthorhombic normal paraffin melting temperatures, T_m, as a function of the number of carbon atoms per molecule, n. That work resulted in an expression,

$$T_m = T_0 \frac{n+a}{n+b} \tag{1}$$

of well-known form in use since 1931. The constants were found to be $a = -1.5$, $b = 5.0$, and $T_0 = \lim_{n \to \infty} T_m(n) = 414.3$ °K (141.1 °C) with an estimated error of ± 2.4 °K.

In 1963 Flory and Vrij [2] reexamined the thermodynamic basis for the paraffiin melting equation and modified the assumption [1] of a linear dependance of the liquid entropy on n, by adding a term, $R \ln n$, to account for the disordering of the methyl layers during melting. The effect of this additional term was to raise the value of T_0 from 414.3 °K (141.1 °C) as predicted by eq (1) to 418.5 ± 1 °K (145.3 °C). The difference between these two values is quite significant when calculating, for instance, the surface free energy of polyethylene crystals from melting data or crystal growth rates. It is the primary purpose of this paper to investigate this discrepancy and to establish more firmly a value for T_0.

2. Liquid Entropies

The n-paraffin melting relationship, $\Delta G(T_m, n) = \Delta H(T_m, n) - T_m \Delta S(T_m, n) = 0$, can be obtained following Flory and Vrij by equating the Gibbs free energy of fusion (written as a function of temperature and n) to zero. If the dependence of ΔG on n is linear, one obtains equation (1). If not, one obtains a more general form of (1) where a and b are functions of n. The limiting value, T_0, depends on the functional form of $\Delta G(T_m, n)$. The solid enthalpies and entropies and the liquid enthalpies are experimentally observed to be linear with n [3], and the problem centers around the functional form of the liquid entropies, $S_l(T, n)$, which experimentally are found to show some nonlinearity. This nonlinearity in $S_l(T, n)$ appears in $\Delta G(T, n)$ and alters T_0 in a way which depends on the magnitude and functional form of the nonlinear terms.

Since it is the liquid entropy that supplies the nonlinear terms to the melting relationship one can investigate these terms independently of the melting temperatures by looking at the n-dependence of experi-

[1] Figures in brackets indicate the literature references at the end of this paper.

mental liquid entropies. Experimental liquid entropies for the *n*-paraffins from C_5H_{12} through $C_{18}H_{38}$ at 300 °K are listed in table 1.[2] If S_l were linear, then differences between consecutive values of $S_l = S_{cl}n + S_{el}$ would be constant, and if $(S_l - R \ln n)$ were linear as indicated by the work of Flory and Vrij then differences between consecutive values of $(S_l - R \ln n) = S_{cl}n + S_{el}$ would be constant. These differences are plotted in figure 1 as a function of n. Figure 1 shows that neither S_l nor $S_l - R \ln n$ are linear with n, and that the $R \ln n$ term is too strong and overcompensates for the non-linearity in S_l. The magnitude of the $R \ln n$ term could be reduced or alternatively a term like $1/n$ could be added with or without the $R \ln n$ term. Included in figure 1 are consecutive differences of the function $(S_l - R \ln n - 5.6/n)$ which do not show any increasing or decreasing trend with n.

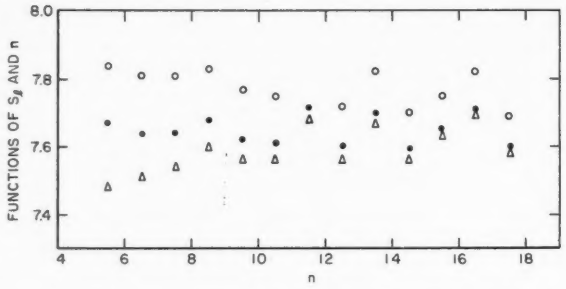

FIGURE 1. *Differences between experimental liquid entropies,* S_l, *(open circles);* $S_l - R \ln n$ *(triangles); and* $S_l - R \ln n - 5.6/n$ *(closed circles), for consecutive n-paraffins at 300 °K versus average number of carbon atoms.*

TABLE 1. *Experimental values of the absolute liquid entropies in cal/mol · deg at 300 °K for the n-paraffins with from 5 to 18 carbon atoms per molecule*

n	S_l(cal/mol/deg)
5	63.21[a]
6	71.05
7	78.86
8	86.67
9	94.505
10	102.272
11	110.019
12	117.869
13	125.591
14	133.407
15	141.111
16	148.865
17	156.68
18	164.37[b]

[a] Data obtained from the U.S. Bureau of Mines, Bartlesville, Oklahoma.
[b] The value for C_{18} was extrapolated to 300 °K from its melting point, 301.3 °K.

A more formal analysis of the entropy data is given in table 2 which shows coefficients and standard deviations resulting from least squares fits of the liquid entropy data for several functions. The lowest standard deviation was obtained using $S_l = S_{cl} + S_{el} + R \ln n + c/n$, but the fit using $S = S_{cl} + S_{el} + cR \ln n$ was also quite satisfactory. The inclusion of a $1/n^2$ term seems an unnecessary complication. But we are still not able to select unambiguously a functional form for S_l based on the data alone. In order to clarify this situation we have examined the statistical theory of polymer chains based on the liquid lattice model. This model allows one to calculate an expression for the entropy of a polymer chain in its liquid phase and leads not only to an unalterable $R \ln n$ term as pointed out by Flory and Vrij but also predicts terms in powers of $1/n$ (see appendix A).

It seems most reasonable to conclude then that the correct expression for the liquid entropy of the *n*-paraffins as a function of n and T is

$$S_l(n, T) = S_{cl}(T)n + S_{el}(T) + R \ln n + 5.6/n, \qquad (2)$$

where terms in $1/n^2$ have been ignored as has the temperature dependence of the relatively unimportant $1/n$ term.

[2] Data were obtained from the United States Bureau of Mines, Bartlesville, Oklahoma. Detailed references are given in reference [3].

TABLE 2. *Least square fits of the liquid n-paraffins entropies at 300 °K for several functions*

Function	Standard deviation of function	Constants and their (standard deviations)			
		S_c	S_e	c	d
$S_l = S_{cl}n + S_{el}$	(0.061)	7.78 (0.004)	24.4 (0.05)		
$S_l = S_{cl}n + S_{el} + cR \ln n$	(0.028)	7.71 (0.010)	23.4 (0.14)	0.38 (0.06)	
$S_l - R \ln n = S_{cl}n + S_{el}$	(0.092)	7.59 (0.006)	21.9 (0.02)		
$S_l - R \ln n = S_{cl}n + S_{el} + c\left(\frac{1}{n}\right)$	(0.027)	7.65 (0.005)	20.7 (0.11)	5.61 (0.49)	
$S_l - R \ln n = S_{cl}n + S_{el} + c\left(\frac{1}{n}\right) + d\left(\frac{1}{n}\right)^2$	(0.028)	7.66 (0.016)	20.4 (0.50)	7.73 (4.61)	−6.04 (13.0)

3. Melting Equation

By expanding $\Delta G = \Delta G_c n + \Delta G_e - RT \ln n - 5.6T/n$ about $T = T_0$ (see reference 2 for details) one finds,

$$n\Delta H \frac{\Delta T}{T_0} - n\frac{\Delta C_p}{2T_0}(\Delta T)^2 - T_m\left[R \ln n + 5.6\left(\frac{1}{n}\right)\right] = T_m \Delta S_e - \Delta H_e + \frac{\Delta C_{pe}}{2T_0}(\Delta T)^2 \qquad (3)$$

which differs from Flory and Vrij's eq (8) only in that it includes the $(1/n)$ term and the ΔC_{pe} term which they chose to neglect. Direct calculations show that neglected terms remain below 1 percent of the magnitude of the leading terms in eq (3). Here $\Delta T = T_0 - T_m$; $-\Delta H/T_0$ and $-\Delta C_p/T_0$ are the first and second temperature derivatives of ΔG_c at $T = T_0$; $-\Delta S_e$ and $-\Delta C_{pe}/T_0$ are the first and second temperature derivatives of ΔG_e at $T = T_0$; and $\Delta H_e = \Delta G_e + T_0 \Delta S_e$. Rewriting (3) in the form of (1) one obtains,

$$T_m = T_0 \frac{n + \dfrac{\Delta H_e - T_0 \Delta C_{pe}/2}{\Delta H - T_0 \Delta C_p/2}}{n + \dfrac{T_0}{\Delta H - T_0 \Delta C_p/2}\left[\left(\Delta S_e - \dfrac{\Delta C_{pe}}{2}\right) + R \ln n + 5.6\left(\dfrac{1}{n}\right) - \left(\dfrac{\Delta C_p}{2} n + \dfrac{\Delta C_{pe}}{2}\right)\dfrac{\Delta T}{T_0}\right]}. \qquad (4)$$

This result is equivalent, except for the ln n and $(1/n)$ terms, to eq (1.6) in reference [1]. Equation (4) can be abbreviated as

$$T_m = T_0 \frac{n + a}{n + B(n)}$$

which can now be treated as a generalization of (1). One can calculate from experimental T_m values

$$B(n) = \frac{T_0}{T_m}(n + a) - n, \qquad (5)$$

and these $B(n)$ values are shown in figure 2 for various values of T_0 and a. The quantity $B(n)$ can also be expressed from equation (4) in the following form:

$$B(n) = \frac{T_0}{\Delta H - T_0 \Delta C_p/2}\left[\left(\Delta S_e - \frac{\Delta C_{pe}}{2}\right) + R \ln n + \frac{5.6}{n} - \left(\frac{\Delta C_p}{2} n + \frac{\Delta C_{pe}}{2}\right)\left(1 - \frac{T_m}{T_0}\right)\right]. \qquad (6)$$

The thermodynamic quantities in eq (6) were assigned values as follows. The molar entropies and enthalpies for the liquid and solid n-paraffins (see footnote 2) were plotted as a function of n. The slopes and intercepts of these curves equal respectively $S_c(T)$, $H_c(T)$ and $S_e(T)$, $H_e(T)$ and differences between the liquid and solid values gave $\Delta S_c(T)$, $\Delta H_c(T)$ and $\Delta S_e(T)$, $\Delta H_e(T)$ which were then extrapolated to $T = T_0$ to give ΔH, ΔS, ΔS_e, and ΔH_e. ΔC_p and ΔC_{pe} were taken as the slopes of the $\Delta H(T)$ and $\Delta H_e(T)$ curves at $T = T_0$. (A more detailed description of this procedure can be found in [3].) The results of these calculations are summarized in table 3. Numbers from table 3 were used to evaluate the various terms in eq (6) and these terms are shown in figure 3.

TABLE 3. *The values of several quantities at 418 °K determined from thermodynamic data on the* n*-paraffins*

Quantity	Value	Estimated possible error[a]
ΔH	1000	±25 cal/mol
ΔC_p	0.5	±0.5 cal/mol deg
ΔG_e	−3400	±500 cal/mol
ΔH_e	−3000	±500 cal/mol
ΔS_e	1.0	±0.5 cal/mol deg
ΔC_{pe}	−8.0	±4.0 cal/mol deg

[a] The estimates of error are intentionally pessimistic and serve only as a guide in examining the sensitivity of eq (4) to extreme variations of these quantities.

Figures 2 and 3 are useful for getting a feeling for how the various terms in $B(n)$ affect T_0 and a. In figure 2 the change in shape of $B(n)$ at small n is associated with a change in a, whereas a change in the slope of $B(n)$ at large n is associated with a change in T_0. Figure 3 shows that the term which accounts mostly for the shape of $B(n)$ at large n is the ln n term and that the remaining three n-dependent terms in $B(n)$ mostly affect the shape of $B(n)$ at small n. The quantity $(\Delta S_e - \Delta C_{pe}/2)$ is treated here as an adjustable parameter and is used to regulate the vertical position of $B(n)$.

When $B(n)$ was assumed constant as was done in [1], curve fitting of the melting equation gave $a = -1.5$ and $T_0 = 414.3$ °K. These results can be anticipated from figure 2 which shows that straightest curve is the $a = -1.5$ curve and the flattest curve would be for T_0 a little less than 415. Including a ln n term and a partially compensating ΔC_p term in $B(n)$ as was done by Flory and Vrij gives $B(n)$ a shape similar to the $a = -3.0$ curve and a large-n slope similar to the 419 °K curve. Thus one can anticipate their results of $T_0 = 418.5$ °K and $a = -2.7$. In this present paper we are adding to $B(n)$ the $1/n$ and ΔC_{pe} terms and from figure 3 we can anticipate that these will raise the small-n end of the curve and thus significantly reduce the magnitude of a but only slightly lower the large-n slope and thus only slightly reduce the T_0 value found by Flory and Vrij.

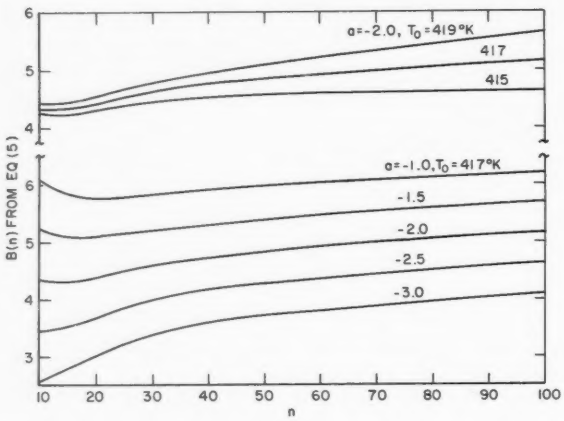

FIGURE 2. B(n), *calculated using eq* (5), *as a function of* n *for different values of parameters* T_0 *and* a.

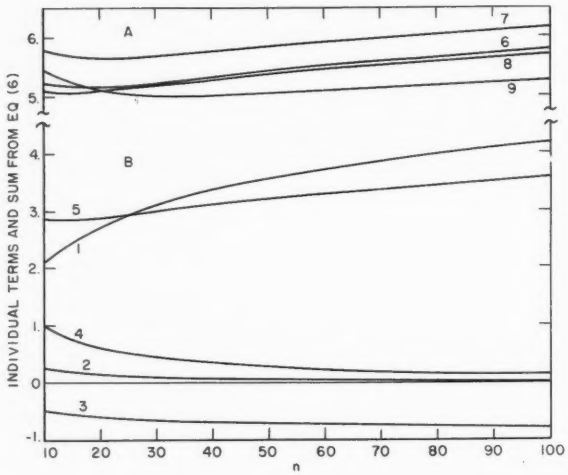

FIGURE 3. A. B(n), *calculated from eq* (6) *using different values for the thermodynamic quantities.* B. *Values of the four variable terms in eq* (6) *and their sum using the values in table 3 and* $T_0 = 418$ °K.

The curves are (1) $b_0 R \ln n$ (where $b_0 = T_0/(\Delta H - T_0\Delta C_p/2) = 0.47$); (2) 5.6 $b_0(1/n)$, (3) $b_0(\Delta C_p/2)n(\Delta T/T_0)$, $\Delta C_p = 0.5$; (4) $b_0(\Delta C_{pe}/2)(1 - T_m/T_0)$, $\Delta C_{pe} = -8$; (5) sum of curves 1–4, (6) same as (5) with $b_0(\Delta S_e - \Delta C_{pe}/2) = 5\ b_0$ added, (7) same as (6) with $\Delta C_{pe} = -12$, (8) same as (6) with $\Delta C_p = 1.0$, (9) same as (6) with $\Delta C_p = 2.0$.

In other words, the ln n term is the crucial one in $B(n)$ as far as establishing T_0 is concerned, and the constants in the other terms can be varied within the generous range of uncertainties given in table 3 without appreciably affecting T_0. In the following section the results of fitting the melting temperatures to eq (4) will be shown to verify these anticipated results.

4. Fitting the Melting Data

Previously, eq (1) was fit to 14 values of T_m for the orthorhombic-liquid transition of the n-paraffins with $44 \leq n \leq 100$ [1]. Flory and Vrij calculated 19 additional values for $11 \leq n < 44$ from data on the enthalpies and temperatures of the orthorhombic-hexagonal and hexagonal-liquid transitions. The resulting 33 values are listed in their paper. The values for the five shortest paraffins were found to be smaller by 0.1, 0.3, 0.2, 0.2, and 0.1 °C respectively than those given by Flory and Vrij, based on quadratic extrapolations of experimental free energies.

These data were fit by least squares using an Omnitab program to eq (4) in the form:

$$T_m(n) = T_0\left(\frac{n}{n+B(n)}\right) + T_0 a\left(\frac{1}{n+B(n)}\right),$$

where $B(n)$ is given by eq (6).

Such a fit yields least squares estimates of T_0 and $T_0 a$ with the assumption that the bracketted terms are known functions of n and that all experimental uncertainty is contained in $T_m(n)$. Thus all constants in $B(n)$ had to be assigned values before fitting. To adapt to these restrictions we assigned values to ΔC_p, ΔC_{pe} and the factor $T_0/(\Delta H - T_0\Delta C_p/2)$ from table 3 and then did the least squares fitting for each of a series of closely spaced values of $(\Delta S_e - \Delta C_{pe}/2)$. The best value for $(\Delta S_e - \Delta C_{pe}/2)$ was taken as that which gave a minimum standard deviation in T_m for fixed values of ΔC_p, ΔC_{pe}, and $T_0/(\Delta H - T_0\Delta C_p/2)$. This method yields a pseudo-least-squares value for $(\Delta S_e - \Delta C_{pe}/2)$, and the standard deviations were adjusted to account for this third constant. The other constants in $B(n)$ could have been handled in the same way except that the fit was fairly insensitive to them. Instead, the values of ΔC_p, ΔC_{pe}, and $T_0/(\Delta H - T_0\Delta C_p/2)$ were varied either together or singly within the range allowed by table 3 and the fit was repeated each time yielding new values for T_0, $T_0 a$ and $(\Delta S_e - \Delta C_{pe}/2)$. In this way the effect of variations in the assigned constants on the values of the derived constants could be observed directly. To eliminate the difficulty of having the ratio $\Delta T/T_0$ appear in $B(n)$, calculated values for this ratio were fed back into $B(n)$ until the calculated T_0 became constant. The results were quite insensitive to the initially assumed value of $\Delta T/T_0$, and T_0 converged to a constant value to better than 4 figures after 2 iterations.

Using $T_0/(\Delta H - T_0\Delta C_p/2) = 0.47$, $\Delta C_p = 0.5$ and $\Delta C_{pe} = -8.0$ gave best fit values of $T_0 = 417.9$ °K, $a = -1.5$ and $(\Delta S_e - \Delta C_{pe}/2) = 5$. The values in table 3 give independently $a = -1.5$ and $(\Delta S_e - \Delta C_{pe}/2) = 5$, which is encouraging agreement. The standard deviations for T_m and T_0 based on 33 minus 3 degrees of freedom were calculated to be 0.30 and 0.12 °K respectively.[3] Changing the assumed values of ΔC_p, ΔC_{pe}, and $T_0/(\Delta H - T_0\Delta C_p/2)$ within the limits allowed in table 3 did not alter the calculated value of T_0 by more than ±0.5 °K. The results are as anticipated by the arguments of the previous section.

[3] For comparison, the melting data were fit to eq (1) and gave $T_0 = 413.8$ °K with standard deviations of 0.36 and 0.14 °K respectively. Hence, eq (4) does offer some improvement of fit over eq (1).

The results lead strongly to the conclusion that T_0 is very nearly equal to 417.9 °K. To apply an uncertainty based on three standard deviations (3×0.12 °K) is misleading since it does not take account of uncertainties in the functional form of (4), but it is difficult to see how T_0 could be altered by more than 0.5 °K by any reasonable means. Hence, the results essentially confirm those of Flory and Vrij with a slight but significant reduction in their estimate of $T_0 = 418.5 \pm 1.0$ °K because of two relatively small terms which they neglected.

5. Discussion

The highest experimentally observed melting temperature for polyethylene is 138.7 °C, and for polymethylene, 141.4 °C [6, 7]. Both of these were extended-chain pressure-crystallized specimens. Brown and Eby [8] used a form of eq (1) to extrapolate the melting temperatures of polyethlene to infinite molecular weight and found $T_0 = 143.5$ °C. By the same procedure Fujiwara and Yoshida [9] found $T_0 = 144.8$ °C. Weeks [10] used a plot of crystallization versus melting temperatures and extrapolated the data to the line $T_c = T_m$ to find $T_0 = 145.5$ °C. Thus, a value of T_0 (paraffins) $\simeq 145$ °C is not out of line with extrapolated values for T_0 (polyethylene), but is significantly higher than experimentally observed melting points for extended chain polyethylene where there should be no effect from chain folded surfaces. An overall explanation of the melting data for polyethylene seems still to be lacking.

It is of interest to examine eq (3) in the limit of large n,

$$T_m \text{ (paraffins, } n \gg 1) = T_0 \left(1 + \frac{\Delta G_e - RT_0 \ln n}{n \Delta H}\right) \qquad (7)$$

For a polymer, one would observe some contribution from the $R \ln n$ term if the chain ends were ordered in the crystal. Given a narrow length-fraction of polyethylene, one might find a high degree of chain end ordering in extended chain crystals, and very little chain end ordering in the folded chain crystals. Assume that ΔG_e is the same for any type of crystal and that a term $RT_0 \ln \alpha n$ takes care of end group ordering effects where α has a value from $1/n$ (completely disordered) to 1 (completely ordered), depending on n, the distribution in length and the mode of crystallization. Assume further that ΔG_f is the free energy contributed to the crystal by a mole of folds in excess of that attributable to the associated CH_2-groups if in a nonfolded configuration, and that the folds, when present in the crystal, occur in regular planes separated by n_f carbon atoms. We can now modify eq (7) as follows,

$$T_m \text{ (polyethylene, } n \gg 1) = T_0 \left[1 + \frac{\Delta G_e - T_0 R \ln \alpha n}{n \Delta H} - \frac{\Delta G_f}{n_f \Delta H}\right] \qquad (8)$$

in order to explicitly account for both chain ends and folds.

Equation (8) can be compared to the well-known equation,

$$T_m = T_0' \left[1 - \frac{2\sigma_e}{l \Delta h_f}\right]. \qquad (9)$$

Here $\sigma_e = -(C/2A)\Delta G_f$ erg/cm^2, $A = 18.5 \times 10^{-16}$ cm^2 = the effective cross-sectional area of a CH_2 chain, $C = 6.95 \times 10^{-17}$ ergs-moles/cal-molecule is a dimensional conversion constant, $l = 1.27\ n_f \times 10^{-8}$ cm and $\Delta h_f = (C/1.27 \times 10^{-8} A)\Delta H = 2.96 \times 10^9$ ergs/cm^3 is the heat of fusion of a CH_2 chain crystal.

One can now write (8) in the form of (9) to a good approximation by letting

$$T_0' = T_0 \left[1 + \frac{\Delta G_e - T_0 R \ln \alpha n}{n \Delta H}\right] \qquad (10)$$

where T_0' is the effective convergence temperature for a polymer containing end groups. T_0' was calculated using $T_0 = 417.9$, $\Delta G_e = -3{,}400$ cal/mole, $\Delta H = 1000$ cal/mole for the two limiting values of α_0, and the results are shown in figure 4, plotted as a function of the number of chain ends per 1000 carbon atoms.

Notice that the apparent convergence temperature for our hypothetical polyethylene is lower when the chain ends are ordered ($\alpha = 1$) than when the chain ends are disordered ($\alpha = 1/n$). This result is of interest primarily because the experimental results mentioned at the beginning of this section give higher values for

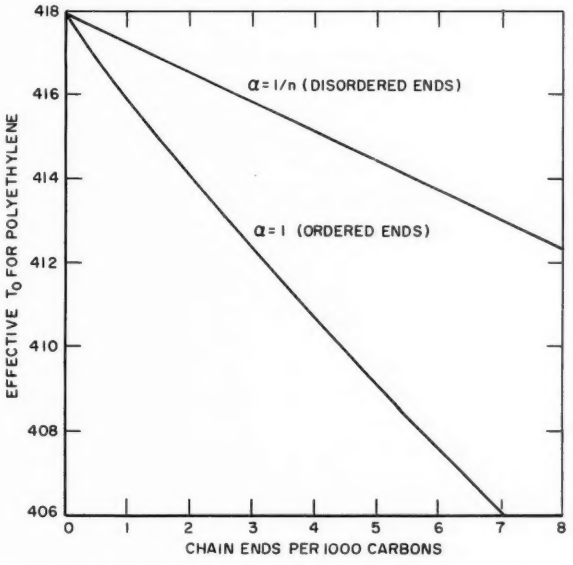

FIGURE 4. *Effective* T_0 *for polyethylene fractions as a function of the number of chain ends (calculated from eq (10)).*

The $\alpha = 1$ line represents the case of extended chain crystals with ordered methyl layers and the $\alpha = 1/n$ line applies to chain folded crystals where the chain ends are supposed to be randomly ordered in the crystal.

230-736 O-66—3

T_0' for folded crystals of polyethylene than the actual measured values for extended chain polyethylene. (The former would presumably exhibit more randomization of ends than the latter.) Also notice that the depression in T_0' is not insignificant for typical polyethylene where the weight average molecule has about 1000 carbons (2 ends per 1000 carbons) [7]. We shall not procede further to include the additional effects of length distribution and side branching but merely emphasize the significant point here that chain ends play an important part in calculating thermodynamic quantities for polyethylene and one can use the $T_0 = 417.9$ °K calculated in this paper only if one includes $\Delta G_e - RT_0 \ln n$ *explicity* in polyethylene melting expressions like (8).

Finally, it should be mentioned that the increase in T_0 to 144.7 °C does not greatly alter the results in reference [3] where the thermodynamic properties of an infinite CH_2 chain crystal and liquid were obtained from paraffin data. Also the introduction of the $R \ln n$ term does not affect those results since the nonlinearity, although not understood, was recognized and taken into account empirically in that paper.

6. Appendix A

In order to examine the theoretical form of the liquid-glass entropy difference, ΔS_{lg}, as predicted by the liquid lattice theory (for a general discussion of the theory see Miller [4]), it is convenient to start with eq 20 in reference [5].[4] This equation includes the important effects of chain stiffness. Letting their z, the primary valance of the backbone chain atoms, equal 4 and writing ΔS_{lg} as a molar quantity, eq 20 [5] is,

$$\Delta S_{lg}/R = n \ln(V_0/S_0) + np \ln(V_0/S_0^z) + \ln 3(n-1) + (n-3)A \qquad \text{(A.1)}$$

where R = molar gas constant, n = number of carbon atoms in the chain, $p = n_0/n\ n_x$ = fraction of vacant, n_0, to occupied, $n\ n_x$, lattice sites (n_x = number of n −mers), $V_0 = n_0/(n\ n_x + n_0) = p/(1+p)$ = volume fraction of vacant to total lattice sites, $S_0 = 2n_0/[(n+1)n_x + 2n_0]$ and

$$A = \ln[1 + 2\exp(-\Delta\beta)] + \frac{2\Delta\beta \exp(-\Delta\beta)}{1 + 2\exp(-\Delta\beta)}$$

where $\Delta\beta = (\epsilon_2 - \epsilon_1)/RT$ and $(\epsilon_2 - \epsilon_1)$ is the energy difference between the trans and gauche configurations for a carbon-carbon bond.

Ignoring p compared to 1 (the derivation was carried out without simplications and gave essentially the same results), writing $V_0/S_0 = (1/2)(1+1/n)$ and dropping the second term in (A.1) gives,

$$\Delta S_{lg}/R = n \ln(1/2)(1+1/n) + \ln 3n(1+1/n) + (n-3)A$$

$$= n(-\ln 2 + A) + (\ln 3 - 3A) + \ln n + (n+1)\ln(1+1/n).$$

Expanding,

$$\ln(1+1/n) = (1/n - 1/2n^2 + 1/3n^3 \ldots)$$

and

$$\Delta S_{lg}/R = n(-\ln 2 + A) + (1 + \ln 3 - 3A) + \ln n + 1/2\,(1/n) - (1/6)(1/n^2). \qquad \text{(A-2)}$$

Thus we have in addition to the linear and constant terms an unalterable $\ln n$ term and a power series in $(1/n)$.

Of some further interest are the predicted magnitudes of the coefficients. Letting $(\epsilon_2 - \epsilon_1) = 500$ cal/mole, then $A = 1.0$ at 300 °K and we have,

$$(\Delta S_{lg}/R) = 0.3n - 0.9 + \ln n + (1/2)(1/n) - (1/6)(1/n^2).$$

Experimentally, the liquid crystal entropy differences at 300 °K for the n-paraffins fit roughly,

$$(\Delta S_{lc}/R) = 1n + 0.5 + \ln n + 2.6(1/n) - 3(1/n^2).$$

The agreement is not good but we can improve things somewhat by taking account of the extra volume of a CH_3 group compared to a CH_2 group. From the x-ray length of the orthorhombic phase $l = (1.27\ n + 2) \times 10^{-8}$ cm indicating an effective CH_3 length of roughly twice a CH_2 length. Replacing n by $n+2$ gives,

$$(\Delta S_{lg}/R) = 0.3n - 0.3 + \ln n + 2.5\,(1/n) - 3.2\,(1/n^2) + \ldots.$$

Even the discrepancy in the constant term is now not too disturbing, and the numerical agreement lends some support to the adoption of the above form for ΔS_{lc}.

[4] This equation actually deals with the configurational entropy difference between the liquid and a zero configurational entropy glass and hence should equally well apply to the configurational entropy difference between the liquid and ordered crystal.

7. References

[1] M. Broadhurst, J. Chem. Phys. **36,** 2578 (1962).
[2] P. J. Flory and Vrij, J. Am. Chem. Soc. **85,** 3548 (1963).
[3] M. Broadhurst, J. Res. NBS, **67A** (Phys. and Chem.) No. 3, 233 (1963).
[4] A. R. Miller, The Theory of Solutions of High Polymers (The Clarendon Press, Oxford, 1948).
[5] J. H. Gibbs and E. A. Dimarzio, J. Chem. Phys. **28,** 373 (1958).
[6] T. Arakawa and B. Wunderlich, J. Polymer Sci. **A2,** 53 (1966).
[7] T. Arakawa, Ph. D. Thesis, Cornell University, 1965.
[8] R. G. Brown and R. K. Eby, J. Appl. Phys. **35,** 1156 (1964).
[9] Y. Fujiwara and T. Yoshida, Polymer Letters **1,** 675 (1963).
[10] J. J. Weeks, J. Res. NBS **67A** (Phys. and Chem.) No. 5, 441 (1963).
[11] J. P. Colson and R. E. Eby, J. Appl. Phys. **37,** 3511 (1966).

(Paper 70A6–421)

JOURNAL OF RESEARCH of the National Bureau of Standards—A. Physics and Chemistry
Vol. 70A, No. 6, November–December 1966

General Treatment of the Thermogravimetry of Polymers

Joseph H. Flynn and Leo A. Wall

Institute for Materials Research, National Bureau of Standards, Washington, D.C., 20234

(August 11, 1966)

Theoretical equations are developed for typical decompositions of polymers including those in which the volatilization does not follow a simple "reaction order" and those made up of a composite of several reactions of differing energies of activation. The effects of order, activation energy, heating rate and temperature dependence upon the calculated thermograms is illustrated. The literature on thermogravimetric kinetics is critically reviewed and coalesced into a logical and coherent development stressing the interrelation of methods and employing a consistent system of notation. As a result, a number of improved methods and new methods for the analysis of kinetic data applicable to the complex systems mentioned above are developed. It is concluded that methods involving a variable rate of heating or involving several thermogravimetric traces at different rates of heating are capable of establishing the uniqueness of kinetic parameters. A new method of determining initial parameters from rate-conversion data is developed. A novel concept is employed of programming reaction variables (in this case, the heating rate) in a manner which greatly simplifies the mathematics of the kinetic system and which shows promise of a wide range of applicability in the area of rate processes.

Key Words: Degradation, nonisothermal kinetics, polymers, pyrolysis, thermal decomposition, thermogravimetry, thermolysis, stability of polymers.

1. Introduction

Thermogravimetric analysis is used widely as a method to investigate the thermal decomposition of polymers and to assess their relative thermal stabilities [1,2,3,4].[1] Also, considerable attention has been directed recently toward the exploitation of thermogravimetric data for the determination of kinetic parameters. A number of these methods will be discussed later in this paper.

Many of the methods of kinetic analysis which have been proposed are based on the hypothesis that, from a single thermogravimetric trace, meaningful values may be obtained for parameters such as activation energy, preexponential factor and reaction order.

Thus, many of these methods make two assumptions, viz, these parameters are useful in characterizing a particular polymer degradation, and that the thermogram for each particular set of these parameters is unique.

Therefore, in this paper, we will test the validity of these assumptions by setting up several idealized typical cases of polymer degradation kinetics, observing how the structures of the calculated thermograms are affected by changes in order, activation energy, heating rate and temperature dependence, and determining by means of a critical evaluation of both existing and new methods if there are any general treatments of these data that will permit the determination of parameters that may be useful in the interpretation of degradation mechanisms.

2. Theory

We shall assume for the present that the isothermal rate of conversion, dC/dt, is a linear function of a single temperature-dependent rate constant, k, and some temperature-independent function of the conversion, C, i.e.,

$$\frac{dC}{dt}=kf(C). \tag{1}$$

[1] Figures in brackets indicate the literature references at the end of this paper.

C, the conversion (degree of completion or advancement, extent of reaction), is defined here as the conversion with respect to initial material. Thus $C=1-(W/W_0)$, where W_0 is the initial weight and W is the weight at any time. Therefore, the residual fraction $(1-C)=W/W_0$ and the rate of conversion, $dC/dt=-1/W_0(dW/dt)$.

Some investigators prefer to define an instantaneous rate of conversion such that $dC'/dt=1/W\ (dW/dt)$ and thence C' is proportional to the logarithm of the residual fraction. However, unless perhaps dealing specifically with first order reaction kinetics, there seems to be little special appeal for this latter definition of conversion.

When the polymer does not completely volatilize at T or $t\rightarrow\infty$, or if the volatilization takes place in steps, the conversion may for convenience, or depending upon one's insight into mechanism, be defined differently based on the total weight loss between two successive horizontal portions of an integral thermogram. Equation (1) excludes composite cases where simultaneous or successive reactions involve several temperature dependent rate constants. Several of these cases will be considered later.

At a constant rate of heating, $\beta=dT/dt$, and assuming k independent of C and $f(C)$ independent of T, the variables in eq (1) may be separated and integrated to obtain:

$$F(C)=\int_0^C\frac{dC}{f(C)}=\frac{1}{\beta}\int_{T_0}^{T}kdT=\Phi \tag{2}$$

where $F(C)$ is the integrated function of conversion and Φ represents the temperature integral.

In analogy to simple cases in homogeneous reaction kinetics, we express the conversion function by

$$f(C)=(\mathbf{n}+1)(1-C)^n \tag{3}$$

where n is defined as the order or reaction. $\mathbf{n}+1$ is the normalization factor for the isothermal cases such that $(\mathbf{n}+1)\int_0^1(dC/kdt)\,dC=1$. $\mathbf{n}$ is equal in value to n and included only in the calculated curves so that they will exhibit maximum thermogravimetric rates at approximately the same temperature.

Substituting eq (3) into eq (1) and integrating, one obtains

$$\begin{aligned}&\frac{(1-C)^{1-n}-1}{(1-n)(\mathbf{n}+1)}=-kt \text{ or } -\Phi \qquad (n\neq 1)\\ &\frac{1}{(\mathbf{n}+1)}\ln(1-C)=-kt \text{ or } -\Phi \qquad (n=1)\end{aligned} \tag{4}$$

($-kt$, if $T=$ const.; $-\Phi$, if $T\neq$ const.).

The normalized isothermal curves from eq (4) for rate versus conversion are plotted in figure 1. Some of these curves indeed do approximate ones obtained in polymer degradation studies. For example, if the depolymerization is initiated at chain ends and the zip length of the depropagation reaction is much shorter than the polymer chain length, as is the case in high molecular weight polymethyl methacrylate, then a large portion of the reaction follows zero order kinetics [5]. If the zip length is much larger than the polymer chain length, first order kinetics results [5]. Other cases of degradation kinetics, such as is found for branched polyolefins, may be fitted over a range of conversion by higher order curves [5].

However, in a large number of polymer decompositions, the isothermal rate of conversion goes through a maximum value. Such behavior describes a wide spectrum of polymers [5].

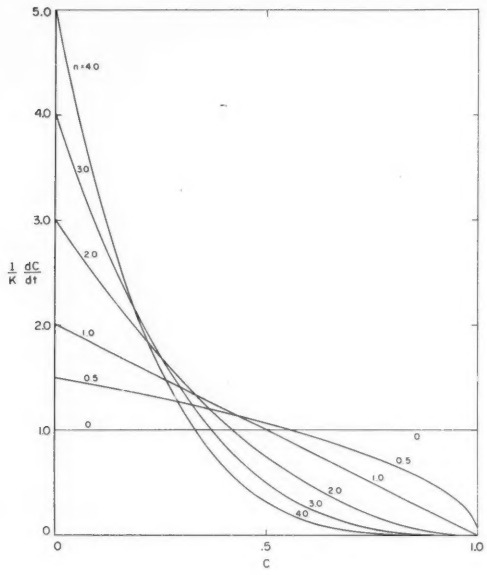

FIGURE 1. *Effect of order on normalized isothermal rate versus degree of conversion.*

Random depolymerization, where most of the early scissions result in fragments too large to distill off, produces an isothermal rate curve with a maximum at 26 percent conversion.

For random depolymerization [6],

$$1-C=(1-\alpha)^{L-1}\left[1+\alpha\frac{(N-L)(L-1)}{N}\right] \tag{5}$$

where $N-1$ is the initial number of carbon atoms in the chain skeleton, L is the number of carbon atoms in the smallest chain that does not evaporate, and α, the fraction of bonds broken.

Differentiating eq (5) with respect to kt,

$$\frac{dC}{dkt}=(L-1)(1-C)-(1-\alpha)^{L}\frac{(N-L)(L-1)}{N} \tag{6}$$

and eliminating α from eqs (5) and (6) for the simplest case, $N \gg L$, $L=2$, result in

$$f(C)=6(C^{1/2}-C)$$

for the normalized isothermal equation. In formulating the above approximation (Case A), the term for the initial isothermal rate, $[L(L+1)]/N$ has been assumed equal to zero since in practice $N \gg L$. Hence the expression goes to zero at $C=0$ and is not applicable to initial situations. The solution of eq (5) for α involves an Lth order polynomial so that it is not practicable to obtain $f(C)$ in analytic form for large L. Also, maximum rates are never obtained at greater than 26 percent conversion from random depolymerization. Therefore, an empirical cubic equation was devised to fit several cases found in isothermal degradation kinetics.

For the equation

$$\frac{dC}{dkt}=N(C^3+a_1C^2+a_2C+a_3) \tag{7}$$

the following boundary conditions:

$$\left(\frac{dC}{dkt}\right)_{C=\omega}=\left(\frac{dC}{dkt}\right)_{\max};\qquad \left(\frac{dC}{dkt}\right)_{C=1}=0;\qquad \frac{\left(\frac{dC}{dkt}\right)_{C=\omega}}{\left(\frac{dC}{dkt}\right)_{C=0}}=\gamma$$

are satisfied when

$$N=\frac{12[(\gamma-1)(1-2\omega)-\omega^2]}{\omega^2(6\omega^2-16\omega-9)-(\gamma-1)(6\omega^2-6\omega-1)},\quad a_1=\frac{2\omega^3-(\gamma-1)(1-3\omega^2)}{(\gamma-1)(1-2\omega)-\omega^2},$$

$$a_2=\frac{\omega[(\gamma-1)(2-3\omega)-\omega^3]}{(\gamma-1)(1-2\omega)-\omega^2},\text{ and }a_3=\frac{\omega^2(\omega-1)^2}{(\gamma-1)(1-2\omega)-\omega^2}.$$

For Case B, we assume the maximum rate at 50 percent conversion and a maximum rate three times the initial rate, ($\omega=0.5$, $\gamma=3$) and obtain,

$$f(C)=-\frac{24}{13}\left(C^3+C^2-\frac{7}{4}C-\frac{1}{4}\right).$$

For Case *C*, ($\omega=0.25$, $\gamma=3$), eq (7) has a minimum as well as a maximum in the range $C=0$ to 1. However, Case *C* was fitted satisfactorily by reduction of the order of eq (7) which gave after normalization,

$$f(C)=-\frac{60}{31}\left(C^{3/2}+C-\frac{7}{4}C^{1/2}-\frac{1}{4}\right).$$

The normalized isothermal rates for Cases A, B, and C are plotted against conversion in figure 2.

Curves A and C closely resemble theoretical curves for pure random depolymerization or for depolymerizations of moderate zip length involving considerable molecular transfer. Case B is representative of depolymerizations in which the initiation occurs at chain ends, the zip length is moderate and either a slight amount of transfer or random initiation take place. Such curves are characterized by a maximum in the 50 percent conversion region [7].

The equation for Case A may be substituted into eq (1) and integrated and if the solutions of the cubic in the equations for Cases B and C are expressed as partial fractions, substituted into

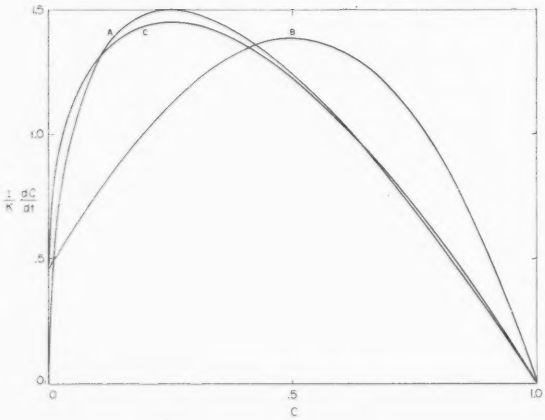

FIGURE 2. *Normalized isothermal rate versus degree of conversion, Cases A, B, and C.*

eq (1) and integrated, one obtains:

for Case A,

$$3 \ln (1-C^{1/2}) = -kt \text{ or } -\Phi,$$

for Case B,

$$\frac{1}{6}\{\ln (1-C) + 0.6547 \ln (C+1.8660) - 1.6547 \ln (C+0.1340) - 1.6219\} = -kt \text{ or } -\Phi,$$

and for Case C,

$$\frac{62}{195}\{\ln (1-C^{1/2}) - 1.2217 \ln (C^{1/2}+1.8660) - 0.2217 \ln (C^{1/2}+0.1340) + 0.5451\} = -kt \text{ or } -\Phi$$

($-kt$, if T = constant; $-\Phi$, if $T \neq$ constant).

The Arrhenius equation,

$$k = Ae^{(-E/RT)} \tag{8}$$

is almost universally assumed for the temperature dependence of k, where A, the "preexponential factor," is usually assumed to be independent of temperature, E is the energy of activation, and R, the gas constant = 1.987 cal mol^{-1} (°K)$^{-1}$ (1 cal = 4.1840 J).

Substituting eq (8) into eq (1), one obtains

$$\frac{dC}{dt} = \beta \frac{dC}{dT} = Ae^{(-E/RT)} f(C) \tag{9}$$

which upon integration becomes

$$F(C) = \int_0^C \frac{dC}{f(C)} = \frac{A}{\beta}\int_{T_0}^{T} e^{(-E/RT)}dT = \Phi = \frac{AE}{\beta R}\left\{-\frac{e^x}{x} + \int_{-\infty}^{x}\frac{e^x}{x}\,dx\right\} = \frac{AE}{\beta R}\,p(x) \tag{10}$$

where $x = (-E/RT)$. It is assumed that T_0 is low enough for the lower limit to be negligible.

If $f(C)$ is given by eq (3) then eq (9) becomes,

$$\frac{dC}{dt} = \beta \frac{dC}{dT} = Ae^{(-E/RT)}(1-C)^n \tag{11}$$

which, upon integration becomes,

$$\frac{(1-C)^{1-n}-1}{1-n} = \frac{AE}{\beta R}\,p(x) \qquad (n \neq 1)$$

$$\ln (1-C) = \frac{AE}{\beta R}\,p(x) \qquad (n = 1). \tag{12}$$

$p(x)$, which includes the exponential integral, has been tabulated for limited ranges [8–11]. There are several series expansions and a semiempirical approximation for $p(x)$. These are given below as they are utilized in many of the kinetic methods which will be discussed later.

2.1. Asymptotic Expansion [12]

$$p(x)=\frac{e^x}{x^2}\left(1+\frac{2!}{x}+\frac{3!}{x^2}+\frac{4!}{x^2}+\ldots\right)$$

$$x\leqslant -10;\ \text{number of terms} \leqslant |x|. \qquad (13a)$$

2.2. Expansion in Series of Bernoulli Numbers [12]

$$p(x)=\frac{e^x}{x}\left(-0.0000035+\frac{0.998710}{x}+\frac{1.98487646}{x^2}+\frac{4.9482092}{x^3}+\frac{11.7850792}{x^4}\right.$$

$$\left.+\frac{20.452340}{x^5}+\frac{21.1491469}{x^6}+\frac{9.5240411}{x^7}\pm 0.35\times 10^{-5}\right) \qquad (x\leqslant -2). \qquad (13b)$$

2.3. Schlömilch Expansion [13]

$$p(y)=\frac{e^{-y}}{y(y+1)}\left(1-\frac{1}{y+2}+\frac{2}{(y+2)(y+3)}-\frac{4}{(y+2)\cdots(y+4)}+\frac{14}{(y+2)\cdots(y+5)}-\cdots\right)$$

$$(y=-x\geqslant 15). \qquad (13c)$$

2.4. Doyle's Approximation [14]

$$\log p(x)\cong -2.315+0.457x$$

$$(-20\geqslant x\geqslant -60). \qquad (13d)$$

Doyle [15] has found that two and three term approximations for eq (13c) are more accurate than the respective approximation for eq (13a). Equation (13b) is almost equivalent to eq (13a) for the first several terms.

At the limits, $-20\geqslant x\geqslant -60$, eq (13d) is accurate within ± 3 percent [11].

An extensive table of log $p(x)$ for various x's was calculated from eq (13b) as this equation gives quite accurate values even for small x. This table was used for the calculation of the thermograms presented subsequently.

If the preexponential factor, A, is linearly dependent on temperature, i.e., $A=\mathbf{A}_1T$

$$k=\mathbf{A}_1Te^{(-E/RT)} \qquad (14)$$

then,

$$\Phi=-\frac{\mathbf{A}_1E^2}{2\beta R^2}\left\{\frac{e^x}{x^2}+\frac{e^x}{x}-\int_{-\infty}^{x}\frac{e^x}{x}\,dx\right\}=-\frac{\mathbf{A}_1E^2}{2\beta R^2}\,p_1(x) \qquad (15)$$

where,

$$p_1(x)=\frac{e^x}{x}\left(-0.0000035-\frac{0.0010290}{x}+\frac{1.9487646}{x^2}+\ldots\right). \qquad (16)$$

A table of log $p_1(x)$ values was composed to investigate the effect of temperature dependence.

Vallet [9] has derived expressions for $A=\mathbf{A}_2T^{1/2}$, $k=\mathbf{A}_2T^{1/2}e^{(-E/RT)}$ and recursion formulas for calculating the above three cases of temperature dependence.

3. Calculated Thermogravimetric Curves

Integral thermograms were obtained by calculating Φ and T at various x and substituting Φ into eq (17).

$$(1-C)=\{(n+1)(n-1)\Phi+1\}^{\frac{1}{1-n}} \qquad (n\neq 1)$$
$$(1-C)=e^{(-2\Phi)} \qquad (n=1). \tag{17}$$

Figure 3 contains curves for the residual fraction, $1-C$, versus temperature for various orders from 0 to 4 for the case $A/\beta=10^{16}/°K$, $E=60{,}000$ cal/mol.

The differential thermograms corresponding to the integral curves in figure 3 were obtained by substitution of values of Φ at various T into

$$\frac{dC}{dT}=\frac{(n+1)A}{\beta}\{(n+1)(n-1)\Phi+1\}^{-\frac{n}{n-1}}e^{(-E/RT)}. \tag{18}$$

These thermogravimetric rate versus temperature curves are contained in figure 4.

Zero and negative orders exhibit ever accelerating rates. Curves for orders between zero and unity go through a maximum rate and, in the idealized case, reach completion at a finite temperature. For curves with $n \geq 1$, increasing order results in a more gradual slope and a more gradual asymptotic approach to the abscissa.

Integral thermograms for the "maximum" Cases A, B, and C were obtained for the same values of A/β and E by calculating Φ at various values of C from the integrated equations for the three cases. The corresponding x and T values were obtained from Φ. Residual fraction versus temperature curves for these cases are contained in figure 5. The early negative-order character of these curves manifests itself by a more precipitous slope than for the zero order curve at the same activation energy.

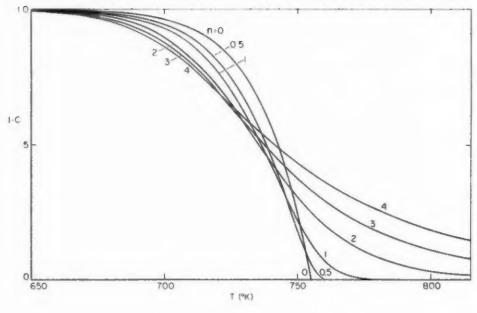

FIGURE 3. *Effect of order on residual fraction versus temperature.*
$n=0$, 0.5, 1.0, 2.0, 3.0, and 4.0;
$A/\beta=10^{16}/°K$; $E=60{,}000$ cal/mol.

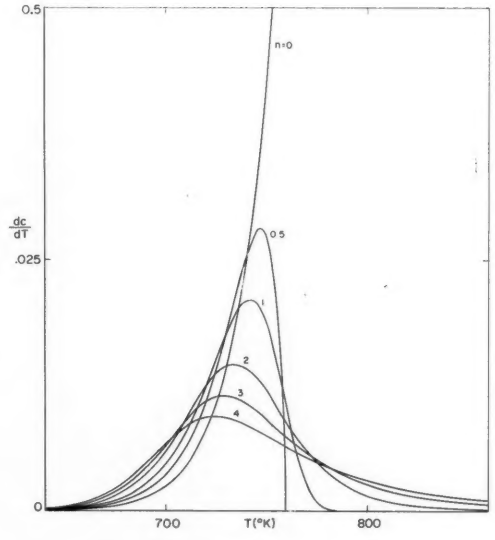

FIGURE 4. *Effect of order on thermogravimetric rate versus temperature.*
$n=0$, 0.5, 1.0, 2.0, 3.0, and 4.0;
$A/\beta=10^{16}/°K$; $E=60{,}000$ cal/mol.

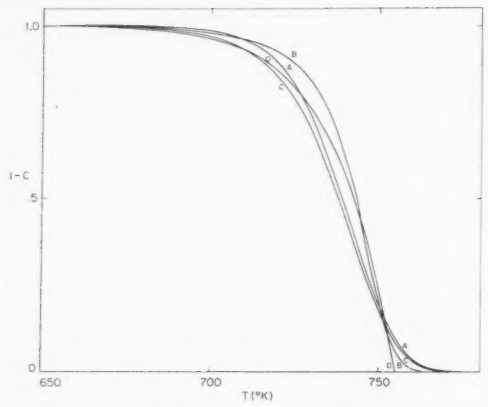

FIGURE 5. *Residual fraction versus temperature for Cases A, B, and C.*
$A/\beta = 10^{16}$/°K; $E = 60{,}000$ cal/mol.

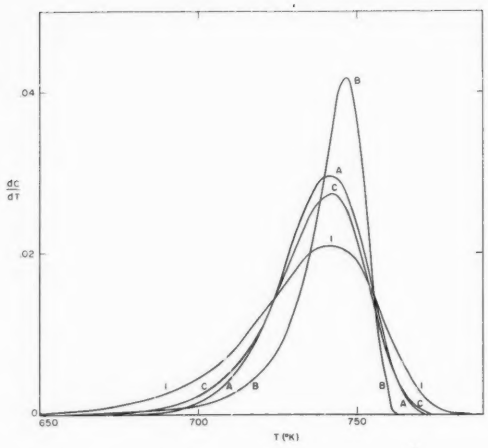

FIGURE 6. *Thermogravimetric rate versus temperature for Cases A, B, and C.*
$A/\beta = 10^{16}$/°K; $E = 60{,}000$ cal/mol.

The corresponding differential thermograms for Cases A, B, and C were obtained by direct substitution of C and the corresponding T values from the integral calculations into eq (9).

The thermogravimetric rate is plotted against temperature for these cases and the same values of A/β and E in figure 6. The first order curve is included for comparison.

The minor detail of the differences among Cases A, B, and C is not significant as these curves are based on asymptotic or semiempirical equations. The slope is greatest in Case B where the maximum isothermal rate is at 50 percent conversion. As γ (maximum rate/initial rate) approaches unity, the curves would more nearly resemble zero order with a tail.

3.1. Thermogravimetric Rate Versus Conversion Curves

The previous figures (figs. 3–6) of residual fraction or thermogravimetric rate versus temperature have been the traditional methods of representing thermogravimetric data. It is surprising that plots of the rate as a function of degree of conversion (dC/dT versus C) have not been utilized as similar presentation has been found to be quite informative in isothermal studies, e.g., figure 1.

Figure 7 exhibits the thermogravimetric rate as a function of conversion for zero through fourth order and Cases A, B, and C for $A/\beta = 10^{16}$/°K and $E = 60{,}000$ cal/mol.

The zero order curve is almost linear while higher order curves go through a maximum rate as $C \to 1$. They approach the zero order curve as $C \to 0$. Curves B and C also approach the zero order curve asymptotically at low conversion but deviate in the direction of negative order. Curve A is anomalous at $C \to 0$ as was mentioned previously.

A better insight into the behavior of the curves in figure 7 may be obtained by differentiating eq (9) with respect to conversion to obtain

$$\frac{d^2C}{dCdT} = \frac{E}{RT^2} + \frac{f'(C)}{f(C)}\frac{dC}{dT} \tag{19}$$

where $f'(C)$ is the derivative of $f(C)$ with respect to C. If $f(C)$ is given by eq (3), then similar differentiation of eq (11) gives

$$\frac{d^2C}{dCdT} = \frac{E}{RT^2} - \frac{n}{1-C}\frac{dC}{dT}. \tag{20}$$

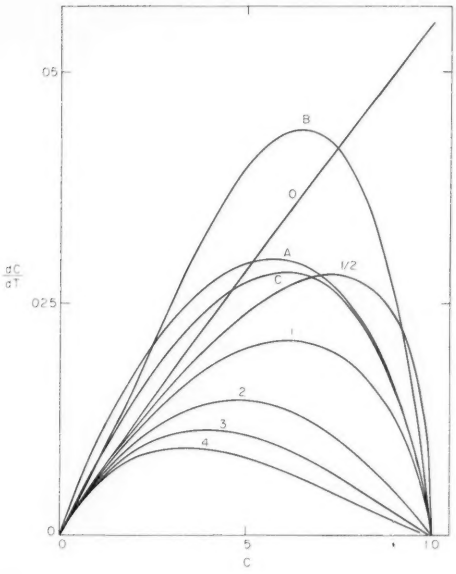

FIGURE 7. *Thermogravimetric rate versus degree of conversion.*
$n = 0, 0.5, 1.0, 2.0, 3.0,$ and 4.0
Cases A, B, and C
$A/\beta = 10^{10}$/°K; $E = 60{,}000$ cal/mol.

Thus the slope of the zero order curve will be given by E/RT^2. At ordinary activation energies, the absolute temperature is a slowly changing variable over the reaction temperature range so the slope will be essentially a constant. The thermogravimetric rate is quite small at low conversion so all other cases approach the zero order case as $C \rightarrow 0$, subject to the condition, $f(C=0) \neq 0$.

Thus, one may obtain a qualitative understanding of the early kinetics from the limiting characteristics of dC/dt versus C. If the curve is initially concave, a negative order character, i.e., an initially increasing isothermal rate as in Cases B and C is indicated. Initial convexity suggests positive order behavior, while approximate linearity connotes kinetics not far removed from zero order. Indeed such a plot may be of great practicable applicability, e.g., to test whether an apparent maximum rate in an isothermal curve is due to an initial temperature lag or an actual initial increase in rate.

3.2. Effects of Activation Energy

The effect of change in energy of activation upon the character and shape of the thermograms was investigated by considering three cases of first order kinetics—I, $E = 60{,}000$ cal/mol, II, $E = 40{,}000$ cal/mol, and III, $E = 80{,}000$ cal/mol. The parameters A/β were adjusted so that the maximum slopes occur at the same temperature in each case. The integral curves are plotted in figure 8 and the corresponding differential curves in figure 9.

The maximum slope increases linearly with increasing energy of activation since, from eq (20), at the maximum

$$\left(\frac{dC}{dT}\right)_{\max} = \frac{E(1-C)_{\max}}{nRT^2_{\max}} \tag{21}$$

Other relationships at the maximum will be discussed in the section on differential methods.

3.3. Effect of a Temperature Dependence of the Preexponential Factor

A slight temperature dependence of the preexponential factor is sometimes noted in isothermal studies. Indeed, according to collision theory, A is proportional to $T^{1/2}$ for a bimolecular gas phase reaction and, according to transition state theory, the preexponential factor contains temperature to the first power.

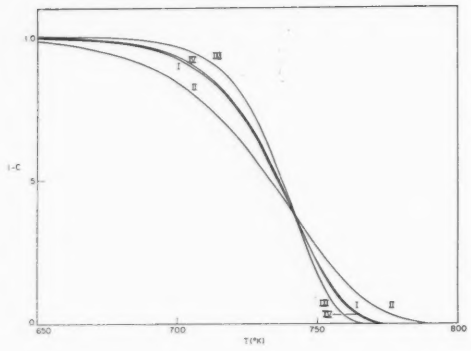

FIGURE 8. *Effects of activation energy and preexponential temperature dependence on residual fraction versus temperature.*

$n=1$
I $E=60{,}000$ cal/mol; $A/\beta=10^{16}$/°K
II $E=40{,}000$ cal/mol; $A/\beta=9.675\times10^{9}$/°K
III $E=80{,}000$ cal/mol; $A/\beta=9.318\times10^{21}$/°K
IV $E=60{,}000$ cal/mol; $A/\beta=1.374\times10^{13}$/°K; $A(T)$.

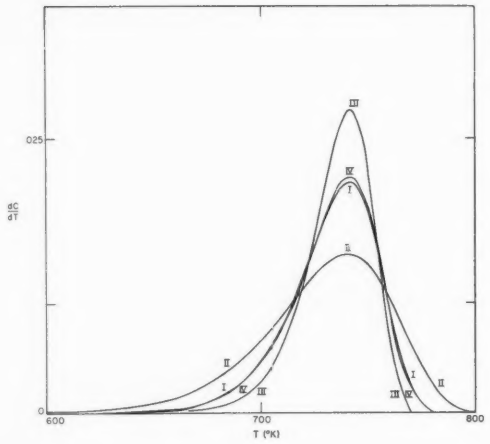

FIGURE 9. *Effects of activation energy and preexponential temperature dependence on thermogravimetric rate versus temperature.*

$n=1$
I $E=60{,}000$ cal/mol; $A/\beta=10^{16}$/°K
II $E=40{,}000$ cal/mol; $A/\beta=9.675\times10^{9}$/°K
III $E=80{,}000$ cal/mol; $A/\beta=9.318\times10^{21}$/°K
IV $E=60{,}000$ cal/mol; $A/\beta=1.374\times10^{13}$/°K; $A(T)$.

Since in both isothermal and thermogravimetric cases usually the same analytic process is involved in activation energy determination, i.e., the logarithm of some function of a rate is plotted against $1/T$(°K), any error resulting from ignoring temperature dependence in the determination of E should be about the same in both cases. If A is linearly dependent on temperature, the differentiation of the logarithm of eq (14) with respect to $1/T$ results in

$$\frac{d\ln k}{d\left(\frac{1}{T}\right)}=-T-\frac{E}{R}. \tag{22}$$

Thus, at $T=500$ °K, the correction for linear temperature dependence of A on the experimentally obtained activation energy will be about 1 kcal/mol.

In order to observe the effect of linear temperature dependence of the preexponential factor on the shape of a thermogram, Case IV, $E=60{,}000$ cal/mol, $\mathbf{A}_1/\beta=1.374\times10^{13}$ (°K)$^{-2}$, was calculated for various orders using $p_1(x)$ values obtained from eq (16). The integral and differential curves for first order kinetics may be compared with Case I, $E=60{,}000$ cal/mol, $A/\beta=10^{16}$ (°K)$^{-1}$ in figures 8 and 9. The difference is trivial for these conditons. The effect is in the direction of increased slope and is greater for higher orders. It will be significant only at very low activation energies.

If a single Arrhenius expression is applied to situations involving simultaneous reactions, the parameters E and A well may exhibit temperature dependence. This aspect is discussed in the section on composite cases.

3.4. Effect of Rate of Heating

Analyses of the changes in thermogravimetric data brought about by variation of the rate of heating, β, are the basis for the most powerful methods for the determination of kinetic parameters and these methods are discussed in subsequent sections.

Figure 10 contains the integral curves for Case B with maximum isothermal rate at 50 percent completion for $A/\beta_2=10^{16}$/°K, $E=60{,}000$ cal/mol and heating rates of $\beta_1=0.05$, $\beta_2=0.10$, and

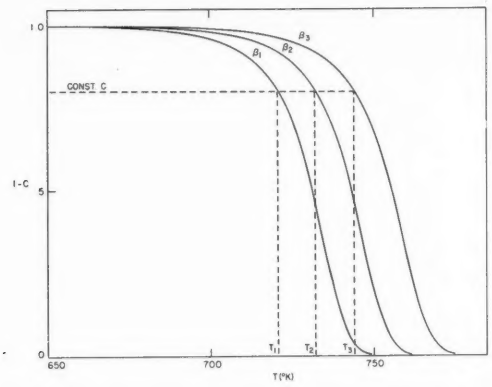

FIGURE 10. *Effect of heating rate on residual fraction versus temperature.*
Case B: $A=10^{15}$/sec, $E=60{,}000$ cal/mol, $\beta_1=0.05$, $\beta_2=0.10$, $\beta_3=0.20$ °K/sec.

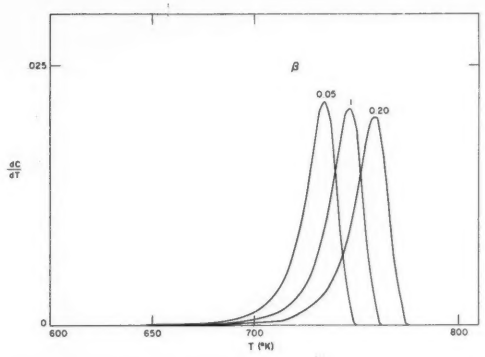

FIGURE 11. *Effect of heating rate on thermogravimetric rate versus temperature.*
Case B: $A=10^{15}$/sec, $E=60{,}000$ cal/mol, $\beta_1=0.05$, $\beta_2=0.10$, $\beta_3=0.20$ °K/sec.

$\beta_3=0.20$ °K/sec. Figure 11 contains the thermogravimetric rate curves for the same case and conditions. Not only are the curves shifted to higher temperatures by increased heating rates but they become less steep.

3.5. Composite Cases

The majority of experimental thermograms found in literature represent cases in which two or more volatilization reactions take place. If the values for the kinetic parameters, e.g., E and A, for each reaction are such that the regions of weight loss occur at separated temperature ranges then a stepwise thermogravimetric trace results. In these cases, each curve between successive horizontal portions may be treated separately. However, many cases are more complex. An example is a polymer which undergoes both depolymerization and side group splitting or ring formation, followed by depolymerization of the thermally more stable product polymer.

Here we investigate only two simple cases:

(1) Two Independent First Order Reactions

If a fraction of the material, a, volatilizes by a first order reaction with Arrhenius parameters A_1 and E_1, and the remainder of the material volatilizes by an independent first order reaction with parameters A_2 and E_2, the residual fraction will be given by

$$1-C=a\left[e^{-\frac{A_1E_1}{\beta R}p\left(-\frac{E_1}{RT}\right)}\right]+(1-a)\left[e^{-\frac{A_2E_2}{\beta R}p\left(-\frac{E_2}{RT}\right)}\right]. \tag{23}$$

(2) Two Competitive First Order Reactions

If the total material may be volatilized by two alternative paths, each having a rate proportional to the first power of all remaining volatilizable material and if the respective Arrhenius parameters are A_1 and E_1 and A_2 and E_2 for the two paths, then the residual fraction will be

$$1-C=e^{-\frac{A_1E_1}{\beta R}p\left(-\frac{E_1}{RT}\right)-\frac{A_2E_2}{\beta R}p\left(-\frac{E_2}{RT}\right)}. \tag{24}$$

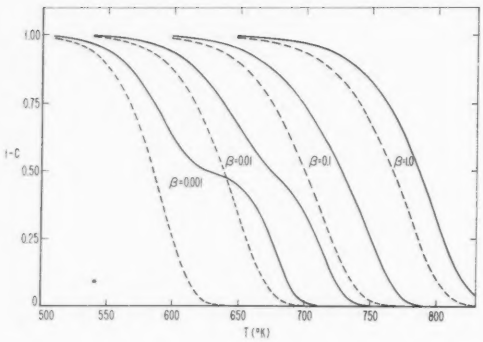

FIGURE 12. *Effect of heating rate on residual fraction versus temperature for composite cases.*
$E_1 = 30{,}000$ cal/mol; $A_1 = 4.458 \times 10^6$/sec
$E_2 = 60{,}000$ cal/mol; $A_2 = 10^{15}$/sec
$\beta = 0.001$, 0.01, 0.1 and 1.0 °K/sec
———— Case (1), independent first order reactions
– – – – – Case (2), competitive first order reactions.

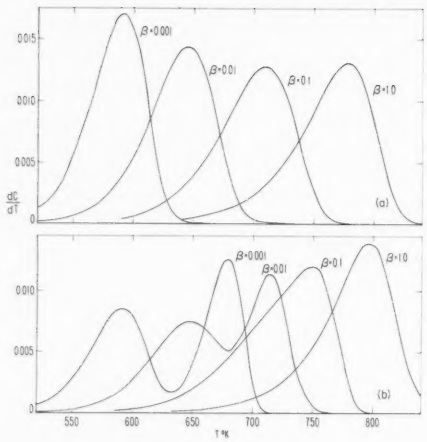

FIGURE 13. *Effect of rate of heating on the thermogravimetric rate versus temperature for composite cases.*
E_1, E_2, A_1, and A_2 as in figure 12
(a) Case (2) competitive first order reactions
(b) Case (1) independent first order reactions.

To observe the effect of variation of heating rate in these composite cases, integral and differential curves were calculated for $a = 0.5$, $E_1 = 30{,}000$ cal/mol, $E_2 = 60{,}000$ cal/mol, $A_2 = 10^{15}$/sec and $A_1 = 4.458 \times 10^6$/sec for heating rates of 1.0, 0.1, and 0.01, and 0.001 °K/sec. The value of A_1 was selected so that for Case (1) at $\beta = 0.1$ °K/sec and $C = 0.5$, the first reaction contributes 75 percent to 1−C and the second reaction, the remaining 25 percent.

The integral curves are shown in figure 12 and the differential curves in figures 13a and 13b for the two cases.

Such a thousand-fold variation in heating rate is not easily realizable experimentally, but was used in these theoretical calculations to illustrate as wide a variety of situations as possible.

It is immediately apparent from inspection of figures 12 and 13 and eqs (23) and (24) that for these cases of two first order reactions with widely differing activation energies, the thermograms for Cases (1) and (2) exhibit quite different variations in structure upon changing the heating rate.

Case (1), (independent reactions), at the highest heating rate (and temperature), ($\beta = 1.0$), gives the appearance of one simple thermogram as the two reactions broadly overlap one another. As the heating rate is lowered, ($\beta = 0.1$), the curve tends to flatten as the two reactions begin to separate. The decrease in the value of the thermogravimetric rate at the maximum with decreasing β is the opposite of simple reactions as seen in figure 11.

At $\beta = 0.01$, the two reactions separate further and two peaks are obtained on the differential curve. It may be noted that at these conditions the "maximum" temperature for the higher activation energy reaction has been shifted five degrees by the perturbing influence of the low energy reaction.

By $\beta = 0.001$, the low energy reaction, favored at the lower temperature, is almost completely separated from the high energy reaction.

On the other hand, in Case (2) (competitive reactions), for the values of parameters considered, the low activation energy reaction takes over almost completely at low temperature and heating rates ($\beta = 0.001$ and $\beta = 0.01$). At the high heating rate, ($\beta = 1.0$), the low activation energy reaction dominates only during the first 30 percent of weight loss, with the high energy reaction considerably modifying the latter portion of the thermogram. Again, the inclusion of the high energy reaction causes a temporary increase in $(dC/dT)_{max}$ with increasing β. In simple reactions the maximum rate decreases upon increasing β and T_{max}, [see eq (21)].

Two competitive first order reactions with equal activation energies ($E_1 = E_2$) appear as a simple first order reaction no matter how great the difference in preexponential factors. This

is true of any set of competitive reactions of the same order. If they are of differing order, then they are, in theory, resolvable.

The differentiation between two independent first order reactions with the same activation energies depends upon how greatly A_1/A_2 deviates from unity. The resolution is relatively unaffected by changing the rate of heating.

Thus, the technique of varying the rate of heating in composite cases not only often permits a separation of reactions but often gives information as to the nature of the competition between reactions. This aspect is discussed further in succeeding sections on methods of kinetic analysis.

The application of more complex empirical substitutes for the Arrhenius equation to experimental data involving composite reactions has been discussed by Farmer [16].

4. Critical Survey of Methods of Kinetic Analysis

The methods of kinetic analysis of thermogravimetric data are divided into five categories to facilitate discussion and comparison. These are—(a) "Integral" methods utilizing weight loss versus temperature data directly, (b) "Differential" methods utilizing the rate of weight loss, (c) "Difference-Differential" methods involving differences in rate, (d) Methods specially applicable to initial rates, and (e) Nonlinear or cyclic heating rate methods.

4.1. Integral Methods

The fundamental criticism of integral methods as applied to a single thermogravimetric trace is that "best values" of A, E, and n are inevitably fitted to the data whether or not these parameters have any significance or even utility in the understanding of mechanism. Also to obtain the activation energy the order must be known or vice versa. This latter problem has been met with varying success in several ways.

As many of these methods involve an approximate integration of the exponential integral, they will be compared to eqs (13a, b, c, d) when applicable.

The first serious theoretical treatment of thermogravimetric data was by van Krevelen et al., [17]. These authors approximated the exponential integral by making the substitution

$$e^{-\frac{E}{RT}} = \left(e^{-\frac{T_{max}}{T}}\right)^{\frac{E}{RT_{max}}} \cong \left(0.368\frac{T}{T_{max}}\right)^{\frac{E}{RT_{max}}} \tag{25}$$

where T_{max} is the temperature at the maximum thermogravimetric rate. Thus, they obtained for eq (4) in logarithmic form

$$\left.\begin{array}{r} \ln\left[\dfrac{(1-C)^{1-n}-1}{1-n}\right] \\ (n \neq 1) \\ \ln\ln(1-C) \\ (n=1) \end{array}\right\} = \ln\left[\frac{AR}{\beta E}\left(\frac{0.368}{T_{max}}\right)^{\frac{E}{RT_{max}}}(T_{max}+1)\right] + \frac{E}{R(T_{max}+1)}\ln T \tag{26}$$

and tested for linearity of $\ln T$ for various values of n. Reactions are insensitive to order at low conversion so in order to obtain n from this or similar methods linearity must be established at high conversion. However, linear plots over much of the conversion range were obtained from eq (26), $n=1$, for Cases B and C with maximum isothermal rates. Thus, the method should be limited to cases in which a known isothermal order is followed.

Baur et al. [18], in 1955 applied a graphical solution of the exponential integral to the case of a linearly temperature dependent preexponential factor (eq (15)) for data on the high pressure oxidation of metals and obtained good agreement between experimental values and theoretical values based on a parabolic rate law. Smith and Arnoff [8] in 1958 calculated a table of $p(x)$ values for $x=1$ to 50 and used it to fit data on the thermodesorption of gases from solids to first and second order kinetics by a method of trial and error.

Doyle [10], in 1961, presented the most formal method for the precise curve fitting of a single thermogram using calculated tables of log $p(x)$. However, as in other such methods, its applicability is limited to cases of known isothermal order. As the method is quite tedious, Doyle devised an approximate method based on the first two terms of the asymptotic expansion (eq (13a)).

$$p_{a,2}(x) \cong e^{-E/RT}\left(\frac{E}{RT}\right)^{-2}. \tag{27}$$

For cases of unknown order, Doyle [10] suggests making calculations as early in the reaction as experimental accuracy allows. However, even using $C=0.05$, one obtains appreciable errors in the determined activation energy when this method is applied to maximum Cases A, B, and C. Nevertheless, such integral curve fitting of a single trace is more generally applicable than similar differential methods.

Farmer [16] defines the relative error using the two term asymptotic approximation as

$$r_2=\frac{p(x)}{p_{a,2}(x)}. \tag{28}$$

This relative error, r_2, and r_3, the relative error in using three terms of the asymptotic approximation, are shown for several values of x in table 1.

TABLE 1. *Relative errors for two- and three-term asymptotic approximations of* p(x) [a] *as a function of* x=(−E/RT) *[15, 16]*

	−x				
	10	20	30	40	50
r_2	0.844	0.913	0.939	0.954	0.962
r_3	1.055	1.014	1.006	1.004	1.002

[a] $p(x)=-\frac{e^x}{x}+\int_{-\infty}^{x}\frac{e^x}{x}dx$.

Farmer [16] substituted eqs (27) and (28) into eq (10) to obtain in logarithmic form

$$\log\frac{\int_0^C\frac{dC}{f(C)}}{T^2}=-\frac{E}{2.303R}\left(\frac{1}{T}\right)+\log\left[r_2\frac{RA}{\beta E}\right] \tag{29}$$

or

$$-T\log\frac{\int_0^C\frac{dC}{f(C)}}{T^2}=-T\log\left[r_2\frac{RA}{\beta E}\right]+\frac{E}{2.303R}.$$

where r_2 is a slowly changing function of temperature. The second expression was found to be sensitive to data point deviation.

As $r_3/r_2=1+2/x=1-(2RT/E)$, if the first three terms of the asymptotic approximation are

utilized and if $f(C)$ is given by eq (3) then

$$\left.\begin{array}{rl} \log\left[\dfrac{1-(1-C)^{1-n}}{T^2(1-n)}\right] & \\ (n\neq 1) & \\ \log\left[\ln\dfrac{1-C}{T^2}\right] & \\ (n=1) & \end{array}\right\} \cong \log\frac{AR}{\beta E}\left[1-\frac{2RT}{E}\right]-\frac{E}{2.303RT} \tag{30}$$

which was developed by Coats and Redfern [2, 19]. A plot of $\log F(C)/T^2$ versus $1/T$ appears to give quite satisfactory results when the kinetics follow a simple order. However, as with previous methods, application to systems of "changing order," e.g., maximum Case B, results in erroneous values for E.

As Doyle has done, Coats and Redfern [20] have gone to low conversion data to get around the problem of determining order.

Assuming all reactions behave as zero order as $C\rightarrow 0$, they obtain from eq (30)

$$\log\frac{C}{T^2}=\log\frac{AR}{\beta E}\left[1-\frac{2RT}{E}\right]-\frac{E}{2.303R}\frac{1}{T} \tag{31}$$

and a plot of $\log C/T^2$ versus $1/T$ for low C or $n\cong 0$ should give a straight line with slope of $-E/4.6$ as $\log AR/\beta E[1-2RT/E]$ is again sensibly constant. It is doubtful that this approximation may be generally used up to $C=0.3$ as is suggested as for at $n=2$, the error in $F(C)$ amounts to 40 percent at $C=0.3$.

Horowitz and Metzger [21] simplify the exponential integral with an approximation similar to but simpler than van Krevelen et al., i.e., defining a characteristic temperature, θ, such that $\theta=T-T_S$ where T_S is a reference temperature at which $1-C=1/e$. Then making the approximation

$$\frac{1}{T}=\frac{1}{T_S+\theta}=\frac{1}{T_S\left(1+\dfrac{\theta}{T_S}\right)}\cong\frac{1}{T_S}-\frac{\theta}{T_S^2} \tag{32}$$

they finally obtain for $n=1$,

$$\ln\ln(1-C)\cong\frac{E\theta}{RT_S^2} \tag{33}$$

so that a plot of $\ln\ln(1-C)$ versus θ should give linearity with a slope of E/RT_S^2.

For cases in which $n\neq 1$, more complicated expressions are suggested [21] involving derivative parameters and T_S is defined as the temperature at the inflection point.

One may obtain from eq (12) using eq (13d) for $\log p(x)$ and making the approximation of eq (32)

$$\ln\ln(1-C)\cong\ln\frac{AE}{\beta R}-5.33-\frac{1.052}{T_S}+\frac{1.052E\theta}{RT_S^2} \tag{34}$$

which gives the same slope as eq (33). However, eq (34) does not include the condition that T_S is the temperature at which $1-C=1/e$.

230-736 O-66—4

Thus, eq (34) suggests the generalization of Horowitz and Metzer's method to the case where $n \neq 1$ and T_S is any reference temperature as in eq (35). (The "constant," 1.052, may be improved upon once an approximate E has been determined from a table of first differences of log $p(-E/RT)$ for various E/RT, [11].)

$$\ln[1-(1-C)^{1-n}] \cong \text{constant} + \frac{1.052E\theta}{RT_S^2} \tag{35}$$

$$(n \neq 1)$$

E may be calculated using eq (33) with fair agreement with theoretical values for $E = 60{,}000$ cal/mol, $A/\beta = 10^{16}/°\text{K}$ for $n = 1$, but theoretical data for $n = 1/2$ as well as, for example, maximum Case C, also give nearly linear plots for ln ln$(1-C)$ versus θ over a wide range and high values for the energy of activation.

Few papers on computational methods have been published [2, 22], but such methods are probably widely used. McCrackin [23], in an unpublished work, has programmed a method in which a series of weights, w_i, and temperatures, T_i, are fed to the computer and values of $(1-C)_i$ and $F(C_i)$ are computed for each temperature, assuming n. From equations

$$F(C_i) = \int_0^C \frac{dC}{(1-C)^n} = \frac{A}{\beta} x_i \tag{36}$$

where $x_i = (E/R)\Gamma_{-1}(E/RT)$ and Γ_{-1} is the incomplete gamma function of -1 order, values of x_i are computed for an assumed E and data fitted to eq (36) to determine A/β. Assuming the error in C_i is only experimental and independent of its value, $F(C_i)$ will have a constant variance so the best estimate for A/β will be given by

$$\frac{A}{\beta} = \frac{\sum_i x_i F(C_i)(1-C_i)^{2n}}{\sum_i x_i^2 (1-C_i)^{2n}}. \tag{37}$$

From eq (36), $F(C_i)$ is computed for each **i** using the calculated values of A/β. Then, $(1-C_i)$ and W_i are computed. The standard error of fit is

$$\sigma(n, E) = \frac{[W_i(\text{calc}) - W_i(\text{expt})]^2}{N-2} \tag{38}$$

$N =$ No. of values of T and W.

This is computed for various values of n and E and the values that give the smallest σ are chosen.

To summarize, the computer calculates and prints σ for values of E for $n = 0, 1/2, 1, 3/2, 2$, and 3. Then, for each n, it chooses the value of E that gives the minimum σ and prints E, σ and A/β for each n. It then prints $W_i(\text{calc}) - W_i(\text{expt})$ for these values of E.

Since only if $W_i(\text{calc}) - W_i(\text{expt})$ remains sensibly constant over the entire range can the system be said to have a particular n and E, it would appear that McCrackin's method tests the validity of its assumptions.

Reich and Levi [24] have developed a method involving the determination of the area under the initial part of an integral thermogram to obtain an approximate expression for the energy of activation. Doyle [25] points out that such a method should be less sensitive to experimental scatter than line or slope methods. The corrected derivation [25] of the equations includes the

approximation in eq (13d), i.e., $p(x)=Ge^{x}$, to obtain for $n=1$,

$$\ln A_i \cong \ln \frac{A}{\beta}\left(\frac{EG}{R}\right)^2 - \frac{E}{RT} \tag{39}$$

which for two different initial areas becomes

$$E \cong \frac{\ln\left(\frac{A_{I+II}}{A_I}\right)}{R\left(\frac{1}{T_I}-\frac{1}{T_{I+II}}\right)} \tag{40}$$

where A_{I+II}/A_I is the ratio of initial areas. As will be shown subsequently, the coefficient of E/RT assumed to be unity in eq (39) is a slowly changing function of E/RT and more accurate values may be obtained for E by successive approximations. Also, the general utility of eq (40) depends on the lack of sensitivity to order in the early conversion range.

Reich [26] has pointed out that at small and constant ΔT from eq (11)

$$\left.\begin{matrix}\ln C \\ (n=0) \\ \\ \ln \ln (1-C) \\ (n=1)\end{matrix}\right\} \cong -\frac{E}{RT}+\ln\frac{A}{\beta}\Delta T \tag{41}$$

$\Delta T=$ constant.

Utility of eq (41) is limited to cases in which a particular reaction order, n, is known to be followed.

Reich [27] using the approximations made by Horowitz and Metzger [21] obtained at constant weight loss for two different heating rates,

$$E \cong \frac{4.6 \log \frac{\beta_2}{\beta_1}\left(\frac{T_1}{T_2}\right)^2}{\left(\frac{1}{T_1}-\frac{1}{T_2}\right)} \tag{42}$$

by assuming that $T_{S,1}/T_{S,2}=T_1/T_2$.

However a simpler expression has been developed [11] by the substitution of eq (13d) into eq (10) to obtain

$$\log F(C) \cong \log\frac{AE}{R} - \log\beta - 2.315 - 0.457\frac{E}{RT} \tag{43}$$

so at constant conversion for several heating rates a plot of $\log\beta$ versus $1/T$ will have a slope of

$$\frac{d\log\beta}{d\frac{1}{T}} \cong 0.457\frac{E}{R} \text{ or } E=-4.35\frac{d\log\beta}{d\frac{1}{T}} \qquad (1-C)=\text{constant.} \tag{44}$$

Activation energies may be quite accurately and simply obtained from eq (44) by successive approximations as tables of $\log p(-E/RT)$ and $\Delta\log p(-E/RT)$ for various E/RT are available [10, 11]. Once an approximate E is obtained from eq (44), the "constant," which changes from 0.477 at $E/RT=20$ to 0.449 at $E/RT=60$, is redetermined for the approximate E/RT and successively more accurate values of E are obtained.

The independence of E from C and T may be tested by determining E at various constant conversion values.

In an excellent and important paper, recently to come to our attention, Ozawa [27a] also develops eq (44) but employs it without further refinement to calculate E at several C values. He sets up appropriate theoretical master-curves of $(1-C)$ versus $\log \Phi[=\log (AE/\beta R)p(x)]$ for, e.g., simple nth order reactions and for the random degradation of polymers [eq (6)] for $N \gg L$ and $L=2$, 3, 4, and 5. A more accurate experimental master curve is obtained by superimposing curves of $\log \beta$ versus $1/T$ at several heating rates by displacement along the abscissa. Values of C and T from this curve are used to construct a plot of $(1-C)$ versus $\log [(E/\beta R)p(E/RT)]$ which may be matched to the appropriate theoretical curve by displacement of $\log A$ along the abscissa, thus determining A and confirming the assumed kinetic equation.

This appears to be one of the best and most generally applicable methods yet developed.

If $F(C)$ may be represented as a simple nth order reaction as in eq (3) then eq (44) becomes,

$$\log \left[\frac{(1-C)^{1-n}-1}{1-n}\right] \cong \log \frac{AE}{R} - \log \beta - 2.315 - 0.457 \frac{E}{RT} \qquad (n \neq 1) \tag{45}$$

so for the slopes of plots of $\log \beta$ versus $1/T$ at constant C, $\log [(1-C)^{1-n}-1]$ versus $1/T$ at constant β, and $\log [(1-C)^{1-n}-1]$ versus $\log \beta$ at constant T, one obtains

$$\frac{d \log \beta}{d \frac{1}{T}} \cong -0.457 \frac{E}{R} \cong \frac{d \ln [(1-C)^{1-n}-1]}{d \frac{1}{T}} \tag{46}$$

$(C = \text{constant}) \qquad (\beta = \text{constant}) \qquad (n \neq 1)$

$$\left.\begin{array}{c} -\dfrac{d \log [(1-C)^{1-n}-1]}{d \log \beta} \\ (n \neq 1) \\ -\dfrac{d \log \ln (1-C)}{d \log \beta} \\ (n=1) \end{array}\right\} \cong 1 \tag{47}$$

$(T = \text{constant}).$

The right-hand side of eq (46) may be applied to a single thermogravimetric trace and has the advantage over the approximate methods of Farmer [16] and Coats and Redfern [19], [eq (29) and (30)], in that successive approximations in the manner described above can be used to determine accurate values of the parameters. The order, n, may be tested by eq (47), the correct n giving a horizontal plot.

Once β, n, E, T, and C are known, one may substitute into eq (45) to determine A. Thence, constancy of A with changing T and C should be a confirmation of the validity of n.

As this method is the most adaptable of the integral methods, we demonstrate its utility with the theorietical cases of "changing order" (maximum Cases A, B, and C) and "changing activation energy" [composite Cases (1) and (2)].

Figure 10 contains the integral curves for $\beta_1 = 0.05$, $\beta_2 = 0.10$, and $\beta_3 = 0.20$ °K/sec for Case B with a maximum isothermal rate at $C = 0.5$. Values of T at constant C were obtained from these curves for $C = 0.02$, 0.10, 0.25, 0.50, 0.75, 0.90, and 0.98 and plots of $\log \beta$ versus $1/T$ are shown in figure 14. The slopes of these lines give, from eq (44), $E_{\text{approx.}} = 59{,}300 \pm 200$ cal/mol. Upon reevaluating the constant in eq (44) for $(E/RT)_{\text{approx.}}$, one obtains $E_{\text{corrected}} = 59{,}850$ cal/mol compared with the theoretical value of 60,000 [11].

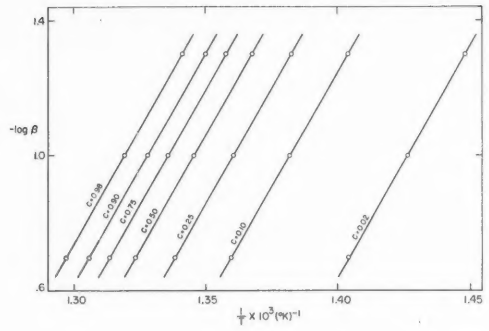

FIGURE 14. *Logarithm of heating rate versus reciprocal absolute temperature for maximum Case B.*
$A = 10^{15}$/sec; $E = 60{,}000$ cal/mol
$\beta_1 = 0.05$, $\beta_2 = 0.10$, $\beta_3 = 0.20$ °K/sec;
$C = 0.02$, 0.10, 0.25, 0.50, 0.75, 0.90, and 0.98.

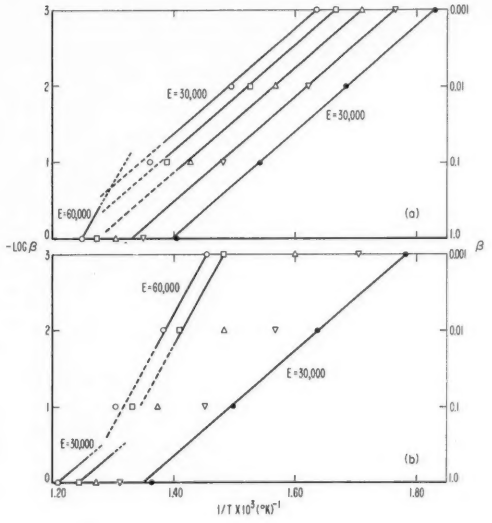

FIGURE 15. *Logarithm of heating rate versus reciprocal absolute temperature for composite cases.*
E_1, E_2, A_1, A_2, and β as in figure 13
(a) Case (2) competitive first order reactions
(b) Case (1) independent first order reactions
●, $C = 0.10$ □, $C = 0.75$
▽, $C = 0.25$ ○, $C = 0.90$.
△, $C = 0.50$

Therefore, this not only permits determination of the correct activation energy for this case of "changing order" but establishes its independence of C and T over the reaction range.

Equation (44) should not be expected to apply to composite cases since it was derived assuming a single temperature dependent rate constant. However, application to the independent and competitive first order reactions shown in figure 12 and 13 demonstrate some of the limitations of the method and how it may be utilized to interpret these simple cases.

In figure 15, log β is plotted against $1/T$ for—(a) two first order competitive reaction, and (b) two first order independent reactions, for $E_1 = 30{,}000$, $E_2 = 60{,}000$ cal/mol, $\beta = 0.001$, 0.01, 0.1 and 1.0 °K/sec and $C = 0.10$, 0.25, 0.50, 0.75, and 0.90. The theoretical slopes for $E_1 = 30{,}000$ and $E_2 = 60{,}000$ cal/mol are included as guidelines.

For two competitive reactions, (fig. 15a), at low conversion, ($C = 0.10$), the low activation energy reaction is dominant at all heating rates so a slope corresponding to 30,000 cal/mol is obtained. At high conversion, ($C = 0.90$), the low energy reaction is still dominant at slow heating rates but the intrusion of the high activation energy reaction can be observed at fast β. A readjustment of the parameters could set up a situation in which the high energy reaction was dominant except at low C and β.

For two independent first order reactions (fig. 15b), at low conversion and slow β, the low energy reaction is dominant but at low C and fast β the slope is perturbed by the high energy reaction. At high conversion, the high energy reaction is dominant at slow β, but, as before, a mixture of E_1 and E_2 reactions contribute at fast β.

In general, employing the lowest practicable heating rate will best isolate competing reactions. However, it may occasionally be expedient to raise the heating rate to pick up a high energy reaction that may not be easily discernible under near-isothermal conditions.

We conclude, therefore, that only methods involving several heating rates can give the correct activation energy for cases of "varying order" (Cases A, B, and C) and reveal and, to some extent, resolve cases of "varying activation energy" (Cases (1) and (2)) in which several competing reactions occur.

The integral methods involving a single thermogram appear to be applicable only in special cases in which the isothermal order is known and meaningful. However, integral curve fitting should be considered important corraborative evidence in the testing of mechanism.

4.2. Differential Methods

"Differential" methods based on rate of weight loss versus temperature data have been devised which are much simpler in application and, in some cases, are able to circumvent difficulties found in many "integral" methods. However, they suffer from an inherent weakness—the magnification of experimental scatter—often rendering their application to experimental data difficult, if not impossible.

Van Krevelen et al. [17], calculated solutions for $p(x)$ using two terms of eq (13c) and plotted families of curves for various T_{max} for log $(T(dC/dT))_{max}$ and log $(\Delta T/T)_{max}$ versus log E/R for first order reactions. ΔT is the half-width of the differential curve.

Turner and Schnitzer [28] used three terms of eq (13c) for $p(x)$ and refined van Krevelen's relationships for $n=1$ to obtain expressions relating E/R to T_{max} and ΔT. ΔT, T_{max} and $(dC/dT)_{max}$ were estimated from a differential curve for each of several composite reactions and values for the parameters obtained. Turner et al. [29], using an identical development, obtained similar expressions for $n=2/3$. However, the equations in references [28] and [29] are in error [15].

Kaesche-Krischer and Heinrick [30] used van Krevelen's method at several heating rates to investigate the composite kinetics of polyvinyl alcohol decomposition. The utility of this method depends on how closely the assumed order of kinetics is followed. If the kinetics, in reality, behaves as a lower order reaction, then the calculated value for E will be too high, and conversely, if n is greater than its assumed value, the calculated E will be too low. Application of this method to maximum Cases A, B, and C gave activation energies from 70 to 150 kcal/mol compared with the theoretical value of 60. Van Krevelen [17], assuming $n=1$, obtained activation energies for polystyrene and polyethylene of 82 and 98 kcal/mol. These polymers which often exhibit maximum type isothermal rate curves usually have activation energies of the order of 55 and 70 kcal/mol, respectively [5].

Equation (11) at the maximum rate becomes

$$\left(\frac{dC}{dT}\right)_{max}=\frac{A}{\beta}(1-C)^n_{max}e^{-E/RT_{max}} \tag{48}$$

which may be combined with eq (21) and eq (30) which utilizes the three term asymptotic approximation to obtain

$$\frac{E}{RT^2_{max}}=\frac{A}{\beta}n(1-C)^{n-1}_{max}e^{-E/RT_{max}} \tag{49}$$

and

$$n(1-C)^{n-1}_{max}\cong 1+(n-1)\frac{2RT_{max}}{E} \tag{50}$$

$$(n>0,\neq 1)$$

$$\ln(1-C)_{max}\cong\left[1-\frac{2RT_{max}}{E}\right]$$

$$(n=1).$$

These eqs (48), (49), and (50) were first derived for first order reactions and used by Murry and White [31]. The solution of eq (49) was facilitated by using several heating rates. Kissinger [32] extended Murry and White's method to any order, n, by deriving eqs (48), (49), and (50) as shown above.

Kissinger [33] differentiated the logarithm of eq (49) to obtain for $n=1$

$$\frac{d \ln \frac{\beta}{T^2_{max}}}{d \frac{1}{T_{max}}} \cong -\frac{E}{R}. \tag{51}$$

Thus the activation energy may be obtained from the shift of the maximum temperature with heating rate. Equation (51) is identical to eq (42) which was also derived assuming $n=1$ and a reference temperature [27, 21]. Substituting eq (50) into (49) and differentiating the logarithm assuming T_{max} changes slowly with β, Kissinger [32] again obtains eq (51) now for any n.

Kissinger [32] also has developed a shape index, s, defined as the absolute value of the ratio of the tangents to the differential curves at the inflection points and related to the order by

$$n=1.26\, s^{1/2}. \tag{52}$$

Such higher derivative methods are seldom practical for polymer degradation studies.

Fuoss et al. [34], suggest determining the three maximum values, T_{max}, $(dC/dT)_{max}$ and $(1-C)_{max}$ from the inflection point of the integral curve and determining the activation energy from eq (21). The method as described [34] is applicable only to first order kinetics and not to all orders as is implied by the omission of n from eq (21). Such an omission leads, obviously, to the exceptionally high value for E for polystyrene indicated in this paper [34].

However, $(1-C)_{max}$ is relatively independent of the heating rate, β. If eq (10) including two terms of the asymptotic approximation, eq (13a), is combined with eq (49) at the maximum, one obtains

$$(1-C)_{max} \cong n^{\frac{1}{1-n}} \qquad (n>0, \neq 1). \tag{53}$$

Equation (53) was first pointed out by Kissinger [32] and also was derived by Horowitz and Metzger [21] from their nearly equivalent approximation. Thus eq (21) becomes

$$E \cong n^{\frac{n}{n-1}} R T^2_{max} \left(\frac{dC}{dT}\right)_{max} \qquad (n>0, \neq 1). \tag{54}$$

The last two columns in table 2 give the approximate $(1-C)_{max}$, [i.e., columns $(1-C)_{max}(x=\infty)$ and $n^{n/n-1}R(x=\infty)$], which may be utilized with eq (54) to determine activation energies if the value and constancy of n have been established. If $(1-C)_{max}$ is independent of β, then from eq (21) $T^2_{max}(dC/dT)_{max}$ must also be independent. Such independence is inherent in the use of the two term asymptotic approximation as differentiation of eq (48) with respect to β assuming $T^2_{max}(dC/dT)_{max}$ and $(1-C)_{max}$ constant results in eq (51).

TABLE 2. *Values of* $(1-C)_{max}$ *for various orders and* x's

n \ $-x$	10	20	30	40	50	∞	$n^{n/n-1}R$ (cal/mol °K)
1/2	0.294	0.273	0.266	0.262	0.260	0.250	3.97
1	.430	.401	.391	.385	.382	.368, 1/e	5.40
3/2	.516	.484	.472	.465	.461	.444	6.71
2	.578	.544	.531	.523	.519	.500	7.95
3	.661	.626	.612	.603	.599	.577	10.32
4	.716	.681	.666	.658	.653	.630	12.62
5	.755	.721	.706	.698	.693	.669	14.85

It also follows that

$$2\frac{d\ln T_{max}}{d\ln\beta}\cong\frac{d\ln\left(\frac{dC}{dT}\right)_{max}}{d\ln\beta}\cong\frac{1}{1+\frac{E}{2RT_{max}}} \tag{55}$$

and from eq (8) that

$$k_{max}=Ae^{-E/RT_{max}}=\frac{\beta\left(\frac{dC}{dT}\right)_{max}}{(1-C)^n_{max}} \tag{56}$$

so, if n is known, E and A may be determined from a plot of $\log\frac{\beta\left(\frac{dC}{dT}\right)_{max}}{(1-C)^n_{max}}$ versus $\frac{1}{T_{max}}$ for several β. Differentiation of eq (56) with respect to β assuming $(1-C)_{max}$ constant results in

$$\frac{d\ln\beta\left(\frac{dC}{dT}\right)_{max}}{d\left(\frac{1}{T}\right)_{max}}\cong-\frac{E}{R} \tag{57}$$

which is an equivalent form of eq (51).

Farmer [16] has developed equations for $T_{1/2}$, the temperature at which $C=0.5$. The relative error [eq (28)], r_2, in using the first two terms of the asymptotic approximation is related to conversion at the maximum by [16]

$$(1-C)_{max}=e^{-r_2}$$
$$(n=1)$$
$$(1-C)_{max}=\left[\frac{1-n}{n}r_2+1\right]^{\frac{1}{n-1}} \tag{58}$$
$$(n\neq 1)$$

Therefore the two-term approximation holds exactly ($r_2=1$) only at $x=-E/RT=\infty$. Utilizing values of r_2 as functions of x from table 1, we can calculate the $(1-C)_{max}$ values for several values of x as is shown in table 2.

The approximate values for $(1-C)_{max}(-x=\infty)$ may be in considerable error for cases of low E/RT_{max} and use of eq (53) will result in large error in determining n. However, if the approximate E/RT_{max} is known, appropriate corrections may be made from table 2.

If $dC/d1/T$ is plotted versus $1/T$, the maximum rate is

$$-\left(\frac{dC}{d\frac{1}{T}}\right)_{max}=\frac{(E+2T_{max})(1-C)_{max}}{nR} \tag{21a}$$

which is practically independent of temperature. Other equations at the maximum will be modified accordingly.

The actual application of these many mathematical excercises at the maximum rate are limited to cases where n is known and its validity over the entire range of conversion has been established. An example of the magnitude of the error which may result in the misapplication of a single point method may be observed from the calculation of E from Case B. First order kinetics would appear to hold as $(1-C)_{max}=0.35$ for this case. However, calculation of E from eq (21) for $n=1$ gives $E_{apparent}=135{,}000$ cal/mol compared with $E_{theoretical}=60{,}000$ cal/mol. Subsequently, it will be shown that a first order curve will give a deceptively good fit for both the differential and integral curves for such cases of maximum isothermal rate.

The simplest differential method for determining kinetic parameters is an Arrhenius plot of the logarithm of the nth order rate constant, k_n, against the reciprocal of the absolute temperature since from eq (11),

$$\log k_n=\log\left[\beta\frac{\frac{dC}{dT}}{(1-C)^n}\right]=\log\beta\frac{d\ln(1-C)}{dT}-(n-1)\log(1-C)=\log A-\frac{E}{2.3RT} \tag{59}$$

or at $\beta=$constant,

$$\log\left[\frac{\frac{dC}{dT}}{(1-C)^n}\right]=\log\frac{A}{\beta}-\frac{E}{2.3RT}.$$

Kofstand [35] used eq (59) to test for linear ($n=0$), parabolic ($n=-1$) and cubic ($n=-2$) rate laws and determine activation energies for the oxidation of metals.

Barrer and Bratt, Newkirk, and others [36–40, 2] have employed eq (59) for $n=1$ to determine activation energies from thermogravimetric data. This method may be used early in the reaction to determine initial parameters as the early parts of most reactions are more or less independent of order. However, it has been suggested that this method be used over the whole range of volatilization [2,37] with values for E obtained from linear portions of the log $(d\ln C)/dT$ versus $1/T$ plot. As with other differential procedures this will lead to too high values for E if $n<1$ and too low values if $n>1$. Thus, when this method is applied to Cases B and C, high values are obtained for E. In order to obtain accurate activation energies, one would have to know or guess the approximate value of n that the reaction appeared to follow in the range of determination.

Ingraham and Marier [41] have used this method for a zero order reaction assuming a linear temperature dependence of the preexponential factor and obtained a linear relationship between log $1/T$ (dC/dT) and $1/T$.

The differential methods treated thus far assume the existence of a single order, n. At worst, they determine order at a single point such as the maximum rate. At best, they do not rigorously and sufficiently test their initial postulate as to the constancy of the parameters as does the integral method at several heating rates or as does a similar differential method which follows.

As in the case of integral methods, it is necessary to perform experiments at several heating rates in order to reveal changes in the kinetic mechanism which might affect the reliability of parameters determined from the data. Anderson [42] solves the three simultaneous equations for eq (59) at three different β with an electronic computer for the parameters A, n, and E at a series of constant $(1-C)$ values. Any systematic drift in parameters with changing conversion would be indicative that the assumptions—single order and single temperature dependent rate constant—do not hold.

The most generally applicable differential method was developed by Friedman [43] who utilized eq (9) in logarithmic form, i.e.,

$$\ln\left(\frac{dC}{dt}\right)=\ln\beta\frac{dC}{dT}=\ln Af(C)-\frac{E}{RT} \tag{60}$$

(dC/dt) and T are determined at constant C for several β, thus a plot of ln (dC/dt) versus $1/T$ will have a slope of E/R and an intercept of ln $Af(C)$. If E proves to be constant over a range of C values then, from eq (59) and (60), a plot of ln $Af(C)$ versus ln $(1-C)$ will have a slope of n and intercept of ln A if an nth order kinetic mechanism is operative.

In general, differentiation of eq (60) at constant C or constant dC/dt gives

$$\frac{d \ln \frac{dC}{dt}}{d\left(\frac{1}{T}\right)} = \frac{E}{R} = \frac{d \ln Af(C)}{d\left(\frac{1}{T}\right)} \tag{61}$$

$$\left(C = \text{const}\right) \qquad \left(\frac{dC}{dt} = \text{const}\right)$$

or if $f(C) = (1-C)^n$,

$$\frac{d \ln \frac{dC}{dt}}{d \frac{1}{T}} = \frac{E}{R} = n \frac{d \ln (1-C)}{d \frac{1}{T}} \tag{62}$$

$$\left(C = \text{const}\right) \qquad \left(\frac{dC}{dt} = \text{const}\right)$$

$$\frac{d \ln \frac{dC}{dt}}{d \ln (1-C)} = n \tag{63}$$

$$(T = \text{const}).$$

The validity of $f(C) = (1-C)^n$ may be tested from several runs at different β either at constant rates or constant temperature.

The right-hand side of eq (62) may be applied to a single differential plot when $n > 0$, since under these conditions dC/dt is a dual-valued function. The constancy of E/n may be tested at a series of constant dC/dt values. However, such constancy does not "prove" that the reaction is nth order. Experiments at several heating rates are essential for such proof.

Chatterjee [44] quite recently has expressed eq (63) in terms of W, the weight of sample remaining,

$$\frac{\Delta \log \left(-\frac{dW}{dt}\right)}{\Delta \log W} = n \tag{64}$$

$$(T = \text{const})$$

and the order n may be determined at several temperatures from two runs differing only in their initial weights.

It may be noted that the preexponential factor of the dC/dt equation is W_0^{-1} times the corresponding preexponential factor of the dW/dt equation [45]. Also, if an initial order is determined by this method, a distinction between the "order with respect to initial weight" and the "order with respect to temperature (time)" may be useful in the interpretation of the mechanism of complex reactions. The order with respect to initial weight, n_w, may be determined from two or more runs

at different W_0 from an integral method, since from eq (43)

$$\frac{\Delta \log W_0}{\Delta \frac{1}{T}} \cong \frac{0.457E}{(n_W - 1)R}$$

at constant W and β.

After the determination of n, Chatterjee [44] suggests determining E from a single run by a difference-differential method. However, his method may be extended to apply to any $f(W) \neq W^n$ since eq (62), for two or more runs at different initial sample weights becomes

$$\frac{d \ln \frac{dW}{dt}}{d \frac{1}{T}} = \frac{E}{R} = \frac{d \ln Af(W)}{d \frac{1}{T}} \qquad (65)$$

$$(\text{const } W) \qquad \left(\text{const } \frac{dW}{dt}\right).$$

Chatterjee [44] suggests using eq (64) to determine the order of competitive reactions by first calculating A_1 and E_1 early in the first reaction and subtracting off the portion of the rate (calculated from A_1 and E_1) due to the first reaction from the second and so on. When change in n is due to competitive reactions this method may be applied only when the orders of the several reactions are different [16] and the rates of each step are proportional to a power of the total weight of material. An added problem is the determination of n early in the reaction.

We may test the applicability of Friedman's method [43] to the cases of "changing order" and "changing activation energy." Figure 16 is a plot of log dC/dt versus $1/T$ for Case B with a maximum isothermal rate at 50 percent conversion. As with the integral method, parallel straight lines are obtained for degrees of conversion ranging between 0.04 and 0.95. The average value of E_{calc} is $59{,}800 \pm 1500$ compared with 60,000 cal/mol, theoretical.

ln β (dC/dT) is plotted against $1/T$ for two first order independent composite reactions in figure 17, as was done for the integral method in figure 15b. Figure 18 is a similar plot for two first order competitive reactions. Again, theoretical slopes for $E_1 = 30{,}000$ and $E_2 = 60{,}000$ cal/mol are included for comparison purposes. The close similarity of these results to those of the integral method is obvious and the interpretation of figures 17 and 18 is identical to that of figure 15. Comparison of eqs (61) and (44) shows the dominance of Δ ln β over Δ ln (dC/dT) and thus, explains the close similarity of the two methods.

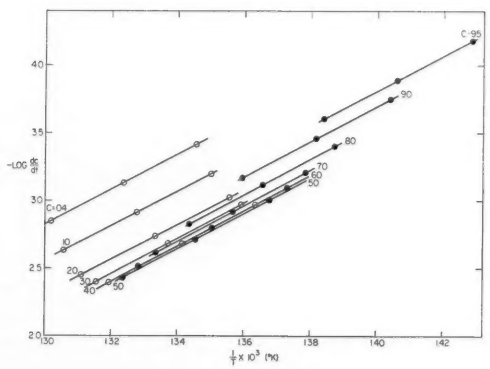

FIGURE 16. *Logarithm of thermogravimetric rate versus reciprocal absolute temperature for Case B.*
$A = 10^{15}$/sec; $E = 60{,}000$ cal/mol
$\beta_1 = 0.05$, $\beta_2 = 0.10$, $\beta_3 = 0.20$ °K/sec
$C = 0.04$, 0.10, 0.20, 0.30, 0.40, 0.50, 0.60, 0.70, 0.80, 0.90, and 0.95.

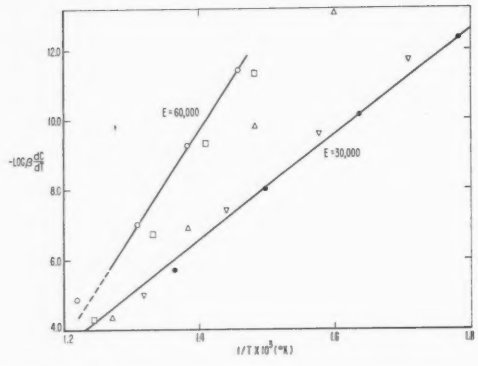

FIGURE 17. *Logarithm of thermogravimetric rate versus reciprocal absolute temperature for Case (1) independent first order reactions.*

E_1, E_2, A_1, A_2, β as in figure 13
●. $C=0.10$ □. $C=0.75$
▽. $C=0.25$ ○. $C=0.90$.
△. $C=0.50$

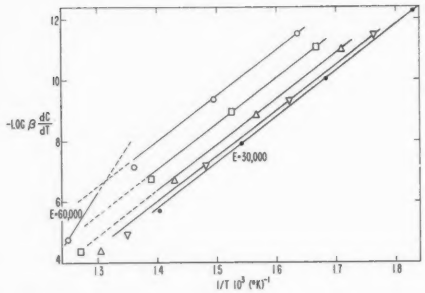

FIGURE 18. *Logarithm of thermogravimetric rate versus reciprocal absolute temperature for Case (2) competive first order reactions.*

E_1, E_2, A_1, A_2, β, as in figure 13
●. $C=0.10$ □. $C=0.75$
▽. $C=0.25$ ○. $C=0.90$.
△. $C=0.50$

The practical merits of the two methods may now be compared. The integral method [eq (44)] is simpler than the differential [eq (61)] method and quicker as it does not involve the determination of rates. However, no successive approximations are necessary for the differential method. (It will be shown that the integral method may become exact by appropriate programming of the heating rate.)

On the other hand, many polymer decompositions are subject to early kinetic irregularities (e.g., a temperature dependent induction period). Such complications may modify parameters obtained from an integral method as they depend upon cumulative values of the experimental parameters. Differential methods which give instanteous values for parameters are not subject to these complications. The preexponential factor, A, and the order, n, if it exists, may be determined directly from the intercept in either method and both methods are equally capable of interpreting cases of changing order or activation energy.

To summarize, of the differential methods, only those involving several thermograms appear to be generally applicable. Methods involving a single thermogravimetric trace should be applied only to systems where all material volatilizes by the same simple kinetic process.

4.3. Difference-Differential Methods

The difference-differential method of Freeman and Carrol [46] and its modification [38] is the most widely used method for the kinetic analysis of thermogravimetric data. It has been applied both to the investigation of inorganic materials [46, 2, 39, 47, 48] and polymers [38, 49, 2, 50, 44].

The difference form of eq (59) is

$$\Delta \log\frac{dC}{dt}=\Delta \log\beta\frac{dC}{dT}=n\Delta \log(1-C)-\frac{E}{2.3R}\Delta\frac{1}{T} \tag{66}$$

and the difference forms of eqs (62) and (63) are

$$\frac{\Delta \log\beta\dfrac{dC}{dT}}{\Delta \log(1-C)}=n-\frac{E}{2.3R}\frac{\Delta\left(\dfrac{1}{T}\right)}{\Delta \log(1-C)} \tag{67}$$

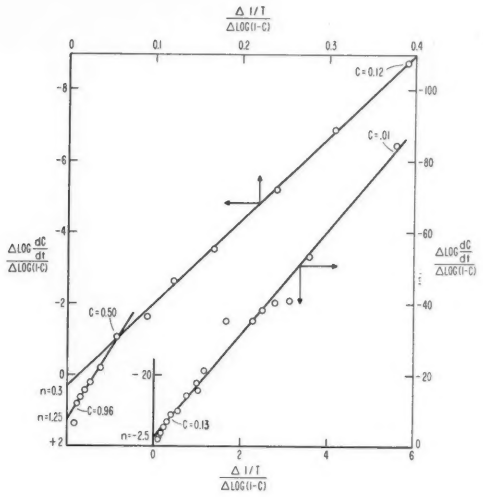

FIGURE 19. $\left[\frac{\Delta \log \frac{dC}{dt}}{\Delta \log(1-C)}\right]$ *versus* $\left[\frac{\Delta \frac{1}{T}}{\Delta \log(1-C)}\right]$ *for Case B.*
$A = 10^{15}$ sec; $E = 60{,}000$ cal/mol; $\beta = 0.10$ °K/sec
intercept $= n$ slope $= E/2.3R$.

$$\frac{\Delta\left(\frac{1}{T}\right)}{\Delta \log \beta \frac{dC}{dT}} = \frac{2.3nR}{E} \frac{\Delta \log (1-C)}{\Delta \log \beta \frac{dC}{dT}} - \frac{2.3R}{E} \tag{68}$$

$$\frac{\Delta \log \beta \frac{dC}{dT}}{\Delta\left(\frac{1}{T}\right)} = n \frac{\Delta \log (1-C)}{\Delta\left(\frac{1}{T}\right)} - \frac{E}{2.3R}. \tag{69}$$

Equations (67) and (69) have been used to obtain the parameters, E and n, from thermogravimetric data with reported success not only for simple inorganic decompositions but also for complex polymeric systems. Therefore it is of interest to apply these equations to Case B with a maximum isothermal rate at 50 percent conversion. Figure 19 is a plot of $\frac{\Delta \log \beta \frac{dC}{dT}}{\Delta \log (1-C)}$ against $\frac{\Delta \frac{1}{T}}{\Delta \log (1-C)}$ for this case with a constant energy of activation of 60,000 cal/mol. Similar results are obtained from eqs (68) and (69).

Three conversion ranges of constant slope may be obtained from figure 19 as might be anticipated for a cubic. These give the following values for n and E,

1–13% conversion	$E = 66{,}500$ cal/mol	$n = -2.4$
13–50% conversion	$E = 105{,}000$ cal/mol	$n = +0.3$
50–95% conversion	$E = 175{,}000$ cal/mol	$n = 1.25$.

The data may be interpeted as follows: between 1 and 13 percent conversion, the data are fitted by the parameters $E = 66{,}500$ cal/mol, and $n = -2.4$, etc. Since n is negative initially and becomes positive the isothermal rate must pass through a maximum value. The value of E does not have any correspondence to its theoretical value except in the initial conversion range. Treating each linear range independently does not improve the results. Therefore, the difference-differential method gives a procedural n and E for the different ranges but these have no mech-

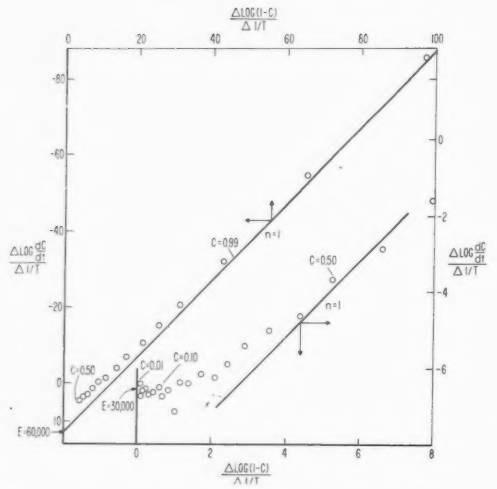

FIGURE 20. $\left[\frac{\Delta \log \frac{dC}{dt}}{\Delta \log(1/T)}\right]$ *versus* $\left[\frac{\Delta \log(1-C)}{\Delta 1/T}\right]$ *for competitive first order reactions.*

E_1. E_2. A_1. A_2 and β. as in figure 13.

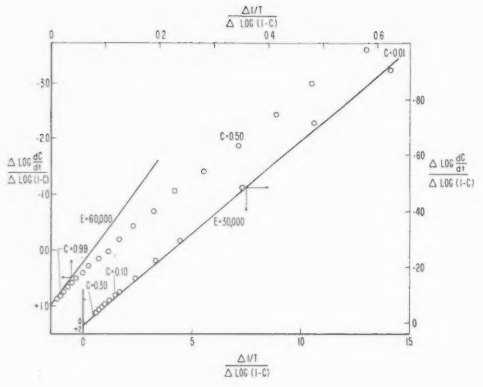

FIGURE 21. $\left[\frac{\Delta \log \frac{dC}{dt}}{\Delta \log(1-C)}\right]$ *versus* $\left[\frac{\Delta 1/T}{\Delta \log(1-C)}\right]$ *for competitive first order reactions.*

E_1. E_2. A_1. A_2, and β as in figure 13.

anistic significance, e.g., the activation energies obtained for the middle conversion range of polystyrene and polyethylene in reference [38] may well be in error.

The Freeman-Carrol method is applied to two competitive first order reactions (Case 2) of 30,000 and 60,000 cal/mol, respectively, in figures 20 and 21.

Analysis of these figures allows a critical investigation of this method as first order kinetics is followed by both reactions. The scatter of points at low conversion in figure 19 due to the determination of $1-C$ and dC/dt values from theoretical curves was cut down by determining them directly from the theoretical equations for figures 20 and 21.

$$\frac{\Delta \log \frac{dC}{dt}}{\Delta \frac{1}{T}} \text{ is plotted against } \frac{\Delta \log (1-C)}{\Delta \left(\frac{1}{T}\right)}$$

in figure 20. The theoretical intercepts at $C \rightarrow 0$ for $E=30{,}000$ and 60,000 cal/mol and the theoretical slopes for $n=1$ are indicated. As $C \rightarrow 0$, the curve approaches the correct intercept, ($E=30{,}000$), but the slight perturbation by the $E=60{,}000$ reaction coupled with the lack of sensitivity toward n at low conversion tends to make the reaction appear to be zero order. The slope approaches $n=1$ only at high conversion, but with an intercept of $E \cong 40{,}000$.

$$\frac{\Delta \log \frac{dC}{dt}}{\Delta \log (1-C)} \text{ is plotted against } \frac{\Delta \frac{1}{T}}{\Delta \log(1-C)}$$

in figure 21. The theoretical intercepts at $C \rightarrow 1.0$ for $n=1$ and the theoretical slopes for $E=30{,}000$ and 60,000 cal/mol are indicated. In the less than 30 percent conversion range, a slope reasonably close to 30,000 may be obtained but the perturbation of the high energy reaction is great enough to throw the intercept toward zero order. The intermediate conversion range gives slopes between 30,000 and 60,000 and intercepts less than unity. Only as $C \rightarrow 1$ may n be accurately determined from the intercept.

It is obvious from the above cases that it is difficult to differentiate between deviations from constancy due to "changing order" and "changing activation energy" with this method.

If the reaction follows a simple order, n may best be determined at high conversion either from the slope of eq (69) or the intercept of eq (67). The activation energy may be determined either from the intercept at low conversion for eq (69) or the slope of eq (67).

In general one may obtain the initial parameters only if values of high accuracy can be obtained for $\Delta\, dC/dt$ at low conversions. The experimental scatter, doubly magnified by taking the difference of a derivative, often will not allow the determination of order at low conversion where the dependence on n is slight.

These methods seem to be of limited applicability to polymeric systems where the kinetics often is complex.

4.4. Initial Rates

Even where $f(C)$ in eq (1) is unknown, the activation energy often can be determined as near to initial conditions as possible since all well-behaved reactions approach zero order as $C \rightarrow 0$.

Since the initial conditions for a thermally decomposing system are usually those most precisely characterized, the initial values of the kinetic parameters are often particularly useful in determining mechanism. Accurate initial weight-loss values are unattainable in isothermal studies due to an inevitable time-lag in reaching experimental temperature.

This independence of order at low conversion means that a plot of the logarithm of a "zero order rate constant," e.g., dC/dt, C/T^2 [20], C [26], or the logarithm of a "first order rate constant," e.g., $(d \ln C)/dT$ [36–40, 4, 16], $\log (1-C)$ [26], or the logarithm of an "nth order rate constant," $[1/(1-C)^n]\, dC/dT$, [35], versus $1/T$ or $1/T + a \ln T$ will give approximately the same values for activation energy at low C. Difference-differential equations, e.g., eq (69), to determine initial E have been suggested [44] but are not usually practical for reasons stressed in the previous section.

The $\ln T$ term which modifies the reciprocal temperature may enter as a temperature dependence of the preexponential factor, through an integral series approximation or a temperature dependence of the heating rate. It has been shown to be trivial except at low E. In general, if the order assumed in calculating E is higher than is actually the case, the resultant activation energy will be greater than the true value, although, where integral expressions are used other approximations may reverse this effect.

From eqs (19) and (20) for $n=0$, the slope of a plot of dC/dT versus C is E/RT^2. [In fact, for any n, plots of $[1/(1-C)^n]\, dC/dT$ versus $(1-C)^{1-n}/1-n$, $(n \neq 1)$, and $d \ln (1-C)/dT$ versus $\ln (1-C)$, $(n=1)$, have a slope of E/RT^2.] E may be determined from the initial slope of a dC/dT versus C curve as the second term in eq (19) is negligible at low C. This is shown for Case B in figure 22. From the slope, one obtains $E_{calc} = R\overline{T}^2\,(\text{slope}) = 670^2 \times 2 \times 0.0068 = 61{,}000$ cal/mol compared with $E_{theor} = 60{,}000$. The error in the calculated E results from difficulty in assigning a value to $\overline{T}$, the average temperature over which the slope was determined.

This problem may be overcome by plotting $-dC/d(1/T)\,(= T^2(dC/dT))$ versus C. The slope then becomes

$$\frac{d}{dC}\left(T^2 \frac{dC}{dT}\right) = -\frac{d^2C}{dC\, d\frac{1}{T}} \begin{cases} = \dfrac{E}{R} + 2\overline{T} - \dfrac{f'(C)}{f(C)} \dfrac{dC}{d\frac{1}{T}} \\ \\ = \dfrac{E}{R} + 2\overline{T} + \dfrac{n}{1-C} \dfrac{dC}{d\frac{1}{T}}. \end{cases} \tag{70}$$

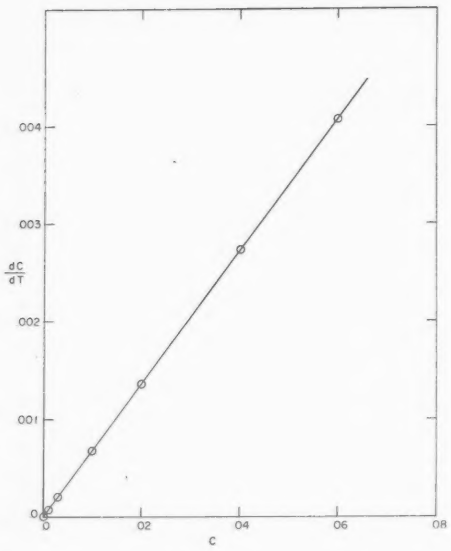

FIGURE 22. *Initial thermogravimetric rate versus conversion for Case B.*
$A/\beta = 10^{16}$/°K; $E_{theor} = 60{,}000$ cal/mol.

Thus at low C, the slope will equal $E/R + 2\overline{T}$ where $E/R \gg 2\overline{T}$. In practice an average E may be obtained from a set of C, dC/dT and T at low C since

$$\frac{\Delta\left(T^2\frac{dC}{dT}\right)}{\Delta C} \cong \frac{E}{R} + 2\overline{T} \text{ or } \frac{T_i^2\left(\frac{dC}{dT}\right)_i}{C_i} \cong E + 2\overline{T}_i$$

$$E \cong \frac{RT_i^2\left(\frac{dC}{dT}\right)_i}{C_i} - 2R\overline{T}_i \text{ at } C \ll 1. \tag{71}$$

Several methods have been applied to determine the initial activation energies for simple orders and the "maximum" cases. At $C=0.05$, Doyle's method [10] give $E=62{,}400$ cal/mol for Case B. Equation (31) of Coats and Redfern [20] gave $E=61{,}800$ at $C=0.04$. Equation (41) of Reich [26] gave a low value of 59,000 as eq (41) differs from eq (31) by 2 ln T.

In general, (dC/dT) versus C plots remain linear to higher conversions than log (dC/dT) versus $1/T$ plots. Methods involving log k_n versus $1/T$ gave the correct slope up to $C \cong 0.01$ for Case B, while dC/dT versus C is linear to $C \cong 0.03$.

If a procedural n may be approximated, log $[(1/(1-C)^n]dC/dT$ versus $1/T$ or $[(1/(1-C)^n]dC/dT$ versus $(1-C)^{1-n}/1-n$ may remain linear over a wide range of concentration. However, a linear plot of log k_n versus $1/T$ at low conversion does not imply nth order kinetics as has been stated by some investigators.

The apparent advantage of thermogravimetric over isothermal methods for the determination of initial parameters is not always experimentally realizable. Accurate data are necessary at low conversions and should be obtained at low heating rates to separate any competing reactions such as volatilization of solvent.

4.5. Nonlinear and Cyclic Heating Rates

Techniques involving the programming of reaction variables are as yet a quite undeveloped tool for the elucidation of kinetic mechanisms. In general, we may write,

$$\frac{dC}{dt} = \frac{1}{y_i}\frac{dY_i}{dt} = f(Y_1, Y_2, \ldots, Y_i, \ldots, Y_n) \tag{72}$$

where the reaction variables, Y_i, may include concentration of any reacting species, temperature, light intensity, dose of ionizing radiation, catalyst concentration, inhibitor concentration, product concentration, intermediate concentration, solvent concentration, dielectric constant of solvent, *p*H, ionic strength, etc.

Time, of course, is a unique monotonously increasing variable. However all other reaction variables may, at least in theory, be programmed to increase or decrease with time during the course of the reaction at a rate given by

$$\frac{dY_j}{dt}=\beta_j=g\left(\sum Y_i\right); \tag{73}$$

β may be any function from zero (isothermal case, if $Y_j=T$) to an integral transform and may include several arbitrary constants and reaction variables.

It may be simpler in some cases, e.g., the *p*H of an unbuffered solution, to allow a reaction variable to change in a prescribed manner rather than to keep it constant. If the change in a reaction variable may be measured, then an empirical equation may be fitted to its change with time. In such a case, any dependence of the empirical constants on the reaction variables should be investigated.

Combining eqs (72) and (73),

$$\frac{dC}{dY_i}=\frac{1}{\beta_i}\frac{dC}{dt}=\frac{\gamma_i f\left(\sum Y_i\right)}{g\left(\sum Y_i\right)}. \tag{74}$$

A judicious selection of g may simplify the kinetics and information concerning the kinetic mechanism may be elicited through the variation of the parameters. Also, this permits the analyses of a large variety of differential expressions of the form $-dY_i/dY_j$.

An application of such techniques has been made recently by Ozawa [27a] and is well adapted to his method of kinetic analysis. For simple random degradation of polymers, the rate of change of fraction of bonds broken, $d\alpha/dt$, is given by a simple first order equation

$$\beta\frac{d\alpha}{dt}=\frac{d\alpha}{dT}=Ae^{-E/RT}(1-\alpha). \tag{75}$$

Equation (75) may be combined, upon integration, with eq (5) to construct master curves of $(1-C)$ versus Φ for $N\gg L$ and $L=2, 3, 4, 5, \ldots$. In general, if $W=W_0(1-C)=g(Y_i)$, and $dY_i/dt=Ae^{-E/RT}h(Y_i)$, then integration results in relationship between conversion and Φ.

Since E and the reduced time, $\theta=\Phi/A=\int_{t_0}^{t}e^{-E/RT}dt=\theta(\beta, E, R, T)$, are independent of C, Ozawa [27a] suggests that they be used to define thermal stability for materials for which the temperature dependence of the measured property can be expressed by a single Arrhenius equation.

Many of the analytical kinetic procedures discussed in this article may be greatly simplified by the appropriate programming of the heating rate, for if

$$\beta=\frac{dT}{dt}=aT^m$$

and the temperature dependence of the preexponential factor is T^0, $T^{1/2}$, or T^1, respectively and

230-736 O-66—5

then if $m=2$, $2\frac{1}{2}$, or 3, respectively, one obtains

$$\frac{1}{\beta}\frac{dC}{dt}=\frac{dC}{dT}=\frac{A}{a}f(C)T^{-2}e^{-E/RT} \tag{76}$$

which is easily integrated to obtain

$$F(C)=\int_0^C \frac{dC}{f(C)}=\frac{AR}{aE}\int_{x_0}^{x} e^x dx=\frac{AR}{aE}\,e^{-E/RT} \tag{77}$$

eliminating all problems associated with the exponential integral.

Programming of $\beta=aT^2$, i.e., time proportional to $1/T$, should pose no special problem; for example, between 200 and 600 °C only a three-fold increase in heating rate would take place.

All integral approximations are now unnecessary as,

$$p(x)=\frac{\beta R^2}{aE^2}\,e^{-E/RT} \tag{13'}$$

and, for example,

$$\frac{d\ln a}{d\frac{1}{T}}=\frac{E}{R}=\frac{d\ln F(C)}{d\frac{1}{T}}=\frac{d\ln[(1-C)^{1-n}-1]}{d\frac{1}{T}} \tag{46'}$$

(const C) (const a)

$$\frac{d\ln[(1-C)^{1-n}-1]}{d\ln a}=-1=\frac{d\ln\ln(1-C)}{d\ln a} \tag{47'}$$

($n\neq 1$) (const T) ($n=1$).

The slope of the rate versus conversion curve now becomes,

$$\frac{d^2C}{dCdT}=\frac{E}{RT^2}-\frac{2}{T}+\frac{f'(C)}{f(C)}\frac{dC}{dT} \tag{19'}$$

and

$$\frac{d}{dC}\left(T^2\frac{dC}{dT}\right)=\begin{cases}\dfrac{E}{R}+\dfrac{f'(C)}{f(C)}\dfrac{dC}{d\frac{1}{T}}\\[2ex] \dfrac{E}{R}-\dfrac{n}{1-C}\dfrac{dC}{d\frac{1}{T}}\end{cases} \tag{70'}$$

so that

$$E\cong\frac{RT_i^2\left(\frac{dC}{dT}\right)_i}{C_i}\ \text{at}\ C\ll 1. \tag{71'}$$

The relationships at the maximum rate are simplified in some cases,

$$\left(\frac{dC}{dT}\right)_{\max}=\frac{(E-2RT_{\max})(1-C)_{\max}}{nRT_{\max}^2} \tag{21'}$$

or

$$\left(\frac{dC}{d\frac{1}{T}}\right)_{max} = -\frac{E}{nR}(1-C)_{max} \tag{21a'}$$

$$n[1-C]_{max}^{n-1} = 1+(n-1)\frac{2RT_{max}}{E} \tag{50'}$$

$$\frac{d \ln a}{d\left(\frac{1}{T}\right)_{max}} = -\frac{E}{R} \tag{51'}$$

etc.

All differential and difference-differential equations are the same if $\beta(dC/dT) = dC/dt$ is replaced by $aT^2(dC/dT)$, thus,

$$\frac{d \ln a \frac{dC}{dT}}{d\frac{1}{T}} = \frac{E}{R} + 2T = n\frac{d \ln(1-C}{d\frac{1}{T}} \tag{61'}$$

(const C) $\qquad \left(\frac{dC}{dt} = \text{const}\right)$

or

$$\frac{d \ln aT^2 \frac{dC}{dT}}{d\frac{1}{T}} = \frac{E}{R} \qquad \text{etc.} \tag{62'}$$

(C = const)

and eq (63) does not change as is true of all equations at constant temperature.

Thus, in summary, the programming of the heating rate proportional to the square of the temperature greatly simplifies integral methods rendering approximate equations exact. Rate versus composition equations are simpler as are expressions relating rate, composition and temperature at the maximum rate. Rate versus temperature methods are modified by the substitution $dC/dt = \beta(dC/dT) = aT^2(dC/dT) = -a\ dC/(d\ 1/T)$.

Other cases of nonlinear heating rates have been developed for the investigation of the ageing of insulating material [51,52]. The case in which the rate of heating increases and decreases as an exponential function of time is of some interest as such behavior approximates the heating and cooling curves of an electrical oven heated at a constant load and then shut off to cool. Thus, at least in theory, once the time constant has been determined, such an apparatus may be used in thermogravimetric investigations without temperature control.

The differential eq (9) is independent of heating rate so in many differential methods in which the simultaneous determination of T, $1-C$, and dC/dt (dW/dt) are utilized, the analytic form or the value of the heating rate need not be known. Thus in eq (59), since $\beta(dC/dT) = dC/dt$, there is no need to know β or to keep it constant unless a method comparing several heating rates is to be used.

On the other hand, all integrated expressions assume a particular function for β so methods including integral forms depend on assumptions made concerning the rate of heating.

Equations at the maximum, e.g., eq (21), are independent of the conditions used in reaching the maximum but assume that β is constant in the region of the maximum, otherwise an additional

term containing the temperature acceleration would be necessary. Many of the other equations at the maximum are combinations of differential and integrated equations.

Equations (61), (62), and (63) should be applicable in a two-point difference form irrespective of the previous variation of β for at any two temperatures at which $(dC/dt)_1=(dC/dt)_2$.

$$\frac{E}{R}\left(\frac{1}{T_1}-\frac{1}{T_2}\right)=n\ln[(1-C)_1/(1-C)_2] \tag{62''}$$

or if the same temperature is obtained by any rate of heating followed by any rate of cooling, then at $T_1=T_2$,

$$\ln\left[\left(\frac{dC}{dt}\right)_1\Big/\left(\frac{dC}{dt}\right)_2\right]\Big/\ln[(1-C)_1/(1-C)_2]=n. \tag{63'}$$

In order to utilize the left-hand sides of eqs (61) and (62), in a similar manner, two separate runs must be performed at different rates of heating such that at the same degree of conversion there will be different rates and temperatures so that at $(1-C)_1=(1-C)_2$

$$\ln\left(\frac{dC}{dt}\right)_1\Big/\left(\frac{dC}{dt}\right)_2\Big/\left(\frac{1}{T_1}-\frac{1}{T_2}\right)=\frac{E}{R} \tag{61''}$$

for any $f(C)$.

Reich, Lee and Levi [53] have applied eq (69) at constant dC/dT,

$$\frac{\Delta\log\beta}{\Delta\frac{1}{T}}=n\frac{\Delta\log W}{\Delta\frac{1}{T}}-\frac{E}{2.3R} \tag{69'}$$

$$\left(\frac{dC}{dT}=\text{const}\right)$$

to cases where β was changed in magnitude and/or sign during a single run to obtain values for n and E. In runs in which the sample was both heated and cooled, eq (63') was also used to determine order.

The above methods should be used with caution for polymeric materials. Except for the most simple systems, the initial starting material may undergo one or more condensed phase physical or chemical transformations before volatilization. In such cases, where two samples at the same degree of conversion have different heating histories, the rates of volatilization may not be comparable. Anderson [42] suggests, as a test for compositional constancy, that a series of M identical heating cycles be performed. If the relationship in eq (78)

$$(1-C)_M=(1-C)_1^M \tag{78}$$

holds, then the kinetics follow a simple nth order relationship and a plot of the logarithm of the residual fraction after M cycles versus the number of cycles, M, should give a straight line whose slope should equal the logarithm of the residual fraction after the first cycle.

Anderson [54] also suggests that since for a case following a simple order n,

$$\left(\frac{dC}{dt}\right)_M=k[(1-C)_1^M]^n \tag{79}$$

a plot of $(dC/dt)_M$ versus M could be matched with curves for various orders. Better still, a plot of $\log(dC/dt)_M$ versus M $\log(1-C)_1$ should yield a slope equal to n.

5. Concerning the Uniqueness of TGA Plots With Respect to Kinetic Parameters

It is quite clear from previous sections that, even for cases in which a single Arrhenius expression is operable, only methods involving several rates of heating determine a reliable activation energy parameter. Single point or even single curve methods may give spurious values for the parameters E and n as both the slope and the inflection point are dependent on $f(C)$ and E/RT. A number of such methods give a reasonable fit for Case B ($E_{\text{theor}}=60{,}000$ cal/mol, isothermal maximum rate at $C=0.5$) with a first order reaction but with an activation energy of approximately 135,000 cal/mol.

Therefore, in the final three figures, we compare these two cases in which the isothermal kinetics differ so drastically and observe to what extent their thermogravimetric curves are distinguishable.

Three integral curves ($1-C$ versus T) are shown in figure 23. Curve 1 is for $n=1$, $E=80{,}000$ cal/mol and $A/\beta=9.3179\times10^{21}$/sec; Curve 2, Case B (isothermal rate rises to a maximum three times the initial rate at 50 percent conversion), $E=40{,}000$ cal/mol, $A/\beta=1.2057\times10^{10}$/sec, and Curve 3, Case B, $E=35{,}000$ cal/mol, $A/\beta=3.6000\times10^{8}$/sec. A/β values were adjusted so that the temperatures of the maximum rates would coincide.

The "maximum" Curves 2 and 3 deviate from the first order curves only in the first 20 percent conversion range. Better fit in this range could undoubtedly be obtained with a different value of n.

Thermogravimetric rate versus temperature curves are shown in figure 24 for the same cases. The closeness of fit well explains the especially poor results obtained when methods involving maximum temperature, rate, conversion, or half-width are applied to Case B.

Thermogravimetric rate versus conversion curves are shown in figure 25 for the same cases. The superiority of this type plot for distinguishing between the two cases is evident. The dependence of the initial slope upon only E and T permits a quick estimate of the initial activation energy whose constancy with increasing conversion may be established through other methods.

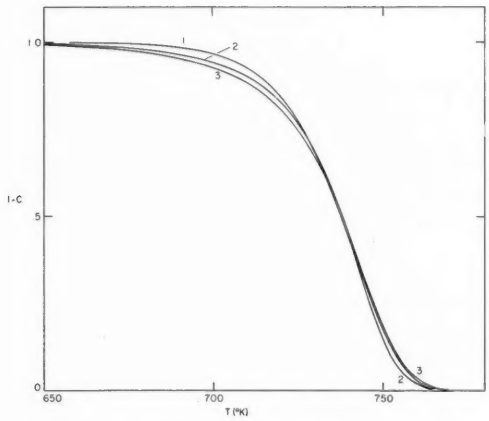

FIGURE 23. *Residual fraction versus temperature.*

1. First order $E=80{,}000$ cal/mol; $\frac{A}{\beta}=9.3179\times10^{21}$/sec.
2. Case B: $E=40{,}000$ cal/mol; $\frac{A}{\beta}=1.2057\times10^{10}$/sec.
3. Case B: $E=35{,}000$ cal/mol; $\frac{A}{\beta}=3.600\times10^{8}$/sec.

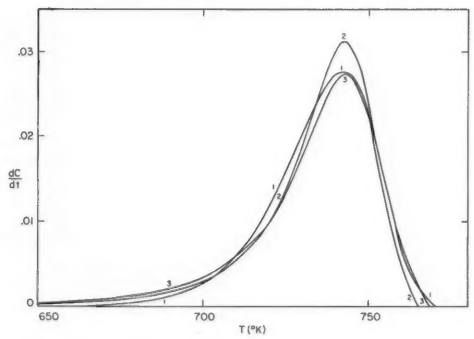

FIGURE 24. *Thermogravimetric rate versus temperature.*

1., 2., and 3. as in figure 23.

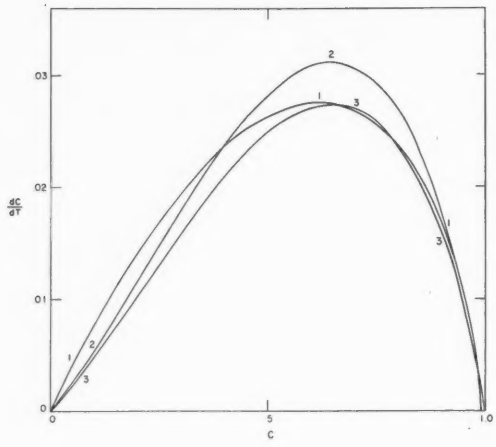

FIGURE 25. *Thermogravimetric rate versus degree of conversion.*
1., 2., and 3. as in figure 23.

To conclude, although there are some special cases for which a theoretical order has real significance, in general, n must be looked upon as a purely empirical parameter, sometimes useful in curve fitting.

6. References

[1] J. H. Flynn and L. A. Wall, Am. Chem. Soc. Meeting, Polymer preprints **6,** 945 (1965).
[2] A. W. Coats and P. J. Redfern, Analyst **88,** 906 (1963).
[3] C. B. Murphy, Analytical Chemistry **36,** 347R (1964).
[4] D. A. Smith, Rubber Chemistry and Technology **37,** 937 (1964).
[5] L. A. Wall and J. H. Flynn, ibid. **35,** 1157 (1962).
[6] R. Simha and L. A. Wall, J. Phys. Chem. **56,** 707 (1952).
[7] L. A. Wall, S. Straus, J. H. Flynn, D. McIntyre, and R. Simha, J. Phys. Chem. **70,** 53 (1966).
[8] A. W. Smith and S. Aranoff, J. Phys. Chem. **62,** 684 (1958).
[9] P. Vallet, Compt. Rendus hebd. Séances Acad. Sci. (Paris) **249,** 823 (1959).
[10] C. D. Doyle, J. Appl. Polymer Sci. **5,** 285 (1961).
[11] J. H. Flynn and L. A. Wall, Polymer Letters **4,** 323 (1966).
[12] E. Jahnke, F. Loesch, and F. Emde, Tables of Higher Functions, 6th ed., p. 18 (McGraw-Hill Book Co. New York, N.Y., 1960).
[13] O. Schlömilch, Vorlesungen über höheren Analysis, 2d ed., p. 266 (Bruenschweig, 1874).
[14] C. D. Doyle, J. Appl. Polymer Sci. **6,** 639 (1962).
[15] C. D. Doyle, Nature **207,** 290 (1965).
[16] R. W. Farmer, Wright-Patterson Air Force Base, Ohio, Aeronautical Systems Division Tech. Doc. Rept. ASD–TDR–62–1043, Part I (1963).
[17] D. W. van Krevelen, C. van Heerden, and F. J. Huntjens, Fuel **30,** 253 (1951).
[18] J. P. Baur, D. W. Bridges, and W. M. Frassell, J. Electro-chem. Soc. **102,** 490 (1955).
[19] A. W. Coats and J. P. Redfern, Nature **201,** 68 (1964).
[20] A. W. Coats and J. P. Redfern, Polymer Letters **3,** 917 (1965).
[21] H. H. Horowitz and G. Metzger, Analytical Chemistry **35,** 1464 (1963).
[22] J. R. Soulen, Analytical Chemistry **34,** 136 (1962).
[23] F. L. McCrackin, Polymer Physics Section, National Bureau of Standards, private communication.
[24] L. Reich and D. W. Levi, Makromol. Chem. **66,** 102 (1963).
[25] C. D. Doyle, Makromol. Chem. **80,** 220 (1964).
[26] L. Reich, Polymer Letters **3,** 231 (1965).
[27] L. Reich, Polymer Letters **2,** 621 (1964).
[27a] T. Ozawa, Bul Chem. Soc. Japan **38** [11], 1881–1886 (Nov. 1965).
[28] R. C. Turner and M. Schnitzer, Soil Science **93,** 225 (1962).
[29] R. C. Turner, I. Hoffman, and D. Chen. Canadian J. of Chem. **41,** 243 (1963).
[30] B. Kaesche-Krischer and H. J. Heinrich, Chemie-Ing.-Techn. **32,** 598 (1960).
[31] P. Murry and J. White, Trans. Brit. Ceram. Soc. **54,** 204 (1955).

[32] H. E. Kissinger, Analytical Chem. **29,** 1702 (1957).
[33] H. E. Kissinger, J. Res. NBS **57,** 217 (1956).
[34] R. M. Fuoss, I. O. Salyer, and H. S. Wilson, J. Polymer Sci. **2A,** 3147 (1964).
[35] P. Kofstad, Nature **179,** 1362 (1957).
[36] R. M. Barrer and G. C. Bratt, J. Phys Chem. Solids **12,** 130 (1959).
[37] A. E. Newkirk, Analytical Chem. **32,** 1558 (1960).
[38] D. A. Anderson and E. S. Freeman, J. Polymer Sci. **54,** 253 (1961).
[39] K. Traore, Soc. Chim. France, 5 serie, Mémoirs, p. 274 (1964).
[40] J. A. Magnuson, Analytical Chem. **36,** 1807 (1964).
[41] T. R. Ingraham and P. Marier, Canadian J. Chem. Eng. **42,** 161 (1964).
[42] H. C. Anderson, J. Polymer Sci. **6C,** 175 (1965).
[43] H. L. Friedman, ibid., **6C,** 183 (1965).
[44] P. K. Chatterjee, J. Polymer Sci. **3A,** 4253 (1965).
[45] J. H. Flynn, Chem. Eng. **69,** 137 (1962).
[46] E. S. Freeman and B. Carroll, J. Phys. Chem. **62,** 394 (1958).
[47] P. Lumme, Suomen Kemistilehti **B32,** 198 (1959).
[48] P. Lumme and J. Peltonen, ibid. **B37,** 162 (1964).
[49] H. C. Anderson, Makromol. Chem. **51,** 233 (1962).
[50] S. Igarashi and H. Kambe, Bul. Chem. Soc. Japan **37,** 176 (1964).
[51] H.-J. Frentz, Elektrotechnische Z. **A78,** 156 (1957).
[52] L. C. Whitman and W. W. Whitman, Amer. Inst. Elect. Eng. Trans. **78,** Pt. I, 308 (1959).
[53] L. Reich, H. T. Lee, and D. W. Levi, J. Applied Polymer Sci. **9,** 351 (1965).
[54] H. C. Anderson, Polymer Letters **2,** 115 (1964).

(Paper 70A6–422)

JOURNAL OF RESEARCH of the National Bureau of Standards—A. Physics and Chemistry
Vol. 70A, No. 6, November–December 1966

Viscoelastic Behavior Under Large Deformations

Louis J. Zapas

Institute for Basic Standards, National Bureau of Standards, Washington, D.C. 20234

(June 7, 1966)

The BKZ elastic fluid theory is used to correlate experimental results obtained in biaxial strain and steady simple shear. With a heuristic potential function involving three material properties, excellent agreement is obtained between theory and experiment. In the special case where one of the material properties is dominant, the behavior in steady simple shear is calculated from dynamic measurements in the infinitesimal range and is compared with actual data.

Key Words: BKZ theory, constant rate of strain, creep, elastic fluid, nonlinear behavior, polyisobutylene, recovery, stress, relaxation.

1. Introduction

In a recent paper [1],[1] excellent agreement was shown between experimental results and predictions of the BKZ elastic fluid theory [2]. This theory involves a potential function, U, but leaves it unspecified. For a given material, a knowledge of the results of a sufficient number of biaxial stress-relaxation experiments will enable one to predict with the BKZ theory the stress response to any other deformation history. However, if one knew a specific functional form by which U could be closely represented, then one would be able to correlate the behavior of different materials and different strain histories from the results of only a few experiments.

Encouraged by these results [1], I constructed a form of U with which the BKZ elastic fluid theory could quantitatively describe biaxial strain at large deformation, biaxial creep, and simple extension of vulcanized rubbers. This form of U involves three material properties. In simple shear it can quantitatively predict non-Newtonian behavior, including normal stresses. The ratio of the shearing stress to the rate of shear depends on the rate of shear in such a way as to describe either shear thinning or shear thickening behavior or both, depending on the relative magnitude of the material properties. In the special case where one material property is dominant, one may use dynamic data taken at infinitesimal strains to predict the dependence of viscosity and normal stresses on rate of shear. This is presented in section 4 of this paper and the agreement is excellent.

I want to emphasize that the form of U presented here is heuristic. The purpose of this paper is to show that with a relatively simple form of U, one may use the BKZ elastic fluid to describe very well the behavior of materials which can be considered isotropic and incompressible.

[1] Figures in brackets indicate the literature references at the end of this paper.

2. Theoretical Considerations

The BKZ elastic fluid is a fluid with an elastic potential. The effect of the configuration at time $\tau < t$ on the stress at time t is equivalent to the effect of a stored elastic energy with the configuration at time τ as the preferred configuration. The effect depends on the amount of time elapsed between τ and t. The stress at time t is the sum of contributions from all past times. For an extensive description of the theory, we refer the reader to the initial papers [2] and [3].

A particular motion of the material may be specified in terms of the Cartesian coordinates x_i of each particle at each time. Let X_1, X_2, X_3 be the position coordinates of the particles in a reference configuration. Then, a motion is given by a set of functions

$$x_i = x_i(X_k, t) \qquad i, k = 1, 2, 3. \tag{2.1}$$

At time τ, (2.1) becomes

$$x_i = x_i(X_k, \tau) \qquad i, k = 1, 2, 3. \tag{2.2}$$

If we eliminate X_1, X_2, X_3 between (2.1) and (2.2) we may write

$$x_i(t) = x_i(x_k(\tau), t, \tau) \qquad i, k = 1, 2, 3$$

where $x_i(t)$ and $x_i(\tau)$ are the position coordinates at time t and τ respectively of the same particle. The relative deformation gradients $x_{ik}(t, \tau)$ are defined by

$$x_{ik}(t, \tau) \equiv \frac{\partial x_i(t)}{\partial x_k(\tau)}.$$

The left Cauchy-Green tensor $c_{ij}(t, \tau)$ is then

$$c_{ij}(t, \tau) \equiv x_{ik}(t, \tau) x_{jk}(t, \tau)$$

where repeated indices indicate summation over the values 1, 2, 3.

The principal invariants of $c_{ij}(t, \tau)$ are

$$I_1(t, \tau) \equiv \zeta_1^2 + \zeta_2^2 + \zeta_3^2$$

$$I_2(t, \tau) \equiv \zeta_1^2\zeta_2^2 + \zeta_2^2\zeta_3^2 + \zeta_3^2\zeta_1^2$$

$$I_3(t, \tau) \equiv \zeta_1^2\zeta_2^2\zeta_3^2$$

where $\zeta_i^2 = \lambda_i^2(t, \tau)$ are the principal values of $c_{ij}(t, \tau)$ and λ_i is the stretch ratio in the x_i direction.

Assuming incompressibility, we have $I_3(t, \tau) = 1$, and the constitutive equations for the BKZ elastic fluid become [4]

$$\sigma_{ij}(t) = -p\delta_{ij} + 2\int_{-\infty}^{t} \left[\frac{\partial U}{\partial I_1} c_{ij}(t, \tau) - \frac{\partial U}{\partial I_2} c_{ij}^{-1}(t, \tau)\right] d\tau \quad (2.3)$$

where σ_{ij} are the components of the stress tensor, p is a hydrostatic pressure, U is a function of I_1, I_2, and $t - \tau$

$$U = U(I_1(t, \tau), I_2(t, \tau), t - \tau),$$

and $c_{ij}^{-1}(t, \tau)$ are the components of the inverse of the matrix $\|c_{ij}(t, \tau)\|$. We may describe an isochoric homogeneous biaxial strain history by writing for (2.1)

$$x_1(t) = \lambda_1(t) X_1$$

$$x_2(t) = \lambda_2(t) X_2$$

$$x_3(t) = \lambda_3(t) X_3 = \frac{1}{\lambda_1\lambda_2} X_3.$$

The matrix of the left Cauchy-Green tensor $c_{ij}(t, \tau)$ becomes

$$\|c_{ij}(t, \tau)\| = \begin{Vmatrix} \dfrac{\lambda_1^2(t)}{\lambda_1^2(\tau)} & 0 & 0 \\ 0 & \dfrac{\lambda_2^2(t)}{\lambda_2^2(\tau)} & 0 \\ 0 & 0 & \dfrac{\lambda_1^2(\tau)\lambda_2^2(\tau)}{\lambda_1^2(t)\lambda_2^2(t)} \end{Vmatrix}$$

and

$$I_1(t, \tau) = \frac{\lambda_1^2(t)}{\lambda_1^2(\tau)} + \frac{\lambda_2^2(t)}{\lambda_2^2(\tau)} + \frac{\lambda_1^2(\tau)\lambda_2^2(\tau)}{\lambda_1^2(t)\lambda_2^2(t)} \quad (2.4)$$

$$I_2(t, \tau) = \frac{\lambda_1^2(\tau)}{\lambda_1^2(t)} + \frac{\lambda_2^2(\tau)}{\lambda_1^2(t)} + \frac{\lambda_1^2(t)\lambda_2^2(t)}{\lambda_1^2(\tau)\lambda_2^2(\tau)}. \quad (2.5)$$

From (2.3), (2.4), and (2.5) we get

$$\sigma_{11}(t) - \sigma_{33}(t) = 2\int_{-\infty}^{t} \left[\frac{\lambda_1^2(t)}{\lambda_1^2(\tau)} - \frac{\lambda_1^2(\tau)\lambda_2^2(\tau)}{\lambda_1^2(t)\lambda_2^2(t)}\right]\left[\frac{\partial U}{\partial I_1} + \frac{\lambda_2^2(t)}{\lambda_2^2(\tau)}\frac{\partial U}{\partial I_2}\right] d\tau \quad (2.6)$$

and

$$\sigma_{22}(t) - \sigma_{33}(t) = 2\int_{-\infty}^{t} \left[\frac{\lambda_2^2(t)}{\lambda_2^2(\tau)} - \frac{\lambda_1^2(\tau)\lambda_2^2(\tau)}{\lambda_1^2(t)\lambda_2^2(t)}\right]\left[\frac{\partial U}{\partial I_1} + \frac{\lambda_1^2(t)}{\lambda_1^2(\tau)}\frac{\partial U}{\partial I_2}\right] d\tau. \quad (2.7)$$

In the case of a single step stress-relaxation experiment where $\lambda_i(\tau) = 1$ for times τ smaller than zero and $\lambda_i(\tau) = \lambda_i(t) = \lambda_i$ for times t, τ greater than zero, (2.6) yields

$$\frac{\sigma_{11}(t) - \sigma_{33}(t)}{\lambda_1^2 - \dfrac{1}{\lambda_1^2\lambda_2^2}} = 2\left(\frac{\partial W}{\partial I_1} + \lambda_2^2 \frac{\partial W}{\partial I_2}\right) \quad (2.8)$$

where

$$W = W(I_1, I_2, t) \equiv \int_t^{\infty} U(I_1, I_2, \xi) d\xi, \quad (2.9)$$

$$\xi = t - \tau,$$

and

$$I_1 = \lambda_1^2 + \lambda_2^2 + \frac{1}{\lambda_1^2\lambda_2^2}$$

$$I_2 = \frac{1}{\lambda_1^2} + \frac{1}{\lambda_2^2} + \lambda_1^2\lambda_2^2$$

Similarly (2.5) becomes

$$\frac{\sigma_{22}(t) - \sigma_{33}(t)}{\lambda_2^2 - \dfrac{1}{\lambda_1^2\lambda_2^2}} = 2\left(\frac{\partial W}{\partial I_1} + \lambda_1^2 \frac{\partial W}{\partial I_2}\right) \quad (2.10)$$

Superficially, expressions (2.8) and (2.10) appear to be the same as the relations given by Rivlin and Saunders [5]. However W, here, depends on time as well as strain and is designed so that (2.10) gives the stress during stress relaxation. On the other hand, the W of Rivlin and Saunders depends only on strain.

In the case of simple shear, we introduce an orthogonal set of coordinates as shown in figure 1, where x_1 is the direction of motion of a particle and x_2 is the direction of shear. In the case of a steady shearing

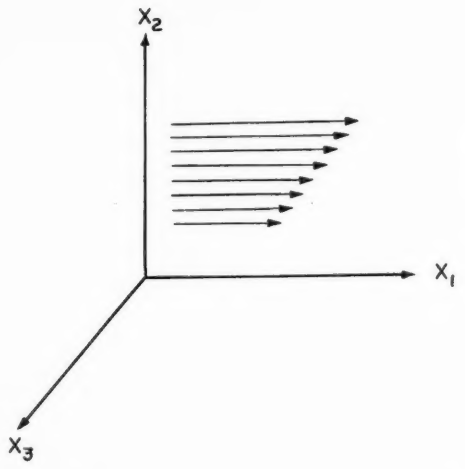

FIGURE 1. *General coordinate axes for description of flow.*

motion with constant rate of shear, $\dot{\gamma}$, (2.1) reads

$$x_1(t)=x_1(\tau)+(t-\tau)\dot{\gamma}x_2(\tau)$$

$$x_2(t)=x_2(\tau)$$

$$x_3(t)=x_3(\tau)$$

Thus,

$$\|c_{ij}(t,\tau)\|=\begin{Vmatrix}1+\dot{\gamma}^2(t-\tau)^2 & \dot{\gamma}(t-\tau) & 0\\ \dot{\gamma}(t-\tau) & 1 & 0\\ 0 & 0 & 1\end{Vmatrix}$$

and

$$\|c_{ij}^{-1}(t,\tau)\|=\begin{Vmatrix}1 & -\dot{\gamma}(t-\tau) & 0\\ -\dot{\gamma}(t-\tau) & 1+\dot{\gamma}^2(t-\tau)^2 & 0\\ 0 & 0 & 1\end{Vmatrix}$$

Substituting in equation (2.3) with $t-\tau=\xi$, one gets

$$\sigma_{12}=2\int_0^\infty\left\{\frac{\partial U}{\partial I_1}+\frac{\partial U}{\partial I_2}\right\}\dot{\gamma}\xi\,d\xi \qquad (2.11)$$

where

$$I_1(t,t-\xi)=I_2(t,t-\xi)=3+\dot{\gamma}^2\xi^2$$

and

$$U=U(I_1,I_2,\xi)$$

$$\sigma_{11}=-p+2\int_0^\infty\left\{\frac{\partial U}{\partial I_1}(1+\dot{\gamma}^2\xi^2)-\frac{\partial U}{\partial I_2}\right\}d\xi \qquad (2.12)$$

$$\sigma_{22}=-p+2\int_0^\infty\left\{\frac{\partial U}{\partial I_1}-\frac{\partial U}{\partial I_2}(1+\dot{\gamma}^2\xi^2)\right\}d\xi \qquad (2.13)$$

$$\sigma_{33}=-p+2\int_0^\infty\left\{\frac{\partial U}{\partial I_1}-\frac{\partial U}{\partial I_2}\right\}d\xi. \qquad (2.14)$$

These relations hold independently of the form of U.

3. Experimental Procedure

From the theoretical considerations of the previous section, we see that we may determine $\partial W/\partial I_1$ and $\partial W/\partial I_2$ as functions of I_1, I_2, and t from data taken in single step stress-relaxation experiments in biaxial strain. For vulcanized rubbers we may regard the long time isochrones in creep to within a good approximation as isochrones of single step stress relaxation. This is true for a material only if the deformation at constant load remains almost constant for long times, although not necessarily to infinite time. For this reason we elected to do our experiments on vulcanized butyl rubber. The experiments were carried out using a test piece in the form of a square sheet having sides of 8 cm and a thickness of about 0.07 cm. The test piece was cut and marked in a fashion described by Rivlin and Saunders [5]. One square surface of the sheet was marked in ink with two sets of four parallel straight lines so as to form a square grid with 1 cm spacings. In drawing the outer lines of the grid, great care was taken that they be straight and form a *perfect* square. In figure 2 is shown part of the ap-

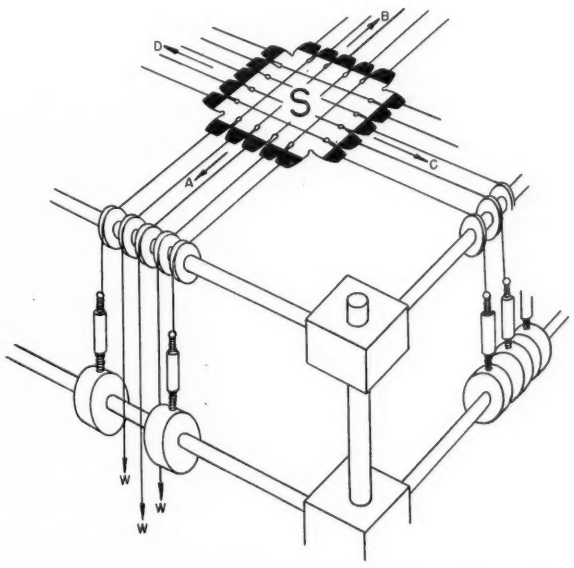

FIGURE 2. *Schematic diagram for the biaxial extension experiments.*

paratus with the sample S. As can be seen from the figure, the sample was stretched in the A–B and C–D directions with the aid of strings. One end of each string was tied to a lug of the sample and the other end was attached to a weight or to a turnbuckle. The strings were made from unspun fibers of Mylar. For the study of the variation of $\partial W/\partial I_1$ and $\partial W/\partial I_2$ with respect to time, the two sets of the three middle lugs in the A and C directions were tied to strings supporting weights. The other 14 lugs were tied to strings in which tension was controlled with the turnbuckles, which could be adjusted to keep the ink lines on the sample straight and parallel. With the aid of a two-way traveling microscope, whose axes of travel were set parallel to the stretch directions, we could check the uniformity of stretch and measure the extensions.

In our other sets of biaxial experiments, we loaded the sample by first stretching it a predetermined amount in the D–C direction and then applying weights in the A–B direction. This was done in order to avoid difficulties due to the history of loading. In these experiments, only the three middle lugs in the A direction carried supporting weights. The strings attached to the other lugs were adjusted to keep the lines straight and parallel to the stretch directions. The final readings were taken after 18 hr from the time of loading. After each measurement the material was allowed to relax for 24 to 48 hr before another loading was started. Thus, the values that we obtained can be considered as isochronal values of stress relaxation at 18 hr.

In order to be able to compare with experiment the predictions of our theory for simple shear flows, we performed dynamic and constant rate of shear measurements on solutions of polyisobutylene B–140 in Mentor 28 oil. Two concentrations were used. They shall be designated as 10 percent and 5 percent. We do not know the actual concentration accurately, because we lost an unknown amount of solvent while preparing what was to be the 10 percent solution. We do know that the ratio of the two concentrations is two to one. The dynamic data at very small deformations were obtained through the cooperation of R. W. Penn, using a torsion pendulum at the W. R. Grace Laboratories. The torsion pendulum is essentially the same as the one described by Morrison, Zapas, and DeWitt [6]. The data on viscosity as a function of rate of shear were obtained in a capillary viscometer.

4. Experimental Results and Discussion

The purpose of this paper is to show that with a relatively simple form of the potential function U, the BKZ elastic fluid can be used to correlate different types of behavior of elastomeric materials. The heuristic form of the potential function U which I shall use here involves three material properties $\alpha(t)$, $\beta(t)$, and $c(t)$. These material properties are positive monotonically decreasing functions of time. The form of U is given by the following expression:

$$-U=\frac{\alpha'}{2}(I_1-3)^2+4.5\beta' \ln\left(\frac{I_1+I_2+3}{9}\right)+24(\beta'-c') \ln\left(\frac{I_1+15}{I_2+15}\right)+c'(I_1-3) \tag{4.1}$$

where

$$\alpha'=\frac{d\alpha(t)}{dt},\ \beta'=\frac{d\beta(t)}{dt},\ \text{and}\ c'=\frac{dc(t)}{dt}.$$

From equations (2.9) and (4.1) we get

$$\frac{\partial W}{\partial I_1}=\alpha(I_1-3)+\frac{4.5\beta}{I_1+I_2+3}+\frac{24(\beta-c)}{I_1+15}+c \tag{4.2}$$

$$\frac{\partial W}{\partial I_2}=\frac{4.5\beta}{I_1+I_2+3}-\frac{24(\beta-c)}{I_2+15} \tag{4.3}$$

where it is understood W, α, β, and c are functions of time.

In a pure shear single step stress-relaxation experiment with $\lambda_2=1$, and $I_1=I_2$, we get from eq (2.8)

$$\frac{\sigma_{11}(t)-\sigma_{33}(t)}{\lambda_1^2-\frac{1}{\lambda_1^2}}=2\left(\frac{\partial W}{\partial I_1}+\frac{\partial W}{\partial I_2}\right)=2\left\{\alpha(I_1-3)+\frac{9\beta}{2I_1+3}+c\right\} \tag{4.4}$$

Since $\alpha(t)$ is taken to be a positive monotonically decreasing function of time, or zero, eq (4.4) says that if one plots $\dfrac{\sigma_{11}(t)-\sigma_{33}(t)}{\lambda_1^2-\frac{1}{\lambda_1^2}}$ at constant t versus $\dfrac{1}{2I_1+3}$, one should get either a curve which is concave upward or a straight line. In the case of a straight line the slope is equal to 18β, the intercept, $2c$, and α equals zero.

In figure 3 we show the data of Rivlin and Saunders [5] on pure shear for vulcanized natural rubber. In this figure we plotted $\dfrac{\sigma_{11}-\sigma_{33}}{2\left(\lambda_1^2-\frac{1}{\lambda_1^2}\right)}-\alpha(I_1-3)$ versus $\dfrac{1}{2I_1+3}$ for $\alpha=0$ and $\alpha=0.06$. As can be seen for the case where $\alpha=0$, the curve is concave upwards. Here $\alpha=0.06$ was found by trial and error. Actually, if there is a well defined minimum, one could obtain α by following the procedure presented in a previous paper [3]. So it is evident that by using the relation (4.4) one could get the three material properties from pure shear experiments.

In figure 4 we present a similar check of the adequacy of the assumed form of U by plotting

$$\frac{\sigma_{11}(t)-\sigma_{33}(t)}{2\left(\lambda_1^2-\frac{1}{\lambda_1^2\lambda_2^2}\right)}-\alpha(I_1-3) \text{ versus } \frac{1+\lambda_2^2}{I_1+I_2+3}$$

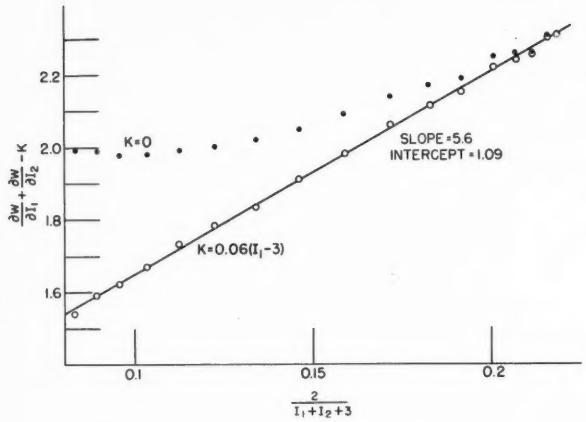

FIGURE 3. *Pure shear data of Rivlin and Saunders on vulcanized natural rubber.*
Open circles, $\alpha=0$. The abscissa is given in kg per cm².

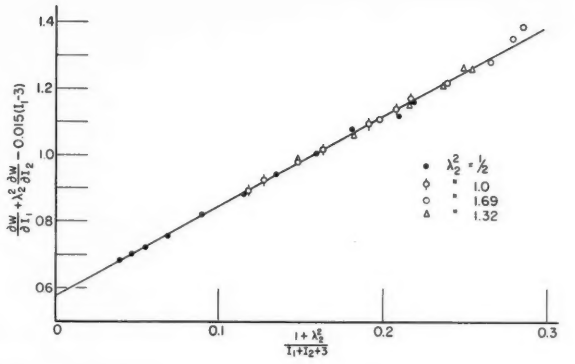

FIGURE 4. *Biaxial extension data of vulcanized butyl rubber.*
The abscissa is given in (dynes/cm²)10⁻⁶.

using data obtained on vulcanized butyl rubber in biaxial and simple extension deformations as described in the previous section. For butyl rubber, the value of $\alpha(t)$ is small and estimated to be 0.015. Since β and c are equal, as determined from the pure shear data, in a plot of this type the experimental points should fall in a straight line. Considering experimental difficulties and uncertainties, the agreement is excellent.

TABLE 1. *Biaxial creep of vulcanized butyl rubber*

Time	I_1	I_2	$\frac{\partial W}{\partial I_1}\times 10^{-6}$	$\frac{\partial W}{\partial I_2}\times 10^{-6}$
Hours			*Dynes/cm²*	*Dynes/cm²*
3	3.1043	3.1050	2.15	−0.10
20	3.1125	3.1125	1.91	.07
23	3.1134	3.1131	1.83	.14
47	3.1160	3.1156	1.80	.16
66	3.1177	3.1172	1.78	.17
90	3.1199	3.1191	1.74	.19
117	3.1211	3.1203	1.71	.20
164	3.1233	3.1224	1.69	.21

In the course of our experiments in biaxial deformation, in a different set of measurements we observed a negative value of $\partial W/\partial I_2$ at very small extensions, while at higher extensions $\partial W/\partial I_2$ was positive. This was observed in three samples with different degrees of vulcanization. For a further study of this peculiarity we selected a relatively high cross-linked specimen of butyl rubber and we studied its biaxial creep behavior at small deformations. In table 1 we show the calculated values of $\partial W/\partial I_1$ and $\partial W/\partial I_2$ as functions of I_1, I_2, and time. This table shows large variations in $\partial W/\partial I_2$ for small changes in I_1 and I_2. A plot of $\partial W/\partial I_1+\partial W/\partial I_2$ versus the logarithm of time is shown in figure 5. We see that even in greatly expanded scale for $\partial W/\partial I_1+\partial W/\partial I_2$ the points fall in a straight line. Moreover, after 150 hr the data still

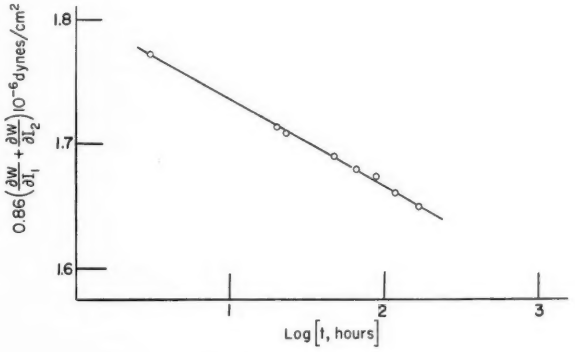

FIGURE 5. *Biaxial creep data on vulcanized butyl rubber.*

did not indicate any suggestions of leveling off. This shows that we cannot neglect the behavior with respect to time. From single step stress-relaxation experiments in simple extension in vulvanized rubbers, we observed that β decays with time much faster than c. From (4.3) we can see that $\partial W/\partial I_2$ will be negative when β is larger than 1.6c. One can see, at least qualitatively, that what seemed to be a paradoxical inversion in sign for $\partial W/\partial I_2$ is predictable from eq (4.3).

4.1. Steady Simple Shearing Flow

We can substitute eq (4.1) into eq (2.11) to get

$$\sigma_{12}=-2\int_0^\infty\left\{\alpha'(\xi)\dot\gamma^2\xi^2+\frac{9\beta'(\xi)}{9+2\dot\gamma^2\xi^2}+c'(\xi)\right\}\dot\gamma\xi\,d\xi. \tag{4.5}$$

Since the viscosity $\eta(\dot{\gamma})$ is defined to be the ratio of σ_{12} to $\dot{\gamma}$, eq (4.5) can be written

$$\eta(\dot{\gamma})=-2\int_0^\infty\left\{\alpha'(\xi)\dot{\gamma}^2\xi^2+\frac{9\beta'(\xi)}{9+2\dot{\gamma}^2\xi^2}+c'(\xi)\right\}\xi d\xi. \tag{4.6}$$

By considering special cases for which the dominant term is that containing $\alpha'(\xi)$, $\beta'(\xi)$, or $c'(\xi)$, one can see that (4.6) could predict a viscosity independent of rate of shear, or viscosities as observed in shear thinning or shear thickening materials.

In figure 6 we show schematically the type of behavior predicted from eq (4.6). For the sake of simplicity we can write

$$\eta(\dot{\gamma})=\eta_\alpha(\dot{\gamma})+\eta_\beta(\dot{\gamma})+\eta_c \tag{4.7}$$

where

$$\eta_\alpha(\dot{\gamma})=-2\int_0^\infty\alpha'(\xi)\dot{\gamma}^2\xi^3d\xi \tag{4.7a}$$

$$\eta_\beta(\dot{\gamma})=-2\int_0^\infty\frac{\beta'(\xi)\xi}{1+\frac{2}{9}\dot{\gamma}^2\xi^2}\,d\xi \tag{4.7b}$$

$$\eta_c=-2\int_0^\infty c'(\xi)\xi d\xi \tag{4.7c}$$

We observe that in the case where $\eta_\alpha(\dot{\gamma})=\eta_\beta(\dot{\gamma})=0$ one gets a viscosity independent of rate of shear. When only $\eta_\alpha(\dot{\gamma})=0$, one gets a behavior shown in curve II of figure 6. Curves III and IV represent the cases where $\eta_\alpha(\gamma)$, $\eta_\beta(\dot{\gamma})$, and η_c all contribute to the viscosity. Naturally, curve IV shows the case where $\eta_\alpha(\dot{\gamma})$ is the dominant quantity.

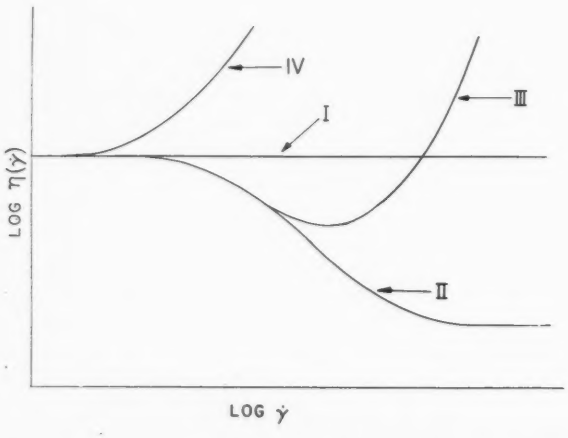

FIGURE 6. *Schematic representation of forms of steady shear viscosity curves which can be predicted by eq (4.6).*

4.2. Comparison of Steady Simple Shearing Flow With Measurements at Infinitesimal Deformations

For a simple shear deformation, which is specified in terms of a single parameter, say $\gamma=\gamma(\tau)$, (2.2) may be written

$$\begin{aligned}x_1(\tau)&=X_1+\gamma(\tau)X_2\\ x_2(\tau)&=X_2\\ x_3(\tau)&=X_3.\end{aligned} \tag{4.8}$$

To represent single step stress relaxation, we take $\gamma(\tau)=0$ for $\tau<0$ and $\gamma(\tau)=\gamma=$constant for $\tau>0$, and we get

$$\begin{aligned}\|c_{ij}\|&=\begin{Vmatrix}1+\gamma^2 & \gamma & 0\\ \gamma & 1 & 0\\ 0 & 0 & 1\end{Vmatrix}\\ \|c_{ij}^{-1}\|&=\begin{Vmatrix}1 & -\gamma & 0\\ -\gamma & 1+\gamma^2 & 0\\ 0 & 0 & 1\end{Vmatrix}\end{aligned} \tag{4.9}$$

where $I_1=I_2=3+\gamma^2$. From (2.3), (2.9), (4.2), (4.3), and (4.9), we obtain

$$\sigma_{12}(t)=2\gamma\left[\gamma^2\alpha(t)+\frac{9\beta(t)}{9+2\gamma^2}+c(t)\right]. \tag{4.10}$$

The limit of $\frac{\sigma_{12}(t)}{\gamma}$ for vanishing γ gives us the relaxation function, $G(t)$, for infinitesimal deformations:

$$G(t)=2\beta(t)+2c(t). \tag{4.11}$$

From the general relation of linear viscoelasticity [7] between periodic and steady-state functions

$$G'(\omega)+i\omega\eta'(\omega)=i\omega\int_0^\infty G(t)e^{-i\omega t}dt,$$

we can express $\eta'(\omega)$ in terms of $\beta(t)$ and $c(t)$ as

$$\eta'(\omega)=\int_0^\infty\{2\beta(t)+2c(t)\}\cos\omega t dt. \tag{4.12}$$

Integrating (4.6) by parts we get

$$\eta(\dot{\gamma})=2\int_0^\infty\left\{3\alpha(\xi)\dot{\gamma}^2\xi^2+\frac{9\beta(\xi)\,(9-2\dot{\gamma}^2\xi^2)}{(9+2\dot{\gamma}^2\xi^2)^2}+c(\xi)\right\}d\xi \tag{4.13}$$

Several interesting observations can be drawn regarding the behavior of a material which can be described by a potential function U of the form of (4.1) by comparing (4.12) and (4.13). First, it is obvious

that in general $\eta(\dot{\gamma})$ cannot be predicted from measurements of $\eta'(\omega)$, since the term in $\alpha(t)$ does not show up in $\eta'(\omega)$ at all. Also, $\beta(t)$ and $c(t)$ cannot be separated by measurements of $\eta'(\omega)$. However, if we encounter a material for which either β or c is the dominant term in (4.13) and (4.9) then in principle $\eta(\dot{\gamma})$ can be calculated from $\eta'(\omega)$. If c is the dominant term, we will have a situation in which $\eta(\dot{\gamma})$ is independent of rate of shear, but $\eta'(\omega)$ may vary with frequency and normal stress effects may be observed in steady shearing flow. If β is dominant, both $\eta'(\omega)$ and $\eta(\dot{\gamma})$ will vary with ω or $\dot{\gamma}$.

For many materials $\alpha(t)$ is negligible, but ordinarily both $\beta(t)$ and $c(t)$ contribute to $\eta(\dot{\gamma})$, with $\beta(t)$ contributing the dominant term within experimentally accessible rates of shear. However, at very high rates of shear, any nonzero c must become dominant. For the range of rates of shear for which

$$\int_0^\infty \frac{9\beta(\xi)\,(9-2\dot{\gamma}^2\xi^2)}{(9+2\dot{\gamma}^2\xi^2)^2}\,d\xi \gg \int_0^\infty c(\xi)d\xi$$

we may utilize $\eta'(\omega)$ to evaluate $\beta(t)$ and calculate a lower bound for the measured $\eta(\dot{\gamma})$. The calculated $\eta(\dot{\gamma})$ should be in close agreement with that measured at low values of $\dot{\gamma}$, but would fall below the measured values at high rates of shear.

For the actual comparison of the two measured functions $\eta'(\omega)$ and $\eta(\dot{\gamma})$, it is better to formulate our expressions in terms of relaxation spectra corresponding to $\beta(t)$ and $c(t)$ entirely analogous to the spectrum representation of $G(t)$. The relaxation spectrum $F(\tau)$ may be defined by [7]:

$$G(t)=\int_0^\infty F(\tau)e^{-t/\tau}d\tau$$

and may be expressed as the sum of two terms $F_\beta(\tau)$ and $F_c(\tau)$ defined by

$$\begin{aligned} 2\beta(t)&=\int_0^\infty F_\beta(\tau)e^{-t/\tau}d\tau \\ 2c(t)&=\int_0^\infty F_c(\tau)e^{-t/\tau}d\tau. \end{aligned} \tag{4.14}$$

In terms of (4.14) we have

$$G'(\omega)=\int_0^\infty \frac{\{F_\beta(\tau)+F_c(\tau)\}\omega^2\tau^2 d\tau}{1+\omega^2\tau^2} \tag{4.15}$$

$$\eta'(\omega)=\int_0^\infty \frac{\{F_\beta(\tau)+F_c(\tau)\}\tau d\tau}{1+\omega^2\tau^2} \tag{4.16}$$

and in the case where $\alpha(t)\equiv 0$ from eq (4.6)

$$\eta(\dot{\gamma})=\int_0^\infty \left\{F_\beta(\tau)\tau\int_0^\infty \frac{xe^{-x}dx}{1+\frac{2}{9}\dot{\gamma}^2\tau^2x^2}+\tau F_c(\tau)\right\}d\tau. \tag{4.17}$$

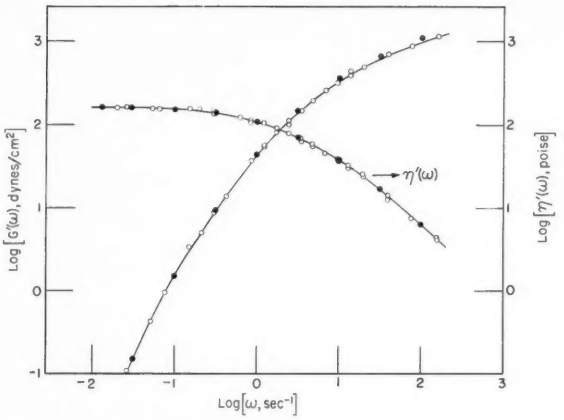

FIGURE 7. *Dynamic data on 5 percent solution of B−140 in Mentor 28 oil.* Solid circles represent the values calculated from data given in table 2.

TABLE 2. *Relaxation spectrum for 5 percent solution of polyisobutylene B−140 in Mentor 28 at 25 °C*

τ	$H(\tau)$
19.0	0.0
15.2	.1
10	.5
3	7.3
1.0	39
0.3	120
.1	245
.03	410
.01	420

We calculated $H(\tau)=\tau F(\tau)$ from measurements of $\eta'(\omega)$ and $G'(\omega)$ on the five percent solution of B−140 by an iterative method which will be described in another paper. In figure 7 we show the dynamic rigidity and viscosity as a function of frequency. The black points represent points calculated from $H(\tau)$ as obtained by our iterative method and tabulated in table 2. The agreement indicates that we have a good representation within the range of measurements. In figure 8 we show the viscosity at steady shearing flow as a function of rate of shear, with the open circles representing values calculated from eq (4.17) assuming that the contribution of the integral of $F_c(\tau)\tau$ is negligible. The agreement between experimental and calculated values is excellent.

The same arguments can be used for the determination of the normal stress differences $\sigma_{11}-\sigma$, $\sigma_{22}-\sigma$, and $\sigma_{33}-\sigma$ (where $3\sigma=\sigma_{11}+\sigma_{22}+\sigma_{33}$) as can be seen from eqs (2.12) to (2.14). An interesting result is that the limiting value of the ratio $\dfrac{\sigma_{22}-\sigma_{33}}{\sigma_{11}-\sigma_{33}}$ at small rates of shear is 0.46 in the case where β is the dominant term. This compares very well with the value of 0.4 reported by Markovitz [8] for a 5.39 percent solution of polyisobutylene in cetane.

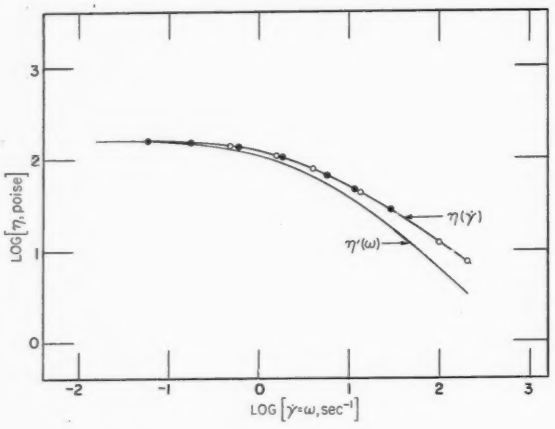

FIGURE 8. *Dynamic viscosity and steady shear viscosity data on 5 percent solution of B–140 in Mentor 28 oil.*

Solid circles are the calculated values.

In conclusion, we should emphasize that all these derivations were obtained with the assumption of incompressibility. In reality $\partial W/\partial I_1$ and $\partial W/\partial I_2$ depend also on I_3, the influence of which can not be evaluated from the experiments reported above.

I thank B. Bernstein, E. A. Kearsley, and R. S. Marvin for their valuable discussions during the preparation of this manuscript.

5. References

[1] L. J. Zapas and T. Craft, J. Res. NBS **69A** (Phys. and Chem.) No. 6, 541–546 (1965).
[2] B. Bernstein, E. A. Kearsley, and L. J. Zapas, J. Res. NBS **68B** (Math. and Math. Phys.) No. 4, 103–113 (1964).
[3] B. Bernstein, E. A. Kearsley, and L. J. Zapas, Trans. Soc. Rheology **VII**, 391–410 (1963).
[4] B. Bernstein, Time-dependent behavior of an imcompressible elastic fluid—Some homogeneous deformations, to be published in Acta Mechanica.
[5] R. S. Rivlin and D. W. Saunders, Phil. Trans, Roy. Soc. London, A **243**, 251 (1951).
[6] J. E. Morrisson, L. J. Zapas, and J. W. DeWitt, Rev. Sci. Instr. **26**, 357 (1955).
[7] J. D. Ferry, Viscoelastic Properties of Polymers, (John Wiley & Sons, New York and London, 1961).
[8] H. Markovitz, Proceedings of the Fourth International Congress on Rheology, Part I, 189 (1963).

(Paper 70A6–423)

JOURNAL OF RESEARCH of the National Bureau of Standards—A. Physics and Chemistry
Vol. 70A, No. 6, November–December 1966

Statistical Aspects of Second and Third Law Heats

William S. Horton

Institute for Materials Research, National Bureau of Standards, Washington, D.C. 20234

(July 19, 1966)

The effects of random errors and of nonconstant heat of vaporization upon the estimation of the second and third law heats of vaporization are examined. The most important conclusion is that the often noticed marked improvement in precision of the third law heat over that for the second law heat is real and is a natural consequence of the difference between the two estimators. The effects of systematic errors upon the two heats are not investigated here. Other results of interest, but of less importance because of the small magnitude of the effects, include: (1) the two heats are negatively correlated, (2) the second law heat is generally biased, (3) the third law heat is not the minimum variance unbiased estimator of the heat of vaporization, and (4) the standard deviation obtained from least squares fitting consistently overestimates the true standard deviation, but by a negligible amount. Any reversible process for which the equilibrium constant is treated by a similar procedure is governed by the same considerations. The results apply approximately at any temperature although the stimulus for these considerations comes from high temperature chemistry.

Key Words: Bias of least squares estimators, coefficient of variation, correlated estimators, enthalpy adjustments, heat of vaporization, high temperature chemistry, overestimation of standard deviation, second law heat, slope estimators, third law heat, vapor pressure.

1. Introduction

For some years it has been the practice when reporting high temperature vapor pressure data to compute and discuss "second law" and "third law" heats of vaporization or sublimation. Because each experimental temperature yields a third law heat, the individual values are often examined for consistency. Since each of these should be estimating the same quantity, grossly different values of one or of a few individuals are suggestive of experimental difficulty. With outliers thus considered, and generally discarded from future consideration, the remaining data are examined for trend, either with temperature or with chronological sequence. Trend with temperature is generally thought to be caused by systematic error in temperature measurement or in vapor pressure measurement, or by systematic error in the tabular free energy functions used to compute the third law heats. Trend with experimental sequence occasionally means that window or similar corrections used for optical pyrometry, were changing from run to run. This could be caused by darkening of the observation window as experimentation proceeds, for example. When the third law heats appear to pass this critical evaluation, the average is generally compared to the second law heat. The latter is usually obtained from the slope of a least-squares fit of the logarithm of the pressure to a straight line in the reciprocal of the absolute temperature. This comparison is also supposed to serve as a test of the experimentation [1][1] ". . . because if the heats calculated by the two procedures do not agree within the carefully calculated errors, then the experiment contains inconsistencies which all too often indicate either serious systematic errors or perhaps unknown species."

The uses described above to which the two estimates of the heat of transformation are put imply that those estimates are not biased by the method of estimation and furthermore that they are independent in the probability sense. It is the purpose of this article to point out the failure of these implicit conditions to apply and to examine the consequences of this failure. In general, the questions of unbiasedness and independence are always pertinent when two experimental values subject to random error are compared. Should either or both be biased by the means of computation, the difference may be due to that rather than to factors under study. Independence is always questionable when, as in the case of the second and third law heats, two estimates are computed using the same data. Lack of independence in the statistical sense would mean that random errors causing one estimate to be high would cause the other to be high also, in the case of positive correlation. Negative correlation would mean that random errors would have opposite effects on the two estimates. Independence would mean that there is no definite relation of this kind. The presence of correlation needs to be taken into account when a comparison is made.

It is found that the bias in the second law heat, as usually calculated, is generally negligible because of the currently attainable precision of most methods for measuring high temperature vapor pressures. The

[1] Figures in brackets indicate the literature references at the end of this paper.

230-736 O-66—6

lack of independence of the two heats does not significantly affect the size of the random error to be attributed to their difference. An important result is the understanding that the greater imprecision of the second law heat compared to that of the mean third law heat is a natural consequence of the difference between the two estimators and of the experimental temperatures usually involved. The usual method of computing the variance for the second law heat overestimates the variance when the simplest linear equation is fitted by least squares. This overestimation is quite small, however, and is naturally on the side of conservatism. Although the usually computed third law heat is not the minimum variance unbiased estimator, the loss of precision is quite small. The vaporization process is the main consideration here, but it is obvious that any reversible process for which the equilibrium constant is treated by a similar procedure is governed by the same considerations. Similar problems arise when estimating the entropy of transformation as the least-squares intercept of the usual second law treatment. As these problems will be obvious after considering the second law heat, entropy problems will not be treated here.

In what follows, the second and third law heats are discussed with a minimum of mathematical statistics. Statistical derivations, which are either already available elsewhere or are straightforward, are relegated to an appendix for statistically minded readers. Following the theoretical discussion of second and third law heats, a numerical example is given to illustrate the magnitudes of the effects.

2. Theoretical

2.1. Second Law Heat

Empirically, the vapor pressure, p, generally fits the equation

$$R \ln p = A - \frac{B}{T} \tag{1}$$

within experimental error, where R is the gas constant, A and B are assumed to be constant and T is the absolute temperature. However, theoretically at a single temperature

$$R \ln p = \Delta S^\circ - \frac{\Delta H^\circ}{T} \tag{2}$$

where ΔS° and ΔH°, the entropy and enthalpy changes, are slowly varying functions of T. The superscript $^\circ$ specifies the substances to be in standard states. Equation (2) assumes that the pressure is sufficiently low for the gas to be assumed ideal. One method of treating the data fits experimental values of $R \ln p$ to $1/T$ and adjusts $\hat{B}$, the least squares estimate of B in eq (1), to a reference temperature T_r. $\hat{B}$ might be considered a reasonable estimate of ΔH° for some representative temperature within the experimental range; the enthalpy change at a commonly used reference temperature far removed from the region of the experiment is somewhat different. Adjustment of $\hat{B}$ to such a temperature is given by

$$\hat{b}_2 = \hat{B} - \int_{T_r}^{T_e} \Delta C_p^\circ dT \tag{3}$$

where $\hat{b}_2$ is used to represent the estimate of the second law heat obtained by adjusting $\hat{B}$ from the experimental temperature, T_e, to the reference temperature, T_r. The quantity ΔC_p° is the heat capacity of the vapor minus the heat capacity of the condensed phase at constant pressure. ΔC_p° is a function of T, but is independent of p.

The reason, of course, that eq (1) is usable without serious error is that ΔC_p° is sufficiently small that its integral over a short range is negligible compared to ΔH°. The use of eq (3) is straightforward as long as one knows the correct value of T_e. Some workers make allowance for this problem by using heat capacity data as in the sigma method [2,3]. More often than not, however, the additional computational labor is not felt to be warranted and is not carried out. Instead, the experimenter chooses some temperature within the range of the experiment as corresponding to the least-squares slope in order that the adjustment by eq (3) may be carried out. Some authors use the arithmetic mean of the experimental temperatures. Others use the temperature corresponding to the arithmetic mean of the reciprocal temperatures. Still others use a rounded value somewhere near the midrange. However, it is shown below that if the data are required to fit eq (1), the quantity $\hat{B}$ does not represent unambiguously the heat of vaporization at any recognizable temperature within the range of experiment. Instead the quantity represents a combination of enthalpy and entropy terms and of the coefficients of the heat capacity equation.

It is particularly convenient in what follows to replace the variable $-T^{-1}$ by x. Then the exact vapor pressure equation may be written as

$$R \ln p = \alpha + \beta x + f(x), \tag{4}$$

where a function of x (and therefore of T) has been added to the simplest form in order to make it exact. There is no other limitation on the form of this function. Then the usual least-squares slope for fitting eq (1) has as its expected value

$$E(\hat{B}) = \beta + \frac{\Sigma(x - \bar{x}) f(x)}{\Sigma(x - \bar{x})^2}. \tag{5}$$

Alternatively it is possible to show that if $g(x)$ represents the slope of the secant connecting the point $(x, R \ln p)$ with the point on the curve at $\bar{x}$,

$$E(\hat{B}) = \frac{\Sigma(x-\bar{x})^2 g(x)}{\Sigma(x-\bar{x})^2}. \quad (6)$$

Thus, the least squares linear slope is a weighted average of the true slopes of the set of secants where the weighting is proportional to the square of the distance from $\bar{x}$.

Because $\hat{B}$ does not represent the slope at any easily defined point, the usual choices for T_e in eq (3) lead to bias in $\hat{b}_2$, the second law heat. The bias, however, is quite small and is given by the integral of ΔC_p° from the chosen T_e to the correct, if unknown, value of T_e. Examples of its magnitude are given later. The main advantage of the modified procedures mentioned earlier appears to be that they avoid the ambiguity of the temperature to which the slope applies. Occasional extended discussions arise, however, about the "correct" temperature to use, and it is well to recognize that there is no easily defined one when the data are fitted directly to eq (1). The bias is not small if the lowest or highest experimental temperature is chosen rather than one near the midrange. Further discussion of this point is relegated to a later section. Removal of the small bias by some means may be considered desirable because, hopefully, vapor pressure data collection will improve over the years and, secondly, because comparison with third law heat for significant difference should be made with estimates known to be unbiased with respect to sources not being tested by the comparison.

Because the experimental data are fitted to a straight line and because theoretically the correct function is known to be more complex, the computed standard deviation is estimating a value larger than the true standard deviation. It is shown in the appendix that the increase in variance (the square of the standard deviation) is given by

$$EVF = (n-2)^{-1}\left\{\Sigma(f-\bar{f})^2 - \frac{[\Sigma(x-\bar{x})(f-\bar{f})]^2}{\Sigma(x-\bar{x})^2}\right\}, \quad (7)$$

where n is the number of observations and $f(x)$ has been shortened to f for convenience. This quantity, the extra variance function, is always positive and, as shown in the numerical example, is negligible for the type of experiments being considered.

2.2. Third Law Heat

Alternative to the second law treatment is that of the third law wherein for each experimental point, i, there is computed

$$b_{3i} = T_i(\delta_i - R \ln p_i), \quad (8)$$

where $\delta_i = \Delta\left[-\frac{G_i^\circ - H_r^\circ}{T_i}\right]$, the change in free energy function for the process [4]. The free energy function, $-\frac{G_i^\circ - H_r^\circ}{T_i}$, for each substance is generally available in tabulations or may be computed from other data. The b_{3i} are examined individually, as suggested in the introduction, and they are also averaged to give

$$\hat{b}_3 = \frac{1}{n}\Sigma b_{3i}, \quad (9)$$

the estimator for the third law heat.

This estimator is unbiased. However, if the random errors are essentially constant when measured in $R \ln p$ at different temperatures, random errors in the b_{3i} will be a function of T because of the term $RT \ln p$. As a consequence $\hat{b}_3$ as given by eq (9) is not the estimate with the least variance. There will generally be a larger error associated with $\hat{b}_3$ than with another estimator, $\tilde{b}_3$, where

$$\tilde{b}_3 = \frac{\Sigma x(R \ln p - \delta)}{\Sigma x^2} = \frac{\Sigma T^{-1}(\delta - R \ln p)}{\Sigma T^{-2}}.$$

This is an unbiased estimator also. It can be shown that $\tilde{b}_3$ is, of all unbiased estimators of the heat, the one with minimum variance and may be called the "minimum variance unbiased estimator" (MVUE). Because $\tilde{b}_3$ has a smaller variance than $\hat{b}_3$, it might be preferred. However, it will be shown in the numerical example that for high temperature experiments the improvement in precision is small and does not warrant the loss of convenient computation. As already pointed out, the individual b_{3i} serve a useful purpose.

2.3. Similarity of Formulas for the Estimators

The estimators $\hat{b}_2$, $\hat{b}_3$, and $\tilde{b}_3$, each of which is an estimate of ΔH_r°, can be written in similar notation and the similarity is striking when these are placed side by side as follows:

$$\left.\begin{aligned} \hat{b}_2 &= \frac{\Sigma(x-\bar{x})(R \ln p - \delta)}{\Sigma(x-\bar{x})^2} = \frac{\Sigma(T^{-1}-\overline{T^{-1}})(\delta - R \ln p)}{\Sigma(T^{-1}-\overline{T^{-1}})^2} \\ \hat{b}_3 &= \frac{\Sigma x^{-1}(R \ln p - \delta)}{n} = \frac{\Sigma T(\delta - R \ln p)}{n} \\ \tilde{b}_3 &= \frac{\Sigma x(R \ln p - \delta)}{\Sigma x^2} = \frac{\Sigma T^{-1}(\delta - R \ln p)}{\Sigma T^{-2}}. \end{aligned}\right\} \quad (10)$$

Although they are not treated in this article the effects of systematic errors, such as in the thermodynamic data, may be readily investigated using these equations. The comparison of the different estimators is particularly facilitated.

2.4. Variance and Covariance of the Estimates

Because the second and third law heats are obtained by an essentially statistical estimation procedure, the statistical properties of the estimators are of interest.

230-736 O-66—7

Of greatest interest are the expected values of the estimators, their variances, the covariance and the correlation coefficient. Knowledge of the law governing the random errors would be desirable, but is not necessary. At this time it can only be stated as likely that the random deviations from eq (1) are of the Gaussian type when measured as deviations in $R \ln p$. That errors are often unwarrantedly assumed to have this characteristic has been shown by Clancey [5]. For least-squares fitting it is merely necessary that the random errors have mean zero, constant variance and be independent of one another in the probability sense. An examination of representative data is proceeding in this laboratory to ascertain the validity of the normal assumption but sufficient information is not yet available. At this point, it does seem very likely that the magnitude of random errors in the logarithm of the pressure is not temperature dependent.

If the vapor pressure data are treated by the sigma method or an alternate, then the slope obtained by the second law is for an unambiguous temperature. Correspondingly, there will be no bias in the second law heat. From the definitions [6] of expected values, variances, covariance and correlation coefficient, ρ, the following relations are found.

$$E(\hat{b}_2) = \Delta H_r^\circ \tag{11}$$

$$E(\hat{b}_3) = \Delta H_r^\circ \tag{12}$$

$$\text{Var } (\hat{b}_2) = \sigma^2/\Sigma(T^{-1} - \overline{T^{-1}})^2 \tag{13}$$

$$\text{Var } (\hat{b}_3) = \sigma^2 \Sigma T^2/n^2 \tag{14}$$

$$\text{Var } (\bar{b}_3) = \sigma^2/\Sigma T^{-2} \tag{15}$$

$$\text{Covar } (\hat{b}_2, \hat{b}_3) = \sigma^2(1 - \overline{T}\,\overline{T^{-1}})/\Sigma(T^{-1} - \overline{T^{-1}})^2 \tag{16}$$

$$\rho(\hat{b}_2, \hat{b}_3) = \frac{n(1 - \overline{T}\,\overline{T^{-1}})}{[\Sigma T^2 \Sigma(T^{-1} - \overline{T^{-1}})^2]^{1/2}}. \tag{17}$$

In these equations σ is the standard deviation of the random errors in $R \ln p$. It follows from Cauchy's inequality that $\overline{T}\,\overline{T^{-1}}$ is always greater than or equal to unity so that the second and third law heats are always negatively correlated in the statistical sense. In most high temperature experiments the degree of correlation is quite small as illustrated by an example later.

Because relative values are more informative, the following ratios are of interest:

$$\frac{\text{Var } (\hat{b}_3)}{\text{Var } (\hat{b}_2)} = \frac{\Sigma T^2 \Sigma(x - \bar{x})^2}{n^2} \tag{18}$$

$$\frac{\text{Cov } (\hat{b}_2, \hat{b}_3)}{\text{Var } (\hat{b}_2)} = 1 + \overline{T}\bar{x} \tag{19}$$

$$\frac{\text{Var } (\hat{b}_3)}{\text{Var } (\bar{b}_3)} = \frac{\Sigma T^2 \Sigma x^2}{n^2}. \tag{20}$$

(In these equations both T and x have been used for compactness.) All of these quantities have identical powers of T and x multiplying one another. Consequently, the magnitude of the mean absolute temperature of the experiments does not greatly affect the magnitude of the ratios. Instead these quantities and the correlation coefficient are functions of the coefficient of variation of the temperatures $CV(T)$, where this represents the relative spread among the temperatures chosen for the experiments rather than relative errors in the temperature. In fact, it can be shown that for moderately small values of $CV(T)$ the following are reasonable approximations.

$$\left.\begin{aligned} \rho(\hat{b}_2, \hat{b}_3) &\approx -CV(T) \\ \frac{\text{Var } (\hat{b}_3)}{\text{Var } (\hat{b}_2)} &\approx [CV(T)]^2 \\ \frac{\text{Cov } (\hat{b}_2, \hat{b}_3)}{\text{Var } (\hat{b}_2)} &\approx -[CV(T)]^2. \end{aligned}\right\} \tag{21}$$

Trial calculations have shown that the approximation for ρ is high by only 2 percent at $CV(T) = 0.15$. At this same value the approximation for the ratio Var $(\hat{b}_3)$/Var $(\hat{b}_2)$ is low by 13 percent, and the covariance ratio approximation is low by 4 percent. The ratio given by eq (18) can be greater than unity, but this is only true for experiments for which the $CV(T)$ is about 0.6 or greater. Application of Cauchy's inequality to eq (20) shows this ratio to be always greater than unity, as it must be if $\bar{b}_3$ is the minimum variance unbiased estimator.

3. Illustrative Calculations

In order to illustrate the magnitude of the effects discussed above, data for the vapor pressure of tungsten [7] will be used. Table 1 shows pertinent data from that study together with third law heats as usually computed. Table 2 compares results from various methods of computing the heat of sublimation from the data of table 1. The number of figures shown is not indicative of uncertainty. The choice was made merely in order to have at least two digits for the smallest difference between values.

TABLE 1. *Vapor pressures and heats of sublimation of tungsten*[a]

Temperature	Vapor pressure	$\Delta H_s^\circ(298)$
°K	atm × 10^9	*kcal mole*$^{-1}$
2786	5.42	203.7
2773	5.21	202.9
2679	1.26	203.5
2574	0.250	203.7
2925	30.8	203.9
3034	98.3	204.6
2614	0.534	203.0
3068	197	202.7
2934	40.0	203.0
3183	542	204.0

[a] Data from reference 7.

TABLE 2. *Comparison of sublimation heats for tungsten*

Second Law, uncorrected (T_l)[a]	201442.5 cal/mole[b]
Second Law, uncorrected ($\overline{T}$)	201619.6
Second Law, uncorrected (T_h)	201885.1
Second Law, corrected	201626.3
Third Law, usual	**203474.9**
Third Law, MVUE	**203457.5**

[a] The temperature indicated in the parentheses is that to which it was *assumed* the slope corresponded: T_l = lowest experimental temperature, T_h = highest temperature, $\overline{T}$ = arithmetic mean temperature.

[b] The number of figures shown is not indicative of the uncertainty. The choice was made merely in order that the smallest difference among values would have at least two digits. For all, the reference temperature was 298 °K.

In order to give an unbiased second law treatment, logarithmic vapor pressures were corrected by an equivalent to the sigma method. The equation

$$R \ln p - \Delta(S^\circ - S_e^\circ) + \frac{\Delta(H^\circ - H_e^\circ)}{T} = \Delta S_e^\circ - \frac{\Delta H_e^\circ}{T} \quad (22)$$

has a form such that the entropy and enthalpy functions are easily evaluated by computer using the OMNITAB language [8] and the JANAF tables [9]. The differences between second law heats from corrected and uncorrected logarithmic vapor pressures is seen to be of the order of hundreds of calories depending upon the temperature assumed to correspond to the slope. In the corrected case the "experimental temperature" was chosen to be the arithmetic mean of those listed in table 1, 2857 °K. If the slope of the uncorrected second law treatment is assumed to correspond to a temperature near $\overline{T}$, the table shows that for the tungsten work the error is of the order of only 10 calories.

Table 2 also shows the usual third law result and the minimum-variance estimator. The difference of 17 calories per mol (0.008%) is also too small to be of importance.

TABLE 3. *Variance functions*

Variance, Second Law heat[a]	1.76×10^8
Variance, Third Law heat, usual[a]	8.20×10^5
Variance, Third Law heat, MVUE[a]	8.05×10^5
Covariance ($\hat{b}_2, \hat{b}_3$)[a]	-8.12×10^5
Correlation coefficient	-0.07
Extra variance function[a]	6.24×10^{-5}

[a] Variances are relative to that for $R \ln p$.

Table 3 is probably of more interest because the improved precision of the third law heat over that for second law heat is very evident. The square root of the first two entries gives the ratio of standard deviations, about 15. It should be emphasized that this is a natural outcome of the methods of estimation and is not a result of imprecision that can be overcome by better experimentation. Also evident in table 3 is the small decrease in variance for the minimum variance estimator compared to that for the usual third law heat. As mentioned earlier there would be little gained and some definite loss in using this estimator.

The correlation coefficient for $\hat{b}_2$ and $\hat{b}_3$ given in table 3 is seen to be a small negative quantity. Because of this, the correlation is of no great importance when comparing second and third law heats. In fact, because the third law heat is also much more precise than the second law heat, the random error in the comparison is contributed almost solely by the latter quantity.

The extra variance function is truly negligible, showing that the use of the simpler method of straight line fitting for these experiments has no important effect upon the estimate of error.

4. Appendix

The question of bias in the second law heat as illustrated by eq (5) is treated by assuming that if the "true" equation is given by (4), experimental values of $R \ln p_i$, represented by y_i, are given by

$$y_i = \alpha + \beta x_i + f(x_i) + \epsilon_i, \quad (23)$$

where the ϵ_i are assumed to behave like random errors. Equation (5) results from application of the well-known formula for the slope of a linear least-squares fit to this equation and taking expected values.

Consider the curve giving the true values, Y_i, as a function of the experimental values, x_i. Let $g(x)$ be the slope of the secant joining any point (x, Y) with the point $(\overline{x}, Y(\overline{x}))$. Then for a given i

$$\frac{Y - Y(\overline{x})}{x - \overline{x}} = \frac{Y - \overline{Y}}{x - \overline{x}} + \frac{\overline{Y} - Y(\overline{x})}{x - \overline{x}} = g(x). \quad (24)$$

Multiplying by $(x - \overline{x})^2$ and summing over i yields

$$\Sigma(x - \overline{x})(Y - \overline{Y}) = \Sigma(x - \overline{x})^2 g(x). \quad (25)$$

Replacing Y by $y - \epsilon$, dividing by $\Sigma(x - \overline{x})^2$ and taking expected values gives

$$\frac{\Sigma(x - \overline{x})(y - \overline{y})}{\Sigma(x - \overline{x})^2} = \frac{\Sigma(x - \overline{x})^2 g(x)}{\Sigma(x - \overline{x})^2}. \quad (26)$$

The left-hand member is the expression used to calculate the least squares slope of a linear fit and the right hand member is that for eq (6).

When a straight line is fitted to data which are known to be nonlinear it is expected that the computed variance will be biased upwards. Although the derivation is straightforward, the expression for the excess appears not to have been presented before. For this purpose let $y = \hat{\alpha} + \hat{\beta}x + f(x) + \epsilon$ represent experimental values and let $\hat{y} = \hat{\alpha} + \hat{\beta}x$ represent estimates obtained by a least-squares linear fit. The ϵ are random errors with zero mean and variance equal to σ^2. Also let $x - \overline{x} = u$ and $\Sigma(x - \overline{x})^2 = \Sigma u^2 = S$. Then for a given i

$$y - \hat{y} = (\beta - \hat{\beta})u + (f - \overline{f}) + (\epsilon - \overline{\epsilon})$$

where for simpler writing $f(x)$ has been replaced by f. But since

$$\beta - \hat{\beta} = -\frac{\Sigma uf}{S} - \frac{\Sigma u\epsilon}{S},$$

$$y_i - \hat{y} = \left[-\frac{u_i \Sigma uf}{S} + (f_i - \bar{f}) \right] + \left[-u_i \frac{\Sigma u\epsilon}{S} + (\epsilon_i - \bar{\epsilon}) \right],$$

where subscript i has now been indicated. The brackets segregate two terms, one with error terms and one without. Thus,

$$y_i - \hat{y} = A_i + e_i.$$

To determine what the usually computed variance is actually giving we need the expected value of the sum of squares for $y - \hat{y}$, or

$$E\{\Sigma(y - \hat{y})^2\} = \Sigma A_i^2 + E(\Sigma e_i^2).$$

The first term of the right-hand member is

$$\Sigma A_i^2 = \Sigma(f - \bar{f})^2 - \frac{(\Sigma uf)^2}{S}.$$

The second term becomes

$$E(\Sigma e_i^2) = \frac{(\Sigma u^2)^2}{S^2}\sigma^2 - \frac{2}{S}E\{\Sigma u(\epsilon - \bar{\epsilon})\Sigma u\epsilon\} + E\{\Sigma(\epsilon - \bar{\epsilon})^2\}$$

where in the right-hand member subscripts have been dropped as they are no longer needed for clarity. This expression is evaluated easily as $(n-2)\sigma^2$. Because the computed variance is given by $(n-2)^{-1}$ $\Sigma(y - \hat{y})^2$, the expected value follows as

$$E\{\text{Var } (\hat{y})\} = \sigma^2 + (n-2)^{-1}\left[\Sigma(f - \bar{f})^2 - \frac{(\Sigma uf)^2}{S}\right].$$

The second term of the right-hand member is equivalent to eq (7) and has been termed by the author the extra variance function. From its equivalent,

$$\frac{\Sigma\Sigma_{ij}[u_i(f - \bar{f})_j - u_j(f - \bar{f})_i]^2}{(n-2)S},$$

wherein the summations over i and j are limited by $i \neq j$ and $j > i$, the extra variance function is seen to be always positive.

The last equation of (10) results from dividing eq (8) by T_i and minimizing the sum of squared residuals with respect to b_3. Equations (13), (14), and (15) are the results of taking the variances of the linear forms, (10). Equation (13) also follows from the well-known results for a straight line. Equation (16) follows from the expected value of $(\hat{b}_2 - \Delta H_r^\circ)(\hat{b}_3 - \Delta H_r^\circ)$. Equation (17) is by definition given as

$$\text{Covar } (\hat{b}_2, \hat{b}_3)/\sqrt{\text{Var } (\hat{b}_2) \cdot \text{Var } (\hat{b}_3)}.$$

In order to obtain the approximations of eqs (21), the Taylor's expansion for x around $\bar{T}$ is useful:

$$x \approx -\frac{1}{\bar{T}} + \frac{(T - \bar{T})}{\bar{T}^2} - \frac{(T - \bar{T})^2}{\bar{T}^3} + \ldots .$$

From this one obtains

$$\bar{x} \approx -\frac{1}{\bar{T}} - \frac{\Sigma(T - \bar{T})^2}{n\bar{T}^3}$$

and

$$\Sigma(x - \bar{x})^2 \approx \frac{\Sigma(T - \bar{T})^2}{\bar{T}^4}.$$

From the expression for $\bar{x}$, the relation

$$1 + \bar{T}\bar{x} \approx -\frac{\Sigma(T - \bar{T})^2}{n\bar{T}^2} = -[CV(T)]^2$$

is obtained, which by virtue of eq (19), gives the third approximation in (21).

In the exact expression $\Sigma T^2 = \Sigma(T - \bar{T})^2 + n\bar{T}^2$ the sum of the squared differences may be neglected when the $CV(T)$ is small, and one can use $\Sigma T^2 \approx n\bar{T}^2$. Using both T and $\bar{x}$ the square of (17) may be written as

$$\frac{n^2(1 + \bar{T}\bar{x})^2}{\Sigma T^2 \Sigma(x - \bar{x})^2} \approx \frac{\Sigma(T - \bar{T})^2}{n\bar{T}^2} = [CV(T)]^2.$$

We note that taking the square root of both sides now gives ambiguity with regard to sign, but it has already been pointed out that this must be negative. Thus, the first approximation of (21) is obtained. The second approximation follows readily from expressions already used here.

It is a pleasure to acknowledge helpful discussions held with staff members of the National Bureau of Standards. The derivation of the extra variance function which appears in this paper is due to J. Mandel and replaces an earlier, less simple one originated by the author. The great utility of Taylor's expansion for the derivation of the approximations was pointed out by J. R. Rosenblatt. Thermodynamic notions were discussed with E. R. Plante and statistical notions with J. R. Rosenblatt, T. A. Willke, and D. Hogben.

5. References

[1] R. J. Ackerman and R. J. Thorn, Vaporization of Oxides in Progress in Ceramic Science, Volume 1, p. 42, ed. by J. E. Burke. (Pergamon Press, N.Y., 1961).

[2] K. K. Kelley, Contributions to the Data on Theoretical Metallurgy. III. The Free Energies of Vaporization and Vapor Pressures of Inorganic Substances, Bulletin 383, U.S. Dept. of Interior, Bur. of Mines, 1935.

[3] G. N. Lewis and M. Randall, Thermodynamics, 2d ed., p. 175, revised by K. S. Pitzer and L. Brewer (McGraw-Hill Book Company, New York, 1961).

[4] S. Glasstone, Thermodynamics for Chemists, pp. 306–309 (D. Van Nostrand Co., New York, N.Y., (1947)).

[5] V. J. Clancey, Nature **159,** 339–40 (1947).

[6] A. M. Mood and F. A. Graybill, Introduction to the Theory of Statistics, 2d ed., ch. 5 (McGraw-Hill Book Company, New York, N.Y., 1963).

[7] R. Szwarc, E. R. Plante, and J. J. Diamond, J. Res. NBS **69A** (Phys. and Chem.) No. 5, 417 (1965).

[8] J. Hilsenrath, G. G. Ziegler, C. G. Messina, P. J. Walsh, and R. J. Herbold, Omnitab, A Computer Program for Statistical and Numerical Analysis, NBS Handbook 101 (1966).

[9] JANAF Thermochemical Tables, Dow Chemical Co., Midland, Michigan, 1961, Tungsten crystal and gas tables dated December 31, 1961.

(Paper 70A6–424)

JOURNAL OF RESEARCH of the National Bureau of Standards—A. Physics and Chemistry
Vol. 70A, No. 6, November–December 1966

Density-Temperature Formulae for Coexisting Liquid and Vapor and for Freezing Liquid Parahydrogen

Robert D. Goodwin*

Institute for Materials Research, National Bureau of Standards, Boulder, Colo.

(June 21, 1966)

A single formula is given for coexistence temperature as a continuous function of the vapor-liquid densities. With six coefficients and seven adjusted exponents, it may conveniently replace the several formulae formerly used in separate regions of the data. Freezing liquid densities are described by a simple power law in temperature, replacing more complicated formulae. Computed results are tabulated and compared with the derived data.

Key Words: Coexistence densities, freezing liquid densities, hydrogen, melting-line liquid densities, orthobaric densities, parahydrogen, vapor-liquid equilibrium.

1. Introduction

Data for densities of the coexisting phases of parahydrogen are derived, not directly experimental. They were obtained as intersections of PVT isochores and isotherms with vapor-pressure and melting-line formulae for $P(T)$ at coexistence [1, 2].[1] Any concise description of these densities is a useful computational aid, as for example, to obtain heats of transition via the Clapeyron and $P(T)$ equations. In [1], however, we had used three formulae, in three regions of the orthobaric densities, with a total of 14 coefficients and about 12 adjusted exponents. The present search for a single formula for orthobaric densities was motivated by the successful application of Ehrlich's simple formula for saturated liquid [5] to our parahydrogen data. This is reported below.

Background on fluid behavior is given by [3], and quantum effects are under study [4]. Additional references on parahydrogen are given in the monograph [6]. Useful with the Clapeyron equation are recent determinations of heats of fusion [7] and of densities of solid parahydrogen [8]. The words: coexisting; at coexistence; orthobaric; at saturation; and saturated vapor, liquid or solid, all refer to one or more of at least two phases in equilibrium. The NBS–1955 low temperature scale used here is the same as in [6], and we define one liter, L, to be 1000 cm^3.

2. Ehrlich's Formula for Saturated Liquid Parahydrogen

Ehrlich's formula, eq (1), employs reduced variables, $\rho \equiv D/D_c$, $\tau \equiv T/T_c$ (where D and T are density and temperature, with subscript c referring to the critical point),

$$(\rho-1)^3/\rho = A\cdot(1-\tau)+B\cdot(1-\tau)^2. \qquad (1)$$

We used iterative methods and a digital computer to find the critical constants for eq (1) which minimize the mean relative deviation between calculated densities and 46 pairs of data for $\rho(\tau)$ [1]. This form of deviation was selected because the data are not directly experimental. Largest relative deviations occur near the critical point and are tabulated in summarizing table 1, while those near the triple point are plotted in figure 1 as open circles. [We define Δ, $\% \equiv 100\cdot(D_{\text{calc}}-D_{\text{ref}})/D_{\text{ref}}$.] Most of the remaining deviations are a mere few hundredths of 1 percent. It is seen that this formula gives an excellent representation of the data.

TABLE 1. *Ehrlich's formula for saturated liquid parahydrogen*

Constants $T_c = 32.984\ 38$ °K, $D_c = 15.17685$ g mol/L, $A = 2.859\ 125$, $B = -0.820\ 205$

Mean deviation (46 points) = 0.0432 percent

Maximum relative deviations near critical point

T, °K	Δ, %	T, °K	Δ, %
32.914	0.000	32.363	−0.044
32.739	−0.195	32.039	−0.140
32.579	−0.110	32.000	+0.038

3. A Formula for Densities of Coexisting Vapor and Liquid

In attempting to modify Ehrlich's formula for densities below critical we note that as $\rho \to 0$ the familiar vapor-pressure and virial equations provide a relation between temperature and density,

$$P \sim P_0\cdot\exp(-T_0/T) \sim D\cdot R\cdot T,$$

* Cryogenics Division, NBS Laboratories, Boulder, Colo.

[1] Figures in brackets indicate the literature references at the end of this paper.

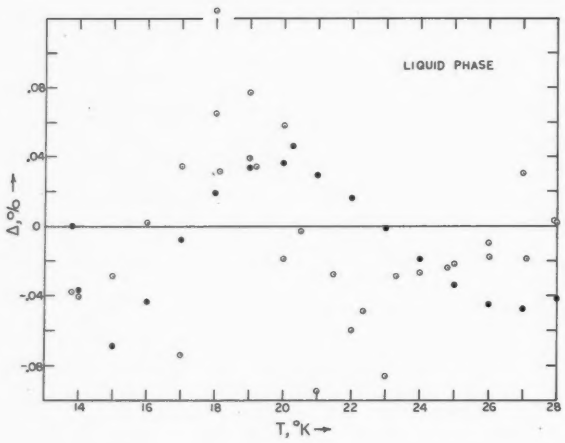

FIGURE 1. *Comparison of calculated densities.*
$\Delta = 100 \cdot (D_{calc} - D_{ref})/D_{ref}$: Open circles, Ehrlich's formula with constants of table 1, using for D_{ref} the derived data of [1]; filled circles from table 4, this report.

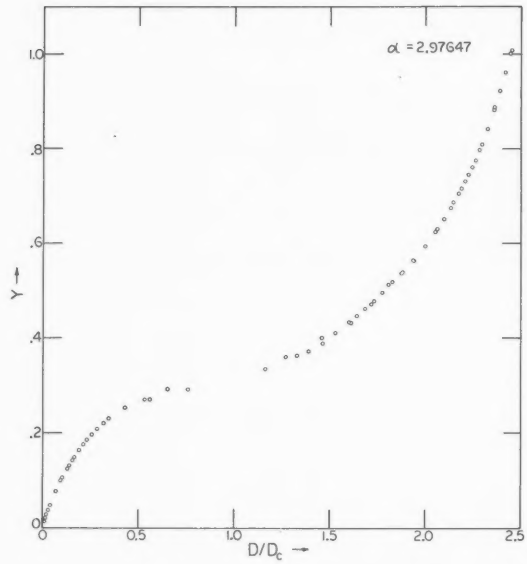

FIGURE 2. $Y(\alpha, \beta, \rho, \tau)$ *versus* ρ *for* $\alpha = 2.97647$, $\beta = 8$.

where P is pressure, R is the gas constant, and P_0, T_0 are constants. At coexistence, $D \cdot R \cdot T$ may be regarded as a function only of the density. Normalizing the above exponential at the critical point in the form, $\exp[\alpha \cdot (1 - 1/\tau)]$ where α is a constant, and comparing its Taylor's series expansion about $\tau = 1$ with eq (1), we have been led to the formula,

$$\exp[\alpha \cdot (1 - 1/\tau)] = 1 - (\rho - 1)^{\beta/3}/\exp[\rho \cdot f(\rho)], \quad (2)$$

wherein $\beta/3$ replaces exponent 3 from eq (1), and $f(\rho)$ is discussed below. This is a single-valued expression for coexistence temperature as a function of the densities, constrained to a given critical point. As the variable τ ranges from 0 to +1 only, β must be an even integer. The expression $[1 - (\rho - 1)^{\beta/3}]$ becomes negative for $2 < \rho \leq 2.45$ where $\rho = 2.45$ is the upper limit for liquid parahydrogen at the triple point.

The exponential on the right side of eq (2) has been introduced as an empirical method for seeking representation of data. We let $f(\rho)$ be a polynomial, and search for the requisite number of terms and powers of ρ, finding coefficients by least-squares in the form $Y/\rho = f(\rho)$, where

$$Y(\alpha, \beta, \rho, \tau) \equiv \mathrm{Log}_e\{(\rho - 1)^{\beta/3}/[1 - e^{\alpha(1 - 1/\tau)}]\}.$$

For each trial β and each form, $f(\rho)$, the value of α is found by an iterative procedure with the high-speed computer. By requisite number of terms and powers of ρ in this report we mean that combination which yields deviations comparable with uncertainty of the data, and a mean relative deviation less than 0.1 percent. We have used only the critical-point constants established by [1], not to be confused with the optimizing values in table 1.

With 75 pairs of data for $\tau(\rho)$ [1], the behavior of Y versus ρ is highly sensitive to the values of α and of β. For $\beta = 6$ and for $\beta = 10$ we find that Y apparently tends to infinite discontinuities as $\rho \to 1$, from below or from above, whereas for $\beta = 8$ the behavior is seen in figure 2, for which $\alpha = 2.97647$, $\beta = 8$. This plot has the qualitative behavior of an isotherm of pressure versus density at temperatures a little above critical, suggesting a cubic polynomial in the density, [or a quadratic for $f(\rho)$ in eq (2)]. Tedious exploration of forms for $f(\rho)$, however, yields

$$f(\rho) \equiv A_1 + A_2 \cdot \rho^{-1/3} + A_3 \cdot \rho^{1/3} + A_4 \cdot \rho^{8/3} + A_5 \cdot \rho^3 + A_6 \cdot \rho^7, \quad (3)$$

to complete eq (2) with above values for α, β. Integer exponents only were explored for the last two terms in eq (3). Mean relative deviation of temperatures using eq (3) is 0.0624 percent. As compared with a three-term expression for $f(\rho)$, we note that an additional term, $A_2 \cdot \rho^{-1/3}$, has been required for data at the lowest densities, and an opposition of similar terms, $A_4 \cdot \rho^{8/3} + A_5 \cdot \rho^{9/3}$, (with opposite signs) apparently is required for the critical region (fig. 2).

TABLE 2. *Constants for eqs (2), (3), parahydrogen*

$D_c = 15.59$ g mol/L,	$T_c = 32.976$ °K
$\alpha = 2.97647$,	$\beta = 8$,
$A_1 = +2.030\ 0583$,	$A_2 = -0.058\ 7951$,
$A_3 = -1.856\ 5706$,	$A_4 = +0.620\ 5095$,
$A_5 = -0.421\ 81139$,	$A_6 = +0.682\ 5745 \cdot 10^{-3}$

Table 2 gives constants for eqs (2) and (3). Table 3 compares calculated temperatures from eq (2) with the data. Table 4 gives densities obtained from eq (2) by an iterative method at integral temperatures, and compares them with densities calculated in [1] with

TABLE 3. *Comparison of calculated temperatures from eq (2) with data of [1]*

DENSTY	T,DATA	T,CALC	T,DIFF	PERCNT	DENSTY	T,DATA	T,CALC	T,DIFF	PERCNT
0.0624	13.8030	13.8051	0.0021	0.0150	25.5526	30.7490	30.7516	0.0026	0.0083
0.0686	13.9900	13.9912	0.0012	0.0082	26.2284	30.3430	30.3445	0.0015	0.0049
0.1100	14.9900	14.9908	0.0008	0.0054	26.7454	30.0000	30.0049	0.0049	0.0163
0.1671	15.9900	15.9889	-0.0011	-0.0071	26.9633	29.8540	29.8543	0.0003	0.0009
0.2430	16.9900	16.9872	-0.0028	-0.0167	27.6451	29.3560	29.3534	-0.0026	-0.0089
0.3409	17.9900	17.9860	-0.0040	-0.0220	28.1314	29.0000	28.9680	-0.0320	-0.1102
0.4642	18.9900	18.9857	-0.0043	-0.0226	28.4499	28.7240	28.7026	-0.0214	-0.0744
0.6164	19.9900	19.9850	-0.0050	-0.0248	29.2443	28.0000	27.9941	-0.0059	-0.0210
0.6636	20.2680	20.2584	-0.0096	-0.0472	29.3123	27.9360	27.9303	-0.0057	-0.0204
1.0850	22.2290	22.2269	-0.0021	-0.0094	30.1841	27.0780	27.0664	-0.0116	-0.0429
1.4969	23.6510	23.6539	0.0029	0.0121	30.2437	27.0000	27.0041	0.0041	0.0153
1.6141	24.0000	24.0032	0.0032	0.0132	31.1471	26.0180	26.0086	-0.0094	-0.0360
1.9919	25.0000	25.0053	0.0053	0.0211	31.1602	26.0000	25.9935	-0.0065	-0.0252
2.1612	25.3940	25.4038	0.0098	0.0387	31.9866	25.0000	24.9917	-0.0083	-0.0332
2.4423	26.0000	26.0100	0.0100	0.0385	32.1482	24.7940	24.7853	-0.0087	-0.0353
2.5671	26.2510	26.2597	0.0087	0.0330	32.7264	24.0000	24.0169	0.0169	0.0702
2.9764	27.0000	27.0074	0.0074	0.0275	33.2393	23.3010	23.2947	-0.0063	-0.0270
3.3330	27.5760	27.5836	0.0076	0.0274	33.4635	23.0000	22.9665	-0.0335	-0.1457
3.6197	28.0000	28.0041	0.0041	0.0148	33.8838	22.3440	22.3296	-0.0144	-0.0643
3.9821	28.4870	28.4890	0.0020	0.0072	34.1067	22.0000	21.9801	-0.0199	-0.0907
4.4062	29.0000	28.9991	-0.0009	-0.0030	34.4222	21.4730	21.4706	-0.0024	-0.0113
4.9653	29.5900	29.5913	0.0013	0.0042	34.6992	21.0000	21.0085	0.0085	0.0406
5.3972	30.0000	29.9951	-0.0049	-0.0163	34.9837	20.5070	20.5189	0.0119	0.0581
6.7196	31.0000	30.9979	-0.0021	-0.0067	35.2509	19.9950	20.0445	0.0495	0.2477
6.7864	31.0480	31.0406	-0.0074	-0.0239	35.2753	20.0000	20.0005	0.0005	0.0024
8.3122	31.8470	31.8460	-0.0010	-0.0032	35.5966	19.3900	19.4087	0.0187	0.0963
8.6917	32.0000	32.0021	0.0021	0.0065	35.7845	18.9930	19.0521	0.0591	0.3111
10.1455	32.4720	32.4671	-0.0049	-0.0152	35.7945	19.0000	19.0329	0.0329	0.1731
11.8156	32.7870	32.7871	0.0001	0.0004	36.2498	18.1150	18.1336	0.0186	0.1028
18.1181	32.9140	32.9140	-0.0000	-0.0001	36.2733	18.0000	18.0858	0.0858	0.4768
19.8043	32.7390	32.7375	-0.0015	-0.0044	36.2989	17.9920	18.0336	0.0416	0.2313
20.7043	32.5790	32.5801	0.0011	0.0033	36.7931	16.9910	16.9931	0.0021	0.0121
21.6233	32.3630	32.3668	0.0038	0.0116	36.8288	17.0000	16.9155	-0.0845	-0.4973
22.7261	32.0390	32.0340	-0.0050	-0.0155	37.2633	15.9900	15.9458	-0.0442	-0.2767
22.7996	32.0000	32.0087	0.0087	0.0273	37.7102	14.9900	14.9117	-0.0783	-0.5224
23.8347	31.6020	31.6082	0.0062	0.0196	38.1286	13.9900	13.9609	-0.0291	-0.2083
24.9013	31.1040	31.1057	0.0017	0.0055	38.2029	13.8030	13.8030	0.0000	0.0002
25.0790	31.0000	31.0127	0.0127	0.0410	38.2029	13.8030	13.8030	0.0000	0.0002

MEAN DEVIATION, PERCENT = 0.0624

the more elaborate formulae. Table 5 gives temperatures from eq (2) at uniformly spaced densities and compares them with values from the monograph [6].

Deviations of temperature (table 3) are relatively large and uniform for liquid densities approaching the triple point, giving alarm that the large exponents used in eq (3) may be responsible. From [6] we find, however, that $(\rho/\tau)(d\tau/d\rho) \approx 3$ to 6 in this region, so that relative temperature deviations will be roughly fivefold greater than corresponding density deviations. We note, also, the experimentalist's estimate of 0.1 percent accuracy [9] for much of the density data used in [1]. Turning to deviations in density, we see in figure 1 that those from eq (2), filled circles, are smaller than or comparable with those from the simple formula eq (1). [To avoid a multiplicity of tables, we have compared densities from eq (2) with the sufficiently precise, calculated results from [1]; hence the relative difference also is a smooth function.] It appears highly improbable that deviations of eq (2) are due entirely to the form of $f(\rho)$ in eq (3). With data for other substances, however, we may expect that this form should be modified.

TABLE 4. *Comparison of calculated densities from eq (2) at uniform temperatures with calculated data of [1]*

	CALCULATED DENSITIES, GMOL/L					
	VAPOR PHASE			LIQUID PHASE		
T,DG.K	CALCLTD	REFRNCE	DIFRNCE	CALCLTD	REFRNCE	DIFRNCE
13.803	0.0623	0.0624	-0.0001	38.2030	38.2068	-0.0038
14.000	0.0689	0.0690	-0.0001	38.1105	38.1246	-0.0141
15.000	0.1104	0.1104	0.0000	37.6723	37.6984	-0.0261
16.000	0.1678	0.1678	0.0000	37.2395	37.2552	-0.0157
17.000	0.2441	0.2440	0.0001	36.7899	36.7928	-0.0029
18.000	0.3424	0.3420	0.0004	36.3153	36.3086	0.0067
19.000	0.4662	0.4653	0.0009	35.8116	35.7997	0.0119
20.000	0.6189	0.6176	0.0013	35.2755	35.2628	0.0127
20.268	0.6653	0.6636	0.0017	35.1260	35.1100	0.0160
21.000	0.8048	0.8030	0.0018	34.7042	34.6940	0.0102
22.000	1.0284	1.0273	0.0011	34.0941	34.0886	0.0055
23.000	1.2955	1.2956	-0.0001	33.4409	33.4411	-0.0002
24.000	1.6130	1.6145	-0.0015	32.7387	32.7448	-0.0061
25.000	1.9897	1.9926	-0.0029	31.9801	31.9910	-0.0109
26.000	2.4374	2.4413	-0.0039	31.1546	31.1685	-0.0139
27.000	2.9721	2.9762	-0.0041	30.2476	30.2622	-0.0146
28.000	3.6168	3.6201	-0.0033	29.2380	29.2502	-0.0122
29.000	4.4070	4.4082	-0.0012	28.0922	28.0991	-0.0069
30.000	5.4027	5.4006	0.0021	26.7526	26.7520	0.0006
31.000	6.7228	6.7170	0.0058	25.1029	25.0946	0.0083
32.000	8.6864	8.6800	0.0064	22.8246	22.8145	0.0101
32.400	9.8926	9.8880	0.0046	21.4947	21.4887	0.0060
32.700	11.2457	11.2425	0.0032	20.0459	20.0463	-0.0004
32.900	12.8997	12.8921	0.0076	18.3203	18.3247	-0.0044

TABLE 5. *Comparison of calculated temperatures from eq (2) at uniform densities with derived results from [6]*

Density	Temperature, deg. K			Density	Temperature, deg. K		
	Calculated	Reference	Difference		Calculated	Reference	Difference
0.5	19.240	19.243	−0.003	19.5	32.780	32.780	0.000
1.0	21.882	21.887	−0.005	20.0	32.707	32.707	0.000
1.5	23.663	23.660	0.003	20.5	32.620	32.620	0.000
2.0	25.025	25.018	0.007	21.0	32.517	32.517	0.000
2.5	26.127	26.119	0.008	21.5	32.399	32.397	0.002
3.0	27.048	27.041	0.007	22.0	32.263	32.261	0.002
3.5	27.833	27.828	0.005	22.5	32.109	32.106	0.003
4.0	28.512	28.509	0.003	23.0	31.938	31.934	0.004
4.5	29.104	29.103	0.001	23.5	31.747	31.742	0.005
5.0	29.625	29.626	−0.001	24.0	31.536	31.532	0.004
5.5	30.085	30.087	−0.002	24.5	31.306	31.301	0.005
6.0	30.492	30.495	−0.003	25.0	31.054	31.050	0.004
6.5	30.853	30.856	−0.003	25.5	30.782	30.778	0.004
7.0	31.172	31.176	−0.004	26.0	30.487	30.484	0.003
7.5	31.455	31.459	−0.004	26.5	30.169	30.168	0.001
8.0	31.705	31.709	−0.004	27.0	29.828	29.829	−0.001
8.5	31.925	31.928	−0.003	27.5	29.464	29.466	−0.002
9.0	32.118	32.120	−0.002	28.0	29.075	29.080	−0.005
9.5	32.285	32.287	−0.002	28.5	28.660	28.668	−0.008
10.0	32.429	32.430	−0.001	29.0	28.219	28.229	−0.010
10.5	32.552	32.553	−0.001	29.5	27.752	27.764	−0.012
11.0	32.656	32.656	−0.000	30.0	27.256	27.270	−0.014
11.5	32.741	32.742	−0.001	30.5	26.732	26.747	−0.015
12.0	32.811	32.811	−0.000	31.0	26.178	26.194	−0.016
12.5	32.866	32.866	−0.000	31.5	25.592	25.608	−0.016
13.0	32.907	32.908	−0.001	32.0	24.975	24.988	−0.013
13.5	32.937	32.938	−0.001	32.5	24.323	24.334	−0.011
14.0	32.957	32.958	−0.001	33.0	23.637	23.642	−0.005
14.5	32.969	32.970	−0.001	33.5	22.912	22.912	0.000
15.0	32.975	32.975	−0.000	34.0	22.148	22.141	0.007
15.5	32.976	32.976	−0.000	34.5	21.342	21.327	0.015
16.0	32.976	32.975	0.001	35.0	20.490	20.469	0.021
16.5	32.972	32.972	−0.000	35.5	19.589	19.564	0.025
17.0	32.963	32.963	−0.000	36.0	18.633	18.612	0.021
17.5	32.946	32.947	−0.001	36.5	17.618	17.609	0.009
18.0	32.921	32.922	−0.001	37.0	16.539	16.556	−0.017
18.5	32.886	32.886	0.000	37.5	15.401	15.451	−0.050
19.0	32.839	32.840	−0.001	38.0	14.245	14.295	−0.050

4. A Formula for Densities of Freezing Liquid

In [2], densities of freezing liquid were derived as intersections of *PVT* isochores and isotherms with an analytically described $P(T)$ melting line, and given a rather complicated, empirical description. We now find that a simple power law [eq (4)] is sufficient. Variables are normalized at the triple point (subscript t):

$$(D/D_t)=(T/T_t)^{\gamma}. \tag{4}$$

For parahydrogen, the constants used are $D_t=(1.0/0.026176)$ g mol/L, $T_t=13.803$ °K [10], and we find the exponent, $\gamma=0.310\,4277$ by minimizing the mean relative deviation. Table 6 shows that eq (4) gives adequate representation. The first four columns are from [2].

The number of digits, given for constants in tables 1, 2, and for γ in eq (4), is more than sufficient to reproduce the calculated results, and is not the result of statistical analysis.

Mr. William J. Hall contributed the essential computer programs for iteration and for least squares.

TABLE 6. *Comparison of calculated densities of freezing liquid with derived data from [2]* [a]

T, deg. K	Publication			Above formula	
	D, data	D, calc	D, percent	D, calc	D, percent
14.171	38.50	38.51	0.03	38.516	0.042
14.416	38.70	38.72	0.05	38.722	0.056
14.764	39.00	39.00	0.01	39.010	0.024
15.247	39.39	39.40	0.01	39.401	0.029
15.375	39.50	39.50	0.01	39.504	0.009
16.006	40.00	39.99	−0.01	40.000	0.000
16.030	40.02	40.01	−0.02	40.019	−0.003
16.655	40.50	40.49	−0.02	40.497	−0.008
16.790	40.60	40.59	−0.01	40.598	−0.004
17.000	40.76	40.75	−0.02	40.755	−0.012
17.323	41.00	40.99	−0.02	40.994	−0.015
17.506	41.13	41.13	−0.01	41.128	−0.005
18.000	41.49	41.49	−0.00	41.485	−0.013
18.012	41.50	41.49	−0.01	41.493	−0.016
18.214	41.65	41.64	−0.02	41.637	−0.031
18.723	42.00	42.00	−0.01	41.995	−0.012
18.883	42.11	42.11	−0.01	42.106	−0.009
19.000	42.19	42.19	−0.00	42.187	−0.007
19.455	42.50	42.50	0.00	42.498	−0.005
19.585	42.58	42.59	0.02	42.586	0.014
20.000	42.86	42.87	0.02	42.864	0.009
20.203	43.00	43.00	0.00	42.999	−0.003
20.218	43.01	43.01	0.01	43.009	−0.003
20.879	43.44	43.44	0.00	43.440	0.000
20.976	43.50	43.50	0.01	43.503	0.006
21.000	43.52	43.52	0.00	43.518	−0.004
21.468	43.81	43.81	0.01	43.817	0.016
21.770	44.00	44.00	0.00	44.007	0.017
22.000	44.14	44.14	0.01	44.151	0.025
23.000	44.77	44.74	−0.05	44.765	−0.012

[a] Densities in g mol/L.

This work was supported by the National Aeronautics and Space Administration.

5. References

[1] H. M. Roder, D. E. Diller, L. A. Weber, and R. D. Goodwin, The orthobaric densities of parahydrogen, derived heats of vaporization, and critical constants, Cryogenics **3,** No. 1, 16–22 (1963).

[2] R. D. Goodwin and H. M. Roder, PVT relations of freezing liquid parahydrogen to 350 atm., Cryogenics **3,** No. 1, 12–15 (1963).

[3] J. S. Rowlinson, Liquids and Liquid Mixtures, Butterworths, London, 1959.

[4] M. E. Fisher, Quantum corrections to critical point behavior, Phys. Rev. Letters **16,** No. 1, 11–14 (1966).

[5] Percy Ehrlich, p. 49 in Advances in thermophysical properties Am. Soc. Mech. Engrs., New York, N.Y. 10017 (1965).

[6] H. M. Roder, L. A. Weber, and R. D. Goodwin, Thermodynamic and related properties of parahydrogen from the triple point to 100 °K at pressures to 340 atmospheres, NBS Monograph 94, August, 1965.

[7] R. F. Dwyer, G. A. Cook, B. M. Shields, and D. H. Stellrecht, Heat of fusion of solid parahydrogen, J. Chem. Phys. **42,** No. 11, 3809–3812 (1965).

[8] R. F. Dwyer, G. A. Cook, O. E. Berwaldt, and H. E. Nevins, Molar volume of solid parahydrogen along the melting line, J. Chem. Phys. **43,** No. 3, 801–805 (1965).

[9] R. D. Goodwin, Apparatus for determination of PVT relations and specific heats of hydrogen to 350 atm at temperatures above 14 °K, J. Res. NBS **65C** (Phys. and Chem.) No. 4, 231–243 (1961).

[10] H. W. Woolley, R. B. Scott, and F. G. Brickwedde, Compilation of thermal properties of hydrogen in its various isotopic and ortho-para modifications, J. Res. NBS **41,** 379–475 (1948) RP1932.

(Paper 70A6–425)

JOURNAL OF RESEARCH of the National Bureau of Standards—A. Physics and Chemistry
Vol. 70A, No. 6, November–December 1966

Solubility of $CaHPO_4 \cdot 2H_2O$ and Formation of Ion Pairs in the System $Ca(OH)_2 - H_3PO_4 - H_2O$ at 37.5 °C

Edgard C. Moreno,* Thomas M. Gregory,* and Walter E. Brown*

Institute for Materials Research, National Bureau of Standards, Washington, D.C. 20234

(June 1, 1966)

The solubility isotherm for $CaHPO_4 \cdot 2H_2O$ (DCPD) in the three-component system $Ca(OH)_2 - H_3PO_4 - H_2O$ was determined in the *p*H range 3.5 to 6.8 by leaching a thermostated column of DCPD with dilute phosphoric acid solutions. In confirmatory experiments, equilibrium was approached both from super- and under-saturation by shaking DCPD with appropriate solutions. The calculated ionic activity product $(Ca^{++}) \times (HPO_4^{=})$, appeared to be a parabolic function of *p*H with a minimum near *p*H 5.0. The *p*H dependence of the ionic product could be accounted for by considering the ion pairs $[CaHPO_4]^\circ$ and $[CaH_2PO_4]^+$ as semi-empirical parameters. Under the condition of saturation with respect to DCPD, the activity of the pair $[CaHPO_4]^\circ$ must be a constant. The activity of the species $[CaH_2PO_4]^+$ was shown to vary directly with hydrogen ion activity. The activities of the two ion pairs were adjusted to give a set of *p*H-independent ionic activity products with a mean of $2.19 \pm 0.011 \times 10^{-7}$. The stability constants for $[CaHPO_4]^\circ$ and $[CaH_2PO_4]^+$ are $5.88 \pm 0.031 \times 10^2$ and 7.49 ± 0.039, respectively. Experiments were conducted to study the hydrolysis of DCPD to more basic calcium phosphates and the kinetics of these transformations is discussed. The significance of the ion pairs in human serum is considered.

Key Words: Solubility of calcium monohydrogen phosphate dihydrate at 37.5 °C, calcium-phosphate ion-pairs, solubility of dicalcium phosphate dihydrate, solubility of dibasic calcium phosphate dihydrate.

1. Introduction

Dicalcium phosphate dihydrate (DCPD), $CaHPO_4 \cdot 2H_2O$, has been found as a component of dental calculi [1][1] and other biological deposits [2]. A role for DCPD as a nucleating agent [3] in calcification of tissues and its presence at the dental caries site [4] have also been suggested. Also, DCPD has chemical properties which are very helpful for the study of chemical interrelations among the various phosphates of biological significance; its high rate of solution for example, makes it possible to prepare reproducible calcium phosphate solutions within a wide range of concentrations and *p*H values which can be used in connection with crystal growth studies, calcification, etc. It has commercial importance as a constituent of fertilizers, feed-grade dicalcium phosphate, and dentifrices.

For these reasons, its solubility is of importance; there is disagreement, however, in reported values of its solubility product constant [5, 6, 7, 8, 9]. Perhaps the most important cause for inconsistent reports is its metastability with respect to the anhydrous salt, $CaHPO_4$, and the more basic calcium phosphates, hydroxyapatite (HA), $Ca_{10}(OH)_2(PO_4)_6$, and octacalcium phosphate (OCP), $Ca_8H_2(PO_4)_6 \cdot 5H_2O$, [10]. Formation of complexes or ion pairs between the calcium and orthophosphate ions, as reported here, also contributes to uncertainty in solubility product constants calculated from solubility data. Its solubility isotherm in the three-component system, $Ca(OH)_2 - H_3PO_4 - H_2O$, at 25 °C is known [9]. The solubility isotherm and solubility product at physiological temperature, 37.5 °C, are reported here. Equilibrations of DCPD with dilute phosphoric acids, using the leaching technique previously described [9], proved successful in minimizing formation of secondary phases. Batchwise equilibrations were used to verify the results obtained with the leaching technique.

* Research Associates, American Dental Association, National Bureau of Standards, Washington, D.C. 20234.

This investigation was supported in part by Research Grant DE-01819 to the American Dental Association from the U.S. Public Health Service and is part of the dental research program conducted by the National Bureau of Standards in cooperation with the Council on Dental Research of the American Dental Association; the National Institutes of Health; the Army Dental Corps; the Aerospace Medical Division, USAF School of Aerospace Medicine; and the Veterans Administration.

[1] Figures in brackets indicate the literature references at the end of this paper.

2. Methods and Experimental Materials

2.1. Preparation of Materials

Dicalcium phosphate dihydrate was prepared by ammoniating in an ice bath an aqueous solution initially saturated with $Ca(H_2PO_4)_2 \cdot H_2O$ and $CaHPO_4 \cdot 2H_2O$; details are described elsewhere [9]. Chemical analysis of this salt yielded Ca, 23.20 percent and P, 17.93 percent (theoretical: Ca, 23.20 percent and P, 18.02 percent). Petrographically, the preparation appeared as pure, homogeneous DCPD.

Phosphoric acid solutions were prepared from doubly crystallized hemihydrate, $2H_3PO_4 \cdot H_2O$, and freshly boiled conductance water. The molarities of the final solutions were checked by chemical analysis.

2.2. Leaching Experiments

The leaching apparatus is shown in figure 1. An 8-cm layer of DCPD crystals was poured on top of the fritted glass (medium porosity), F; phosphoric acid solution was poured into the column; the solid was stirred to remove air bubbles; finally about 300 ml of phosphoric acid solution was poured into the reservoir, S, continuosly flushing the apparatus with nitrogen. Water, from a constant temperature bath, was pumped through the jackets, W, maintaining the temperature at 37.5 ±0.1 °C as measured by thermometer T. The effluent from the column was collected in the thermostated cup D in which were mounted glass and calomel electrodes of a commercially available *p*H meter (claimed relative accuracy ±0.0037 *p*H units) and through which flowed a slow current of CO_2-free and water-saturated nitrogen. When the *p*H of the solution entering the cup D became constant, several samples for analysis were collected through stopcocks C or E. The *p*H was rechecked several times during sampling and at various flow rates to be sure that the effluent was saturated. Standardization of the *p*H meter was made with certified NBS buffer standards [11]. The uncertainty in *p*H measurements was estimated to be about ±0.008 *p*H units. The hydraulic head was kept constant by means of the Mariotte valve M. The rate of flow at which the samples were collected was about 25 ml per hour. When faster rates were needed, nitrogen pressures of up to 3 psi were used to supplement the hydraulic head.

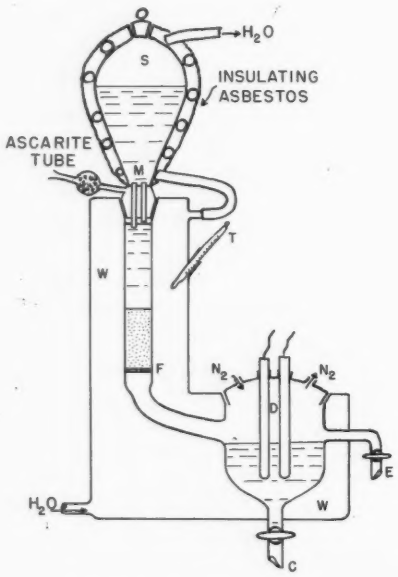

FIGURE 1. *Leaching apparatus.*

2.3. End-Over-End Equilibrations

A series of equilibrations was made in glass-stoppered bottles, each of which contained 5 g of DCPD and 120 ml of phosphoric acid (1.00×10^{-4}, 1.00×10^{-3}, 5.00×10^{-3}, or $5.00 \times 10^{-2} M$) by slowly rotating end-over-end in a water bath at 37.5 ±0.1 °C. In addition to the DCPD, 0.1 g of octacalcium phosphate, $Ca_8H_2(PO_4)_6 \cdot 5H_2O$, (OCP), was added to replicates of the two most dilute systems. At selected time intervals the contents of the bottles were filtered through the sintered glass in the thermostated apparatus shown in figure 1; *p*H values were determined and samples were collected for calcium and phosphorus analyses in the manner described above.

Equilibrium was also approached from supersaturation, taking advantage of the negative thermal coefficient of solubility of DCPD: a column of DCPD in the apparatus shown in figure 1 was leached with $5.00 \times 10^{-3} M$ phosphoric acid at 25 ±0.1 °C; the *p*H of the effluent was determined and a sample was taken for calcium and phosphorus analyses. The effluent was collected under a CO_2-free atmosphere in a glass bottle containing about 2 g of DCPD; when the volume was about 120 ml, the bottle was stoppered and equilibrated in a water bath at 37.5 ±0.1 °C as described above. The *p*H and the calcium and phosphorus concentrations of the liquid phase were determined after 16 days of equilibration.

2.4. Calcium and Phosphorus Determinations

Calcium was determined colorimetrically by the indirect technique described by Banerjee et al. [12]. Phosphorus was determined using the vanadomolybdate reagent of Brabson et al. [13]. In both analyses, samples were compared directly with blanks and standards in a double beam spectrophotometer. Uncertainties in phosphorus and calcium determinations were estimated as 1.0 and 2.5 percent of the amounts present, respectively.

3. Calculations

3.1. Apparent Solubility Product Constants, K'_{sp}

The ionic strength, μ, is defined in these calculations

by

$$\mu = P[\nu + H^+/2P + \Phi/\lambda] \quad (1)$$

in which P and H^+ represent molar concentrations of phosphorus and hydrogen ion and the other symbols are defined as:

$$\nu = 2M/P \quad (2)$$

$$\Phi = \frac{(H^+)}{2K_2 f'} + \frac{2}{f''} \quad (3)$$

$$\lambda = \frac{(H^+)^2}{K_1 K_2} + \frac{(H^+)}{K_2 f'} + \frac{1}{f''}. \quad (4)$$

In eqs (2), (3), and (4), (H^+) and M represent the hydrogen ion activity and the molar concentration of calcium, respectively, K_1 and K_2 are the first and second dissociation constants for phosphoric acid, and f' and f'' are the molar activity coefficients for the species $H_2PO_4^-$ and $HPO_4^=$, respectively. The numerical values for K_1 and K_2 used here were 6.53×10^{-3} [14] and 6.57×10^{-8}, respectively. The value of K_2 at 37.5 °C was interpolated by means of the equation

$$pK_2 = 7.1994 - 1.135 \times 10^{-2}\, X + 1.998 \times 10^{-3}\, X^2 - 6.64 \times 10^{-5}\, X^3 \text{ with } X = (T\,°\text{K} - 298.15)/5$$

derived from a portion (0–45 °C) of the experimental data of Bates and Acree [15].

Equations (1), (2), (3), and (4) are consistent with the assumptions that the only ionic phosphate species present in significant concentrations are $H_2PO_4^-$ and $HPO_4^=$ and that the contribution of hydroxyl ion to the ionic strength is negligible in comparison with that of the other ionic species present. These assumptions are justifiable in the pH range of the present investigation.

An approximate ionic strength was obtained by the use of eqs (1) to (4) assuming unitary values for f' and f'', improved ionic activity coefficients, f_i, were then calculated from the extension of the Debye-Hückel limiting law,

$$-\log f_i = \frac{AZ_i^2\sqrt{\mu}}{1 + Ba_i\sqrt{\mu}} \quad (5)$$

in which Z_i represents the valence of the ith ion, a_i its distance of closest approach, and A and B are temperature-dependent constants; the numerical values chosen [16] for B and A were 0.331×10^8 and 0.522, respectively; the numerical values for a_i were Ca^{++}, 6×10^{-8} cm; $HPO_4^=$ and $H_2PO_4^-$, 4×10^{-8} cm [17]. With activity coefficients obtained by the use of eq (5), a new value for μ was calculated from eqs (1) to (4) and iteration was continued until convergence was attained, which usually occurred after three cycles.

The activity of $HPO_4^=$, $(HPO_4^=)$, was calculated from

$$(HPO_4^=) = P/\lambda \quad (6)$$

and a solubility product for dicalcium phosphate dihydrate, K'_{sp}, was calculated according to eq (7), assuming a value of unity for the activity of water,

$$K'_{sp} = Mf_{Ca}\,(HPO_4^=) = MP\,\frac{f_{Ca}}{\lambda}. \quad (7)$$

The solubility product calculated in this way was found to be dependent on concentration and is referred to here as the "apparent" solubility product. A more nearly constant value, K_{sp}, was obtained by allowing for the presence of the ion pairs, $[CaHPO_4]°$ and $[CaH_2PO_4]^+$ as described below.

3.2. Stability Constants

The several stability and ionization constants considered in this paper are defined as the equilibrium constants of the following reactions in solution:

(a) Associative reactions (stability constants)

$$Ca^{++} + HPO_4^= \rightleftarrows CaHPO_4 \qquad [K_x^*] \quad (8)$$

$$Ca^{++} + H_2PO_4^- \rightleftarrows Ca(H_2PO_4)^+ \qquad [K_y^*]. \quad (9)$$

(b) Dissociative reactions (ionization constants)

$$Ca(H_2PO_4)^+ \rightleftarrows CaHPO_4 + H^+ \qquad [K_y] \quad (10)$$

$$CaHPO_4 \rightleftarrows CaPO_4^- + H^+ \qquad [K_x]. \quad (11)$$

For systems saturated with respect to DCPD, the concentration of the uncharged species $[CaHPO_4]°$, $X°$, is given by

$$X° = K_x^*\,(Ca^{++})(HPO_4^=)/f_{x°} = K_x^*\,K_{sp}/f_{x°} \quad (12)$$

in which (Ca^{++}) is the activity of ionic calcium and K_{sp} is the activity product $(Ca^{++})(HPO_4^=)$. Therefore, $X°$ is constant, assuming, as customary, that the activity coefficient, $f_{x°}$, of an uncharged species in a dilute electrolyte solution is unity. The activity, (Y^+), of the charged species $[CaH_2PO_4]^+$ is given by

$$(Y^+) = Y^+ f_{y^+} = X°(H^+)/K_y \quad (13)$$

in which Y^+ represents the concentration of the species $[CaH_2PO_4]^+$; accordingly, the activity of the charged species is proportional to the activity of hydrogen ion. In the calculations reported here, it was assumed that $f_y^+ = f'$. It follows then, that if any two solutions designated by "a" and "b" are considered, the concentration Y_b^+ in solution "b" is related to that in

solution "a" by the equation

$$Y_b^+ = \frac{(H^+)_b f_a'}{(H^+)_a f_b'} Y_a^+ \tag{14}$$

For the calculations in this paper, solution "a" was taken as the most dilute solution in table 1. The selection of values of X° and Y_a^+ was made from an array of reasonable pairs set up for exploratory purposes; the choice of the values finally selected was based upon considerations outlined in the discussion.

TABLE 1. *Solubility of* $CaHPO_4 \cdot 2H_2O$. *Solution compositions obtained in leaching experiments*

System No.	Concentration of H_3PO_4 $M \times 10^4$	Composition of effluent			$K_{sp}' \times 10^7$	$K_{sp} \times 10^7$
		pH	Ca, $M \times 10^4$	P, $M \times 10^4$		
1	5	6.74_8	10.0_1	14.4_8	2.68_0	2.15_0
2	10	6.29_3	13.7_4	24.3_9	2.59_6	2.22_3
3	10	6.29_6	13.9_7	23.7_8	2.59_4	2.22_2
4	50	5.11_1	53.1	$101._4$	2.43_6	2.22_5
5	100	4.58_7	$105._0$	$203._4$	2.41_1	2.14_8
6	200	4.12_5	$201._9$	$407._3$	2.57_2	2.18_7
7	200	4.13_5	$196._8$	$403._5$	2.55_8	2.17_6
8	500	3.56_2	$484._2$	$979._0$	2.86_5	2.21_1
				S. D.[a]	0.14	0.03
				Avg.[b]	$2.59 \pm 0.05_6$	$2.19 \pm 0.01_1$

[a] Standard deviation.
[b] Averages given with the standard error of the mean.

3.3. Corrected Solubility Product Constant, K_{sp}

The ionic strength was now calculated considering the balance equations (15) to (19)

$$\tau = Y^+ + X^\circ \tag{15}$$

$$M = [Ca^{++}] + \tau \tag{16}$$

$$P = \sum_{j=0}^{2} P^{(j)} + \tau \tag{17}$$

$$[Ca^{++}] = M(1-\beta) \tag{18}$$

$$\sum_{j=0}^{2} P^{(j)} = P\left(1 - \frac{1}{2}\beta\nu\right). \tag{19}$$

In eqs (15) to (19), τ is the total concentration of calcium (or phosphorus) in ion pairs, $[Ca^{++}]$ is the concentration of unpaired calcium; $P^{(j)}$ is the concentration of unpaired phosphate species of charge j; β, the fraction of total calcium in paired forms, is $\beta = \tau/M$. The ionic strength, μ, is given by

$$\mu = P\left[\nu - \frac{3}{2}\left(\frac{1}{2}\beta\nu\right) + (\Phi/\lambda)\left(1 - \frac{1}{2}\beta\nu\right) - (1/2P)\,(X^\circ - H^+)\right] \tag{20}$$

and the solubility product constant, K_{sp}, is given by

$$K_{sp} = MP(1-\beta)\,(1 - \tfrac{1}{2}\beta\nu)\,(f_{Ca}/\lambda). \tag{21}$$

For each selected pair of values for X° and Y_a^+, eq (20) was solved by successive approximations starting with unitary activity coefficients analogously to the procedure outlined above.

4. Results

The composition of effluents in the leaching experiments and the corresponding calculated solubility products are shown in table 1. All the compositions are averages of at least two samples. Within experimental error, the final phosphorus concentration equaled the original phosphoric acid concentration plus the calcium concentration in the effluent, indicating that congruent dissolution took place in each case.

The calcium and phosphorus concentrations in the various effluents at 37.5 °C are plotted against pH in figure 2; corresponding curves for 25 °C [9] are shown as broken lines. It is apparent that DCPD is more soluble at 25 °C than at 37.5 °C.

Apparent solubility products, K_{sp}', listed in table 1, are plotted against pH in figure 3. The concave shape of this curve is consistent with a model in which the ion pairs $[CaHPO_4]^\circ$ and $[CaH_2PO_4]^+$ are present in solution. The corrected solubility product constants, K_{sp}, calculated on the basis of this model are also plotted in figure 3. The maximum variation in K_{sp}, about 4 percent, is satisfactory in view of the analytical uncertainties. In contrast, K_{sp}' varied by about 20 percent.

In table 2 are listed the parameters used in the calculations along with pertinent stability and ionization

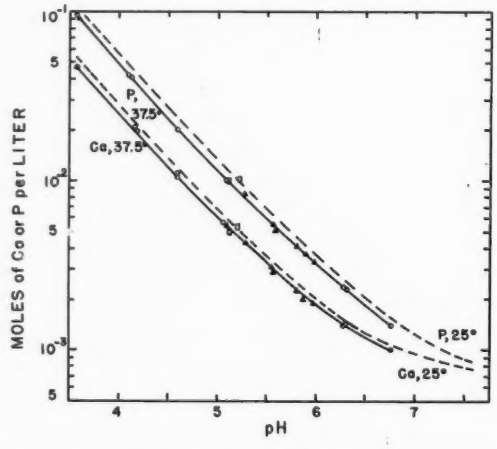

FIGURE 2. *Solubility isotherm of DCPD at 37.5 °C, full line, and at 25 °C, broken line* [9].
Open circles, compositions obtained in leaching apparatus; triangles, compositions obtained in end-over-end experiments; squares, initial and final compositions in super-saturation experiments (see tabulation in text).

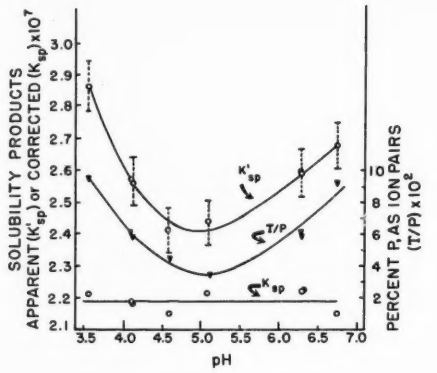

FIGURE 3. *Solubility product constants (apparent and corrected) and percent* P *in ion pairs plotted against* p*H.*

Calculated errors, based on analytical uncertainties, are shown for each point.

TABLE 2. *Ionic strengths and concentrations and stability constants of ion pairs* [a]

System No.	$\mu \times 10^2$	$\tau \times 10^4$	β	$Y^+ \times 10^4$	$K_x^* \times 10^{-2}$	K_y^*
1	0.300	1.34_1	0.134	0.0475	6.00_0	7.64_2
2	.408	1.42_8	.104	$.133_1$	5.80_3	7.39_1
3	.410	1.42_9	.102	$.136_2$	5.80_8	7.39_4
4	1.51_0	3.49_5	.066	2.20_0	5.79_8	7.38_4
5	2.94_1	8.95_1	.085	7.65_8	6.00_6	7.64_9
6	5.57_4	24.5_8	.120	23.2_8	5.89_9	7.51_3
7	5.46_4	24.0_1	.124	22.7_2	5.92_8	7.55_1
8	12.6_0	92.9_6	.192	91.6_8	5.83_5	7.43_1
				S. D. [b]	0.09	0.11
				Avg. [c]	$5.88 \pm 0.03_1$	$7.49 \pm 0.03_0$

[a] Values in table calculated for the final set $X^\circ = 1.293 \times 10^{-4}$ and $Y_a^+ = 0.0475 \times 10^{-4}$ *M*

[b] Standard deviation.

[c] Averages given with the standard error of the mean.

The value for K_y was 5.160×10^{-6}.

constants. The values for K_x^* and K_y were calculated using eqs (12) and (13), respectively. The values for K_y^* were calculated from

$$K_y^* = \frac{(Y^+)K_2}{K_{sp}(\mathrm{H}^+)}. \tag{22}$$

The constancy in the value of K_y is imposed by the calculative procedure, as will be explained later. The near constancy in the values of K_X^* and K_y^* (table 2) lends strong support for the existence of the complexes postulated here.

The fraction of phosphorus complexed, τ/P, is also plotted in figure 3. There appears to be a minimum of complexing at *p*H 5. As might be anticipated, the minimum in the fraction of P present as ion pairs is nearly coincident with the minimum in the K'_{sp} curve in the same figure.

The compositions of all the solutions obtained in the end-over-end equilibrations, listed in table 3 and shown in figure 2 as triangles, lie close to the isotherm obtained in the leaching experiments. However, only

TABLE 3. *End-over-end equilibrations*

Initial solid phases	Concentration of H_3PO_4	Equilibration time—hours	Solution composition		
			*p*H	Ca, $M \times 10^4$	P, $M \times 10^4$
	$M \times 10^2$				
DCPD + OCP	0.01	264	5.98_4	19.8_3	34.9_2
DCPD + OCP	.1	288	5.65_3	28.1_5	52.7_1
DCPD	.01	5	7.42_8	7.20	8.24
DCPD	.01	24	5.88_3	20.2_8	37.9_4
DCPD	.01	48	5.80_9	22.7_6	42.6_2
DCPD	.01	240	5.55_0	30.5_7	58.4_4
DCPD	.01	960	5.28_1	43.2_1	84.8_2
DCPD	0.5	192	5.13_2	51.4_0	99.9_4
DCPD	5.0	192	3.57_0	$473._8$	$963._9$

two of the systems, the last two entries in table 3, showed congruent dissolution. These contained only DCPD and were equilibrated with $5.00 \times 10^{-3} M$ and $5.00 \times 10^{-2} M$ phosphoric acid, respectively. The compositions of these two solutions are the only ones that are essentially the same as those obtained in the corresponding leaching experiments, table 1.

In the OCP-free systems equilibrated with $1.00 \times 10^{-4} M$ phosphoric acid, table 3, a more basic phosphate precipitated as evidenced by the changes in composition with time. The rate of this precipitation was relatively fast at the beginning and then decreased.

The two systems containing both DCPD and OCP, table 3, were included with the hope of obtaining the singular point for the two salts (i.e., the solution which would be in equilibrium with both salts). The lack of agreement in the final composition of the two solutions indicates that at least one of them did not remain at the singular point composition. Hydrolysis of OCP to a more basic phosphate, presumably hydroxyapatite, would account for this result.

The initial and final compositions in the experiment in which equilibrium was approached from supersaturation are shown in the tabulation:

	*p*H	Ca $M \times 10^4$	P $M \times 10^4$
Initial	5.20_2	52.9_8	$101._9$
Final	5.14_2	48.2_2	$100._8$

The initial and final compositions are shown as squares in figure 2. It is apparent that the former lies on the 25 °C isotherm and the latter on the 37.5 °C isotherm.

5. Discussion

5.1. Leaching Experiments

The more basic calcium phosphates (such as HA and OCP) were not formed in the leaching experiments as long as the phosphoric acid solutions were more concentrated than $1.00 \times 10^{-4} M$. Attempts to attain

equilibrium with $1.00\times10^{-4}M$ acid failed because considerable hydrolysis of DCPD was evident even at flow rates 3 to 4 times higher than the rate used with more concentrated acids. This behavior is in marked contrast to that at 25 °C [9] which showed no evidence of hydrolysis with the same acid.

The following facts show that equilibrium was closely approached in the experiments reported here: (a) the plots of experimental points yielded smooth curves; (b) the end-over-end experiments (systems 8 and 9, table 3), which represent much longer equilibration times, gave solution compositions in agreement with those obtained in the leaching experiments; (c) the system in which equilibrium was approached from supersaturation, agreed with that in which equilibrium was attained from undersaturation with the same acid; (d) within experimental error, a constant solubility product was obtained when corrections for the presence of complexes in solution were introduced.

Dicalcium phosphate dihydrate is metastable with respect to anhydrous dicalcium phosphate over the entire range studied and with respect to OCP and HA, in part of the range. The material in the column was examined after each experiment with the petrographic microscope. With one exception, the system in which the most concentrated acid was used, no anhydrous dicalcium phosphate was found. The trace found in the one exception is believed to be too small to influence the corresponding point on the isotherm because it is known that the rate of precipitation of the anhydrous salt is much less than the rate of dissolution of DCPD [18].

5.2. End-Over-End Experiments

Since all the compositions shown in table 3 fall on the DCPD isotherm (fig. 2) obtained in the leaching experiments, the rate of precipitation of more basic calcium phosphates (such as OCP and HA) in the end-over-end experiments must have been significantly lower than the rate of dissolution of DCPD.

With only DCPD and OCP present as solid phases, the solution composition should approach the DCPD–OCP singular point. The formation of HA in such a system would cause compositions to shift toward the more acid region. This would create a condition of undersaturation with respect to OCP; the OCP would then dissolve, leading to supersaturation with respect to DCPD. The dissolution of OCP and precipitation of DCPD would thus tend to maintain the *p*H at a higher level, approaching that of the OCP–DCPD singular point. Therefore, depending upon the relative rates of these three reactions, the solution composition would be either at the DCPD–OCP singular point or somewhere on the acid side of this point. In agreement with these considerations, the $1.00\times10^{-3}\,M$ acid yielded an equilibrium *p*H of 6.295 in the leaching experiments; the same acid after 288 hr in the end-over-end experiments gave a *p*H of 5.653. The difference must be attributed to the formation of HA. Likewise, it is probable that the DCPD–OCP singular point has a *p*H above the value 5.984 obtained with the $1.00\times10^{-4}\,M$ acid after 264 hr.

The ionic product for OCP, $(Ca^{++})^4(H^+)(PO_4^{\equiv})^3$, calculated for the solution with *p*H 5.984 ($\beta=0.08$) is 3.8×10^{-48}. Because of the foregoing reasons, the solubility product of OCP at 37.5 °C must be greater than 3.8×10^{-48} which puts it in the neighborhood of the product reported for 25 °C, 1.25×10^{-47} [10].

In the absence of OCP, the $1.00\times10^{-4}\,M$ acid gave solutions with *p*H values below 5.984, the value obtained in the presence of OCP; at 24 hr the *p*H was 5.883 and it decreased to 5.281 after 960 hr. Precipitation of HA liberates acid which is not neutralized by dissolution of OCP when the latter is absent. Consequently, the *p*H in the time series with $1.00\times10^{-4}\,M$ acid in the absence of OCP, decreased fairly rapidly to approach that of the DCPD–HA singular point. The results suggest that the *p*H of the DCPD–HA singular point is below 5.281, and probably above 5.132, the value obtained in system 8, table 3, in which no hydrolysis was detected after 192 hr.

The hydrolysis steps outlined in the foregoing discussion are consistent with the known behavior of DCPD [9, 10] and of OCP [19]. The formation of OCP by hydrolysis of DCPD in aqueous solutions occurs at 25 °C, but it was possible [10] to determine the singular point for these two salts, because at 25 °C hydrolysis of OCP to HA is too slow to displace the composition from that of the singular point.

5.3. Ion-Pair Formation

The values for the concentrations of the ion-pairs $[CaHPO_4]^\circ$ and $[CaH_2PO_4]^+$, X° and Y^+, in the most dilute solution were selected from an array according to the following criteria:

(a) The calculated value for K_{sp} cannot be higher than the minimum value for K'_{sp} in table 1; (b) the sum of the concentrations of the ion pairs cannot be higher than either the total Ca or *P* concentrations in any of the systems considered; (c) there must be a minimum in the fraction (τ/P) of *P* complexed and it should coincide with the minimum in the value of K'_{sp} in figure 3; (d) the variance of K_{sp} obtained with the final values of X° and Y^+_a should be an absolute minimum with respect to all other possible pairs of values for these parameters.

Designating values for X° and Y^+ for the most dilute solution fixes a numerical value of K_y for all the other solutions because the quantities $(Y^+)/(H^+)$ and X° in eq (13) are constants in the adopted model. This is why the quantity K_y does not appear in table 2 along with the calculated values for K^*_x and K^*_y. The value derived for K_y is 5.16×10^{-6}.

The value for the acid ionization constant, K_y, of the species $[CaH_2PO_4]^+$, 5.16×10^{-6}, is one hundred times the second ionization constant of phosphoric acid; this ion-pair is thus a stronger acid than $H_2PO_4^-$, presumably due to the proximity of the charge of the calcium ion.

If the reasonable assumption is made that the ratio of K_y/K_x is of the same order of magnitude as K_1/K_2 or K_2/K_3 for phosphoric acid, the value of K_x would be of the order of 10^{-11}. This means that the activity of the species $[CaPO_4]^-$ in the system with the highest pH would be of the order of 10^{-8} M, which is negligible relative to the activities of Ca^{++} and $HPO_4^=$. Therefore, ignoring the concentration of the species $[CaPO_4]^-$ in the calculations is justified.

In a previous study of the solubility of DCPD at 25 °C [9], the possibility of complexing was not ruled out, but the data were treated by an empirical method that gave K_{sp} by extrapolation to zero ionic strength. The 25° data are being re-evaluated in this laboratory, taking into account ion-pair formation.

According to the present treatment, it appears that as much as 20 percent of the calcium was ion-paired (e.g., system No. 8, table 1). The model adopted for the treatment of the ion pairs is not exempt from uncertainties; for example, it is impossible to ascertain the adequacy of eq (5) for calculating activity coefficients. On the other hand, the variation of the solubility product constant could not be explained simply in terms of activity coefficients because (a) the extended Debye-Hückel limiting law should give reasonably good values for activity coefficients in solutions as dilute as those used here, and (b) it is unlikely that the minimum in the value of K'_{sp} which occurs at $\mu \approx 0.025$ is related to minima in mean activity coefficients which are sometimes observed; such minima occur at concentrations much higher than those described here.

5.4. Comparison With Reported Data

Davies and Hoyle [20] reported dissociation constants at 25 °C for systems containing sodium and potassium phosphate buffers and calcium iodate. Allowing for experimental differences, the constants obtained by Davies and Hoyle, K_x^* (25°) = 1/.002 = 5×10^2 and K_y^* (25°) = 1/.084 = 11.8, are in reasonable agreement with those given here, K_x^* (37.5°) = 5.88×10^2 and K_y^* (37.5°) = 7.49.

Bjerrum [21] studied the three component system $Ca(OH)_2$—H_3PO_4—H_2O at 18 °C in the pH range 6 to 8 in the absence of solid phases. He concluded that a model involving the ion-pair $[CaHPO_4]^\circ$ or any of the ion pairs $[Ca(HPO_4)_2]^{2-}$, $[Ca(HPO_4)(PO_4)]^{3-}$, or $[Ca(PO_4)_2]^{4-}$, would fit his data. Models involving $[CaHPO_4]^\circ$ alone or in combination with any of the above ion pairs with Ca/P ratios of 1/2 gave variable K_{sp} values when used with the present data. The only model giving reasonably constant K_{sp} values was the one with the ion pairs $[CaHPO_4]^\circ$ and $[CaH_2PO_4]^+$. It is believed that the condition of saturation with respect to DCPD, which demands a constant activity for the species $[CaHPO_4]^\circ$, is more determinative than the conditions used by Bjerrum.

More recently, Greenwald [22] used Bjerrum's data to calculate values for the instability constant of $[CaHPO_4]^\circ$; these varied from 1.01 to 9.55×10^{-3}. As in previous reports by the same author [23, 24], ionic concentrations were used instead of activities. For this reason, and because the procedure used in his calculations is not detailed, a direct comparison of his results with those given here is not possible. His average value for the instability constant, 2.77×10^{-3}, gives a K_x^* (18 °C) = $1/(2.77 \times 10^{-3}) = 3.61 \times 10^2$. This, too, gives order of magnitude agreement with the value of K_x^* (37.5 °C) = 5.88×10^2 given here.

Similar rough agreement is found with the result of Gosselin and Coghlan [25], K_x^* (25 °C) = $1/1.38 \times 10^{-2} = 0.72 \times 10^2$, who also used ionic concentrations instead of activities in their calculations.

The negative temperature coefficient for the solubility of DCPD relates to properties of both the solution and the solid. For example, with an increase in temperature the activity of water increases and it is conceivable that less water is associated with the calcium and phosphate ions which, then, for comparable concentrations, would display a higher activity; this should result in lower solubility of DCPD as the temperature increases. However, if the solubility product, K_{sp}, decreases as the temperature increases, the magnitude of the standard free energy of formation of DCPD must increase with temperature more rapidly than the sum of the free energies of formation of Ca^{++}, $HPO_4^=$, and $2H_2O$. The solubility product of DCPD at 25 °C [9], 2.77×10^{-7}, is higher than the value, 2.19×10^{-7}, at 37.5 °C. However, since no consideration was given to the formation of ion pairs in solution at 25 °C, a meaningful comparison is not possible at present.

An important application of the stability constants relates to the formation of ion pairs in biological fluids. Representative figures cited for ionic Ca^{++} and $HPO_4^=$ activities in adult human serum, 4.7×10^{-4} and 1.9×10^{-4} M, respectively [26], give the result at pH = 7.4 that about five percent of the calcium or inorganic phosphorus is in the form of the ion pair $[CaHPO_4]^\circ$. In infant serum, with Ca^{++} and $HPO_4^=$ activities of 4.7×10^{-4} and 3.7×10^{-4}, the percentage of calcium and phosphorus in paired forms would amount to 8 and 5, respectively. For both adults and infants, the concentrations of the ion pairs $[CaH_2PO_4]^+$ and $[CaPO_4]^-$ in serum appear to be negligible.

6. References

[1] S. W. Leumg and A. Tovborg-Jensen, Intern. Dental J. **8**, 613 (1958).

[2] G. Chihara, N. Kurosawa, and E. Takasaki, Chem. and Pharm. Bull (Tokyo) **7**, 622 (1959).

[3] W. F. Neuman and M. W. Neuman, The Chemical Dynamics of Bone Mineral, p. 169 (University of Chicago Press, Chicago, Ill., 1958).

[4] J. A. Gray and M. D. Francis, Physical Chemistry of Enamel Dissolution. In Mechanisms of Hard Tissue Destruction, R. F. Sognnaes, ed., p. 213 (AAAS, Washington, D.C., 1963).

[5] N. Bjerrum, Selected papers, p. 245 (Copenhagen, Denmark, 1949).

[6] Tennessee Valley Authority, Chem. Eng. Rept. No. 8, (1950).

[7] M. J. Shear and B. Kramer, J. Biol. Chem. **79,** 125 (1928).
[8] B. S. Strates, W. F. Neuman, and G. J. Levinskas, J. Phys. Chem. **61,** 279 (1957).
[9] E. C. Moreno, W. E. Brown, and G. Osborn, Soil Sci. Soc. Amer. Proc. **24,** 94 (1960).
[10] E. C. Moreno, W. E. Brown, and G. Osborn, Soil Sci. Soc. Amer. Proc. **24,** 99 (1960).
[11] R. G. Bates, J. Res. NBS **66A** (Phys. and Chem.) No. 2, 179 (1962).
[12] D. K. Banerjee, C. C. Budke, and F. D. Miller, Anal. Chem. **33,** 418 (1961).
[13] J. A. Brabson, R. L. Dunn, E. A. Epps, Jr., W. M. Hoffman, and K. D. Jacob, J. A.O.A.C. **41,** 517 (1958).
[14] L. F. Nims, J. Am. Chem. Soc. **56,** 1110 (1934).
[15] R. G. Bates and S. F. Acree, J. Res. NBS **30,** 129 (1943) RP1524.
[16] G. G. Manov, R. G. Bates, W. J. Hamer, and S. F. Acree, J. Am. Chem. Soc. **65,** 1765 (1943).
[17] J. Kielland, J. Am. Chem. Soc. **59,** 1675 (1937).
[18] W. E. Brown and J. R. Lehr, Soil Sci. Am. Proc. **23,** 7 (1959).
[19] W. E. Brown, J. P. Smith, J. R. Lehr, and A. W. Frazier, Nature **196,** 1050 (1962).
[20] C. W. Davies and B. E. Hoyle, J. Chem. Soc. 4134 (1953).
[21] N. Bjerrum, Mat. Fys. Medd. Dan. Vid. Selsk, **31,** 69 (1958).
[22] I. Greenwald, J. Phys. Chem. **67,** 2853 (1963).
[23] I. Greenwald, J. Biol. Chem. **161,** 697 (1945).
[24] I. Greenwald, J. Redish, and A. C. Kilbrick, J. Biol. Chem. **135,** 65 (1940).
[25] R. E. Gosselin and E. R. Coghlan, Arch. Biochem. and Biophys. **45,** 301 (1953).
[26] Ref. 3, pp. 17 and 21.

(Paper 70A6–426)

JOURNAL OF RESEARCH of the National Bureau of Standards—A. Physics and Chemistry
Vol. 70A, No. 6, November–December 1966

Dissociation of Some Substituted Phenols in 50-Percent Aqueous Methanol as Solvent

R. A. Robinson and Roger G. Bates

Institute for Materials Research, National Bureau of Standards, Washington, D.C., 20234

(June 7, 1966)

The dissociation constants of the following substituted phenols in 50 wt percent methanol have been measured at 25 °C: *o*-nitrophenol, *p*-nitrophenol, 4-methyl-2-nitrophenol, 2,6-dichlorophenol, pentachlorophenol. The respective values found, expressed as pK values, are 7.91_7, 7.69_2, 8.28_4, 7.68_0, and 5.27_8. The dissociation constants of 4-methyl-2-nitrophenol and pentachlorophenol, again expressed as pK values, have been measured in water as solvent at 25 °C and found to be 7.59_7 and 4.82_0, respectively.

Key Words: Dissociation constant, methanol-water mixtures, solvent effects, substituted phenols.

1. Introduction

The dissociation constants of protonated tris(hydroxymethyl) aminomethane [1][1] and of the ammonium ion in 50 wt percent aqueous methanol [2] have been determined recently over the temperature range 10 to 40 °C. The dissociation constants of acetic acid and of the dihydrogen phosphate ion have also been determined [3] over this temperature range. The emf measurements needed to evaluate the dissociation constants of acetic acid and dihydrogen phosphate ion also yielded values of the acidity function $p(a_H\gamma_{Cl}) \cong -\log (a_{H^+} \cdot \gamma_{Cl^-})$ for a buffer solution containing equimolar acetic acid, sodium acetate, and sodium chloride (Solution A) and another buffer solution containing equimolar potassium dihydrogen phosphate, disodium hydrogen phosphate, and sodium chloride (Solution B) in 50 percent methanol. The $p(a_H\gamma_{Cl})$ value of Solution A is approximately 5.7, that of Solution B 8.2, the exact value depending on the temperature and the total ionic strength of the solution.

Advantage has now been taken of these buffer solutions to determine the dissociation constants of the following substituted phenols in 50 percent methanol at 25 °C: *o*-nitrophenol, *p*-nitrophenol, 4-methyl-2-nitrophenol, 2,6-dichlorophenol, and pentachlorophenol. The order of magnitude of the pK values of these phenols is such that either Solution A or Solution B is a suitable buffer solution for spectrophotometric measurements of the dissociation constants. Comparison with the pK values in aqueous solution can be made because such pK values have already been determined for the following; *o*-nitrophenol [4], *p*-nitrophenol [5], and 2,6-dichlorophenol [6]. In order to complete the series, the dissociation constants of 4-methyl-2-nitrophenol and of pentachlorophenol have now been measured in aqueous solution at 25 °C.

2. Outline of Method

In the spectrophotometric method the optical densities of three solutions of the phenol are measured. One contains sufficient acid to convert the phenol entirely into its undissociated form, HN; the optical density is denoted by D_1. The second solution contains sufficient alkali to convert the phenol entirely into its anion, N^-, the optical density of this solution being D_2. The third solution, of optical density D, contains a buffer solution whose $p(a_H\gamma_{Cl})$ value is known. It is an advantage if a series of such buffer solutions of different total ionic strengths are available. The stoichiometric concentration of phenol in each solution is the same. Measurements of optical density are made at a wavelength where D_2 is large and D_1 small.

[1] Figures in brackets indicate the literature references at the end of this paper.

230-736 O-66—8

The fraction, α, of the phenol present in the anionic form in the third solution is given by

$$\alpha = \frac{D - D_1}{D_2 - D_1}. \quad (1)$$

The dissociation constant of the phenol is defined as:

$$K = \frac{a_{H^+} \cdot m_{N^-}}{m_{HN}} \cdot \frac{\gamma_{N^-}}{\gamma_{HN}} \quad (2)$$

whence

$$pK = p(a_H\gamma_{Cl}) - \log \frac{D - D_1}{D_2 - D} - \log \frac{\gamma_{N^-}}{(\gamma_{Cl^-} \cdot \gamma_{HN})}. \quad (3)$$

The last term in eq (3) is either negligible or small; in the latter case, the true value of pK can be obtained by extrapolation to zero total ionic strength. A small correction is needed because the $p(a_H\gamma_{Cl})$ value of the buffer solution is changed slightly on addition of the phenol; this correction has already been considered [7].

3. Materials

o-Nitrophenol, *p*-nitrophenol, and 2,6-dichlorophenol were available from previous work [4, 5, 6]. 4-Methyl-2-nitrophenol was twice recrystallized from a mixture of petroleum ether and heptane; mp 32 °C. It has absorption maxima in aqueous alkali solution at 433 mμ (ϵ_2 4,480) and 368 mμ (ϵ_1 2,880) in acid solution with an isosbestic point at 388 mμ (ϵ 2,380). Pentachlorophenol was recrystallized twice from a mixture of water and methanol; mp 193 °C. In aqueous solution the spectrum exhibits maxima at 320 mμ (ϵ_2 4,870) in alkali solution and at 302 mμ (ϵ_1 2,000) in acid solution; it has no isosbestic point in this region of the spectrum.

4. Spectrophotometric Measurements

The details of the measurements are given in tables 1 through 7. For the determination of the pK value of 4-methyl-2-nitrophenol in aqueous solution both tris(hydroxymethyl)aminomethane and phosphate buffer solutions were used; $p(a_H\gamma_{Cl})$ values for these buffer solutions have been tabulated [8]. The equimolal sodium hydrogen succinate-sodium chloride buffer solutions proved satisfactory for measuring the pK value of pentachlorophenol; $p(a_H\gamma_{Cl})$ values for these buffer solutions have also been tabulated [8]. The acidity functions $p(a_H\gamma_{Cl})$ listed in tables 1 through 7 for both solvent media relate to the buffer mixtures without added phenol. A correction for the change in acidity produced by the phenol is, however, included in the values of pK' (corr) given in the last column of each of these tables.

TABLE 1. *Dissociation constant of 4-methyl-2-nitrophenol in aqueous solution at 25 °C*

Phenol concentration 1.83×10^{-4} M, cell length 1 cm, wavelength 433 mμ, D_1 0.075, D_2 0.819

I	$p(a_H\gamma_{Cl})$	D	$\log \frac{D - D_1}{D_2 - D}$	pK	pK(corr)
0.01	8.176	0.660	0.566	7.610	7.598
.02	8.207	.669	.598	7.609	7.603
.03	8.232	.675	.620	7.612	7.608
.04	8.251	.685	.658	7.593	7.590
.05	8.266	.684	.653	7.613	7.611
.06	8.280	.690	.678	7.602	7.600
.08	8.302	.697	.707	7.595	7.594
.10	8.321	.700	.720	7.601	7.600

The buffer solution contained tris(hydroxymethyl)aminomethane (m), and its hydrochloride (0.9843m). $I = 0.9843$m.

Phenol concentration 1.83×10^{-4} M, cell length 1 cm, wavelength 433 mμ, D_1 0.076, D_2 0.820

I	$p(a_H\gamma_{Cl})$	D	$\log \frac{D - D_1}{D_2 - D}$	pK	pK(corr)
0.02	7.080	0.247	−0.525	7.605	7.598
.04	7.040	.239	−.552	7.592	7.589
.05	7.026	.233	−.573	7.599	7.596
.06	7.013	.230	−.578	7.591	7.589
.08	6.992	.226	−.598	7.590	7.588
.10	6.974	.218	−.627	7.601	7.600

The buffer solution contained equimolar amounts of potassium dihydrogen phosphate (m) and disodium hydrogen phosphate (m). $I = 4$m.

TABLE 2. *Dissociation constant of pentachlorophenol in aqueous solution at 25 °C*

Phenol concentration 1.69×10^{-3}M, cell length 10 cm, wavelength 320 mμ, D_1 0.015, D_2 0.823

I	$p(a_H\gamma_{Cl})$	D	$\log \frac{D - D_1}{D_2 - D}$	pK	pK (corr)
0.040	4.851	0.435	0.034	4.817	4.816
.064	4.838	.426	.015	4.823	4.822
.096	4.827	.422	.006	4.821	4.821
.144	4.814	.415	−.009	4.823	4.823
.200	4.802	.411	−.017	4.819	4.819

The buffer solution contained sodium hydrogen succinate (m) and sodium chloride (m). $I = 2$m.

TABLE 3. *Dissociation constant of o-nitrophenol in 50 percent methanol at 25 °C*

Phenol concentration 1.50×10^{-4} M, cell length 1 cm, wavelength 418 mμ, D_1 0, D_2 0.718

I	$p(a_H\gamma_{Cl})$	D	$\log \frac{D - D_1}{D_2 - D}$	pK'	pK' (corr)
0.02	8.248	0.488	0.302	7.946	7.922
.04	8.178	.463	.233	7.945	7.933
.06	8.127	.444	.182	7.945	7.937
.08	8.085	.426	.135	7.950	7.944
.10	8.049	.409	.092	7.957	7.952

The buffer solution contained potassium dihydrogen phophate (m), disodium hydrogen phosphate (m), and sodium chloride (m). $I = 5$m.

TABLE 4. *Dissociation constant of p-nitrophenol in 50 percent methanol at 25 °C*

Phenol concentration 5.18×10^{-3} M, cell length 1 cm, wavelength 402 mμ, D_1 0, D_2 1.042

I	$p(a_H\gamma_{Cl})$	D	$\log \frac{D-D_1}{D_2-D}$	pK'	pK' (corr)
0.02	8.248	0.810	0.543	7.705	7.697
.04	8.178	.773	.458	7.720	7.716
.06	8.127	.743	.396	7.731	7.728
.08	8.085	.722	.353	7.732	7.730
.10	8.049	.698	.307	7.742	7.740

The buffer solution contained potassium dihydrogen phosphate (m), disodium hydrogen phosphate (m), and sodium chloride (m). $I = 5$m.

TABLE. 5. *Dissociation constant of 4-methyl-2-nitrophenol in 50 percent methanol at 25 °C*

Phenol concentration 1.81×10^{-4} M, cell length 1 cm, wavelength 436 mμ, D_1 0.041, D_2 0.875

I	$p(a_H\gamma_{Cl})$	D	$\log \frac{D-D_1}{D_2-D}$	pK'	pK' (corr)
0.02	8.248	0.431	−0.056	8.304	8.285
.04	8.178	.403	−.115	8.293	8.283
.06	8.127	.377	−.171	8.298	8.292
.08	8.085	.359	−.210	8.295	8.290
.10	8.049	.324	−.244	8.293	8.289

The buffer solution contained potassium dihydrogen phosphate (m), disodium hydrogen phosphate (m), and sodium chloride (m). $I = 5$m.

TABLE 6. *Dissociation constant of 2,6-dichlorophenol in 50 percent methanol at 25 °C*

Phenol concentration 1.55×10^{-4} M, cell length 1 cm, wavelength 298 mμ, D_1 0.012, D_2 0.971

I	$p(a_H\gamma_{Cl})$	D	$\log \frac{D-D_1}{D_2-D}$	pK'	pK' (corr)
0.02	8.248	0.757	0.542	7.706	7.669
.04	8.178	.738	.494	7.684	7.665
.06	8.127	.724	.460	7.667	7.655
.08	8.085	.711	.430	7.655	7.646
.10	8.049	.700	.405	7.644	7.637

The buffer solution contained potassium dihydrogen phosphate (m), disodium hydrogen phosphate (m), and sodium chloride (m). $I = 5$m.

TABLE 7. *Dissociation constant of pentachlorophenol in 50 percent methanol at 25 °C*

Phenol concentration 1.99×10^{-4} M, cell length 1 cm, wavelength 323 mμ, D_1 0.002, D_2 1.013

I	$p(a_H\gamma_{Cl})$	D	$\log \frac{D-D_1}{D_2-D}$	pK'	pK' (corr)
0.04	5.660	0.709	0.364	5.296	5.290
.08	5.659	.705	.358	5.301	5.298
.12	5.659	.694	.336	5.323	5.321
.16	5.659	.692	.332	5.327	5.326
.20	5.658	.686	.320	5.338	5.337

The buffer solution contained acetic acid (m), sodium acetate (m), and sodium chloride (m). $I = 2$m.

Inspection of tables 1 and 2 shows that the pK values of 4-methyl-2-nitrophenol and pentachlorophenol in aqueous solution are almost independent of the total ionic strength of the buffer solution, the difference between any one value and the mean being within the experimental error. This is in accordance with previous experience with other aqueous solutions; the mean of the recorded pK values was, therefore, taken as the best value.

This does not hold for phenols in 50 percent methanol, as tables 3 through 7 show. For this reason, the quantity

$$p(a_H\gamma_{Cl}) - \log \frac{D-D_1}{D_2-D}$$

in tables 3 through 7 has been called pK'; it is identical with $pK + \log \gamma_N - /(\gamma_{Cl} - \cdot \gamma_{HN})$. The variation of pK' is linear with total ionic strength. It is not great in the case of 4-methyl-2-nitrophenol, but it is considerable with the other four phenols; moreover, while the pK' values of four of the phenols increase with increasing ionic strength, they decrease in the case of 2,6-dichlorophenol. It is clear that the activity coefficient term in eq (3) is very specific to each phenol. For this reason, the true values of pK were obtained by extrapolating pK' to zero ionic strength, using the method of least squares.

Since the data for $p(a_H\gamma_{Cl})$ have been recorded in molality units, all pK values in this paper are also on the molality scale.

5. Results

Table 8 gives the pK values obtained in this work and values for some phenols in aqueous solutions obtained in earlier work [4, 5, 6].

In aqueous solution the substitution of a methyl group in the para position raises the pK value of *o*-nitrophenol by 0.36_7. A similar substitution of a methyl group in phenol itself has been found to raise the pK value by 0.26_4 [9] or 0.25_6 [10]. The joint effects of *p*-CH_3 and *o*-NO_2 are, therefore additive only to a poor approximation. The same has been shown to be true, to a greater degree [11], for 2,4-dinitrophenol with $pK = 4.09$ [12]; here the substitution of a *p*-NO_2 group in *o*-nitrophenol has lowered the pK value by 3.14 whereas the lowering would have been 2.84 if additivity held.

The pK values of *o*-, *m*-, and *p*-chlorophenol are 8.53_4, 9.13_0, and 9.41_8, respectively [13], so that *o*-, *m*-, and *p*-Cl substitution lowers the pK value of phenol by 1.46_4, 0.86_8, and 0.58_0. If the effects were additive, one would expect $pK = 4.75_4$ for pentachlorophenol compared with the observed value of 4.82_0. It has been found [6] that an additivity principle is moderately successful in accounting for the pK values of the dichlorophenols, except for 2,6-dichlorophenol for which an additivity rule would predict a pK value 0.27 greater than the observed. It is interesting to observe that when substitution of chlorine atoms occurs at all five possible positions in the phenol

TABLE 8. *Values of* pK *for substituted phenols in aqueous solution and in 50 percent methanol at 25 °C*

	Water	50 percent Methanol	Δ^a
o-Nitrophenol	7.23_0	7.91_7	0.68_7
p-Nitrophenol	7.15_6	7.69_2	$.53_6$
4-Methyl-2-nitrophenol	7.59_7	8.28_4	$.68_7$
2,6-Dichlorophenol	6.79_1	7.68_0	$.88_9$
Pentachlorophenol	4.82_0	5.27_8	$.45_8$

[a] $\Delta = pK$ (in 50 percent methanol) $- pK$ (in water).

molecule, the anomaly is greatly reduced; an additivity principle, as shown above, predicts a pK value within 0.07 of the observed.

The information available about the dissociation constants of weak acids in 50 percent methanol is not extensive. The dissociation constant of *p*-nitrophenol in a number of water-methanol solvents has been determined by de Ligny, Loriaux, and Ruiter [14]; interpolation at 50 percent methanol gives $pK = 7.74$ compared with 7.69_2 in table 8.

Our measurements [3] of the pK value of dihydrogen phosphate ion show that it is 0.245 higher in 50 percent methanol than in water (at 25 °C). The corresponding difference for acetic acid is 0.904, in good agreement with values interpolated from the conductance data of Shedlovsky and Kay [15] and the emf results of Bacarella, Grunwald, Marshall, and Purlee [16]. Interpolation of the data of the latter at 50 percent methanol gives the following differences between pK in 50 percent methanol and pK in water for formic acid, propionic acid, butyric acid, and benzoic acid, respectively, 0.70, 1.03, 1.02, and 1.18.

The medium effect, therefore, as measured by the difference in pK in the two solvents, covers a wide range of values. It is difficult to see why, in a series of four aliphatic acids, the medium effect should increase with increasing size of the molecule. The Born equation or any modification of it would lead one to predict the opposite order.

The five acids listed in table 8 might be thought to resemble benzoic acid in configuration, yet the medium effect for benzoic acid ($\Delta pK = 1.18$) is considerably higher than that found for these five acids (0.45_8–0.88_9). In selecting these five phenols it was hoped that a more or less constant medium effect would be observed which could be taken as characteristic of phenolic acids. It may be disappointing to find that this is not so, but it is useful to realize now that the problem is complicated and that apparently minor changes in structure can lead to differences in the medium effect.

6. References

[1] M. Woodhead, M. Paabo, R. A. Robinson, and R. G. Bates, J. Res. NBS **69A** (Phys. and Chem.) No. 3, 263 (1965).
[2] M. Paabo, R. G. Bates, and R. A. Robinson, J. Phys. Chem. **70,** 247 (1966).
[3] M. Paabo, R. A. Robinson, and R. G. Bates, J. Am. Chem. Soc. **87,** 415 (1965).
[4] R. A. Robinson and A. Peiperl, J. Phys. Chem. **67,** 1723 (1963).
[5] G. F. Allen, R. A. Robinson, and V. E. Bower, J. Phys. Chem. **66,** 171 (1962).
[6] R. A. Robinson, J. Res. NBS **68A** (Phys. and Chem.) No. 2, 159 (1964).
[7] R. A. Robinson and A. K. Kiang, Trans. Faraday Soc. **51,** 1398 (1955).
[8] R. G. Bates and R. Gary, J. Res. NBS **65A** (Phys. and Chem.) No. 6, 495 (1961).
[9] A. I. Biggs, Trans. Faraday Soc. **52,** 35 (1956).
[10] D. T. Y. Chen and K. J. Laidler, Trans. Faraday Soc, **58,** 480 (1962).
[11] R. A. Robinson, M. M. Davis, M. Paabo, and V. E. Bower, J. Res. NBS **64A** (Phys. and Chem.) No. 4, 347 (1960).
[12] H. von Halban and G. Kortüm, Z. Physik. Chem. **A170,** 351 (1934).
[13] A. I. Biggs, J. Chem. Soc. (London) **388** (1961).
[14] C. L. de Ligny, H. Loriaux, and A. Ruiter, Rec. Trav. Chim. **80,** 725 (1961).
[15] T. Shedlovsky and R. L. Kay, J. Phys. Chem. **60,** 151 (1956).
[16] A. L. Bacarella, E. Grunwald, H. P. Marshall, and E. L. Purlee, J. Org. Chem. **20,** 747 (1955).

(Paper 70A6–427)

JOURNAL OF RESEARCH of the National Bureau of Standards—A. Physics and Chemistry
Vol. 70A, No. 6, November–December 1966

Publications of the National Bureau of Standards*

Selected Abstracts

Reproducibility of germanium resistance thermometers at 4.2 °K, M. H. Edlow and H. H. Plumb, *J. Res. NBS* **70C4** (*Engr. and Instr.*), No. 4, 245–254 (*Oct.–Dec. 1966*).

NBS has needed a set of very reproducible germanium resistors that would be capable of maintaining temperature scales. This paper describes our procedure for selecting such a set.

A group of germanium resistors from three commercial sources have been thermally cycled between 4.2 °K and room temperature. The resistance-temperature calibrations at 4.2 °K were made with reference to a liquid helium bath so that reproducible temperatures could be determined from liquid helium vapor pressure measurements. Seven resistors out of 25 demonstrated reproducibilities (of the 4.2 °K calibration) of about 0.001 °K after undergoing the multiple cyclings. Guided by these results, we procured twelve, new, similar resistors which were cycled in a comparable procedure. After 85 cycles, in which 14 resistance-temperature calibrations were performed at 4.2 °K for each resistor, ten of the twelve resistors demonstrated reproducibilities of approximately 0.001 °K.

The resulting set of secondary thermometers have undergone calibrations in the temperature ranges, 2 to 5 °K and 2 to 20 °K; reports of this work will be published in the near future.

Key Words: Germanium resistors, germanium resistor reproducibility, low temperature thermometry, reproducibility of germanium resistors, thermal cycling at low temperatures, thermometry.

Standard x-ray diffraction powder patterns, H. E. Swanson, M. C. Morris, and E. H. Evans, *Mono. 25, Section 4* (*June 28, 1966*), *55 cents.*

Standard x-ray diffraction powder data are presented for 103 substances. Thirty-two of these patterns represent experimental data and 71 are calculated. Ten experimental patterns replace eleven cards already in the X-ray Powder Diffraction File published by the American Society for Testing and Materials; twenty-two experimental patterns and seventy-one calculated patterns are for substances not previously included in the File. The experimental x-ray powder diffraction patterns were made with a Geiger counter x-ray diffractometer, using samples of high purity. All *d*-values were assigned Miller indices determined by comparison with theoretical interplanar spacings and from space group extinctions. The densities and lattice constants were calculated, and the refractive indices were measured whenever possible. The calculated x-ray powder diffraction patterns were obtained from single crystal structure data. The reported peak height intensities for calculated patterns were converted from integrated intensities.

Accurate cell determination measurements for the internal standards were obtained by using a flat-plate back reflection focusing camera.

Key Words: Standard, x-ray, diffraction, powder, patterns, crystal, structure, measurements, lattice, constants.

A bibliography on ion-molecule reactions. January 1900 to March 1966, F. N. Harllee, H. M. Rosenstock, and J. T. Herron, *Tech. Note 291* (*June 28, 1966*) *30 cents.*

The present document is a bibliography on ion-molecule reactions of chemical interest. The bibliography is listed in a chronological-alphabetic arrangement and includes 431 titles and references taken from the published literature since 1900. The coverage is limited to reactions between ions and molecules leading to changes in the atomic composition of either the projectile ion or target molecule. No attempt has been made to completely cover resonant charge exchange or elastic scattering.

Key Words: Bibliography, ions, molecules, reactions.

Equilibrium pressures of oxygen over oxides of lead at various temperatures, E. M. Otto, *J. Electrochem. Soc.* **113,** *No. 6, 525–527* (*June 1966*).

PbO_2 apparently requires four stages of decomposition to reach PbO. Based on thermogravimetric studies the intermediate products appear to be $5PbO_2 \cdot 4PbO$, $4PbO_2 \cdot 5PbO$ and Pb_3O_4. Though the first three stages seem irreversible, they too come to a steady state in decomposition, but no recombination takes place. $\Delta H°$ and $\Delta S°$ values have been calculated for the four stages.

Key Words: Dissociation, entropy, equilibrium, heat of reaction, intermediate oxides, irreversibility, lead oxides, oxygen pressures, thermogravimetry.

Liquid immiscibility in the rare earth oxide-boric systems, E. M. Levin, *Phys. Chem. Glasses* **7,** *No. 3, 90–93* (*June 1966*).

Three experimental methods were used to determine the composition of the modifier-rich liquids in the following binary systems with B_2O_3: La_2O_3, Nd_2O_3, Sm_2O_3, Eu_2O_3, Gd_2O_3, Dy_2O_3, Y_2O_3, Ho_2O_3, Er_2O_3, Tm_2O_3, Yb_2O_3, Lu_2O_3, Sc_2O_3. With decreasing ionic radius (increasing atomic number), the extent of immiscibility increased from 21.5% for the La_2O_3 system to 34.0 mol% for the Sc_2O_3 system. With the exception of the La_2O_3 and the Nd_2O_3 systems temperatures of the monotectics increased monotonically from 1136° for Sm_2O_3 to 1526 °C for Sc_2O_3. Index of refraction of the quenched modifier-rich liquid was a maximum (1.732) for Eu_2O_3. Competing ionic field strengths between the glass-forming and modifier cations with oxygen govern the existence of immiscibility. Structural considerations governing the number of oxygens associated per modifier cation determine the extent of immiscibility.

Key Words: Boric oxide, liquid immiscibility, phase equilibria, rare earth oxides.

Low-frequency motions and barrier to rotation in phosphonium iodide, J. J. Rush, *J. Chem. Phys.* **44,** *No. 4, 1722–1723* (*Feb. 15, 1966*).

The vibrational spectrum of PH_4I has been investigated by the energy-gain scattering of cold neutrons ($Er < 5$ milli-electron volts). Three distinct inelastic scattering maxima are observed at energy gains corresponding to 110, 335, and 614 cm^{-1}. The 335 and 614 cm^{-1} peaks are attributed to the torsional oscillations of the PH_4^+ ion and the 110 cm^{-1} peak to the translational optic vibrations. The barrier to rotation for the torsional mode of 335 cm^{-1} was computed to be 7.1 ± 0.5 kcal/mole based on the observed energy of the peak. This agrees well with the value of 7.5 kcal/mole derived from an electrostatic model.

Key Words: Inelastic neutron scattering, phosphonium iodide (PH_4I), barrier to rotation, electrostatic model.

Matrix-isolation study of the infrared and ultraviolet spectra of the free radical CNN, D. E. Milligan and M. E. Jacox, *J. Chem. Phys.* **44,** *No. 8, 2850–2856* (*Apr. 15, 1966*).

Features appearing at 393, 1241, and 2847 cm^{-1} after photolysis of matrix-isolated cyanogen azide with 2100–2800 Å radiation are shown to exhibit parallel behavior. Isotopic data are consistent with the assignment of these three features as fundamentals of the free radical CNN, produced by the reaction of carbon atoms with molecu-

lar nitrogen. Ultraviolet absorptions at 4189 and 3964 Å can also be assigned to CNN. The force constants and thermodynamic properties of CNN have been derived. The carbon-nitrogen bond is found to have approximately triple bond character, and the nitrogen-nitrogen bond approximately double bond character.

Key Words: NCN free radical, thermodynamic properties, ultraviolet spectrum, C atom reactions, C atom sources, carbon suboxide photolysis, CNN free radical, cyanogen azide photolysis, force constants, infrared spectrum, matrix isolation.

Microwave spectra of alkali hydroxides: evidence for linearity of CsOH and KOH, R. L. Kuczkowski, D. R. Lide, Jr., and L. C. Krisher, *J. Chem. Phys.* **44,** *No. 8, 3131–3132 (Apr. 15, 1966).*
The microwave spectra of CsOH and KOH have been observed. Both molecules show a spectrum characteristic of a linear molecule. The K–O and Cs–O distances are found to be 2.18 and 2.40 Å, respectively.

Key Words: Alkali hydroxides, CsOH, KOH, microwave spectra.

Neutron and infrared spectra of $HCrO_2$ and $DCrO_2$, J. J. Rush and J. R. Ferraro, *J. Chem. Phys.* **44,** *No. 6, 2496–2498 (Mar. 15, 1966).*
The vibrational spectra of $HCrO_2$ and $DCrO_2$ have been investigated by the energy-gain scattering of cold-neutrons, and by infrared absorption spectra from 4000–30 cm^{-1}. The infrared measurements are in agreement with previous results above 400 cm^{-1}. In addition, no absorptions are observed between 400 and 30 cm^{-1}, a region not covered in previous measurements. These results appear to support previous evidence for asymmetric hydrogen bonds in $DCrO_2$ and essentially symmetric bonds in $HCrO_2$. The neutron spectra exhibit a number of maxima, including a band peaked at about 225 cm^{-1} in $HCrO_2$ (and a less intense peak around 180 cm^{-1} in $DCrO_2$), probably due to low-frequency optic lattice modes. A comparison of the neutron and infrared results appears to raise some uncertainty concerning the assumption of symmetric hydrogen bonds in $HCrO_2$.

Key Words: Chromous acid, $HCrO_2$, $DCrO_2$, neutron spectra, infrared spectra, hydrogen bond, isotope effect, vibration spectra, lattice modes.

A survey of the thermodynamic data on heavier elements and their compounds: high-temperature enthalpy and vaporization equilibria, T. B. Douglas, *Proc. 3d Meeting Interagency Chemical Rocket Propulsion Group, Working Group on Thermochemistry, El Segundo, Calif., Mar. 17–18, 1965, 1, No. 82U, 5–16 (Chemistry Propulsion Information Agency, Silver Spring, Md., July 1965).*
A comprehensive, though not all-inclusive, survey of the published literature was undertaken for the purpose of determining where high-temperature enthalpy and vaporization-equilibrium data appear to be lacking or inadequate for Ti, Zr, W, Pb, Hg, I, Hf, Th, U, and their light-element compounds considered to be of possible importance in chemical propulsion and refractory applications. The results of this survey are summarized, and several examples are presented of the effects of uncertainties in the standard thermodynamic properties on calculated equilibria at high temperatures. It is pointed out that the first ionization potential of a molecule containing one alkali atom can be expected to exceed that of the free alkali atom by approximately the dissociation energy of the neutral molecule; and this relation is verified, within experimental uncertainty, for several examples.

Activation-analysis program and facilities at the National Bureau of Standards, J. R. DeVoe and G. W. Smith, *Proc. 1965 Intern. Conf. Modern Trends in Activation Analysis, Texas A&M University, College Station, Texas, pp. 225–229 (Apr. 1965).*
The National Bureau of Standards' Radiochemical Analysis Section is now developing a capability in activation analysis to compliment other analytical techniques using radioisotopes in analysis.
Activation analysis can be likened to spectrometric methods in which the re-emitted radiation from excited states (e.g., radioisotopes) which are often long (e.g., milliseconds to years) are measured and related to the kind and amount of element which interacted with the primary radiation. The analyst learns to discriminate from unwanted excitation processes by varying the type and energy of incident radiation, the length of time of the excitation, and the type of detector that measures the re-emitted or secondary radiation. To be most effective for our applications of activation analysis a computer is best used in a regenerative feed-back loop which consists of selecting, in sequence: the proper nuclear reaction, time of irradiation, complexity of radiochemical separation, appropriate detector, stripping of time dependent radiation spectra, and judgment of the analyst. It should be emphasized that a selective combination of the above variables does not place too large a burden on any one of the variables.
Plans for the development of facilities to carry out these concepts are discussed. Facilities which are planned or under construction are: a 10 MWth nuclear reactor, a 40KW-100 MeV Linac linear electron accelerator, a wide variety of pneumatic tube facilities, hot laboratories, a clean room complex, and low background counting facility.

Determination of trace amounts of tellurium in standard reference materials by neutron-activation analysis, D. A. Becker and G. W. Smith, *Proc. 1965 Intern. Conf. Modern Trends in Activation Analysis, Texas A & M University, College Station, Texas, pp. 230–235 (Apr. 1965).*
For the first time, neutron activation was used for elemental analysis of NBS Standard Reference Materials at the National Bureau of Standards. The reference materials were of two general types, cartridge brass and white cast iron, and were analyzed for their tellurium content. Utilizing the nuclear reaction $Te^{130}(n, \gamma)Te^{131} \xrightarrow{\beta-} I^{131}$, the samples were irradiated and the I^{131} separated by a destructive distillation and solvent extraction technique. Chemical yields were obtained through the use of I^{125} tracer. Tellurium concentrations of 2 to 800 ppm were determined, and the results compared to the results on identical samples obtained by polarography and emission spectroscopy.

Equilibrium pressures of oxygen over Ag_2O—Ag at various temperatures, E. M. Otto, *J. Electrochem. Soc.* **113,** *No. 7, 643–645 (July 1966).*
Although earlier investigators showed the dissociation of Ag_2O to be reversible and equilibrium points had been obtained there was a range from 101 °C to 302 °C that had not been studied. This region has now been studied. From all the data available and heat capacity data ΔH°_{298} and ΔS°_{298} have been calculated to be 14.690 kcal/mol O_2 and 31.916 cal/deg, respectively.

Key Words: Dissociation by heat, entropy, equilibrium, heat of reaction, silver oxide, oxygen pressures.

Force fields for some group VI hexafluorides, S. Abramowitz and I. W. Levin, *J. Chem. Phys.* **44,** *No. 9, 3353–3356 (May 1, 1966).*
The Coriolis zeta constants were determined for the infrared active F_{1u} modes of SF_6 and TeF_6 from gas phase band contour measurements. These Coriolis data were applied toward determining the general force fields for these Group VI hexafluorides.

Key Words: Force fields, sulphur hexafluoride, tellurium hexafluoride, gas phase, infrared, vibration-rotation, band contours.

Franck-Condon factors and the mass spectra of small molecules, H. M. Rosenstock, (Proc. Intern. *Mass Spectrometry Conf., ASTM E–14, The Hydrocarbon Research Group and GAMS, Paris, France, Sept. 1964), Adv. Mass Spectrometry* **3,** *435–439 (1966).*
This paper is not a review paper but is rather a status report of the theory relating to the mass spectra of small molecules and includes, in outline, some recent work carried out at the National Bureau of Standards.

Key words: Franck-Condon factors, vibrational, photoionization, transition, acetylene probability.

Infrared spectrum of the free radical CF_3 isolated in inert matrices, D. E. Milligan, M. E. Jacox, and J. J. Comeford, *J. Chem. Phys.* **44,** *No. 10, 4058–4059 (May 1966).*
The free radical CF_3 has been stabilized in inert gas and nitrogen matrices at cryogenic temperatures following (1) the reaction of photolytically produced CF_2 and F atoms, (2) the vacuum ultraviolet photolysis of HCF_3 and of CF_3Br[2], and (3) the reaction of photolytically produced C and F atoms. The concentration of CF_3 obtained in these studies has been sufficient for direct infrared observation of three of its vibrational fundamentals, at 703, 1084, and 1248 cm^{-1}. It is concluded that CF_3, unlike CH_3, is nonplanar in its ground state.

Key words: CF_2 reactions, CF_3 free radical, CF_3Br photolysis, F atom reactions, HCF_3 photolysis, infrared spectrum, matrix isolation technique.

Microwave spectrum of perchlorylfluoride, D. R. Lide, Jr., *J. Chem. Phys.* **43,** *No. 10, 3767–3768 (Nov. 1965).*
The microwave spectrum of perchlorylfluoride has been measured and analyzed. Digital averaging techniques were used to improve the signal-to-noise ratio of the very weak lines. The molecular constants determined for $Cl^{35}O_3F$ are $B_0 = 5258.682$, $D_J = 0.0014$, $D_{JK} = 0.0018$, and $eqQ = -19.2$ Mc/s. The OC10 angle is found to be in the range 114°–116°.

Key words: Dipole moment, microwave, perchlorylfluoride, quadrupole coupling constant structure.

Nuclear magnetic resonance studies of inorganic fluorides. II. Solvent effects on J(^{29}Si–^{19}F) in silicon tetrafluoride, T. D. Coyle, R. B. Johannesen, F. E. Brinckman, and T. C. Farrar, *J. Phys. Chem.* **70,** *No. 5, 1682–1684 (May 1966).*
Solvent dependence of the $^{29}Si-^{19}F$ nuclear spin coupling constant has been observed for SiF_4 in solutions in a range of 24 solvents. Similar effects are noted in related molecules.

Key Words: Nuclear magnetic resonance; fluorine, silicon, fluorosilanes, SiF_4, spin coupling constants, solvent.

Phase relations between Cr_2O_3 and IrO_2 in air, C. L. McDaniel and S. J. Schneider, *J. Am. Ceramic Soc.* **49,** *No. 5, 285–286 (May 1966).*
A study has been made by x-ray diffraction analysis of the reactions that occur in an air environment between Cr_2O_3 and Ir or IrO_2. In air Ir oxidizes at low temperatures to form IrO_2 which in turn dissociates at 1020 °C. The pseudo binary system $Cr_2O_3-IrO_2$ contained a quasi-solid solution region existing from 100 mole percent IrO_2 to approximately 21 mole percent Cr_2O_3 with a maximum dissociation temperature at 1040 °C. Up to at least 2100 °C no reaction occured between Cr_2O_3 and Ir.

Key Words: $Cr_2O_3-IrO_2$ system, dissociation, phase relations, platinum metal oxides, solid solution.

Photoionization of propylene at 1236Å. reactions of $C_3D_6^+$ with added alkanes, R. Gorden, Jr., R. Doepker, and P. Ausloos, *J. Chem. Phys.* **44,** *No. 10, 3733–3740 (May 1966).*
C_3H_6-C_3D_6-O_2 mixtures have been irradiated at 1236 Å (10 eV) in the presence and absence of an applied electrical field with the purpose of obtaining information about the ion-molecule reaction mechanism. On the basis of a number of observations, It was calculated that the product, propane, can be ascribed to the reaction $C_{3m}H_{6m}^+ + C_3H_6 \rightarrow C_{3m}H_{6m-2}^+ + C_3H_8$, $(m > 2)$. When alkanes (RH_2) whose ionization energy is less than 10 eV are added to C_3D_6-O_2 mixtures, the following H_2^--transfer reaction occurs: $C_3D_6^+ + RH_2 \rightarrow CD_3CDHCD_2H + R^+$. Relative rates of the reaction of $C_3D_6^+$ with various alkanes have been determined and compare favorably with values obtained in a recent radiolytic study in which cyclopentane-d_1 was used as a source of $C_3D_6^+$ ions.
The optimum experimental conditions, under which meaningful saturation ion currents can be obtained in the photoionization apparatus, are described. On the basis of measurements of the saturation ion current in NO and propylene at 1236 Å, values of 0.197 and 0.208 were obtained for the photoionization efficiencies of C_3H_6 and C_3D_6, respectively. The latter measurements made it possible to express the products in the number of molecules formed per ion pair as well as in the number of molecules formed per quantum absorbed.

Key Words: H_2^--transfer reactions, hydrocarbons, ion-molecule reaction, photoionization, photolysis, propylene.

Some aspects of the coulomb hole of the ground state of H_3^+, W. Lester and M. Krauss, *J. Chem. Phys.* **44,** *No. 1, 207–212 (Jan. 1966).*
The Coulomb hole for the linear and equilateral configurations of the ground state of H_3^+ is calculated using a Gaussian basis set. A modification of the method of Coulson and Neilson which determines the distribution function, $f(r_{12})$, instead of the distribution function of the interelectronic distance $f(r_{12})$ was used. Curves of $f(r_{12})$ and the Coulomb hole function are plotted for selected orientations of the electron-pair to the nuclear arrangements. The method allows a graphic presentation of the dependence of the size of the Coulomb hole on the nuclear geometry of the polyatomic system.

Key Words: Electronic structure, molecular quantum mechanics, H_3^+.

The microwave spectrum of dinitrogen trioxide, R. L. Kuczkowski, *J. Am. Chem. Soc.* **87,** *5259–5260 (1965).*
The microwave spectrum of four isotopic species of dinitrogen trioxide is reported which support the planar ON-NO_2 model with C_s symmetry and from which the N-N bond is determined to be 1.85 with an estimated uncertainty of ±0.03Å.

Key Words: Dinitrogen trioxide, equilibrium, microwave spectrum, structure.

High resolution infrared spectra of cyanogen and cyanogen $-{}^{15}N_2$, A. G. Maki, *J. Chem. Phys.* **43,** *No. 9, 3193–3199 (Nov. 1965).*
The infrared absorption of $^{12}C_2{}^{14}N_2$ and $^{12}C_2{}^{15}N_2$ has been studied with a resolution of 0.08 to 0.04 cm^{-1}. The vibration-rotation band constants were determined for eight vibrational transitions of $^{12}C_2{}^{14}N_2$ and three vibrational transitions of $^{12}C_2{}^{15}N_2$. Many unresolved hot band Q-branches were also measured. The values for many vibrational and rotational constants are given. The bond distances determined from the rotational analysis, and their three-standard-deviation error limits, are r_0 (C-C) = $1.38_9 \pm 0.030$Å and r_0 (C≡N) = $1.15_4 \pm 0.017$Å. The N-N distance and corresponding error limits are $3.69_7 \pm 0.010$A.

Newly observed structure in the photoionization continua of Kr and Ze below 160Å, K. Codling and R. P. Madden, *Appl. Opt.* **4,** *1431–1434 (Nov. 1965).*
The absorption spectra of Kr and Xe have been photographed in the 70–200Å region, revealing many weak, previously unobserved, resonances in the photoionization continua of these gases. The new structures occuring in the 110–115Å region for Kr and 145–160Å for Xe are due to two-electron excitation states involving an inner-shell *d* electron and an outer-shell *p* electron. The resulting configurations are characteristic of the neutral atom, although they lie, in energy, well above the 3rd ionization limits for these atoms. Additional resonances in Xe, photographed in the 90Å region, are due to the excitation of an inner-shell 4*p* electron. An improved value has been obtained for the N_{III} edge of Xe, namely 145.6(±0.5) eV. These spectra were obtained using the pure continuum radiated by the NBS 180 MeV electron synchrotron as a background source.

Observations of dislocations in ammonium dihydrogen phosphate: production of dislocation-free crystals, R. D. Deslattes, J. L. Torgesen, B. Parketzkin, and A. T. Horton, *J. Appl. Phys.* **37,** *No. 2, 541–548 (Feb. 1966).*
The results of etch pit and diffraction topographic studies on ammonium dihydrogen phosphate (ADP) are reported. These studies were carried out on specimens sectioned by abrasive wheel and string-saw from large single crystals grown from aqueous solution. The two characterization methods are shown to be in approximate one-to-one correspondence in the case of sections produced by abrasive sawing.

Absence of both etch pits and topographic images in sections made by string-sawing of material well removed from the seed region is taken to indicate that this material is dislocation free. Preliminary results on the plasticity of ADP are reported. The mechanical results are consistent with dominant slip along the equivalent pair of tetragonal axes and minor, although significant, slip along the unique tetragonal axis. Diffraction contrast profiles calculated on the basis of these slip assignments by means of the schematic theory of contrast due to Bonse are in disagreement with the shape and parity of the observed images.

Structure in the photo-ionization continuum of N_2 near 500Å, K. Codling, *Astrophys. J.* **143,** *No. 2, 552–558 (Feb. 1966).* The absorption spectrum of neutral N_2 has been studied in the 100–600Å region, utilizing the pure continuum radiated by the 180 MeV electron synchrotron as a background source. A 3-meter grazing incidence spectrograph of 0.06Å resolution was used to photograph the spectrum. Discrete structure was observed only in the 470–570Å region. This previously unobserved structure appears to correspond basically to a single state of neutral N_2 having vibrational spacings very similar to those of the known $C^2\Sigma_u^+$ state of N_2^+. There are signs of a second state; the two states appear to form a Rydberg series converging to a limit at 23.6 eV. The structure involves transitions to autoionizing electronic states lying at higher energies than any previously reported for neutral N_2.

Other NBS Publications

J. Res. NBS 70C (Engr. and Instr.), No. 4 (Oct.–Dec. 1966). 75 cents.

Some techniques for measuring small mutual inductances. D. N. Homan.

Deflection of centrally loaded thin circular elastic plates on equally spaced point supports. A. F. Kirstein, W. H. Pell, R. M. Woolley, and L. J. Davis.

Reproducibility of germanium resistance thermometers at 4.2 °K. M. H. Edlow and H. H. Plumb. (See above abstracts.)

Calibration of vibrating-sample magnetometers. W. E. Case and R. D. Harrington.

Notes on the use of propagation of error formulas. H. H. Ku.

The apparent thermal radiation properties of an isothermal V-groove with specularly reflecting walls. R. B. Zipin.

Electrical parameters of precision, coaxial, air-dielectric transmission lines, R. E. Nelson and M. R. Coryell, NBS Mono. 96 (June 30, 1966), $1.25.

Dimensional metrology. Subject-classified with abstracts, I. H. Fullmer, NBS Misc. Publ. 265 (August 1, 1966), $3.00.

Periodicals and serials received in the Library of the National Bureau of Standards as of October 1965, N. J. Hopper, NBS Misc. Publ. 274 (July 1, 1966), 50 cents. Supersedes Mono. 57.

Measures for progress. A History of the National Bureau of Standards, R. C. Cochrane, NBS Misc. Publ. 275 (1966), $5.25.

Cooperation, convertibility, and compatibility among information systems: A literature review, M. M. Henderson, J. S. Moats, M. E. Stevens, and S. M. Newman, NBS Misc. Publ. 276 (June 15, 1966), $2.00.

Atomic transition probabilities. Hydrogen through neon, W. L. Wiese, M. W. Smith, and B. M. Glennon, NSRDS–NBS4, Vol. I (May 20, 1966), $2.50.

The band spectrum of carbon monoxide, P. H. Krupenie, NSRDS–NBS5 (July 8, 1966), 70 cents.

Interrelations between cement and concrete properties. Part 2. Sulfate expansion, heat of hydration, and autoclave expansion, R. L. Blaine, H. T. Arni, and D. N. Evans, Bldg. Sci. Series 5, Pt. 2 (July 1, 1966), 35 cents.

Hosiery lengths and sizes excluding women's, CS46–65 (Dec. 31, 1965), 15 cents. Supersedes CS46–49.

Cast iron soil pipe and fittings, CS188–66 (July 1, 1966), 40 cents. (Supersedes CS188–59).

Southern pine plywood, Comm. Std. CS259–63 (as amended through Feb. 1, 1966) (Nov. 15, 1963), 15 cents.

Expanded vinyl fabrics for furniture upholstery use, Comm. Std. CS273–65 (Dec. 31, 1965), 10 cents.

TFE-Fluorocarbon (polytetrafluoroethylene) resin sintered thin coatings for dry film lubrication, CS274–66 (Jan. 20, 1966), 10 cents.

Quarterly radio noise data March, April, May 1965, W. Q. Crichlow, R. T. Disney, and M. A. Jenkins, NBS Tech. Note 18–26 (May 2, 1966), 45 cents. (Formerly the Central Radio Propagation Laboratory of the National Bureau of Standards, now the Environmental Sciences Services Administration, Boulder, Colo.)

Transistorized building blocks for data instrumentation, P. G. Stein, NBS Tech. Note 268 (May 28, 1966), 60 cents.

Analytical mass spectrometry section: instrumentation and procedures for isotopic analysis, ed. W. R. Shields, Tech. Note 277 (July 25, 1966), 60 cents.

Status report. National Standard Reference Data System April 1966, ed. E. L. Brady, NBS Tech. Note 289 (June 1, 1966), 50 cents.

Information handling in the National Standard Reference Data System, F. L. Alt, NBS Tech. Note 290 (July 1, 1966), 25 cents.

The viscosity and thermal conductivity coefficients of dilute argon between 100 and 2000 °K, H. J. M. Hanley, NBS Tech. Note 333 (March 11, 1966), 25 cents.

Zonal harmonics in low frequency terrestrial radio wave propagation, J. R. Johler, NBS Tech. Note 335 (Apr. 13, 1966), 25 cents. (Formerly the Central Radio Propagation Laboratory of the National Bureau of Standards now the Environmental Science Services Administration, Boulder, Colo.)

Calculation of the admittance of a parallel plate capacitor containing a toroid-shaped sample, E. G. Johnson, Jr., NBS Tech. Note 336 (April 21, 1966), 30 cents.

Advances in ionospheric mapping by numerical methods, W. B. Jones, R. P. Graham, and M. Leftin, NBS Tech. Note 337 (May 12, 1966), 45 cents. (Formerly the Central Radio Propagation Laboratory of the National Bureau of Standards, now the Environmental Science Services Administration, Boulder, Colo.)

A quick, direct method for the determination of activation energy from thermogravimetric data, J. H. Flynn and L. A. Wall, Polymer Letters **4,** Pt. B, No. 5, 323–328 (May 1966).

A standard reference material for Mossbauer spectrometry of iron and its compounds, J. J. Spijkerman, F. C. Ruegg, and J. R. DeVoe, Technical Reports Series 50, Applications of the Mossbauer Effect in Chemistry and Solid-State Physics, pp. 254–259 (International Atomic Energy Agency, Vienna, Austria, 1966).

Action of zinc dust and sodium iodide in *N,N*-dimethylformamide on contiguous, secondary sulfonyloxy groups: a simple method for introducing nonterminal unsaturation, R. S. Tipson and A. Cohen, Carbohydrate Res. **1,** No. 4, 338–340 (1965).

Approximate eigenfunctions of the Liouville operator in classical many-body systems, R. Zwanzig, Phys. Rev. **144,** No. 1, 170–177 (Apr. 8, 1966).

Crystal growth of bone mineral, W. E. Brown, Clin. Orthopaed. **44,** 205–219 (1966).

Infrared-red spectra of hydroxyapatite, octacalcium phosphate and pyrolysed octacalcium phosphate, B. O. Fowler, E. C. Moreno, and W. E. Brown, Arch. Oral. Biol. **11,** 477–492 (1966).

Phase rule considerations and the solubility of tooth enamel, W. E. Brown and B. M. Wallace, Ann. N.Y. Acad. Sci. **131,** Art. 2, 690–693 (Sept. 30, 1965).

Preparation of inososes from their phenylhydrazones by use of a cation-exchange resin; separation of certain phenylhydrazones from phenylosazones, A. J. Fatiadi, Carbohydrate Res. **1,** No. 6, 489–491 (1966).

Pyrolysis of vinyl and vinylidene fluoride polymers: Influence of prior gamma-irradiation, L. A. Wall, S. Straus, and R. E. Florin, J. Polymer Sci. **4,** Pt. A-1, 349–365 (1966).

Random-walk model of adsorption of a chain-polymer molecule on a long rigid-rod molecule, R. J. Rubin, J. Chem. Phys. **44,** No. 5, 2130–2138 (Mar. 1, 1966).

Rodlike behavior of poly(*n*-butyl)isocyanate from dielectric measurements, H. Yu, A. J. Bur, and L. J. Fetters, J. Chem. Phys. **44,** No. 7, 2568–2576 (Apr. 1, 1966).

Soft tissue response to implants of gallium alloys and silver amalgam alloys, H. W. Lyon, R. M. Waterstrat, and G. C. Paffenbarger, J. Am. Dental Assoc. **72,** No. 3, 659–664 (Mar. 1966).

A statistical model of flicker noise, J. A. Barnes and D. W. Allan, Proc. IEEE **54,** No. 2, 176–178 (Feb. 1966).

An automatic ellipsometer. Automatic polarimetry by means of an ADP polarization modulator III, H. Takasaki, Appl. Opt. **5,** No. 5, 759–764 (May 1966).

An intercomparison of atomic standards, R. Beehler, D. Halford, R. Harrach, D. Allan, D. Glaze, C. Snider, J. Barnes, R. Vessot, H. Peters, J. Vanier, L. Cutler, and L. Bodily, Proc. IEEE **54,** No. 2, 301–302 (Feb. 1966).

Bone-air cancellation, E. L. Smith, H. S. Bowman, P. G. Weissler, and R. K. Cook, Bull. Lab. Electroacoustique, No. 9, 45–50 (Apr. 1966).

Convenient safety cutoff device for water cooled equipment, J. J. Ritter and T. D. Coyle, Rev. Sci. Instr. **37,** No. 4, 523 (Apr. 1966).

Study suggests value of shared computers, A. E. Rikli, S. I. Allen, and S. N. Alexander, Mod. Hosp. **106,** No. 5, 100–108 (May 1966).

The NBS-A time scale—its generation and Dissemination, J. A. Barnes, D. H. Andrews, and D. W. Allen, IEEE Trans. Instr. Meas. **IM-14,** 228–232 (Dec. 1965).

Inequalities for the permanental minors of non-negative matrices, R. A. Brualdi and M. Newman, Can. J. Math. **18,** 608–615 (1966).

Real two-dimensional representations of the free product of two finite cyclic groups, J. Lehner and M. Newman, Proc. Camb. Phil Soc. **62,** 135–141 (1966).

Absolute determination of refractive indices of gases at 47.7 gigahertz, A. C. Newell and R. C. Baird, J. Appl. Phys. **36,** No. 12, 3751–3759 (Dec. 1965).

International comparison of measurements at high frequencies, M. C. Selby, IEEE Spectrum **3,** No. 1, 89–98 (Jan. 1966).

LF-VLF frequency and time services of NBS, D. H. Andrews, IEEE Trans. Instr. Meas. **IM-14,** No. 4, 233–237 (Dec. 1965).

The system of electromagnetic quantities at 30 kHz to GHz, M. C. Selby, Metrologia **2,** No. 1, 37–45 (Jan. 1966).

The system of electromagnetic quantities at frequencies above 1 GHz, R. W. Beatty, Metrologia **2,** No. 1, 46–54 (Jan. 1966).

The "volt standard" moves to Gaithersburg, Maryland, W. J. Hamer, J. Wash. Acad. Sci. **56,** 101–108 (May 1966).

A nomogram for determining azimuth and horizontal trace velocity from tripartite measurements, H. Matheson, Earthquake Notes **XXXVII,** No. 1, 33–37 (Mar. 1966).

Correction in the laboratory measurement of the rate constant for $N_2^+ + O_2 \rightarrow N_2 + O_2^+$ at 300 °K, F. C. Fehsenfeld, A. L. Schmeltekopf, and E. E. Ferguson, Planetary Space Sci. **13,** 919–920 (Sept. 1965).

Electromagnetic wave propagation and relativistic damping effects in a uniformly magnetized electron-positron gas, L. A. Steinert, Il Nuovo Cimento **40,** No. 10, 345–374 (Dec. 1965).

Energy gap of superconducting tin films in a magnetic field, R. S. Collier and R. A. Kamper, Phys. Rev. **143,** No. 1, 323–328 (Ocf. 1966).

Extended dislocation nodes in a silver-tin alloy, L. K. Ives and A. W. Ruff, Jr., J. Appl. Phys. **37,** No. 4, 1831–1837 (Mar. 15, 1966).

Force fields for group IV tetrafluorides and group V trifluorides, I. W. Levin and S. Abramowitz, J. Chem. Phys. **44,** No. 7, 2562–2567 (Apr. 1, 1966).

Longitudinal magnetoresistance of copper, R. L. Powell, Low Temp. Phys. **LT-9,** Pt. B, 732–735 (1965).

On the definition of the stacking-fault energy in binary alloys, R. deWit and R. E. Howard, Acta. Met. **14,** No. 3, 431–433 (1966).

Possible nuclear contribution to thermal expansion, E. C. Hirschkoff and N. N. Wolcott, Proc. Phys. Soc. **86,** No. 6, 1372 (1965).

Possible observation of In^{115} nuclear electric hexadecapole transitions, R. J. Mahler, L. W. James, and W. H. Tantilla, Phys. Rev. Letters **16,** No. 7, 259–261 (Feb. 14, 1966).

Random-walk method for calculating correlation factors: Tracer diffusion by divacancy and impurity-vacancy pairs in cubic crystals, R. E. Howard, Phys. Rev. **144,** No. 2, 650–651 (Apr. 15, 1966).

Relaxations in polyethylene: orientation of the lamellar crystals, R. K. Eby and J. P. Colson, J. Acoust. Soc. Am. **39,** No. 3, 506–510 (Mar. 19, 1966).

Role of surface diffusion in stabilizing the surface of a solid growing from solution or vapor, S. R. Coriell, and R. L. Parker, J. Appl. Phys. **37,** No. 4, 1548–1550 (Mar. 15, 1966).

The optical constants of some oxide glasses in the strong absorption region, G. W. Cleek, Appl. Opt. **5,** No. 5, 771–775 (May 1966).

Three-body photodisintegration of He^3, H. M. Gerstenberg and J. S. O'Connell, Phys. Rev. **144,** No. 3, 834–838 (Apr. 22, 1966).

Use of ellipsometry in the study of corrosion, J. Kruger, Corrosion **22,** No. 4, 88–97 (Apr. 1966).

Wave propagation in a three-element linear spring and dashpot model filament, J. C. Smith, J. Appl. Phys. **37,** No. 4, 1697–1704 (Mar. 15, 1966).

Perturbation theorems for waveguide junction, with applications, D. M. Kerns and W. T. Grandy, IEEE Trans. Microwave Theor. Tech. **MTT-14,** No. 12, 85–92 (Feb. 1966).

The effect of atmospheric noise on the probability of error for an NCFSK system, A. M. Conda, IEEE Trans. Commun. Technol. **CT-13,** No. 3, 280–284 (Sept. 1965).

Acids, bases, and buffers, R. G. Bates (Proc. Symp. Current Concepts of Acid-Base Measurements, New York Academy of Sciences, New York, N.Y., Nov. 23, 1964), Ann. N.Y. Acad. Sci. **133,** Art. 1, 25–33 (1966).

Comparative strengths of aliphatic acids and some other carboxylic acids in benzene at 25°, M. M. Davis and M. Paabo, J. Organic Chem. **31,** 1804–1810 (1966).

Crystal chemistry of calcium phosphates, W. E. Brown, Proc. 1964 Technical Session on Cane Sugar Refining Research, New Orleans, Louisiana, Nov. 9–10, 1964, pp. 26–34 (Agriculture Research Service, New Orleans, Louisiana, Mar. 1966).

Emission spectrometry, M. Margoshes and B. F. Scribner, Anal. Chem. **38,** No. 5, 297R–310R (Apr. 1966).

Structure of cubic ammonium fluosilicate: neutron-diffraction and neutron-inelastic scattering studies, E. O. Schlemper, W. C. Hamilton, and J. J. Rush, J. Chem. Phys. **44,** No. 6, 2499–2502 (Mar. 15, 1966).

Application of sulfur coatings to integrating spheres, S. T. Dunn, Appl. Opt. **4,** No. 7, 877 (July 1965).

Simple contact type temperature controller, L. A. Marzetta, Rev. Sci. Instr. Note **37,** No. 6, 789 (June 1966).

Some statistical properties of pulses from photomultipliers, M. Gadsden, Appl. Opt. **4,** No. 11, 1446–1452 (Nov. 1965).

Use of an auxiliary sphere with a spectrophotometer to obtain absolute reflectance, D. G. Goebel, B. P. Caldwell, and H. K. Hammond, J. Opt. Soc. Am. **56,** No. 6, 783–788 (June 1966).

Anniversaries in 1965 of interest to statisticians, C. Eisenhart, Am. Stat. **19,** No. 5, 21–29 (Dec. 1965).

The assumptions underlying the analysis of variance, C. Eisenhart, (Spanish Translation by Jose Otaduy), Book, Sobre el Analisis de la Variancia, pp. 1–24 (Comision de Education Estadistica del Instituto Interamerican de Estadistica, Rosario, Argentina, 1953).

Debye relaxation in symmetric-top-foreign-gas mixtures; temperature dependence of collision cross sections, L. Frenkel, S. J. Kryder, and A. A. Maryott, J. Chem. Phys. **44,** No. 7, 2610–2619 (Apr. 1, 1966).

Demountable high power source for soft x-ray region, R. D. Deslattes and B. G. Simson, Rev. Sci. Instr. **37,** No. 6, 753–754 (June 1966).

EPR spectrum of gas-phase sulfur atoms, R. L. Brown, J. Chem. Phys. **44,** No. 7, 2827–2828 (Apr. 1, 1966).

Gas density stabilizer for flow proportional counters, R. D. Deslattes, B. G. Simson, and R. E. LaVilla, Rev. Sci. Instr. **37,** No. 5, 596–599 (May 1966).

Inelastic scattering cross sections for 20-keV electrons in Al, Be, and polystyrene, N. Swanson and C. J. Powell, Phys. Rev. **145,** No. 1, 195–208 (May 6, 1966).

Influence of an external magnetic field on nuclear resonance in ferromagnetic materials, L. H. Bennett, J. Appl. Phys. **37,** No. 3, 1242–1243 (Mar. 1, 1966).

Measurement of absolute wavelength stability of lasers, K. D. Mielenz, R. B. Stephens, K. E. Gillilland, and K. F. Nefflen, J. Opt. Soc. Am. **56,** No. 2, 156–162 (Feb. 1966).

Measurement of the 633-nm wavelength of helium-neon lasers, K. D. Mielenz, R. B. Stephens, K. E. Gillilland, K. F. Nefflen, and R. B. Zipin, Appl. Phys. Letters **7,** No. 10, 277–279 (Nov. 1965).

Methods of determining Coriolis zeta constants, S. Abramowitz and I. W. Levin, J. Mol. Spectry. **19,** No. 4, 461–462 (Apr. 1966).

Plasmon damping metals, B. W. Ninham, C. J. Powell, and N. Swanson, Phys. Rev. **145,** No. 1, 209–217 (May 6, 1966).

Polycrystalline spin wave theory of ferro-magnetic resonance compared with the tilting experiment, A. S. Risley, E. G. Johnson, and H. E. Bussey, J. Appl. Phys. **37,** No. 2, 656–668 (Feb. 1966).

Shock wave propagation in cubic lattices, D. H. Tsai and C. W. Beckett, J. Geophys. Res. **71,** No. 10, 2601–2608 (May 15, 1966).

Some applications of the wave front shearing interferometer, J. B. Saunders, Japanese J. Appl. Phys. Suppl. **I,** 4, 99–105 (1965).

Superconducting behavior of indium-lead alloys, S. Gygax, J. L. Olsen, and R. H. Kropschot (Proc. IXth Intern. Conf. Low Temperature Physics, Columbus, Ohio, Aug. 31–Sept. 4, 1964), Book, Low Temperature Physics LT9, Pt. A, ed. J. G. Daunt, D. O. Edwards, F. J. Milford, and M. Yaqub, pp. 587–590 (Plenum Press Inc., New York, N.Y., 1965).

Superconductivity in ceramic, mixed titanates, H. P. R. Frederikse, J. F. Schooley, W. R. Thurber, E. Pfeiffer, and W. R. Hosler, Phys. Rev. Letters **16,** No. 13, 579–581 (Mar. 28, 1966).

The measurement of homogeneity of optical materials in the visible and near infrared, F. W. Rosberry, Appl. Opt. **5,** No. 6, 961–966 (June 1966).

Two-state model for the free volume of vitreous B_2O_3, P. B. Macedo, W. Capps, and T. A. Litovitz, J. Chem. Phys. **44,** No. 9, 3357–3364 (May 1, 1966).

Additional observations on the electronic spectrum of copper (II) acetate monohydrate, C. W. Reimann, G. F. Kokoszka, and G. Gordon, J. Inorg. Chem. **4,** No. 7, 1082–1084 (July 1965).

Density and specific gravity, J. K. Taylor, Encyclopedia of Industrial Analysis **1,** 546–560 (Interscience Publ. Inc., New York, N.Y., 1965).

Electron paramagnetic resonance and nuclear magnetic resonance as analytical tools, T. C. Farrar (Proc. Conf. Purification of Materials, New York Academy of Sciences), Ann. N.Y. Acad. Sci. **137,** 323–334 (Jan. 1966).

Formation of crystallites of benzophenone in hydrocarbon glass, R. Keller and D. Breen, J. Chem. Phys. **43,** No. 7, 2562–2563 (Oct. 1965).

Gas-phase radiolysis of cyclopentane. Relative rates of H_2-transfer reactions from various hydrocarbons to $C_3H_6^+$, R. D. Doepler and P. Ausloos, J. Chem. Phys. **44,** No. 5, 1951–1958 (Mar. 1966).

Ion-molecule reaction in the liquid and solid phase radiolysis of hydrocarbon mixtures, P. Ausloos, A. A. Scala, and S. G. Lias, J. Am. Chem. Soc. **88,** 1583–1584 (1966).

Ion-pair process in CH_3Cl by photoionization, V. H. Dibeler and J. A. Walker, J. Chem. Phys. **43,** No. 5, 1842–1843 (Sept. 1965).

Progress report on a test for cleanability, M. D. Burdick, Proc. Porcelain Enamel Institute Forum **26,** 41–48 (1965).

Progress report on the development of a standardized test for continuity of porcelain enamel coatings, M. A. Rushmer, Proc. Porcelain Enamel Institute **27,** 49–56 (1965).

Purification of single crystal growth, J. L. Torgesen, Ann. N. Y. Acad. Sci. **137,** 30–43 (1966).

Shear relaxation times of simple fluids, R. D. Mountain and R. Zwanzig, J. Chem. Phys. **44,** No. 7, 2777–2779 (Apr. 1966).

Silicon-fluorine chemistry. II. Silicon-boron fluorides, P. L. Timms, T. O. Ehlert, J. L. Margrave, F. E. Brinckman, T. C. Farrar, and T. D. Coyle, J. Am. Chem. Soc. **87,** No. 17, 3819–3823 (Sept. 1965).

Spectrochemical analysis of high-temperature alloys by spark excitation in argon and nitrogen, H. C. Dilworth, Am. Soc. Testing Mater. Spec. Tech. Publ. **376** (1965).

Standardization of the differential chemical shift for Fe^{57}, J. J. Spijkerman, F. C. Ruegg, and J. R. DeVoe, (Proc. New England Nuclear Mossbauer Symp., New York, N.Y., Jan. 1964), Book, Mossbauer Effect Methodology, pp. 115–120 (Plenum Press Inc., New York, N.Y., 1965).

The electron paramagnetic resonance spectrum of tetrakis-*t*-butoxyvanadium(IV), G. F. Kokoszka, H. C. Allen, Jr., and G. Gordon, Inorg. Chem. **5,** 91–93 (1966).

A cooling system for a laboratory magnet, R. A. Forman and T. McKneely, Appl. Spectry. **20,** 189 (May–June 1966).

A large signal IGFET DC source follower, D. P. Stokesberry, Proc. IEEE **54,** No. 1, 66 (Jan. 1966).

A method for calibrating volt boxes, with analysis of volt-box self-heating characteristics, R. F. Dziuba and T. M. Souders, IEEE Intern. Conf. Record, Pt. 10, pp. 17 (Mar. 21–25, 1966).

A semi-automatic technique for tuning a reflectometer, M. H. Zanboorie, IEEE Trans. Microwave Theory Tech. **MTT-13,** No. 5, 709–710 (Sept. 1965).

A simple current generator, J. K. Whittaker, Nuclear Instr. Methods **39,** No. 1, 183–184 (Jan. 1966).

A zero-crossing discriminator with picosecond time slewing, J. K. Whittaker, IEEE Trans. Nuclear Sci. **NS-13,** No. 1, 399–405 (Feb. 1966).

Anomalous conductance behavior in polymers, A. H. Scott (1965 Annual Report Conf. Electrical Insulation, NAS–NRC Publ. 1356, pp. 98–102) (Natl. Acad. Sci.–Natl. Res. Council, Washington, D.C., 1966).

Apparent negative impedances and their effect on three-terminal dielectric loss measurements, W. P. Harris (1965 Annual Report Conf. Electrical Insulation), NAS–NRC Publ. 1356, pp. 83–86) (Natl. Acad. Sci.–Natl. Res. Council, Washington, D.C., 1966).

Effects of thermal shrinkage on built-up roofing, W. C. Cullen, J. Bldg. Res. Inst. **2,** No. 4, 23 (July–Aug. 1965).

Fire test methods for paints, A. F. Robertson, Bldg. Res. pp. 48–52 (July–Aug. 1965).

Flow measurement standardization, T. Filban and M. R. Shafer, Proc. ISA Conf. 1964, 19, Pt. 1, Paper No. 12-2-4-64 (1964).

Guide to dental materials, 1966–1967, G. C. Paffenbarger, J. W. Stanford, M. P. Kumpula, and W. T. Sweeney, Am. Dental Assoc. 3d ed., 188 pages (Chicago, Ill., 1966).

Human engineering with design of a console for the comparison of volt boxes, P. H. Lowrie, Jr., ISA J. pp. 67–71 (July 1965).

International intercomparison of standards for microwave power measurement, G. F. Engen, IEEE Trans. Microwave Theory Tech. **MTT-13,** No. 5, 713–715 (Sept. 1965).

Measuring the coordinates of a number of points in a complex laboratory-scale model, F. D. Ordway, Rev. Sci. Instr. **36,** No. 8, 1156–1159 (Aug. 1965).

Modular software for on-line handling of nuclear data, J. M. Wyckoff, IEEE Trans. Nuclear Sci. **NS-13,** No. 1, 199 (Feb. 1966).

National Bureau of Standards offers method to prevent built-up roof splitting failure, W. C. Cullen, Roofing Siding Insulation Mag. **40,** No. 4, 28–30 (Apr. 1965).

1965 Meeting of IEC Committee TC45, Progress in Nuclear Instrumentation, L. Costrell, Mag. Std., p. 9 (Jan. 1966).

Roofing research in Guam and Okinawa, W. C. Cullen, Am. Roofer Bldg. Improvement Contractor, pp. 10 (Oct. 1965).

Standards for galvanomagnetic devices, S. Rubin, Solid State Electronics **9,** 5, 559–566 (May 1966).

Suppression of 60 c/s pickup when using sensitive DC amplifiers, R. L. Nuttall and D. C. Ginnings, Electron. Design **12,** No. 26, pp. 34–35 (Dec. 20, 1965).

Tapered inlets for pipe culverts, discussion and author's closure, J. L. French, J. Hydraulics (Div. Am. Soc. Civil Eng.) pp. 286 (May 1965).

The effect of insulation on the durability of a smooth-surfaced built-up roof, W. C. Cullen and W. H. Appleton, Coal Tar Asphalts and Related Mater. **3,** 122–124 (Mar. 1965).

The NBS instrumentation for use in the measurement of spectral irradiances of solar simulators, R. Stair and W. E. Schneider, Proc. Intern. Symp. Solar Radiation Simulation, Los Angeles, Calif., Jan. 18–20, 1965, pp. 75–94 (Inst. Environmental Sciences and Am. Soc. Testing and Materials, 1965).

The response of flush diaphragm pressure transducers to thermal gradients, L. Horn, ISA 20th Annual Conf. and Exhibit, Los Angeles, Calif., Oct. 4–7, 1965, 20, Pt. III, ISA Preprint No. 13. 3–4–65 (1965).

Thermal insulation in buildings, F. J. Powell, Military Engr. **58,** No. 38, 275–276 (July–Aug. 1966).

Voltmeter calibration to 1 GHz, M. C. Selby, W. J. Blank, and R. P. Chairton, (Proc. 1965 Wescon Conf., San Francisco, Calif., Aug. 1965), IEEE WESCON Tech. Papers **9,** Pt. 6, No. 8.8, 1–12 (1965).

Congruence subgroups of positive genus of the modular group, M. Newman and M. Knopp, Ill. J. Math. **9,** No. 4, 577–583 (Nov. 1965).

Scattering properties of concentric soot-water spheres for visible and infrared light, R. W. Fenn and H. Oser, J. Appl. Opt. **4,** 1504–1509 (Nov. 1965).

The design of a federal statistical data center, D. Rosenblatt, E. Glaser, and M. K. Wood, Statistical Evaluation Report No. 6, Office of Statistical Standards, Bureau of the Budget, Appendix C, pp. 1–19 (Office of the President, Washington, D.C., Dec. 1965).

Color designation and specification, D. B. Judd, Encyclopedia of Industrial Analysis, **1,** 315 (1966).

Electrical testing in chemical technology, A. H. Scott, Encyclopedia of Chemical Technology, 2d ed., 7, 716–726 (1965).

Measurement of DC dielectric conductance (reciprocal resistance)

at elevated temperatures, A. H. Scott, Proc. 6th Electrical Insulation Conf., Sept. 13–16, 1965, pp. 252–254 (1965).

Metrology essential to the space age, A. G. McNish, George Washington University Mag. 1, No. 4, 10–14 (1965).

Progress report for OSA Committee on uniform color scales, D. B. Judd, Proc. Intern. Color Comm., Lucerne, Switzerland, 1965, 1, 399–407 (Mar. 1966).

Specification and designation of color, D. B. Judd and I. Nimeroff, Treatise Anal. Chem. **36,** 2873–2942 (1964).

The calibration of permanent magnet standards, I. L. Cooter, ISA 20th Annual Conf. and Exhibit, Part 1. Measurement Standards and Instrumentation, Los Angeles, Calif., Oct. 4–7, 1965, 20, Pt. 1, ISA Preprint 14.1–3–65 (1965).

The international system of units, A. G. NcNish, American Society for Quality Control Annual 1965 Tech. Conf. Trans. Industrial Quality Control **22,** No. 9, 465–469 (Mar. 1966).

The nature of measurement, A. G. McNish, Book, Industrial Metrology (Sponsored by the American Society of Tool and Manufacturing Engineers), chap. 1, 4, No. 2, 24–31 (Mar. 1966).

Color appearance, D. B. Judd, Proc. Intern. Color Comm., Lucerne, Switzerland, 1965, 1, 27–51 (Mar. 1966).

Cooler for semiconductor light emitters, lasers and photodetectors, H. K. Kessler, Rev. Sci. Instr. **37,** 517–518 (Apr. 1966).

Decays of positive-parity baryon resonances in a broken U(12), H. Harari, D. Horn, M. Kugler, H. J. Lipkin, and S. Meshkov, Phys. Rev. **140,** No. 4B, B1003 (Nov. 1965).

Discussion of ASME paper 60–WA–333, November 30, 1960, D. P. Johnson and U. O. Hutton, Book, High Pressure Measurement, ed. A. A. Giardini and E. C. Lloyd, pp. 350–351 (Butterworth, Inc., London, England, 1963).

Effects of space radiation on refractive properties of optical glass, I. H. Malitson, M. J. Dodge, and M. E. Gonshery, Proc. Annual Conf. Photography, Science and Engineering, San Francisco, Calif., May 9–13, 1966, p. 75 (1966).

Elastic constants of single crystal UO_2 at 25 °C., J. B. Wachtman, Jr., M. L. Wheat, H. J. Anderson, and J. L. Bates, J. Nuclear Mater. **16,** 39–41 (1965).

Electron energy bands in $SrTiO_3$ and TiO_2 (theory and experiment), A. K. Kahn, H. P. R. Frederikse, and J. H. Beckerd, (Informal Proc. Bull., Intern, Conf. Materials, Pittsburgh, Pa., 1963), Book, Transition of Metal Compounds, ed. E. R. Schatz, pp. 53–64 (Gordon and Breach Sci. Publ., New York, N.Y., 1964).

Fundamental studies of color vision from 1860 to 1960, D. B. Judd, Proc. Natl. Acad. Sci. **55,** No. 6, 1313–1330 (June 1966).

Geomagnetic and solar data, J. V. Lincoln, J. Geophys. Res. **70,** No. 13, 3227–3228 (July 1965); **70,** No. 15, 3761–3763 (Aug. 1965); **70,** No. 17, 4383–4384 (Sept. 1965); **70,** No. 19, 4963–4964 (Oct. 1965).

Interspecimen comparison of the refractive index of fused silica, I. H. Malitson, J. Opt. Soc. Am. **55,** No. 10, 1205 (Oct. 1965).

Intrinsic and lattice-induced distortion of the tetrachlorocuptrate ion, M. Sharnoff and C. W. Reimann, J. Chem. Phys. **43,** No. 9, 2993–2996 (Nov. 1965).

Line broadening, W. L. Wiese, Book, Plasma Diagnostic Techniques, ed. R. H. Huddleston and S. L. Leonard, 21, 265–317 (Academic Press Inc., New York, N.Y., 1965).

Magnetic susceptibility of insulating and semiconducting strontium titanate, H. P. R. Frederikse and G. A. Candela, Phys. Rev. **147,** No. 2, 583–584 (July 15, 1966).

Magnetoacoustic adsorption and the fermi surface in potassium, H. J. Foster, P. H. Meijer, and E. V. Mielczarek, Phys. Rev. **139,** No. 6A, A1849–A1857 (Sept. 1965).

Magnetoresistance of semiconducting $SrTiO_3$, H. P. Frederikse, W. R. Hosler, and W. Thurber, Phys. Rev. **143,** No. 2, 648–651 (Mar. 1966).

Measurements of ion-optical properties of a high resolution spectrometer for electron scattering, S. Penner and J. W. Lightbody, Proc. Intern. Symp. Magnetic Technologies, Stanford Linear Accelerator Center, Stanford Univ., Calif., Sept. 8–10, 1965, pp. 154–163 (Oct. 1965).

Observatory reports, spectroscopy, C. E. Moore, Astron. J. **70,** No. 9, 637–639 (Nov. 1965).

Optical absorption of cobalt in manganese fluoride, R. F. Blunt, J. Chem. Phys. **44,** No. 6, 2317–2320 (Mar. 15, 1966).

Photon absorption cross section of spherical nuclei, M. G. Huber, H. J. Weber, M. Danos, and W. Greiner, Phys. Rev. Letters **15,** No. 12, 529–531 (Sept. 1965).

Photoneutron reactions, E. G. Fuller, (Proc. Intern. Conf. Study of Nuclear Structure with Neutrons, Antwerp, Belgium, July 14–23, 1965), Book, Nuclear Structure Study with Neutrons, ed. M. Neve De Mevergnies, P. VanAssche, and J. Vervier, pp. 359–375 (North-Holland Publ. Co., Amsterdam, The Netherlands, 1966).

Photonuclear reactions. M. Danos and E. G. Fuller, Ann. Rev. Nuclear Sci. **15,** 29–66 (1966).

Radiative recombination lifetimes in laser excited silicon, N. N. Winogradoff and H. K. Kessler, Appl. Phys. Letters **8,** No. 4, 99 (Feb. 1966).

Radiation of sound by earthquakes, R. K. Cook, 5^{e} Cong. Intern. Acoustique, Liege, Belgium 1b, K19 (1965).

Relation of strength of thermally tempered glass to fraeture mirror size, M. K. Kerper and T. G. Scuderi, Am. Ceramic Soc. Bull. **44,** No. 12, 953–955 (Dec. 1965).

Resolving power related to aberration, F. E. Washer, Photogrammetric Eng. **XXXII,** No. 2, 213–226 (Mar. 1966).

Second breakdown and current distributions in transistors, H. A. Schafft and J. C. French, Solid-State Electron. **9,** No. 7, 681–688 (July 1966).

Secondary electron trajectories in a Faraday cup magnetic field, J. S. Pruitt, Nuclear Instr. Methods **39,** 329 (Feb. 1966).

Symmetry conditions on jump rates occuring in relaxation times associated with point defect motion, H. S. Peiser and J. B. Wachtman, Jr., J. Phys. Chem. Solids **27,** 975 (1966).

Tables of dielectric constants, dipole moments and dielectric relaxation times, F. I. Mopsik, (1964 Digest of Literature on Dielectric Conf. Electrical Insulation), NAS-NRC Publ. 1342, 28, 33–66 (Natl. Acad. Sci.–Natl. Res. Council, Washington, D.C., 1965).

The interaction of radiation with charged particles. I, W. H. Chappell, W. E. Brittin, and S. J. Glass, Il Nuovo Cimento **38,** No. 3, 1186–1191 (1965).

The interaction of radiation with charged particles. II. Dispersion relation for transverse modes, S. J. Glass and W. R. Chappel, Il Nuovo Cimento **38,** No. 1, 79–88 (1966).

The paramagnetic resonance spectrum of W^{5+} in rutile (TiO_2), T. T. Chang, Phys. Rev. **147,** No. 1, 264–267 (July 8, 1966).

Atmospheric research and electromagnetic telecommunication, Part I, H. G. Booker and C. G. Little, IEEE Spectrum **2,** No. 8, 44–52 (Aug. 1965).

Atmospheric research and electromagnetic telecommunication, Part II, H. G. Booker and C. G. Little, IEEE Spectrum **2,** No. 9, 98–103 (Sept. 1965).

**Publications for which a price is indicated are available by purchase from the Superintendent of Documents, U.S. Government Printing Office, Washington, D.C. 20402 (foreign postage, one-fourth additional). The NBS nonperiodical series are also available from the Clearinghouse for Federal Scientific and Technical Information, Springfield, Va., 22151. Reprints from outside journals and the NBS Journal of Research may often be obtained directly from the authors.*

JOURNAL OF RESEARCH of the National Bureau of Standards—A. Physics and Chemistry
Vol. 70A, No. 6, November–December 1966

Index to Volume 70A

January to December 1966

A

Page
Absolute isotopic abundance ratios and atomic weight of magnesium 453
Absolute isotopic abundance ratios and the atomic weight of a reference sample of chromium 193
Allen, H. C., Jr., C. W. Reimann, G. F. Kokoszka, Optical and magnetic spectra of bis-*N*-propylsalicylaldiminato copper (II) 1
Aluminum carbide, dissociation pressure of, using a rotating Knudsen cell 253
Annealing of a borosilicate glass, further studies 147
Antonucci, J. M., L. A. Wall, High-temperature reactions of hexafluorobenzene 473
Atomic weight of a reference sample of chromium, absolute isotopic abundance ratios ... 193
Atomic weight of magnesium and absolute isotopic abundance ratios 453

B

Bates, R. G., R. A. Robinson, Dissociations of some substituted phenols in 50-percent aqueous methanol as solvent 553
Billick, I. H., G. H. Weiss, The solution to a nonlinear Lamm equation in the Faxén approximation 17
Bis-*N*-propylsalicylaldiminato copper (II), optical and magnetic spectra 1
Block, S., C. Robbins, A. Perloff, Crystal structure of $BaGe[Ge_3O_9]$ and its relation to benitoite 385
Borates, hydrated, infrared spectra 153
Borosilicate glass, further studies in the annealing 147
Bower, V. E., R. A. Robinson, Properties of aqueous mixtures of pure salts. Thermodynamics of the ternary system: water-calcium chloride-magnesium chloride at 25 °C 305
—, —, Properties of the aqueous mixtures of pure salts: Thermodynamics of the ternary system: water-sodium chloride-calcium chloride 313
Brillouin scattering in liquids, thermal relaxation 207
Broadhurst, M. G., The melting temperatures of the *n*-paraffins and the convergence temperature for polyethylene 481
Brown, W. E., E. C. Moreno, T. M. Gregory, Solubility of $CaHPO_4 \cdot 2H_2O$ and formation of ion pairs in the system $Ca(OH)_2 - H_3PO_4 - H_2O$ at 37.5 °C 545

C

Calcium molybdate ($CaMoO_4$) and other single crystals having the scheelite structure ... 379
Calibration of germanium resistors at low temperatures (2–20 ° Kelvin) 243
Cataland, G., H. H. Plumb, Calibration of germanium resistors at low temperatures (2–20 °Kelvin) 243
Catanzaro, E. J., T. J. Murphy, E. L. Garner, W. R. Shields, Absolute isotopic abundance ratios and atomic weight of magnesium 453
—, *W. R. Shields, T. H. Murphy, E. L. Garner,* Absolute isotopic abundance ratios and the atomic weight of a reference sample of chromium 193
Ceramic oxide specimens from 1200 to 1600 °K, a rotating cylinder method for measuring normal spectral emittance 393
Chromium, absolute isotopic abundance ratios and atomic weight of a reference sample 193
Clark, H. E., D. G. Moore, A rotating cylinder method for measuring normal spectral emittance of ceramic oxide specimens from 1200 to 1600 °K 393
Cobalt (II)-doped trisphenanthrolinezinc nitrate dihydrate, electron absorption 417
Configuration $4d^n + 4d^{n-1}5s$ in doubly ionized atoms 435
Consistency of the check in the vector verification method, use 319
Corliss, C. H., W. F. Meggers, Wavelengths, intensities, and Zeeman patterns in ytterbium spectra (Yb I, II, III, IV) 63
—, *B. Warner,* Oscillator strengths for ultraviolet lines of Fe I 325
Corundum, synthetic single crystal, elastic constants 277
Crissman, J. M., E. Passaglia, Mechanical relaxation in polyethylene crystallized with various degrees of lammellar orientation 225
Crystal structure in the system niobium pentoxide-tungsten trioxide, phase equilibria ... 281
Crystal structure of $BaGe[Ge_3O_9]$ and its relation to benitoite 385
Crystallization, spherulitic, of isotactic polypropylene from solution: On the evolution of monoclinic spherulites from dendritic chain-folded crystal percursors 29

D

Dendritic crystals of polypropylene, evolution of monoclinic spherulites 29
Density of polyethylene crystals grown from solution 221
Density-temperature formulae for coexisting liquid and vapor and for freezing liquid parahydrogen 541
Dibeler, V. H., J. A. Walker, H. M. Rosenstock, Mass spectrometric study of photoionization V. water and ammonia 459
Dissociation of some substituted phenols in 50-percent aqueous methanol as solvent ... 553
Dissociation pressure of aluminum carbide using a rotating Knudsen cell 253
Determination of intermolecular potential functions from macroscopic measurements ... 259

E

Page
Effect of some halogenated hydrocarbons on the flame speed of methane 133
Eisenstein, J. C., M. H. L. Pryce, Interpretation of the solution absorption spectra of $(PuO_2)^{++}$ and $(NpO_2)^{+}$ ions 165
Elastic constants of synthetic crystals corundum 277
Electron absorption spectrum of cobalt (II)-doped trisphenanthrolinezinc nitrate dihydrate 417

F

Farabaugh, E. N., H. S. Peiser, J. B. Wachtman, Jr., Orientation of calcium molybdate ($CaMoO_4$) and other single crystals having the scheelite structure 379
Fe I, oscillator strengths for ultraviolet lines 325
Fetters, L. J., Procedures for homogeneous anionic polymerization 421
Florin, R. E., M. S. Parker, L. A. Wall, Mechanism of the depolymerization of polytetrafluoroethylene with pyrolytic and radiolytic initiation 115
Flynn, J. H., L. A. Wall, General treatment of the thermogravimetry of polymers 487
Formal solution for slit corrections in small-angle x-ray scattering 467
Further studies in the annealing of a borosilicate glass 147

G

Garner, D. L., E. J. Catanzaro, T. J. Murphy, W. R. Shields, Absolute isotopic abundance ratios and atomic weight of magnesium 453
—, *W. R. Shields, T. J. Murphy, E. J. Catanzaro,* Absolute isotopic abundance ratios and the atomic weight of a reference sample of chromium 193
General treatment of the thermogravimetry of polymers 487
Germanium resistors, calibration of, at low temperatures (2–20 °Kelvin) 243
Glasgow, A. R., Jr., Rupture-disk ampoule for anhydrous addition of hydrogen fluoride ... 143
Glass, borosilicate, annealing of, further studies 147
Gold (au III), interpretation of the third spectrum 465
Goodwin, R. D., Density-temperature formulae for coexisting liquid and vapor and for freezing liquid parahydrogen 541
Gregory, T. M., E. C. Moreno, W. E. Brown, Solubility of $CaHPO_4 \cdot 2H_2O$ and formation of ion pairs in the system $Ca(OH)_2 - H_3PO_4 - H_2O$ at 37.5 °C 545

H

Halpern, C., Effect of some halogenated hydrocarbons on the flame speed of methane ... 133
Hexafluorobenzene, high-temperature reactions 473
High-temperature reactions of hexafluorobenzene 473
Horton, W. S., Statistical aspects of second and third law heats 533
Hydrocarbons, halogenated, effect of, on the flame speed of methane 133
Hydrogen fluoride, rupture-disk for anhydrous addition 143

I

Iglesias, L., Interpretation of the third spectrum of gold (Au III) 465
Infrared spectra of the hydrated borates 153
Intermolecular potential functions from macroscopic measurements, determination ... 259
Interpretation of the solution absorption spectra of the $(PuO_2)^{++}$ and $(NpO_2)^{+}$ ions ... 165
Interpretation of the third spectrum of gold (Au III) 465
Isotactic polypropylene, the spherulitic crystallization of, from solution: On the evolution of monoclinic spherulites from dendritic chain-folded crystal percursors 29

J

Jacobson, R. A., A. D. Mighell, Use of the consistency check in the vector verification method 319

K

Khoury, F., The spherulitic crystallization of isotactic polypropylene from solution: On the evolution of monoclinic spherulites from dendritic chain-folded crystal precursors 29
Klein, M., Determination of intermolecular potential functions from macroscopic measurements 259
Knudsen, cell, rotating, dissociation pressure of aluminum carbide 253
Kokoszka, G. F., C. W. Reimann, H. C. Allen, Jr., Optical and magnetic spectra of bis-*N*-propylsalicylaldiminato copper (II) 1

L

Page

Lamm equation, nonlinear, the solution to, in the faxen approximation..... 17
Laun, D. D., Self-reversal in the spectral lines of uranium..... 323
Levin, E. M., Phase equilibria in the system niobium pentoxide-boric acid..... 11
–, Phase equilibria in the system niobium pentoxide-germanium dioxide..... 5
Line formula notation for coordination compounds: III Deviations from idealized configurations..... 23

M

Macroscopic measurements, determination of intermolecular potential functions..... 259
Magnesium, absolute isotopic abundance ratios and atomic weight..... 453
Martin, G. M., E. Passaglia, Density of polyethylene crystals grown solution..... 221
Mass spectrometric study of photoionization V. water and ammonia..... 459
Mazur, J., A. M. Wims, A formal solution for slit corrections in small-angle x-ray scattering..... 467
Mechanical relaxation in polyethylene crystallized with various degrees of lamellar orientation..... 225
Mechanism of the depolymerization of polytetrafluoroethylene with pyrolytic and radiolytic initiation..... 115
Meggers, W. F., C. H. Corliss, Wavelengths, intensities, and Zeeman patterns in ytterbium spectra (Yb I, II, III, IV)..... 63
Melting temperatures of the *n*-paraffins and the convergence temperature for polyethylene..... 481
Methane, the flame speed of, effect of some halogenated hydrocarbons..... 133
Methanol, 50-percent aqueous, as solvent, dissociation of some substituted phenols... 553
Mighell, A. D., Jacobson, R. A., Use of the consistency check of the vector verification method..... 319
Moore, D. G., H. E. Clark, A rotating cylinder method for measuring normal spectral emittance of ceramic oxide specimens from 1200 to 1600 °K..... 393
Moreno, E. C., T. M. Gregory, W. E. Brown, Solubility of $CaHPO_4 \cdot 2H_2O$ and formation of ion pairs in the system $Ca(OH)_2 - H_3PO_4 - H_2O$ at 37.5 °C..... 545
Mountain, R. D., Thermal relaxation and Brillouin scattering in liquids..... 207
Murphy, T. J., W. J. Catanzaro, E. L. Garner, W. R. Shields, Absolute isotopic abundance ratios and atomic weight of magnesium..... 453
–, *W. R. Shields, E. J. Catanzaro, E. L. Garner*, Absolute isotopic abundance ratios and the atomic weight of a reference sample of chromium..... 193

N

Napolitano, A., S. Spinner, Further studies in the annealing of a borosilicate glass..... 147
Niobium pentoxide-boric acid, phase equilibria in the system..... 11
Niobium pentoxide-germanium dioxide, phase equilibria in the system..... 5
Niobium pentoxide-tungsten trioxide, phase equilibria in the system to crystal structure..... 281
n-paraffins, the melting temperatures of, and the convergence temperature for polyethylene..... 481

O

Optical and magnetic spectra of bis-*N*-propylsalicylaldiminto copper (II)..... 1
Orientation of calcium molybdate ($CaMoO_4$) and other single crystals having the scheelite structure..... 379

P

Palladium group, configuration $4d^n + 4d^{n-1}5s$ in doubly ionized atoms..... 435
Parahydrogen, liquid, density-temperature formulae for coexisting liquid and vapor and for freezing..... 541
Parker, M. S., R. E. Florin, L. A. Wall, Mechanism of the depolymerization of polytetrafluoroethylene with pyrolytic and radiolytic initiation..... 115
Passaglia, E., J. M. Crissman, Mechanical relaxation in polyethylene cyrstallized with various degrees of lamellar orientation..... 225
–, *G. M. Martin*, Density of polyethylene crystals grown from solution..... 221
Pasternack, R. F., E. Silverton, A line formula notation system for coordination compounds: III Deviations from idealized configurations..... 23
Peiser, H. S., E. N. Farabaugh, J. B. Wachtmann, Jr., Orientation of calcium molybdate ($CaMoO_4$) and other single crystals having the scheelite structure..... 379
Pentafluorophenyl alkyl and vinyl ethers..... 233
Perloff, A., C. Robbins, S. Block, Crystal structure of BaGe $[Ge_3O_9]$ and its relation to benitoite..... 385
Phase equilibria as related to crystal structure in the system niobium pentoxide-tungsten trioxide..... 281
Phase equilibria in the system niobium pentoxide-boric acid..... 11
Phase equilibria in the system niobium pentoxide-germanium dioxide..... 5
Phenols, some substituted, in 50-percent aqueous methanol as solvent..... 553
Plante, E. C., R. Szwarc, Vapor pressure and heat of sublimation of rhenium..... 175
–, *C. H. Schreyer*, Dissociation pressure of aluminum carbide using a rotating Knudsen cell..... 253
Plumb, H. H., G. Cataland, Calibration of germanium resistors at low temperatures (2–20 °Kelvin)..... 243
P-N junction type, diffused, to x rays, steady-state response of silicon radiation detectors. II: Photodiode mode of operation..... 181
Polyethylene crystallized with various degrees of lamellar orientation, mechanical relaxation..... 225
Polyethylene crystals, density of, grown from solution..... 221
Polyethylene, the melting temperatures of the *n*-paraffins and the convergence temperature..... 481
Polymerization, homogeneous anionic, procedures..... 421
Polypropylene, isotactic, the spherulitic crystallization of, from solution: On the evolution of monoclinic spherulites from dendritic chain-folded crystal precursors..... 29
Polymers, general treatment of the thermogravimetry..... 487
Polytetrafluoroethylene, mechanism of the depolymerization of, with pyrolytic and radiolytic initiation..... 115
Procedures for homogeneous anionic polymerization..... 421
Properties of aqueous mixtures of pure salts. Thermodynamics of the ternary system: water-calcium chloride-magnesium chloride at 25 °C..... 305
Properties of aqueous mixtures of pure salts. Thermodynamics of the ternary system: water-sodium chloride-calcium chloride at 25 °C..... 313
Pryce, M. H. L., J. C. Eisenstein, Interpretation of the solution absorption spectra of the $(PuO_2)^{++}$ and $(NpO_2)^{+}$ ions..... 165
Pummer, W. J., L. A. Wall, Pentafluorophenyl alkyl and vinyl ethers..... 233
Pyrolytic and radiolytic initiation, mechanism of the depolymerization of polytetrafluoroethylene..... 115

R

Reimann, C. W., Electron absorption spectrum of cobalt (II)-doped trisphenanthroline-zinc nitrate dihydrate..... 417
–, *G. F. Kokoszka, H. C. Allen, Jr.*, Optical and magnetic spectra of bis-*N*-propylsalicylaldiminato copper (II)..... 1
Rhenium, vapor pressure and heat of sublimation..... 175
Robbins, C., A. Perloff, S. Block, Crystal structures of BaGe $[Ge_3O_9]$ and its relation to benitoite..... 385
Robinson, R. A., R. G. Bates, Dissociation of some substituted phenols in 50-percent aqueous methanol as solvent..... 553
–, *V. E. Bower*, Properties of aqueous mixtures of pure salts. Thermodynamics of the ternary system: water-calcium chloride-magnesium chloride at 25 °C..... 305
–, –, Properties of aqueous mixtures of pure salts. Thermodynamics of the ternary system: water-sodium chloride-calcium chloride..... 313
Rosenstock, H. M., V. H. Dibeler, J. A. Walker, Mass spectrometric study of photoionization V. water and ammonia..... 459
Rotating cylinder method for measuring normal spectral emittance of ceramic oxide specimens from 1200 to 1600 °K..... 393
Roth, R. S., J. L. Waring, Phase equilibria as related to crystal structure in the system niobium pentoxide-tungsten trioxide..... 281
Rupture-disk ampoule for anhydrous addition of hydrogen fluoride..... 143

S

Scharf, K., J. H. Sparrow, Steady-state response of silicon radiation detectors of the diffused P-N junction type to x rays. II: Photodiode mode of operation..... 181
Scheelite structure, orientation of calcium molybdate ($CaMoO_4$) and other single crystals..... 379
Schreyer, C. H., E. R. Plante, Dissociation pressure of aluminum carbide using a rotating Knudsen cell..... 253
Self-reversal in the spectral lines of uranium..... 323
Shadmi, Y., The configuration $4d^n + 4d^{n-1}5s$ in doubly ionized atoms of the palladium group..... 435
Shields, W. R., E. J. Catanzaro, T. J. Murphy, E. L. Garner, Absolute isotopic abundance ratios and atomic weight of magnesium..... 453
–, *T. J. Murphy, E. J. Catanzaro, E. L. Garner*, Absolute isotopic abundance ratios and the atomic weight of a reference sample of chromium..... 193
Silicon radiation detectors of the diffused P-N junction type to x rays. II: Photodiode mode of operation..... 181
Silverton, E., R. F. Pasternack, A line formula notation system for coordination compounds: III Deviations from idealized configurations..... 23
Solubility of $CaHPO_4 \cdot 2H_2O$ and formation of ion pairs in the system $Ca(OH)_2 - H_3PO_4 - H_2O$ at 37.5 °C..... 454
Solution to a nonlinear Lamm equation in the Faxen approximation..... 17
Sparrow, J. H., K. Scharf, Steady-state response of silicon radiation detectors of the diffused P-N junction type x rays. II: Photodiode mode of operation..... 181
Spectra, solution absorption, of the $(PuO_2)^{++}$ and $(NpO_2)^{+}$ ions..... 165
Spectral emittance, normal, of ceramic oxide specimens from 1200 to 1600 °K, a rotating method for measuring..... 393
Spherulitic crystallization of isotactic polypropylene from solution: On the evolution of monoclinic spherulites dendritic chain-folded crystal precursors..... 29
Spinner, S., A. Napolitano, Further studies in the annealing of a borosilicate glass..... 147
Steady-state response of silicon radiation detectors of the diffused P-N junction type x rays. II: Photodiode mode of operation..... 181
Szwarc, R., E. R. Plante, Vapor pressure and heat of sublimation of rhenium..... 175

T

Tefft, W. E., Elastic constants of synthetic single crystals corundum..... 277
Ternary system: water-calcium chloride-magnesium chloride at 25 °C, thermodynamics of, properties of aqueous mixtures of pure salts..... 305
Ternary system: water-sodium chloride-calcium chloride at 25 °C, thermodynamics of, properties of aqueous mixtures of pure salts..... 313
Thermal relaxation and Brillouin scattering in liquids..... 207
Thermodynamics of the ternary system: water-calcium chloride-magnesium chloride at 25 °C..... 305
Thermodynamics of the ternary system: water-sodium chloride-calcium chloride at 25 °C..... 313
Thermogravimetry of polymers, general treatment..... 487

U

Ultraviolet lines of Fe I, oscillator strengths..... 325
Uranium, self-reversal in the spectral lines..... 323
Use of the consistency check in the vector verification method..... 319

V

Page

Vapor pressure and heat of sublimation of rhenium..... 175
Vector verification method, use of the consistency check..... 319
Vinyl ethers and pentafluorophenyl alkyl..... 233
Viscoelastic behavior under large deformations..... 525

W

Wachtmann, J. B., Jr., E. N. Farabaugh, H. S. Peiser, Orientation of calcium molybdate ($CaMoO_4$) and other single crystals having scheelite structure..... 379
Walker, J. A., V. H. Dibeler, H. M. Rosenstock, Mass spectrometric study of photoionization V. Water and ammonia..... 459
Wall, L. A., J. M. Antonucci, High-temperature reactions of hexafluorobenzene..... 473
—, *R. E. Florin, M. S. Parker,* Mechanism of the depolymerization of polytetrafluoroethylene with pyrolytic and radiolytic initiation..... 115
—, *J. H. Flynn,* General treatment of the thermogravimetry of polymers..... 487
—, *W. J. Pummer,* Pentafluorophenyl alkyl and vinyl ethers..... 233
Waring, J. L. Roth, R. S., Phase equilibria as related to crystal structure in the system niobium pentoxide-tungsten trioxide..... 281
Warner, B., C. H. Corliss, Oscillator strengths for ultraviolet lines of Fe I..... 325
Wavelengths, intensities, and Zeeman patterns in ytterbium spectra (Yb I, II, III, IV)... 63
Weir, C. E., Infrared spectra of the hydrated borates..... 153

Page

Weiss, G. H., I. H. Billick, The solution to a nonlinear Lamm equation in the Faxén approximation..... 17
Wims, A. M., J. Mazur, A formal solution for slit corrections in small-angle x-ray scattering..... 467

X

X-ray scattering, small-angle, a formal solution for slit corrections..... 467
X rays, steady-state response of silicon radiation detectors of the diffused P-N junction type. II: Photodiode mode of operation..... 181

Y

Ytterbium spectra (Yb I, II, III, IV), wavelengths, intensities, and Zeeman patterns..... 63

Z

Zapas, L. J., Viscoelastic behavior under large deformations..... 525
Zeeman patterns in ytterbium spectra (Yb I, II, III, IV)..... 63

U.S. GOVERNMENT PRINTING OFFICE : 1966 OL—230-736

UNIVERSITY MICROFILMS, INC
ATT SERIALS SECTION
313 NORTH FIRST ST
ANN ARBOR, MICHIGAN

UNITED STATES
GOVERNMENT PRINTING OFFICE
DIVISION OF PUBLIC DOCUMENTS
WASHINGTON, D.C. 20402

OFFICIAL BUSINESS

POSTAGE AND FEES PAID
U.S. GOVERNMENT PRINTING OFFICE

JOURNAL OF RESEARCH of the National Bureau of Standards Vol. 70A, No. 6 November–December 1966
A. Physics and Chemistry

Contents

	Page
Absolute isotopic abundance ratios and atomic weight of magnesium. Edward J. Catanzaro, Thomas J. Murphy, Ernest L. Garner, and William R. Shields.	453
Mass spectrometric study of photoionization V. Water and ammonia. Vernon H. Dibeler, James A. Walker, and Henry M. Rosenstock.	459
Interpretation of the third spectrum of gold (Au III). Laura Iglesias.	465
A formal solution for slit corrections in small-angle x-ray scattering. Jacob Mazur and Andrew M. Wims.	467
High-temperature reactions of hexafluorobenzene. Joseph M. Antonucci and Leo A. Wall.	473
The melting temperatures of the *n*-paraffins and the convergence temperature for polyethylene. Martin G. Broadhurst.	481
General treatment of the thermogravimetry of polymers. Joseph H. Flynn and Leo A. Wall.	487
Viscoelastic behavior under large deformations. Louis J. Zapas.	525
Statistical aspects of second and third law heats. William S. Horton.	533
Density-temperature formulae for coexisting liquid and vapor and for freezing liquid parahydrogen. Robert D. Goodwin.	541
Solubility of $CaHPO_4 \cdot 2H_2O$ and formation of ion pairs in the system $Ca(OH)_2$-H_3PO_4-H_2O at 37.5 °C. Edgard C. Moreno, Thomas M. Gregory, and Walter E. Brown.	545
Dissociation of some substituted phenols in 50-percent aqueous methanol as solvent. R. A. Robinson and Roger G. Bates.	553
Publications of the National Bureau of Standards.	557
Index to volume 70A, January to December 1966.	565

Library of Congress Catalog Card Number: 62–37059

For sale by the Superintendent of Documents, U.S. Government Printing Office, Washington, D.C. 20402. Price $1.00 (single copy)
Subscription price: $5 a year; $1.00 additional for foreign mailing.
UNITED STATES GOVERNMENT PRINTING OFFICE, WASHINGTON : 1966